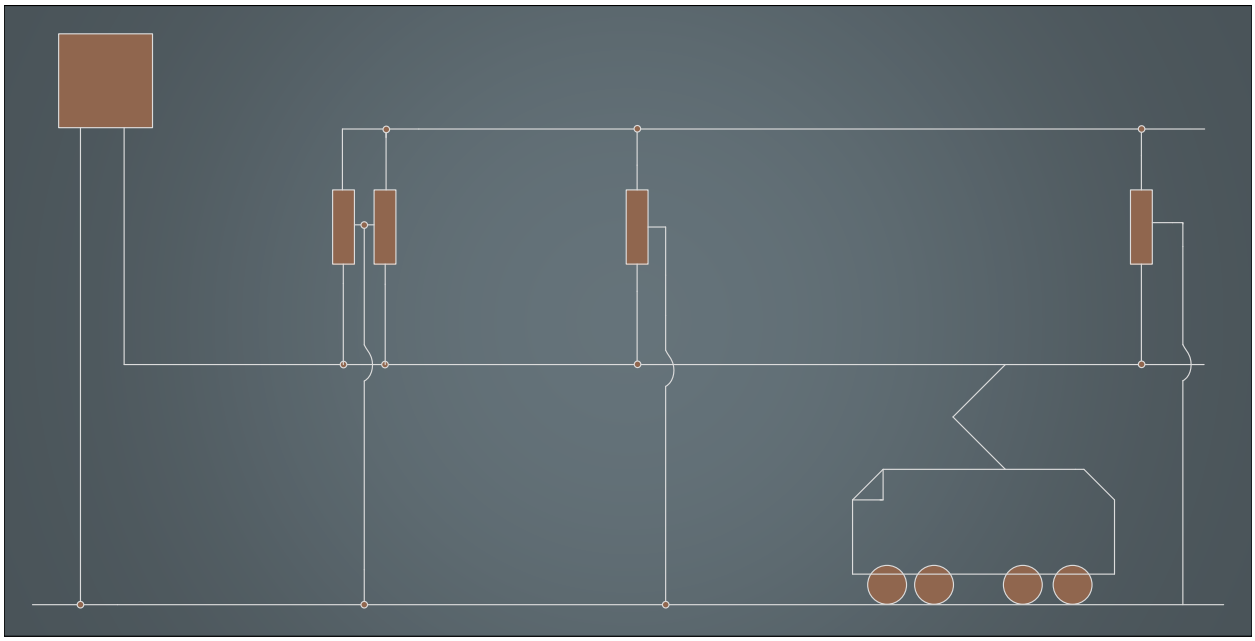

Impact of Converter Size Asymmetry on Power Transfer in Railway Power Systems

Power transfer optimization based on adjustable converter parameters

Master's thesis in Sustainable Electric Power Engineering and Electromobility

FILIP ALRUP

WILLIAM HIDEVIK

DEPARTMENT OF ELECTRICAL ENGINEERING

CHALMERS UNIVERSITY OF TECHNOLOGY
Gothenburg, Sweden 2026
www.chalmers.se

Master's thesis EENX30 2026

Impact of converter size asymmetry On power transfer in railway power systems

FILIP ALRUP
WILLIAM HIDEVIK

CHALMERS
UNIVERSITY OF TECHNOLOGY

Department of Electrical Engineering
Division of Electric Power Engineering
Chalmers University of Technology
Gothenburg, Sweden 2026

Impact of converter size asymmetry on power transfer in railway power systems
FILIP ALRUP
WILLIAM HIDEVIK

Supervisor: Lars Abrahamssom, Trafikverket
Supervisor: Anders Forsmark, Trafikverket
Examiner: Anh Tuan Le, Chalmers University of Technology

Master's Thesis 2026
Department of Electrical Engineering
Division of Electric Power Engineering
Chalmers University of Technology
SE-412 96 Gothenburg
Telephone +46 31 772 1000

Cover: Schematic diagram of the structure of an AT-system in the Swedish railway power system.

Typeset in LaTeX
Printed by Chalmers Reproservice
Gothenburg, Sweden 2026

Abstract

This thesis investigated the impact of converter station capacity asymmetry on power transfer for different system impedances. The scope of this thesis was to investigate the significance of the adjustable static converter parameters, in order to minimize active power losses in the railway power system. This thesis only considers the static frequency converter (SFC), and since an SFC solely consists of power electronics and is modeled to mimic the behaviors of a rotary frequency converter (RFC) through software, the parameters are adjustable. This means that it was possible to adjust the quadrature reactances for instance, which would not be possible if the RFC were modeled. The Y-bus matrices and the load profiles were made in Matlab whilst the optimization and load flow models were constructed in the General Algebraic Modeling System (GAMS), which was used to optimize the system with the objective function to minimize active power losses. Various cases were simulated where the converter parameters were optimized for both the auto-transformer (AT) - and booster transformer (BT)-systems to understand the system for representative cases. The models were used for studying realistic cases as well as cases with large asymmetry in terms of power capacity and different load locations between substations. This was done to shed further light regarding the philosophy of local production, whether it should be prioritized or not. The results show, for both the AT- and BT-system, that if the load is located in the middle of the line, it is optimal for the substations to share the load as evenly as possible. If the load is located closer to one substation than the other, then the system should prioritize local production regardless of the substation capacities. If there is a large asymmetry between the substations, in terms of installed total power capacity, it is more optimal to control the load-sharing with the no-load angle than other parameters. Optimization of the no-load angle reduced power losses for all cases, particularly when the substations had highly asymmetric power capacities. However, it was shown that the no-load voltage should always be kept as high as possible. The results also show that the quadrature reactances should be as low as possible in order to minimize losses, this is possible since the SFC quadrature reactances can be set in the software controlling the power electronics. In regards to the active- and reactive power droops, it was shown that with optimization they were not able to reduce the losses significantly. In contrast, it was shown and discussed that the active power droop, when solely optimized, was able to reduce the voltage drops and decrease the overall voltage variations. However, during the full optimized cases, the droop factor did not give such significant change since it was probably de-prioritized. It was also discussed that the reactive power droop got very small for the BT-system when the no-load voltage also were optimized, which probably is a result of the high no-load voltage and limited load model. In order to reach clarification regarding the droop constants, a load model with higher complexity would be needed.

Keywords: Railway, Power transfer, AT-system, BT-system, Voltage variations, Static Frequency Converter, Optimization, Loss reduction

Acknowledgements

I would like to acknowledge and thank everyone who supported William and I during this thesis and those who contributed to this thesis work. My deepest appreciation goes out to my supervisor Lars Abrahamson who helped guide us provided many valuable modeling considerations to achieve the work in this thesis. Your expertise and support were instrumental in shaping our modeling approach and helping us identify the right areas of focus. Your contributions were essential for this thesis.

Thank you Anders Forsmark for generously sharing your knowledge of the Swedish railway system. Your insights gave us a much deeper understanding of the operational context, which greatly informed our work.

Special thanks Anh Tuan Le, our examiner. Thank you for your engagement throughout this thesis and the confidence you showed in our work. Your approach in our meetings made for a smooth and encouraging work experience.

Lastly I would like to thank Trafikverket for providing William and I with the opportunity to do this work. It has been an enriching, and very motivating experience to work on a project with practical significance in the Swedish railway

Filip Alrup, Gothenburg, June 2026

Firstly, I would like to thank my supervisors and examiners Lars Abrahamsson, Anders Forsmark and Anh Tuan Le for their endless help, guidance and support throughout this thesis. I would also like to thank my colleagues at Trafikverket for providing an excellent work environment and many joyful coffee-breaks.

I would of course also like to thank my family and friends for always supporting me during my studies and in life in general.

Lastly, I would like to dedicate this work to my great-grandmother, Ingrid Ahlén, who sadly passed away during the time of this thesis. Thank you for your endless love and support, and may you forever rest in peace.

William Hidevik, Gothenburg, June 2026

List of Acronyms

Below is the list of acronyms that have been used throughout this thesis listed in alphabetical order:

AT-system	Auto-Transformer System
BT-system	Booster-Transformer System
GAMS	General Algebraic Modeling System
IORE	Iron ore
RFC	Rotating Frequency Converter
SFC	Static Frequency Converter
X/R - ratio	Ratio between Reactance (X) and Resistance (R)
Y-bus	Admittance matrix

Nomenclature

Below is the nomenclature of indices, sets, parameters, and variables that have been used throughout this thesis.

Indices

i,j	Indices for nodes in the network
ss	Indices for substation nodes in the network, subset to i, j
sc	Indices of sub-converters within a converter station

Sets

N	Set of nodes
s	Set of operation scenarios

Parameters

G_{ij}	Electrical conductance between node i and node j
B_{ij}	Electrical susceptance between node i and node j
$P_{D,i}$	Active power load at node i
$Q_{D,i}$	Reactive power load at node i
S	Total amount of operation scenarios
C	Total amount of converters in substation
$S_{rated,ss,sc}$	Rated apparent power of a converter in a substation
$\tau_{ss,sc}$	Scaling factor

Variables

P_i	Active power injection at node i
P_{ij}	Active power flow from node i to node j
Q_i	Reactive power injection at node i
Q_{ij}	Reactive power flow from node i to node j
U_i	Voltage at node i
U_{ss}	Voltage at a substation busbar
θ_i	Angle at node i
$P_{G,ss}$	Generated active power at substation node ss
$Q_{G,ss}$	Generated reactive power at substation node ss
$P_{G,i}$	Generated active power at node i
$Q_{G,i}$	Generated reactive power at node i
$X_{q,m}^{ss,sc}$	Quadrature reactance at the motor side for a converter, sc, at a substation, ss
$X_{q,g}^{ss,sc}$	Quadrature reactance at the generator side for a converter, sc, at a substation, ss,
J_{total}	Cost function of the optimization
$K_{p,Q}^{ss}$	Voltage droop with respect to reactive power for a converter
$K_{p,P}^{ss}$	Voltage droop with respect to active power for a converter

Contents

List of Figures

List of Tables

1
Introduction

This chapter describes the background and problem overview of this thesis, along with its scope, limitations and structure

1.1 Background

The impedance in the Swedish railway power supply network (15 kV, $16\frac{2}{3}$ Hz, 1 PH) decrease with the transition from BT- to AT-system. When investing in new lines, as well as in reinforcements and reinvestments, Trafikverket tends to choose converter units with larger amount of installed power. This is because it would provide a higher power per cost of unit (MVA/SEK). This applies particularly to static converters since the upcoming rotary converter has a relatively modest power capacity of 12 MVA.

Since static converters in synchronous-synchronous networks are modeled to behave like mechanically coupled synchronous machines, the power fed relative to other units in the same converter station are mainly dependent on the installed power and the machine's reactances. Load sharing between converter stations also depends on grid impedance to a high degree. This means that future networks with asymmetrically distributed converter sizes may result in geographically distant large converters contributing more power to the loads than geographically closer and smaller converters.

This phenomena will be most significant when the load is low, since in general only a few converters will be active at each station. Stations with small converters will then have a relatively small installed power in operation compared to stations with a few large converters.

1.2 Problem overview

The national grid and the railway grid are connected by converters, located together with other converters in converter stations, which is used for the conversion from 50 Hz to, in Sweden, $16\frac{2}{3}$ Hz. Since the national grid is typically a lot stronger than the railway power grid, it is a fair assumption that the voltage on the 50 Hz side is constant. However, on the railway side it is possible to control the voltages. Although the railway is the most efficient land-based transportation in terms of energy, there

is still a lot of possibilities to operate the railway power systems more efficiently. At the time of writing, the settings of the voltage droop is experience-based and have a lot of potential improvements to be investigated [5]. By investigating and determining the possibilities of the converter controllable parameters, an improvement in system losses may be achievable.
Based on the problem overview, the following questions will be examined in this thesis:

- Is it possible to increase the efficiency of the system without risking the stability of the system?
- What is an optimal solution for power transfer between stations with significant converter size differences?
- What is the philosophy regarding local supply with small converters and larger converters that are geographically distant from demand?

1.3 Research methodology

A review of the literature will be conducted in order to find equations, methods and knowledge needed in order to create the models of the system. A simple network will first of all be constructed in the GAMS software, which then will be compared to PowerFactory in order to verify that the model works properly. When the GAMS model is verified, data regarding the power network will be used in order to construct a representative power system with a realistic load profile. When the full network is constructed with a realistic load profile, the GAMS modeling will be performing optimization of the calculations in order to ultimately find answers to the questions in the problem overview.

1.4 Scope and limitations

The scope of this thesis is to investigate the significance of manipulating the converter parameters and if it could improve the power transfer, and thus improve the system losses. The thesis will mainly be focusing on following converter parameters:

- No-load voltage
- No-load angle
- Droop on active and reactive power
- Quadrature reactances of the converter

The limitations of this thesis can be described in a bullet list:

- The thesis will not investigate the full railway network, only certain parts of it. Due to confidentiality, the exact locations will not be named in the report.
- The thesis will not take into account the short-circuit capacity, which could affect the maximum amount of active units. In this project, each substation will have 2 units active at all times.

- Due to complexity and time constraints, the modeling of the trains will be considered as static loads.
- Due to time limitations, this thesis will only consider static frequency converters as the type of converter.

1.5 Thesis structure

After this chapter the thesis will be structured accordingly:

- **Chapter 2 -** Provides a theoretical background regarding the railway power system in Sweden and its components.

- **Chapter 3 -** Shows the background regarding the system setup and the used equations to optimize the converter parameters.

- **Chapter 4 -** Shows the results from the validation system, as well as the results from the representative-, exaggerated converter size- and asymmetric load distribution cases for both the AT- and BT-system.

- **Chapter 5 -** Discusses the results and the reasoning behind the behaviors that can be seen from the simulations.

- **Chapter 6 -** Through the discussion, this chapter draws the main conclusions regarding the results of the simulations. The chapter also describes what kind of improvements that can be made and done, in the form of future work, that can improve this thesis.

2
Theory

This chapter presents the necessary theory and information required for this thesis.

2.1 Background of the Swedish railway system

The Swedish railway power system consists of a 15 kV and $16\frac{2}{3}$ Hz network. The origin of this standard was set during the early days of electrification, a low frequency was used due to limitations in the used electrical machines. In comparison to the national grid, the railway power system can be seen as very weak and its voltage levels are sensitive to the flow of power [2].
The connection between the national grid and the railway power network in a decentralized system can be seen in figure 2.1:

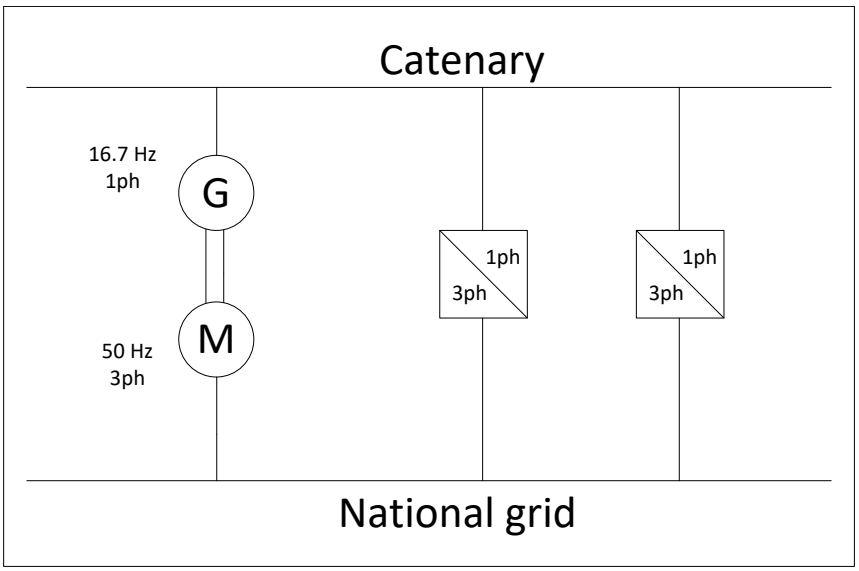

Figure 2.1: Visualization of the connection between the national grid and catenary for a decentralized system, from [1].

In the late 70's there was a problem within the Swedish railway power system that larger voltage drops occurred. A possible solution to this problem would've been to increase the amount of substations in the system. However, since that was considered to be very expensive, a solution of adding a single phased 130 kV transmission line was made [1]. An illustration of the centralized system can be seen in figure 2.2:

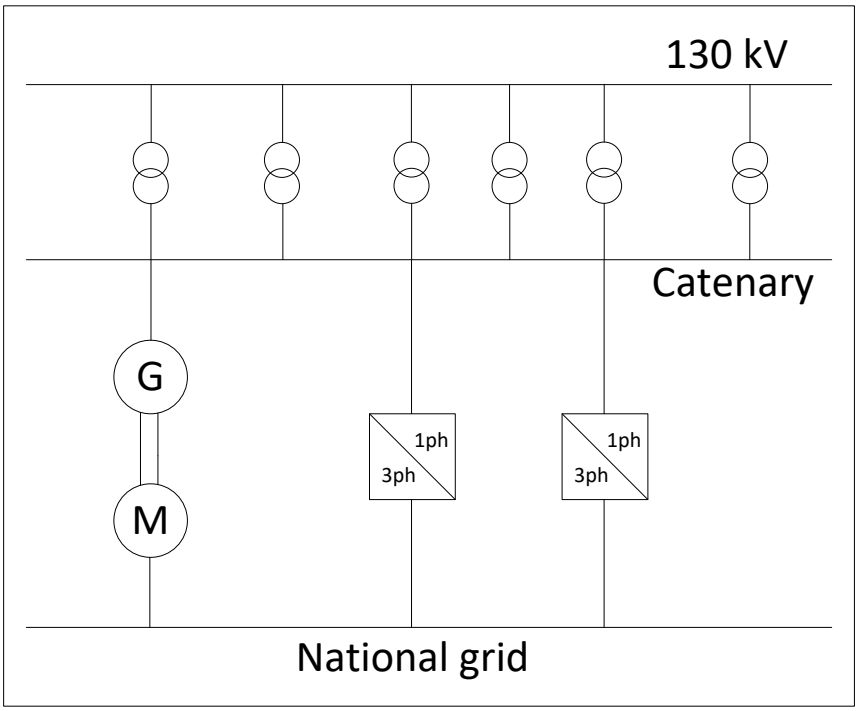

Figure 2.2: Visualization of the connection between the national grid, catenary and 130 kV grid in a centralized system, from [1].

The addition of the 130 kV transmission line made it possible to decrease the number of converter stations, it also improved the voltage profiles and reduced network losses. The first 130 kV transmission line was completed in 1992 and since then the network has increased to a larger network as a whole [1].

2.2 Converters in the railway power system

In order to achieve the frequency conversion between the national grid (50 Hz) and the railway grid ($16\frac{2}{3}$ Hz), different types of converters are used. The different converters can either be a static frequency converter, which is based on power electronics, or a rotary frequency converter which is a machine based converter [6].

The RFC consists of a motor on the public grid side, and a generator on the catenary side. If the motor is of the synchronous type, the railway power grid will be synchronous to the public grid and if it is of the asynchronous type, the railway power grid will not be synchronous to the public grid. In Sweden and Norway, the motor is of the synchronous type, hence the frequency of the railway power grid is synchronous to the national grid. The generator is also of synchronous type and is connected with a common axis to the synchronous motor [7]. The number of pole pairs of the generator is one third of the numbers of pole pairs of the motor and due to the difference, the converter is able to convert the power from the 50 Hz side to $16\frac{2}{3}$ Hz on the railway side. The rotary converter is connected to the public grid through a transformer to its motor side, and is connected to the catenary side through a transformer to its generator side [2].

The connection between the public grid (50 Hz) and the railway grid ($16\frac{2}{3}$ Hz) can be seen in figure 2.3:

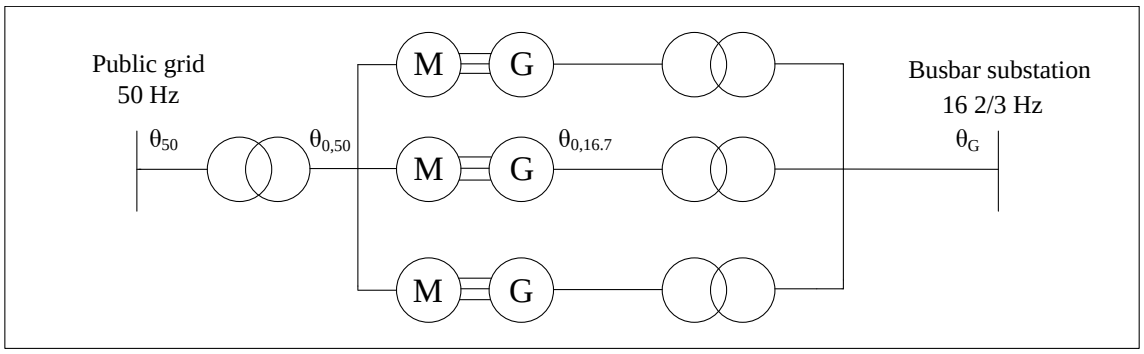

Figure 2.3: Visualization of the conversion from the public grid to the catenary, inspired by fig 2.3 in [2].

There are certain limitations with the rotary converter. Since it is, in the Swedish railway system, composed of two synchronous machines there are certain parameters that are uncontrollable due to the fact that they are directly related to the characteristics of the motor and generator. For instance, the quadrature reactances of the converter which is entirely dependent on the construction of the machines, and hence can not be changed [8]. The only parameters that can be controlled is the voltage magnitudes of the motor and generator sides, or the reactive power on the same sides [7].

Although static converters only consist of power electronics, instead of synchronous machines like the RFC, they are still used to mimic the behaviors of the RFCs. The main difference is that the modeling of the SFC is able to control the quadrature reactances, phase angles and voltages. However, a drawback is that the SFC cannot be overloaded and hence it is important to include a limit on the output of apparent power [2][9].

2.2.1 Voltage control on substation busbar

In the Swedish railway power system, the busbar voltage is today mainly controlled by the reactive power output of the converters, i.e the voltage at the busbar will drop if the reactive power output increases. Since there is usually more than one converter at each busbar, it means that they control the voltage at the busbar together, hence a control system needs to be implemented. This concept is called voltage droop, where a droop coefficient is applied on the reactive power, and describes how sensitive the voltage should be to the change of reactive power. It is possible to add a droop-control with respect to the active power as well. This could be beneficial because in the Swedish railway power system, the ratio between line resistance and reactance is almost equal to 1. This means that the traditional strong relation between voltage and reactive power, which is a typical assumption that can be made in the national grid, is weakened since it requires a high X/R-ratio. Due to the fact that the X/R-ratio in the railway system is close to 1, voltage has a strong relation with both

active- and reactive power [6]. In [6] a modified voltage control law was made, which investigated the inclusion of droop on active power and how the system behaviors changed with it. The conclusion was that the load sharing between the substations improved, but with the cost of lower voltage level and higher system losses. Although it is suggested that the disadvantages could be fixed by changing the no-load voltage and implement proper settings for droop coefficients.

2.3 Power transfer

Within railways the most common type of power supply system is to use an overhead contact line to supply the trains. Typically in the railway power system, the overhead line usually goes by the name of catenary and is mainly made of copper alloy [2].

2.3.1 System for return currents

Although the ground itself in Sweden has a relatively high resistance as compared to e.g. central Europe, using the rail as the return conductor could potentially cause problems that the current starts to flow through the ground in addition to the rail, since the ground has less impedance than the rail. If this happens, unwanted currents might occur at the surroundings. Because of these problems there is a high need for a separate system for the return currents. A solution is to use transformer based systems that forces the return current to flow through the track and return circuitry [2].
In order to limit the stray currents, the transformers needs to be distributed within different intervals. For the BT-system the booster transformers are distributed approximately every 5 km on the line, whilst for the AT-system the auto transformers are distributed about every 10 km [9].

2.3.1.1 BT-system

The BT-system was first introduced to the Swedish railway power system and was seen as a solution to the problems related to the high ground resistances in the Nordics. The high ground resistance complicates the return currents through the rail and ground, which could potentially cause communication disturbances. The purpose of the booster transformer is to draw the currents from the rail to an overhead return conductor [9]. The booster transformer forces the supply current, that flows through the train and track, to flow into the transformer via a return circuit. Due to the transformer having a 1:1-ratio and both of its sides are connected in series to the catenary and the return circuit, the transformer will force the currents to match as long as the transformer is operated within its operating zone. If a fault occurs, and a large amount of current is drawn to the booster transformer, the transformer could eventually reach its saturation level. The result of this will then be that the transformer loses its control to force the current via the return circuit and the current will then start to also flow through the track and ground [10]. By making sure that the same current that runs through the contact line goes back via the return circuit, the rail potential can be reduced. The booster-transformers

and return circuit have much higher impedance than the ground and due to the fact that the currents have to run through each booster transformer on the line, the total system impedance increases [9]. Although the BT-system is used in various countries, it should be noted that it is not needed everywhere since some places do not have the problem with high ground resistance [11]. A visualization of the BT-system with its current flows can be seen in figure 2.4:

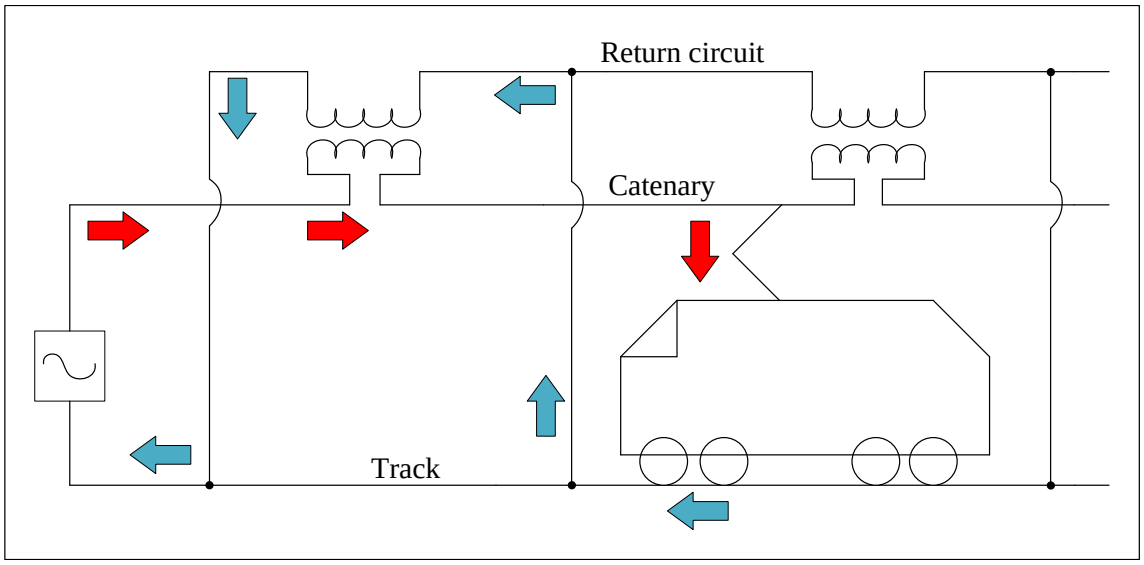

Figure 2.4: Visualization of a BT-system with its current flow, inspired by [2].

The red arrows shows the current flow from the substation to the train, whilst the blue arrows shows the current flow from the train to the booster transformer and then eventually back to the substation.

2.3.1.2 AT-system

Instead of balancing the supply and return currents as in the BT-system, the AT-system balances the voltage. By introducing a secondary conductor, which is phase shifted 180° to the primary conductor, the system will then have a positive- and a negative feeder [2]. Although the voltage between the catenary and negative feeder line doubles, due to the 180° phase shift, the voltage between the rail and catenary stays the same. The reasoning behind the increased voltage potential is to electrically reduce the impedance, since higher voltage leads to smaller currents, thus reducing network active power losses [9].
A schematic diagram of the AT-system can be seen in figure 2.5:

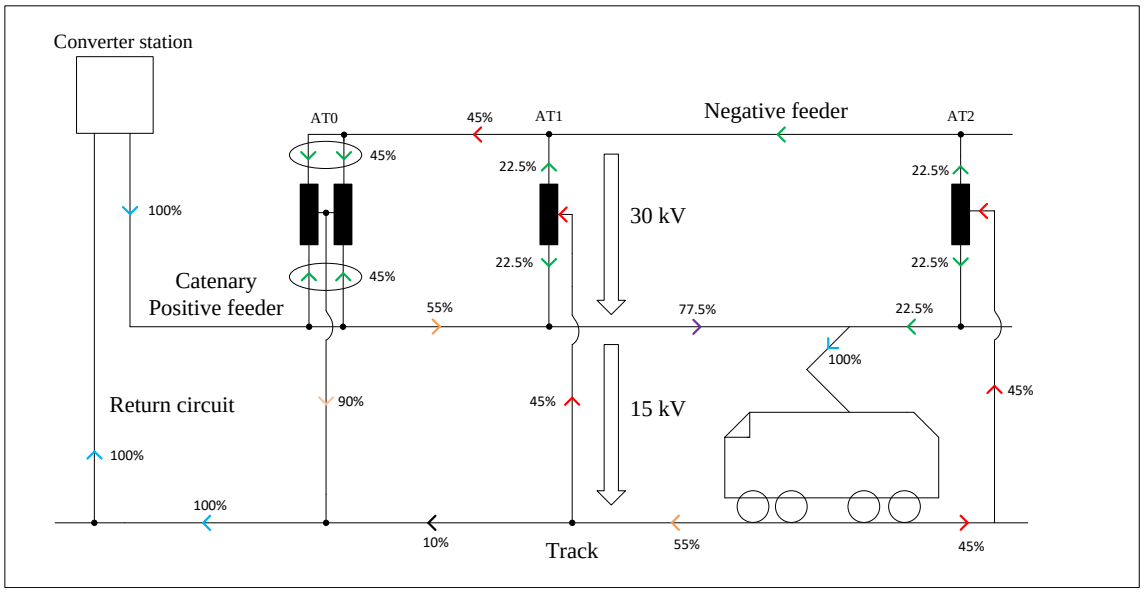

Figure 2.5: Visualization of an AT-system with its current flows, inspired by figure 2.5 in [3].

The current flows for a simple case can also be seen in figure 2.5. Worth mentioning is that the distribution does not always follow the ones given in the figure. It is just an example to understand the concept of the AT-system.

2.4 Trains as loads

Trains in the railway power system are able to produce and consume power. This production and consumption can be gathered over a period of time to form a profile of the train as a positive or negative load. Older trains tend to have a lower power factor while newer trains tend to have a power factor closer to one, i.e only consuming active power [10]. Most modern trains are able to achieve a unity power factor during motoring, an example of this are trains using an iron ore (IORE) locomotive. However, due to regenerative braking for most but not all trains, the reactive power demand from a train increases since the feed back power from the braking train will increase the catenary voltage. The train is then allowed to increase its reactive power demand to decrease the voltage at the catenary [2].

Another important element to take into account when modeling the load profile is the designated route. For instance, if a route is mainly used for transporting goods it is more likely to experience a lower amount of moving trains during a day in comparison to a route that is used for commuting people. If a route is mainly used for commuting people then it will result in a different load profile since the number of trains along the route is much higher [12].

3

Power system modeling and optimization

This chapter contains the methods regarding the modeling and optimization of the simulated power system. How the simulations were structured and what was done to accurately represent the system that was modeled.

3.1 Assumptions to the modeling and simulation

In order to scale the complexity of the project, certain assumptions were needed. Following assumptions have been taken in this thesis:

- Assuming constant frequency values
- Assuming that the load has a constant $cos(\phi) = 1$, i.e. only considers active power.
- Assuming a very strong national grid
- The converters in each substations is sharing its demand proportionally in relation to their size. This has been done through a scaling factor.

3.2 Power system simulations in PowerFactory

PowerFactory is a modeling software mainly used for analyzing transmission, distribution and generation within power systems [13]. In order to validate that the structure of the GAMS model is correct, the PowerFactory software has been used as a reference. A system containing 5 stations and 4 loads can be seen in figure 3.1:

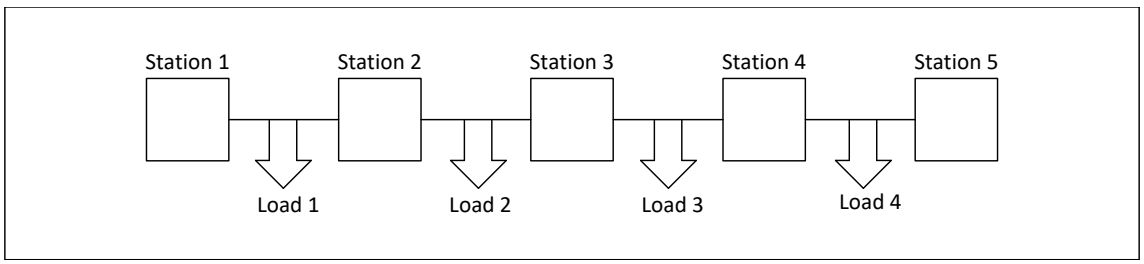

Figure 3.1: Schematic diagram of the model structure that have been used to simulate in PowerFactory

It should be noted that the loads are located in the middle of the lines for the validation system. There is no specific reason to locate the load in the middle, since in reality the train is moving, but it is of utmost importance that the load is located on a similar location between GAMS and PowerFactory. If not, the GAMS model will not be able to be validated properly since the system setup would differ.
A schematic diagram of a substation can be seen in figure 3.2:

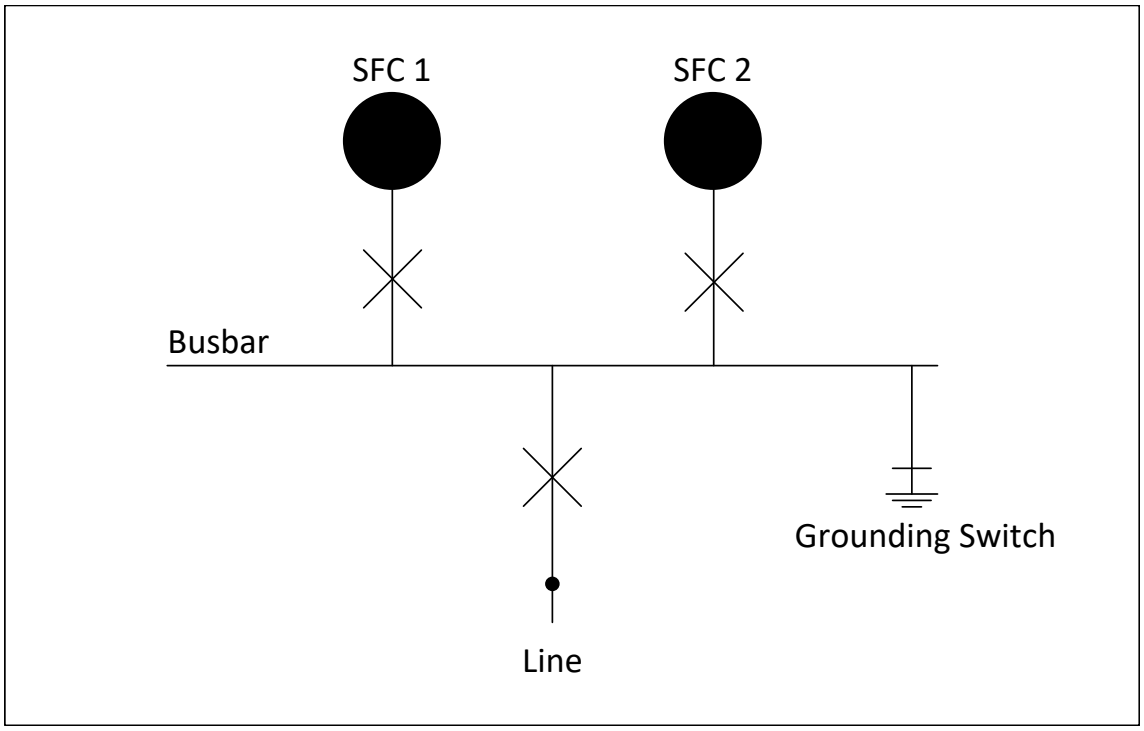

Figure 3.2: Schematic diagram of a substation

As can be seen in figure 3.2 the substations for the validation system has 2 static converters active. The capacities of the converters in the substation are different and asymmetrical to other substations. This means that the total capacity of each substation is different throughout the system. This was done to make it more realistic and to expose potential problems in the GAMS model. The capacities of the substations are based on real substations in the grid, but not exactly as to retain anonymity. By using the load flow calculation with the Newton-Raphson classical power equations as setting, it was possible to simulate in both programs and then to compare them against each other.
In the railway power system the phase technology is of 1PH-N, with the neutral being connected through the grounding switch. This is so that, when simulating, the neutral will not be floating for measurement reasons.

3.3 Modeling and optimization in GAMS

The modeling and optimiztion in GAMS was done by constructing the system as in terms of system admittance matrix and load profile. Then a mathematical model was set up in order to simulate the power system.

3.3.1 System structure with admittance matrix

In order to describe a power system, and to be able to mathematically calculate the power flow of the system, an admittance matrix was used. The definition of admittance can be described as the inverse of the impedance:

$$Y = \frac{1}{Z} = G + jB \tag{3.1}$$

In equation 3.1 the admittance is described in rectangular form, where the real part G is the conductance and the imaginary part B is the susceptance. A power system containing 5 stations, which is in accordance to the system structure of this thesis, can be seen in figure 3.3:

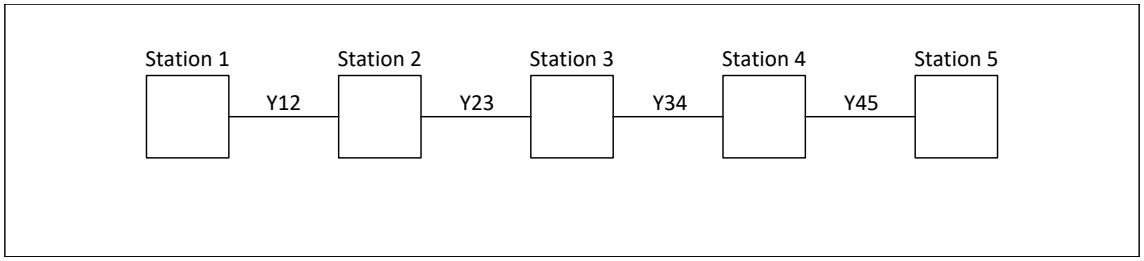

Figure 3.3: Power system structure with 5 substations

From the power system structure in figure 3.3, its admittance matrix Y_{bus} looks like:

$$Y_{bus} = \begin{bmatrix} Y_{12} & -Y_{12} & 0 & 0 & 0 \\ -Y_{12} & (Y_{12}+Y_{23}) & -Y_{23} & 0 & 0 \\ 0 & -Y_{23} & (Y_{23}+Y_{34}) & -Y_{34} & 0 \\ 0 & 0 & -Y_{34} & (Y_{34}+Y_{45}) & -Y_{45} \\ 0 & 0 & 0 & -Y_{45} & Y_{45} \end{bmatrix}$$

From the Y_{bus} matrix, the structure of the power system is described mathematically. The admittance matrix was then used to calculate the power flow equations in order to describe the system behaviors.

3.3.2 Load profiles

By using real-life data of the power- and current output from each substation, a load profile for both the AT- and BT-system have been created.

3.3.2.1 Using power output data from each station

In order to properly simulate a representative version of the railway power system, load profiles for both AT- and BT-system needs to be taken into account. The way to, as accurately as possible, model the load profiles is to use real-life data for the power output of the substations. Since this thesis has the assumption that the modeled trains are of a modern type using IORE locomotives, it was assumed that the load has a $cos\phi = 1$, which means that the load only absorbs active power. Due

to this assumption, the used data only focused on the active power output. The load between two substations has been calculated as the summation of the active power flow injection from each substations toward each other. This can be visualized in figure 3.4:

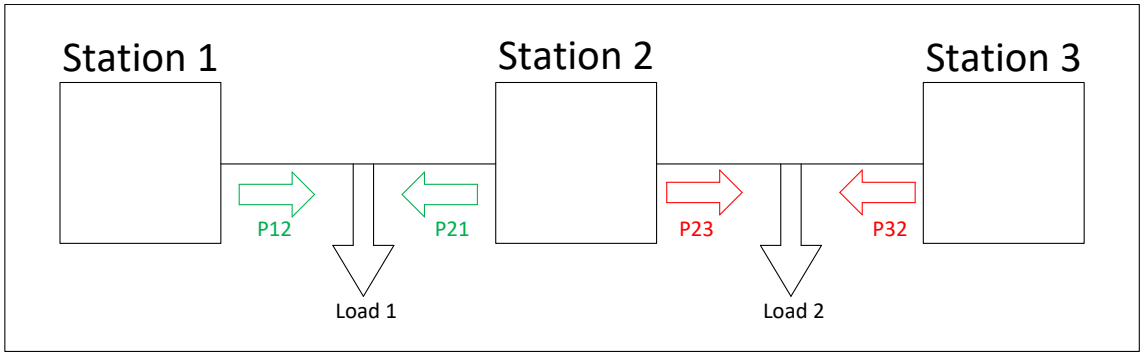

Figure 3.4: Visualization of power flow in order to calculate the load

The active power flow towards load 1 and 2 can be seen in figure 3.4. According to the picture, the load was calculated as following:

$$Load_1 = P_{12} + P_{21} \tag{3.2}$$

$$Load_2 = P_{23} + P_{32} \tag{3.3}$$

A proper modeling of the loads in the AT- and BT-system requires that the activity of the routes is taken into account. If a route is more actively used, as in there are more trains moving along the route, then the load will become evenly distributed whereas if it is less active then there is a risk of error in modeling the load profile. If the time step of the acquired data is too large then there is a risk of miscounting the number of trains along the route. For example, if there is a train between station 1 and 2, and within the same hour the train is between station 2 and 3, the data would've said that there are two loads if the time-step was one hour. Due to this, the used data has a time-step of a minute.

At some parts of the railway power system, there is a distribution station in between converter stations. Due to this, it was possible to calculate and distribute the load more evenly along the line. A visualization of a power system network with a distribution station can be seen in figure 3.5:

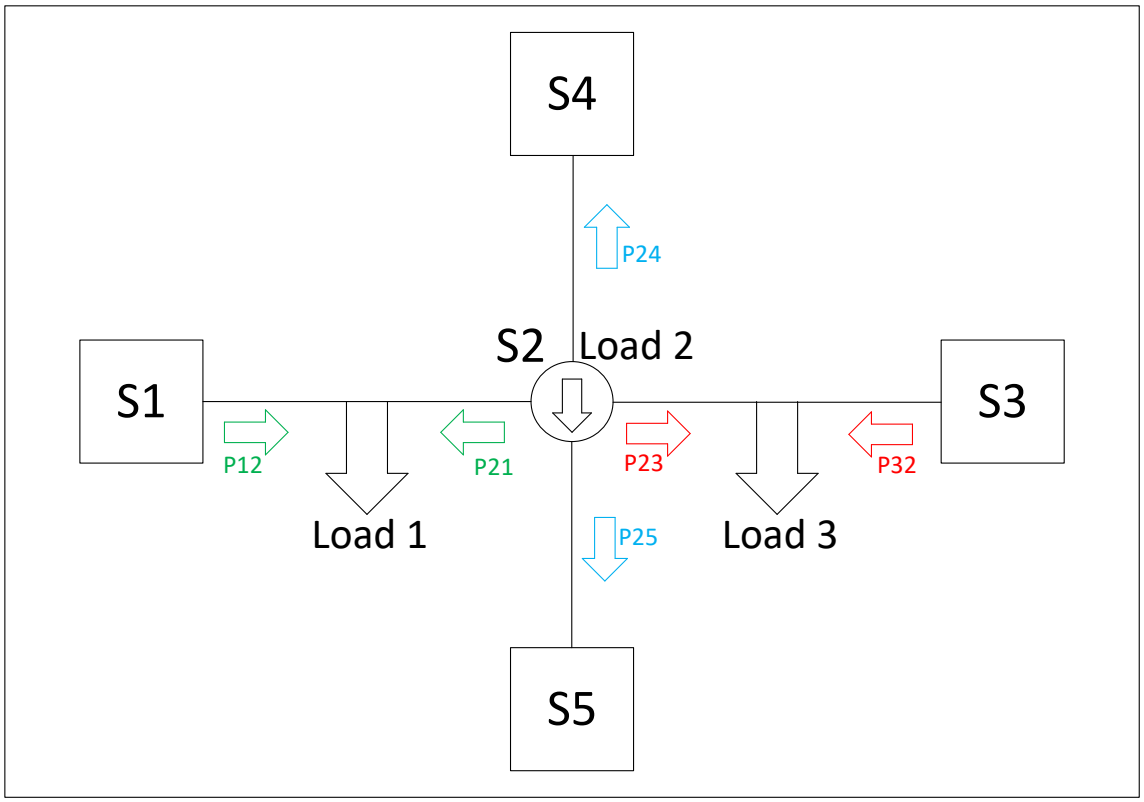

Figure 3.5: Visualization of power flow with a distribution station

The stations labeled as S1, S3, S4 and S5 are in this case four converter stations, whilst station S2 is a distribution station. To simplify the system modeling, only the interaction between substations 1 and 3 has been considered. Hence the contribution from substation 1 and 3 to feed the load towards the fourth and fifth substations, can be modeled as an equivalent load. This system can be modeled as a single line, between substation 1 and 3, with three loads according to equation 3.4, 3.5 and 3.6:

$$Load_1 = P_{12} + P_{21} \tag{3.4}$$

$$Load_2 = P_{24} + P_{25} \tag{3.5}$$

$$Load_3 = P_{23} + P_{32} \tag{3.6}$$

In the railway power system there may also be double tracks that the converter station is feeding individually. In figure 3.6 a visualization of a system with double tracks can be seen:

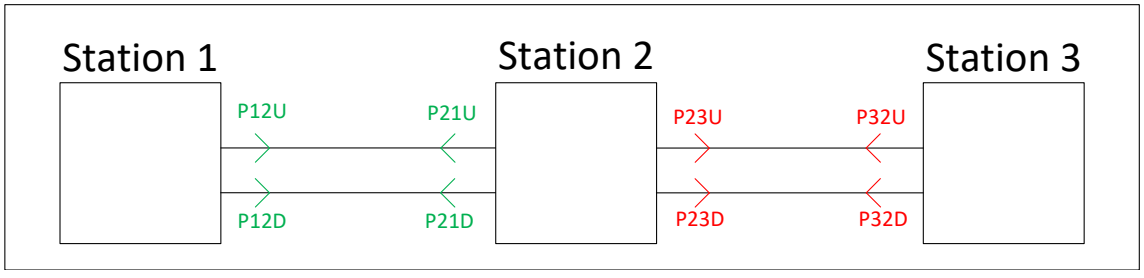

Figure 3.6: Visualization of a system feeding up- and down tracks

As told, for a system with double tracks it means that the substation needs to feed for both the up- and down track. However, in order to simplify the modeling and simulation in GAMS, the double track was modeled as a single track system. This was done by summing the total power from each substation at each direction:

$$P_{12} = P_{12U} + P_{12D} \tag{3.7}$$

$$P_{21} = P_{21U} + P_{21D} \tag{3.8}$$

$$P_{23} = P_{23U} + P_{23D} \tag{3.9}$$

$$P_{32} = P_{32U} + P_{32D} \tag{3.10}$$

Since the transmission line between the stations is in parallel, the equivalent impedance for a single track system is calculated accordingly:

$$Z_{12} = \frac{Z_{12U} \cdot Z_{12D}}{Z_{12U} + Z_{12D}} \tag{3.11}$$

$$Z_{23} = \frac{Z_{23U} \cdot Z_{23D}}{Z_{23U} + Z_{23D}} \tag{3.12}$$

Since the used data consists of the power output from each substation, the output data considers both the actual load but also compensation for the losses caused by the line impedance. In order to calculate a representative load profile, it is necessary to estimate the compensation of the line losses and subtract them from the power output.

3.3.2.2 Subtracting the added power to feed the line losses

By using data of the measured current of the station for the same time, the line losses is calculated as accordingly:

$$P_{losses} = R \cdot I^2 \tag{3.13}$$

The line losses in equation 3.13 consider the resistive losses by multiplying the squared measured current with the resistance of the known impedance of the transmission line. However, since the load is assumed to typically be in the middle and is fed from both stations, the equation should be properly applied to the system. Due to this, both substations current outputs have been considered in order to calculate the total line losses for a transmission line between two substations:

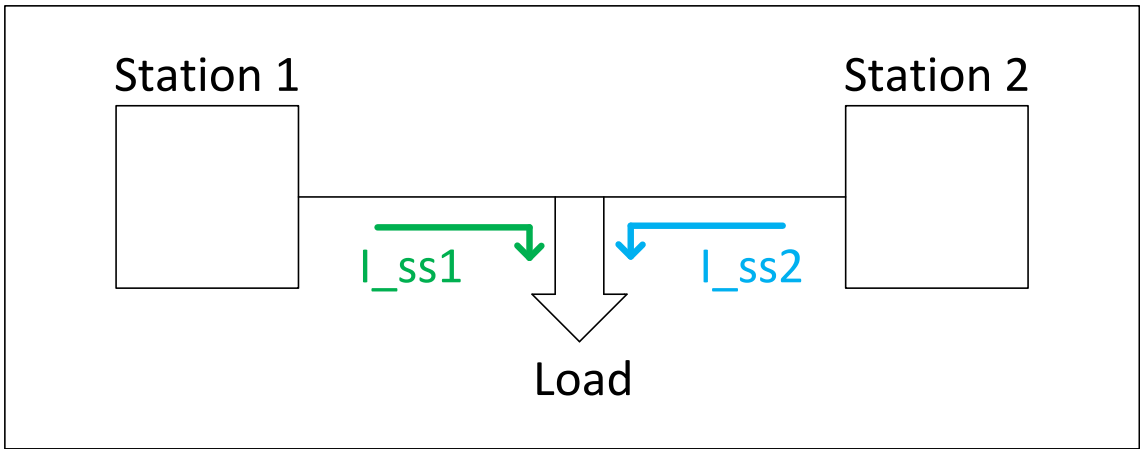

Figure 3.7: Visualization of current output of each substation

In figure 3.7, the current from both substations can be seen. Since both the stations contribute to feed the desired load, the line losses need to be calculated accordingly to where the current travels. Since the load is mostly assumed to be in the middle of the line, the resistive part of the impedance can be split into half. Assuming the impedance of the transmission line between station 1 and 2 is homogeneous, the line losses are calculated accordingly:

$$P_{loss,s1} = \frac{R}{2} \cdot I_{sub1}^2 \tag{3.14}$$

$$P_{loss,s2} = \frac{R}{2} \cdot I_{sub2}^2 \tag{3.15}$$

Using equation 3.14 and 3.15, the total line loss between station 1 and 2 has been calculated as:

$$P_{Loss,tot} = P_{loss,s1} + P_{loss,s2} \tag{3.16}$$

By subtracting the total power output from the stations with the calculated line losses, the representative load was calculated as:

$$P_{load} = P_{sum,stations} - P_{losses} \tag{3.17}$$

3.3.3 Power flow in power system

In order to optimize the system it needs to be able to simulate the active- and reactive power flow for each scenario. This was done by using the load flow equations which determine the active- and reactive power that is injected into a node and is dependent on the power that is sent from its neighboring nodes. The equations can be seen in equation 3.18 and 3.19, from [14]:

$$P_i = U_i \sum_j^n U_j \left(G_{ij} \cos(\theta_i - \theta_j) + B_{ij} \sin(\theta_i - \theta_j)\right) \tag{3.18}$$

$$Q_i = U_i \sum_j^n U_j \left(G_{ij} \sin(\theta_i - \theta_j) - B_{ij} \cos(\theta_i - \theta_j)\right) \tag{3.19}$$

The load flow equations allow the system to accommodate any load with the required active- and reactive power in order to reach an equilibrium point. In order to reach power balance for each node, equations showing the relation between generated-, absorbed- and injected power to a node can be seen in equation 3.20 and 3.21, from [6]:

$$0 = P_{G,i} - P_{D,i} - P_i \tag{3.20}$$

$$0 = Q_{G,i} - Q_{D,i} - Q_i \tag{3.21}$$

The parameters P_D and Q_D are the static load values that are determined by the load profile. P_G and Q_G in equation 3.20 and 3.21, respectively, is the generated active- and reactive power in each node. Since the system have multiple converters in each station, the active- and reactive power output of the substation is the summed power from the contribution of all converters. Equation 3.22 and 3.23 shows the summation of the active- and reactive power for each substation:

$$P_{G,ss}(s) = \sum_{m=1}^{C} P_{\mathrm{G,ss,sc}}(m, s) \tag{3.22}$$

$$Q_{G,ss}(s) = \sum_{m=1}^{C} Q_{\mathrm{G,ss,sc}}(m, s) \tag{3.23}$$

Equation 3.22 and 3.23 aggregate the active and reactive power, respectively, of each converter for each generator node so that the simulation will accurately keep track of the power sent from a node. In order to calculate the total system loss for each scenario, the active power injected into each node have been summed for the whole network. Equation 3.24 shows the summation in order to get the total system losses for each scenario:

$$P_{\mathrm{loss,tot}}(s) = \sum_{i=1}^{N} P_i(s) \tag{3.24}$$

Worth mentioning is that in equation 3.24, N in the summation stands for the number of nodes in the system. By using equation 3.18, 3.19, 3.20, 3.21, 3.22, 3.23 and 3.24, the load flows and voltage at each node of the system can be calculated. In order for the modeling to work properly, the system needs to have an objective function that it should optimize around. The objective function of the system is to minimize total system losses for each scenario, which can be seen in equation 3.25:

$$\min(J_{\mathrm{total}}) = \min(\sum_{s=1}^{S} P_{\mathrm{loss,tot}}(s)) \tag{3.25}$$

The minimization of the total system losses is the objective function that GAMS have used to optimize its given variables to find the most optimal values to achieve the objective. Through the optimization, the results from GAMS then shows the most optimal values on the converter parameters in order to minimize losses.

3.3.4 Modeling structure of a converter

In order to model a converter, the voltage and angle at the generator side needs to be determined. However, since the converter is fed by the national grid, a conversion between the 50 Hz and $16\frac{2}{3}$ Hz sides needs to be taken into account.
The phase angle shift between the motor- (50 Hz) and generator($16\frac{2}{3}$ Hz) sides can be seen in equation 3.26, in accordance with [9]:

$$\Psi = -\frac{1}{3}\arctan\left(\frac{X_{\mathrm{q,m}}^{\mathrm{ss,sc}} \cdot P_{\mathrm{G,ss,sc}}}{U_{50}^2 + X_{\mathrm{q,m}}^{\mathrm{ss,sc}} \cdot Q_{50}}\right) - \arctan\left(\frac{X_{\mathrm{q,g}}^{\mathrm{ss,sc}} \cdot P_{\mathrm{G,ss,sc}}}{U_{\mathrm{ss}}^2 + X_{\mathrm{q,g}}^{\mathrm{ss,sc}} Q_{\mathrm{G,ss,sc}}}\right) \tag{3.26}$$

As can be seen in equation 3.26, the phase angle shift is determined by the quadrature reactances of the specific converter. This means that for the optimization, when the quadrature reactances are floating variables, it will mainly optimize $X_{\mathrm{q,m}}$ and $X_{\mathrm{q,g}}$ to find the most suitable values on Ψ for the converters in order to minimize the system losses. The parameter Ψ is shared between the converters in the station, but it will differ between the stations.
The phase angle shift has then been used to determine the angle of the substations busbar, which depends on the no-load angle θ_0 on the $16\frac{2}{3}$ Hz side and the phase angle shift.
The conversion of the no-load angle between the 50- and $16\frac{2}{3}$ Hz sides can be seen in equation 3.27, and the calculation for the angle of the busbar can be seen in equation 3.28:

$$\theta_{0,16.7} = \frac{\theta_{0,50}}{3} \tag{3.27}$$

$$\theta_g = \theta_{0,16.7} + \Psi \tag{3.28}$$

As can be noted, there are two types of no-load angles, $\theta_{0,50}$ and $\theta_{0,16.7}$. They describe the no-load angle on the 50- and $16\frac{2}{3}$ Hz sides, which can be seen in figure 2.3. Due to the assumption that the national grid is very strong, the no-load angle on the 50 Hz side is not controllable, hence it is the no-load angle on the catenary side that this thesis has investigated. By being able to change the no-load angle, it is possible to change how much a converter contributes in order to provide for the load, but at the same time find the most optimal cooperation between substations in order to minimize losses.
In order to control the voltage at the substations busbars, an equation with a droop constant of the power output is used. The droop constant describes how sensitive the voltage at a generator node is to changes in the power output. The droop equation can be seen in equation 3.29:

$$U_{\mathrm{ss}}(\mathrm{s}) = U_{0,16.7}^{\mathrm{ss}}\left(1 - \left(K_{\mathrm{p,Q}}^{\mathrm{ss}} \cdot Q_{\mathrm{G,ss}}(\mathrm{s}) + K_{\mathrm{p,P}}^{\mathrm{ss}} \cdot P_{\mathrm{G,ss}}(s)\right)\right) \tag{3.29}$$

It can be noted in equation 3.29 that the busbar voltage at each generator is highly related to both the reactive- and active power. At the time of writing, the converters in the Swedish railway power system are only compensated with a droop on the reactive power. However, it is possible to compensate with a droop-factor on the

active power as well, hence this thesis has investigated the impact of potentially including it.
While it is important to maintain the voltage level at the substation busbar, it is also very necessary in the simulation that no converter is able to exceed its rated power limits. The relation between the total power output in relation to the converters capacity can be seen in equation 3.30, from [2]:

$$(S_{\text{rated,ss,sc}})^2 \geq (P_{\text{G,ss,sc}})^2 + (Q_{\text{G,ss,sc}})^2 \tag{3.30}$$

Equation 3.30 limits the possible amount of generated active and reactive power of any single converter to its total rated power. Worth mentioning is that the unit for the powers is in per unit, the conversion to per unit can be seen in Appendix A.1.
The scaling constant τ is calculated as a parameter using equation 3.31 taking the power of each converter and dividing it by the system base. This ensures that the simulation is able to proportionally distribute its production in relation to the converters size

$$\tau_{ss,sc} = \frac{S_{\text{rated,ss,sc}}}{S_{\text{rated,ss,Tot}}} \tag{3.31}$$

The last equations that involves the converters are the scaling equations 3.32 and 3.33 which allows the system to produce the appropriate amount of active and reactive power:

$$P_{G,ss,sc}(s) = \tau_{ss,sc} \cdot P_{G,i}(m,s) \tag{3.32}$$

$$Q_{G,ss,sc}(s) = \tau_{ss,sc} \cdot Q_{G,i}(m,s) \tag{3.33}$$

3.3.5 Constraints of model

In order for the model to properly optimize the system, the equations and variables need proper constraints so the system still reflects the reality. The main constraints in the system are set on the optimization variables, which have been given upper- and lower boundaries that they are able to be optimized within. The constraints on the optimized variables are based on what is theoretically possible and plausible for a converter to use in reality. The designated boundaries that have been given for each variable can later be seen in the results section.

4
Results

This chapter contains the results from the different power systems and the variable-optimization. The chapter also shows the cross-validation between the software which proves that the GAMS model is constructed mathematically correct.

4.1 Cross-validation between PowerFactory and GAMS

In order to validate that the GAMS-model is properly constructed, the settings of the power systems in GAMS and PowerFactory needs to be equal. The power system consists of five different substations, with two SFCs in each substation with various capacities. The system structure can be seen in figure 3.3 and the sizes of the converters in each substation can be seen in Table 4.1:

Table 4.1: Converter sizes of each substation for validation of GAMS model

Substation 1	SFC1: 10 MVA SFC2: 15 MVA
Substation 2	SFC1: 13 MVA SFC2: 10 MVA
Substation 3	SFC1: 10 MVA SFC2: 17 MVA
Substation 4	SFC1: 20 MVA SFC2: 10 MVA
Substation 5	SFC1: 5 MVA SFC2: 10 MVA

The line impedance used for the validation system is based on an AT-system with the impedance of $0.034 + \text{j}0.032\ \Omega/\text{km}$, and an initial impedance of $0.215 + j0.343\ \Omega$ at each end of the substation , according to [4]. The length between each substations can be seen in Table 4.2:

Table 4.2: Distances between substations

Station 1 - Station 2	120 km
Station 2 - Station 3	100 km
Station 3 - Station 4	40 km
Station 4 - Station 5	80 km

The distances between the substations can be seen in Table 4.2. For simplicity, this project assumes the load to be in the middle of the lines. Later the load will be estimated through real life data with different kinds of scenarios. But for validation, the load-values has been very roughly estimated to a single value. The given parameter values for the different loads can be seen in Table:

Table 4.3: Load values for validation of the GAMS model

$Load_1$	22, 061 MW
$Load_2$	13, 417 MW
$Load_3$	16, 263 MW
$Load_4$	13, 555 MW

It is worth mentioning that the parameter values on the loads do not represent the values that later will be estimated for the remaining simulations. Since the GAMS model was optimized with the objective of minimizing total system losses, there was a need to define constraints to the system variables, otherwise the solver would have found unrealistic solutions. The different constraints can be seen in Table 4.4:

Table 4.4: Limits on different parameters in GAMS

Level	$U_{\text{NoGenNode}}$ [p.u]	U_{GenNode} [p.u]	$U_{0,16.7}$ [p.u]	θ $\theta_{0,16.7}$ ψ [rad]	$P_{\text{G,ss,sc}}$ $Q_{\text{G,ss,sc}}$ [p.u]	$X_{\text{q,m}}$ $X_{\text{q,g}}$ [p.u]	$K_{\text{p,Q}}$ $K_{\text{p,P}}$ [p.u]
Max:	1.2	1.15	1.1	π	$\frac{S_{base}}{S_{rated}}$	$1.5\frac{S_{\text{base}}}{S_{\text{rated}}}$	$0.15\frac{S_{\text{base}}}{S_{\text{rated}}}$
Min:	0.6	0.8	0.9	$-\pi$	$-\frac{S_{\text{base}}}{S_{\text{rated}}}$	$0.4\frac{S_{\text{base}}}{S_{\text{rated}}}$	$-0.15\frac{S_{\text{base}}}{S_{\text{rated}}}$

In addition to the maximum and minimum limits, the variables were also given a starting value that is very close to zero. This value is mainly a precaution so that the system will not accidentally divide an equation with zero at first iteration, which could cause the system to not find an optimal solution. Although, due to licensing limitations, the GAMS model will not be simulated with a global solver. This means that the initial value might have an affect on the given system solution, hence the given starting value is very close to zero.
Through the GAMS solver, the system was able to optimize its given variables in order to minimize the total system losses. The given values for the variables for the validation system can be seen in Table 4.5:

Table 4.5: Optimized values for the variables from GAMS

Converter station:	$X_{q,m}$ [p.u]	$X_{q,g}$[p.u]	θ_0 [deg]	$K_{p,Q}$ [%]	$K_{p,P}$ [%]	U_{50} [kV]
Substation 1	1.00	0.60	-3.52	15.00	-10.53	16.5
Substation 2	0.40	0.40	-3.91	15.00	-5.93	16.5
Substation 3	0.40	0.66	-5.37	-13.21	-7.65	16.5
Substation 4	0.40	0.95	-5.68	8.59	-10.29	16.5
Substation 5	0.40	1.10	-6.86	15.00	-12.34	16.5

Inserting the values given from the GAMS simulation into the PowerFactory model, it was possible to do a static load flow simulation in order to verify that the system behaviours in GAMS were correct. The system results from both the GAMS model and PowerFactory can be seen in Table 4.6:

Table 4.6: Results from simulations in PowerFactory and GAMS

Position	**PowerFactory**	**GAMS**
Substation 1	PG_{SFC1}=4.91 MW PG_{SFC2}=7.365 MW QG_{SFC1}=0.416 MVAr QG_{SFC2}=0.624 MVAr $\theta = -20.8725°$	PG_{SFC1}=4.91 MW PG_{SFC2}=7.365 MW QG_{SFC1}=0.416 MVAr QG_{SFC2}=0.624 MVAr $\theta = -20.8724°$
Load 1	U = 1.039 p.u	U = 1.039 p.u
Substation 2	PG_{SFC1}=11.215 MW PG_{SFC2}=8.627 MW QG_{SFC1}=0.495 MVAr QG_{SFC2}=0.381 MVAr $\theta = -21.0745°$	PG_{SFC1}=11.215 MW PG_{SFC2}=8.627 MW QG_{SFC1}=0.495 MVAr QG_{SFC2}=0.380 MVAr $\theta = -21.0745°$
Load 2	U =1.097 p.u	U = 1.097 p.u
Substation 3	PG_{SFC1}=6.00 MW PG_{SFC2}=10.20 MW QG_{SFC1}=−0.035 MVAr QG_{SFC2}=-0.059 MVAr $\theta = -22.2024°$	PG_{SFC1}=6.00 MW PG_{SFC2}=10.20 MW QG_{SFC1}=-0.035MVAr QG_{SFC2}=−0.059 MVAr $\theta = -22.2023°$
Load 3	U = 1.121 p.u	U = 1.121 p.u
Substation 4	PG_{SFC1}=9.595 MW PG_{SFC2}=4.798 MW QG_{SFC1}=0.909 MVAr QG_{SFC2}=0.455 MVAr $\theta = -23.2922°$	PG_{SFC1}=9.595 MW PG_{SFC2}=4.798 MW QG_{SFC1}=0.909MVAr QG_{SFC2}=0.455 MVAr $\theta = -23.2922°$
Load 4	U = 1.106 p.u	U = 1.106 p.u
Substation 5	PG_{SFC1}=2.159 MW PG_{SFC2}=4.318 MW QG_{SFC1}=0.261 MVAr QG_{SFC2}=0.522 MVAr $\theta = -23.9818°$	PG_{SFC1}=2.159 MW PG_{SFC2}=4.318 MW QG_{SFC1}=0.261 MVAr QG_{SFC2}=0.522 MVAr $\theta = -23.9818°$

From the results it is possible to notice that the two systems behaves equally, which makes the validation of the GAMS model successful.

4.2 Load profiles and Y-buses

Since the AT- and BT-system are different it is needed to have one profile for each system. For both the AT- and the BT-system, the system voltage is 15 kV and the system apparent power is 15 MVA.

4.2.1 Representative AT-system

In order to create a representative load profile for the AT-system, a representative power network of an AT-system is needed. A schematic visualization of a representative AT-system that was used can be seen in:

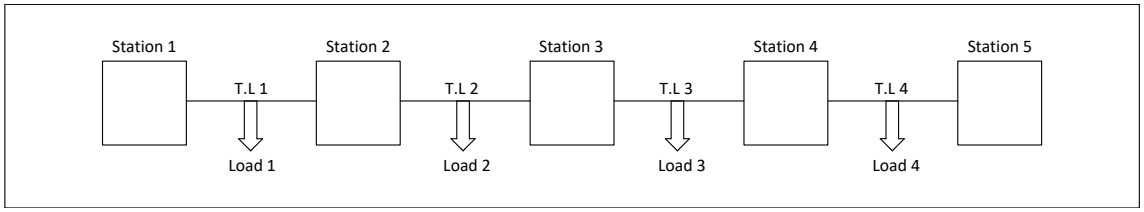

Figure 4.1: Visualization of the AT-system

In figure 4.1 the AT-system considers a single track between the substations, with a load that is assumed to be in the middle of the transmission line. The length and impedance of the different transmission lines used for the AT-system can be seen in Table 4.7:

Table 4.7: Data of transmission lines for the AT-system, impedance values taken from [4]

Transmission line	Length	Impedance
T.L 1	70	$0.034 + j0.032\ \Omega/km$
T.L 2	90	$0.034 + j0.032\ \Omega/km$
T.L 3	80	$0.034 + j0.032\ \Omega/km$
T.L 4	90	$0.034 + j0.032\ \Omega/km$

Since this thesis have used minute-data of the power- and current output of each substation for a full day, the load profile contains of 1440 different scenarios for each of the 17 nodes. Due to the size of the matrix, it is not possible to show the full load profile. However, in Appendix A.1, a table of the first 20 minutes of the load profile for the AT-system can be seen.
The Y-bus was created in regards to the numbers of nodes in the system. In order to have the possibility to have loads at different locations of the transmission line, the transmission lines between each stations have been designated three nodes. The distances have also been distributed equally, which means that the distance between

each nodes is $\frac{1}{4}$ of the total distance of the transmission line. A schematic diagram that visualizes the nodes in the network can be seen in figure 4.2:

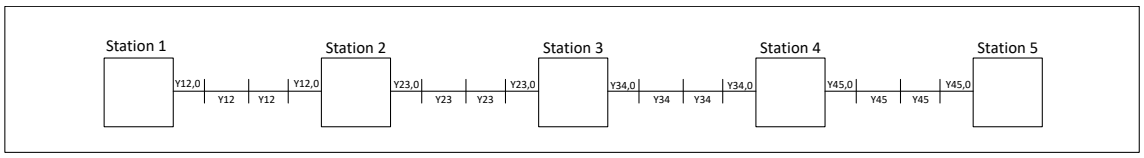

Figure 4.2: Schematic diagram of all the nodes of the AT-system

The different admittance values can be seen in figure 4.2 and as seen there are two types of admittance values between each station. For instance, between station 1 and 2 there is an admittance value labeled $Y_{12,0}$ and Y_{12}. This is due to the auto-transformers in the AT-system, where $Y_{12,0}$ is the line impedance plus the initial impedance which is supposed to represent the impedance of the first auto-transformer at each outage from the stations. The rest of the auto-transformer is then included in the line admittance in the Y_{12}. The impedance of the initial impedance is $0.215 + j0.343\Omega$.
The Y-bus of the total network for the AT-system can be seen in figure A.1 in Appendix.

4.2.2 Representative BT-system

In comparison to the AT-system, the representative network of the BT-system is a little bit trickier to model. A visualization of the chosen BT-system network can be seen in figure 4.3:

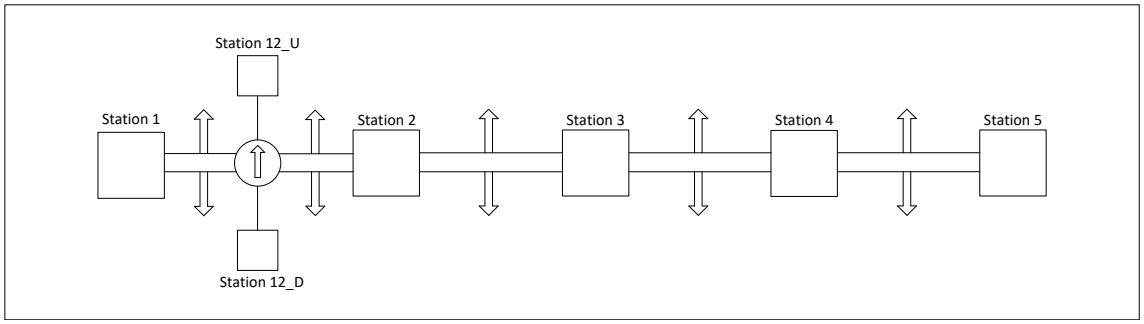

Figure 4.3: Power system of a representative BT-system

As can be seen in figure 4.3, the chosen route for the BT-system is fairly more difficult than the AT-system to model due to the double track and distribution station between station 1 and 2. For simplicity, the system was modeled as a single track system without a distribution system which can be seen in figure 4.4:

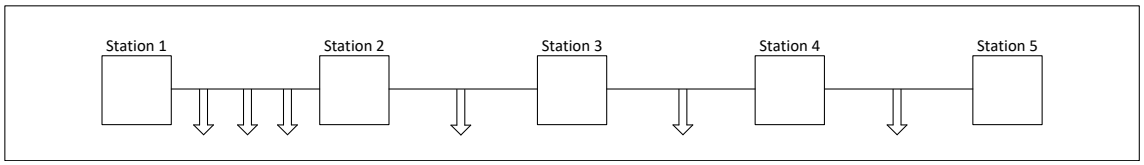

Figure 4.4: Visualization of an equivalent network to the representative BT-system

The configuration of the conversion between the representative model and the equivalent network model can be seen in chapter 3.3.2. The first 20 minutes of the load profile and the Y-bus for the BT-system can be seen in Table A.2 and figure A.2, respectively, in Appendix.
The values for the length and impedance of the transmission lines for the BT-system can be seen in Table 4.8:

Table 4.8: Length and impedance of the transmission lines for the BT-system

Transmission line	**Length [km]**	**Impedance [Ω/km]**
T.L 1	70	$0.21 + j0.2$
T.L 2	40	$0.21 + j0.2$
T.L 3	70	$0.13 + j0.16$
T.L 4	70	$0.21 + j0.2$

Worth mentioning is that the values given in Table 4.8 is for each track in the BT-system, which has a double track configuration.

4.3 Simulation of a representative system

This section contains the results of the simulations with the representative system with representative load and converter sizes. Due to a lot of plots from the simulation, all figures will not be shown in the results chapter. However, all the plots from the simulation for the AT- and BT-system in the representative case can be seen in A.4.
The order of simulation cases can be viewed in Table 4.9:

Table 4.9: Case numbering and its optimized variable(s)

Case	Optimized variable
1	All variables fixed
2	$X_{\mathrm{q,M}}$
3	$X_{\mathrm{q,G}}$
4	$K_{\mathrm{p,Q}}$
5	$K_{\mathrm{p,P}}$
6	$\theta_{0,16.7}$
7	$U_{0,16.7}$
8	$X_{\mathrm{q,M}}$ and $X_{\mathrm{q,G}}$
9	$K_{\mathrm{p,Q}}$ and $K_{\mathrm{p,P}}$
10	$\theta_{0,16.7}$ and $K_{\mathrm{p,Q}}$
11	$\theta_{0,16.7}$ and $K_{\mathrm{p,P}}$
12	$\theta_{0,16.7}$ and $U_{0,16.7}$
13	$\theta_{0,16.7}$, $U_{0,16.7}$, and $K_{\mathrm{p,Q}}$
14	Full optimization without $K_{\mathrm{p,P}}$
15	Full optimization with $K_{\mathrm{p,P}}$

4.3.1 Converter sizes of each substation

Due to the differences in the AT- and BT-system, the converter sizes in the substation are not the same. For the simulation with a representative system, the converter sizes for both the AT- and BT-system can be seen in Table 4.10:

Table 4.10: Converter sizes for the representative AT- and BT-systems

Substation:	AT-system [MVA]	BT-system [MVA]
1	$SFC_1 : 10$ $SFC_2 : 15$	$SFC_1 : 10$ $SFC_2 : 15$
2	$SFC_1 : 13$ $SFC_2 : 10$	$SFC_1 : 13$ $SFC_2 : 10$
3	$SFC_1 : 10$ $SFC_2 : 17$	$SFC_1 : 20$ $SFC_2 : 30$
4	$SFC_1 : 20$ $SFC_2 : 10$	$SFC_1 : 18$ $SFC_2 : 10$
5	$SFC_1 : 5$ $SFC_2 : 10$	$SFC_1 : 25$ $SFC_2 : 10$
Total system capacity	**120**	**161**

The converter sizes seen in Table 4.10 have been used throughout the simulations with the representative systems.

4.3.2 AT-system

This sub-chapter contains the results for the representative AT-system. The optimized values for each variable for different simulation cases can be seen in Table 4.11:

Table 4.11: Values on variables for different cases for the AT-system

Cases:	$X_{\mathbf{q,m}}[\mathbf{p.u}]$	$X_{\mathbf{q,g}}[\mathbf{p.u}]$	$\theta_{\mathbf{0,16.7}}[\mathbf{deg}]$	$K_{\mathbf{p,Q}}[\%]$	$K_{\mathbf{p,P}}[\%]$	$U_{\mathbf{0,16.7}}[\mathbf{kV}]$
All variables fixed (1)	SS1 : 0.49	SS1 : 0.53	SS1 : 0	SS1 : 4	SS1 : 0	SS1 : 16.5
	SS2 : 0.49	SS2 : 0.53	SS2 : 0	SS2 : 4	SS2 : 0	SS2 : 16.5
	SS3 : 0.49	SS3 : 0.53	SS3 : 0	SS3 : 4	SS3 : 0	SS3 : 16.5
	SS4 : 0.49	SS4 : 0.53	SS4 : 0	SS4 : 4	SS4 : 0	SS4 : 16.5
	SS5 : 0.49	SS5 : 0.53	SS5 : 0	SS5 : 4	SS5 : 0	SS5 : 16.5
All variables fixed except $X_{\mathbf{q,m}}$ (2)	SS1 : 0.40	SS1 : 0.53	SS1 : 0	SS1 : 4	SS1 : 0	SS1 : 16.5
	SS2 : 0.40	SS2 : 0.53	SS2 : 0	SS2 : 4	SS2 : 0	SS2 : 16.5
	SS3 : 0.40	SS3 : 0.53	SS3 : 0	SS3 : 4	SS3 : 0	SS3 : 16.5
	SS4 : 0.40	SS4 : 0.53	SS4 : 0	SS4 : 4	SS4 : 0	SS4 : 16.5
	SS5 : 0.74	SS5 : 0.53	SS5 : 0	SS5 : 4	SS5 : 0	SS5 : 16.5
All variables fixed except $X_{\mathbf{q,g}}$ (3)	SS1 : 0.49	SS1 : 0.40	SS1 : 0	SS1 : 4	SS1 : 0	SS1 : 16.5
	SS2 : 0.49	SS2 : 0.40	SS2 : 0	SS2 : 4	SS2 : 0	SS2 : 16.5
	SS3 : 0.49	SS3 : 0.40	SS3 : 0	SS3 : 4	SS3 : 0	SS3 : 16.5
	SS4 : 0.49	SS4 : 0.40	SS4 : 0	SS4 : 4	SS4 : 0	SS4 : 16.5
	SS5 : 0.49	SS5 : 0.54	SS5 : 0	SS5 : 4	SS5 : 0	SS5 : 16.5
All variables fixed except $K_{\mathbf{p,Q}}$ (4)	SS1 : 0.49	SS1 : 0.53	SS1 : 0	SS1 : 30.00	SS1 : 0	SS1 : 16.5
	SS2 : 0.49	SS2 : 0.53	SS2 : 0	SS2 : 8.11	SS2 : 0	SS2 : 16.5
	SS3 : 0.49	SS3 : 0.53	SS3 : 0	SS3 : 19.21	SS3 : 0	SS3 : 16.5
	SS4 : 0.49	SS4 : 0.53	SS4 : 0	SS4 : 18.17	SS4 : 0	SS4 : 16.5
	SS5 : 0.49	SS5 : 0.53	SS5 : 0	SS5 : 30.00	SS5 : 0	SS5 : 16.5
All variables fixed except $K_{\mathbf{p,P}}$ (5)	SS1 : 0.49	SS1 : 0.53	SS1 : 0	SS1 : 4	SS1 : −8.95	SS1 : 16.5
	SS2 : 0.49	SS2 : 0.53	SS2 : 0	SS2 : 4	SS2 : −5.66	SS2 : 16.5
	SS3 : 0.49	SS3 : 0.53	SS3 : 0	SS3 : 4	SS3 : −4.37	SS3 : 16.5
	SS4 : 0.49	SS4 : 0.53	SS4 : 0	SS4 : 4	SS4 : −6.73	SS4 : 16.5
	SS5 : 0.49	SS5 : 0.53	SS5 : 0	SS5 : 4	SS5 : −9.68	SS5 : 16.5
All variables fixed except $\theta_{\mathbf{0,16.7}}$ (6)	SS1 : 0.49	SS1 : 0.53	SS1 : 0.35	SS1 : 4	SS1 : 0	SS1 : 16.5
	SS2 : 0.49	SS2 : 0.53	SS2 : 1.43	SS2 : 4	SS2 : 0	SS2 : 16.5
	SS3 : 0.49	SS3 : 0.53	SS3 : 1.91	SS3 : 4	SS3 : 0	SS3 : 16.5
	SS4 : 0.49	SS4 : 0.53	SS4 : 1.50	SS4 : 4	SS4 : 0	SS4 : 16.5
	SS5 : 0.49	SS5 : 0.53	SS5 : −0.17	SS5 : 4	SS5 : 0	SS5 : 16.5
All variables fixed except $U_{\mathbf{0,16.7}}$ (7)	SS1 : 0.49	SS1 : 0.53	SS1 : 0	SS1 : 4	SS1 : 0	SS1 : 17.17
	SS2 : 0.49	SS2 : 0.53	SS2 : 0	SS2 : 4	SS2 : 0	SS2 : 17.16
	SS3 : 0.49	SS3 : 0.53	SS3 : 0	SS3 : 4	SS3 : 0	SS3 : 17.13
	SS4 : 0.49	SS4 : 0.53	SS4 : 0	SS4 : 4	SS4 : 0	SS4 : 17.13
	SS5 : 0.49	SS5 : 0.53	SS5 :: 0	SS5 : 4	SS5 : 0	SS5 : 17.14

The values on the variables for scenarios with optimization of more than one variable at the same time can be seen, as different combinations, in Table 4.12:

Table 4.12: Values on variables for different combinations for the AT-system

Cases:	$X_{\mathbf{q,m}}[\mathbf{p.u}]$	$X_{\mathbf{q,g}}[\mathbf{p.u}]$	$\theta_{\mathbf{0,16.7}}[\mathbf{deg}]$	$K_{\mathbf{p,Q}}[\%]$	$K_{\mathbf{p,P}}[\%]$	$U_{\mathbf{0,16.7}}[\mathbf{kV}]$
All variables fixed except $X_{\mathbf{q,m}}$ and $X_{\mathbf{q,m}}$ (8)	SS1 : 0.40	SS1 : 0.40	$SS1 : 0$	SS1 : 4	SS1 : 0	SS1 : 16.5
	SS2 : 0.40	SS2 : 0.40	SS2 : 0	SS2 : 4	SS2 : 0	SS2 : 16.5
	SS3 : 0.40	SS3 : 0.40	SS3 : 0	SS3 : 4	SS3 : 0	SS3 : 16.5
	SS4 : 0.40	SS4 : 0.40	SS4 : 0	SS4 : 4	SS4 : 0	SS4 : 16.5
	SS5 : 0.40	SS5 : 0.52	SS5 : 0	SS5 : 4	SS5 : 0	SS5 : 16.5
All variables fixed except $K_{\mathbf{p,Q}}$ and $K_{\mathbf{p,P}}$ (9)	SS1 : 0.49	SS1 : 0.53	SS1 : 0	SS1 : 24.97	SS1 : -11.25	SS1 : 16.5
	SS2 : 0.49	SS2 : 0.53	SS2 : 0	SS2 : 30.00	SS2 : -13.15	SS2 : 16.5
	SS3 : 0.49	SS3 : 0.53	SS3 : 0	SS3 : 30.00	SS3 : -12.46	SS3 : 16.5
	SS4 : 0.49	SS4 : 0.53	SS4 : 0	SS4 : 30.00	SS4 : -12.97	SS4 : 16.5
	SS5 : 0.49	SS5 : 0.53	SS5 : 0	SS5 : 25.39	SS5 : -8.29	SS5 : 16.5
All variables fixed except $\theta_{\mathbf{0,16.7}}$ and $K_{\mathbf{p,Q}}$ (10)	SS1 : 0.49	SS1 : 0.53	SS1 : 2.22	SS1 : 26.20	SS1 : 0	SS1 : 16.5
	SS2 : 0.49	SS2 : 0.53	SS2 : 3.30	SS2 : 7.94	SS2 : 0	SS2 : 16.5
	SS3 : 0.49	SS3 : 0.53	SS3 : 3.79	SS3 : 20.62	SS3 : 0	SS3 : 16.5
	SS4 : 0.49	SS4 : 0.53	SS4 : 3.39	SS4 : 24.11	SS4 : 0	SS4 : 16.5
	SS5 : 0.49	SS5 : 0.53	SS5 : 1.65	SS5 : 30.00	SS5 : 0	SS5 : 16.5
All variables fixed except $\theta_{\mathbf{0,16.7}}$ and $K_{\mathbf{p,P}}$ (11)	SS1 : 0.49	$SS1 : 0.53$	SS1 : 0.83	SS1 : 4	SS1 : -7.87	SS1 : 16.5
	SS2 : 0.49	SS2 : 0.53	SS2 : 1.92	SS2 : 4	SS2 : -5.17	SS2 : 16.5
	SS3 : 0.49	SS3 : 0.53	SS3 : 2.40	SS3 : 4	SS3 : -4.49	SS3 : 16.5
	SS4 : 0.49	SS4 : 0.53	SS4 : 2.00	SS4 : 4	SS4 : -5.45	SS4 : 16.5
	SS5 : 0.49	SS5 : 0.53	SS5 : 0.26	SS5 : 4	SS5 : -6.22	SS5 : 16.5
All variables fixed except $\theta_{\mathbf{0,16.7}}$ and $U_{\mathbf{0,16.7}}$ (12)	SS1 : 0.49	SS1 : 0.53	SS1 : 0.63	SS1 : 4	SS1 : 0	SS1 : 17.18
	SS2 : 0.49	$SS2 : 0.53$	SS2 : 1.74	SS2 : 4	SS2 : 0	SS2 : 17.19
	SS3 : 0.49	SS3 : 0.53	SS3 : 2.14	SS3 : 4	SS3 : 0	SS3 : 17.19
	SS4 : 0.49	SS4 : 0.53	SS4 : 1.82	SS4 : 4	SS4 : 0	SS4 : 17.18
	SS5 : 0.49	SS5 : 0.53	SS5 : 0.02	SS5 : 4	SS5 : 0	SS5 : 17.15
All variables fixed except $\theta_{\mathbf{0,16.7}}$, $K_{\mathbf{p,Q}}$, and $U_{\mathbf{0,16.7}}$ (13)	SS1 : 0.49	SS1 : 0.53	SS1 : -7.26	SS1 : 5.55	SS1 : 0	SS1 : 17.16
	SS2 : 0.49	SS2 : 0.53	SS2 : -6.18	SS2 : 6.96	SS2 : 0	SS2 : 17.16
	SS3 : 0.49	SS3 : 0.53	SS3 : -5.83	SS3 : 8.22	SS3 : 0	SS3 : 17.14
	SS4 : 0.49	SS4 : 0.53	SS4 : -6.11	SS4 : 18.46	SS4 : 0	SS4 : 17.15
	SS5 : 0.49	SS5 : 0.53	SS5 : -7.89	SS5 : 6.84	SS5 : 0	SS5 : 17.10
No variables fixed except $K_{\mathbf{p,P}}$ (14)	SS1 : 0.40	SS1 : 0.40	SS1 : 3.10	SS1 : 3.62	SS1 : 0	SS1 : 17.19
	SS2 : 0.40	SS2 : 0.40	SS2 : 3.92	SS2 : 4.67	SS2 : 0	SS2 : 17.19
	SS3 : 0.40	SS3 : 0.40	SS3 : 4.20	SS3 : 5.57	SS3 : 0	SS3 : 17.17
	SS4 : 0.40	SS4 : 0.40	SS4 : 3.99	SS4 : 14.14	SS4 : 0	SS4 : 17.18
	SS5 : 0.40	SS5 : 0.40	SS5 : 2.62	SS5 : 4.97	SS5 : 0	SS5 : 17.15
No fixed variables (15)	SS1 : 0.40	SS1 : 0.40	SS1 : 3.10	SS1 : 3.31	SS1 : -0.51	SS1 : 17.18
	SS2 : 0.40	SS2 : 0.40	SS2 : 3.94	SS2 : 7.32	SS2 : -0.58	SS2 : 17.19
	SS3 : 0.40	SS3 : 0.40	SS3 : 4.20	SS3 : 5.94	SS3 : -0.56	SS3 : 17.16
	SS4 : 0.40	SS4 : 0.40	SS4 : 3.99	SS4 : 16.66	SS4 : -2.03	SS4 : 17.15
	SS5 : 0.40	SS5 : 0.40	SS5 : 2.61	SS5 : 5.36	SS5 : 0.06	SS5 : 17.14

Since the objective function of the optimization is to minimize losses, it is fairly interesting to see how each scenario performs in that area. Since the load profile is set up minute-wise, the total losses for the day will be given if all the losses for each scenario is summed together. A bar chart showing the total active losses for a day can be seen in figure 4.5:

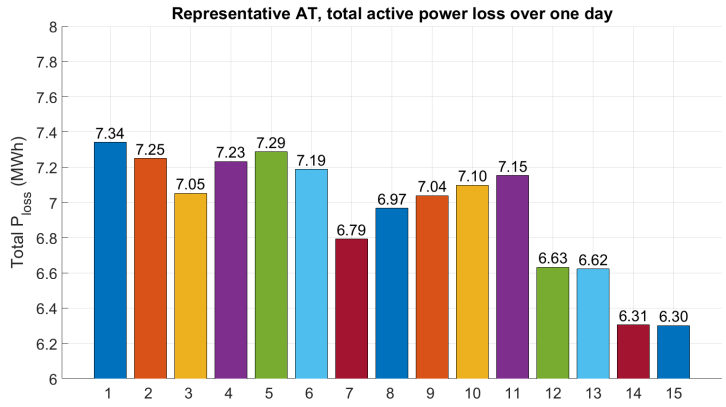

Figure 4.5: Losses for representative AT system

Figure 4.5 displays how each scenario impacts the total system losses, and also which parameters are more significant. It may also be easier to understand the significance of the decreasing losses by seeing the decrease as a percentage. The loss-graph is normalized by comparing it to the case with the highest system loss and can be seen in figure 4.6:

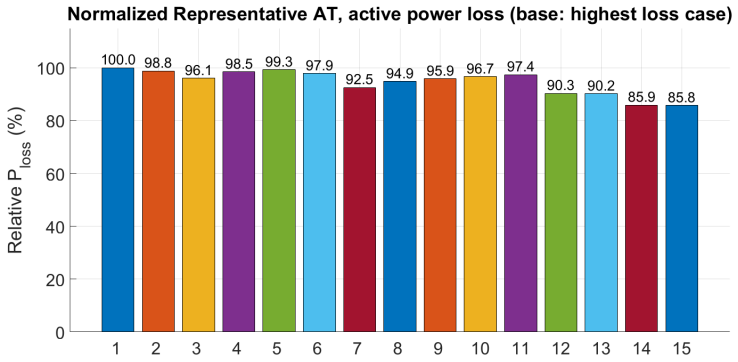

Figure 4.6: Normalized losses for representative AT system

Figure 4.5 and 4.6 shows how the efficiency of the representative AT system can be changed by optimizing different variables of the converters in different combinations. It is important to mention that optimizing with the objective function to minimize losses means that optimizing losses in the system could affect the voltage stability of the system. In order to further understand system voltage stability, the voltage profiles showing the maximum, average and minimum value of the voltage for each node can be seen in figures 4.7, 4.8, and 4.9:

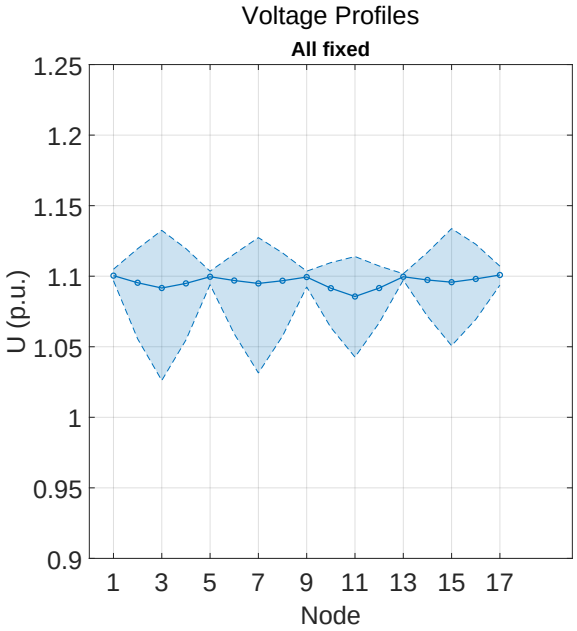

Figure 4.7: Voltage of system nodes for representative AT-system, all variables fixed

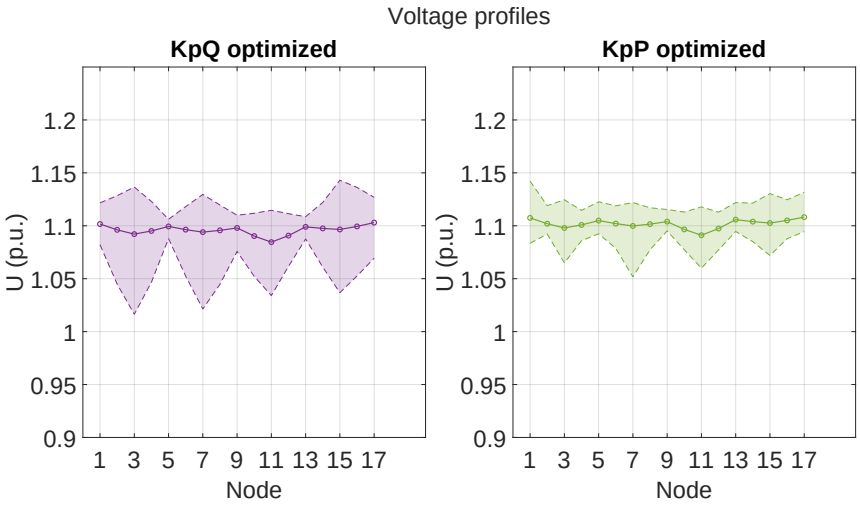

Figure 4.8: Voltage of system nodes for representative AT-system, $K_{\mathrm{p,Q}}$ optimized (left) and $K_{\mathrm{p,P}}$ optimized (right)

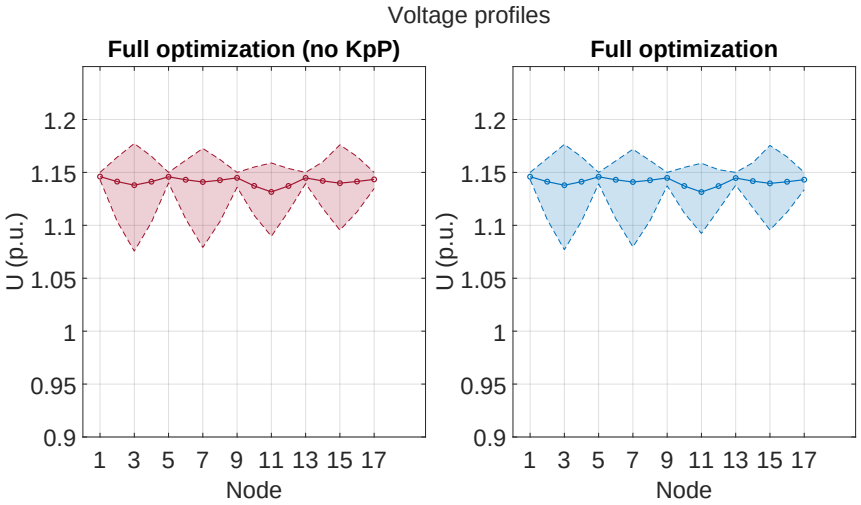

Figure 4.9: Voltage of system nodes for representative AT-system, full optimization except $K_{p,P}$ (left) and Full optimization with $K_{p,P}$ (right)

The figures of the voltage levels provide a picture of the systems voltage stability. The figures showing this production show the substation node and the generator that is producing. Since each substation has two converters the decimal in the figure shows which converter of the generator node is producing. For further clarification of the system behaviors, the production of active and reactive power for the all-fixed, $K_{p,P}$ only and full optimized cases can be seen in figure 4.10, 4.11, 4.12, and 4.13, respectively:

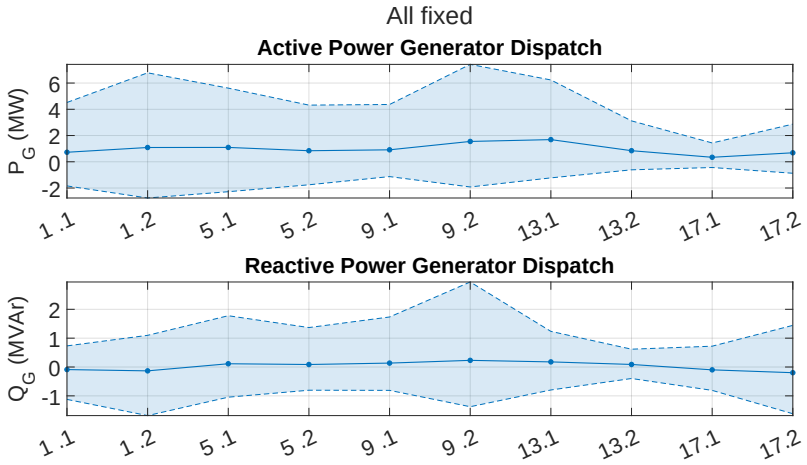

Figure 4.10: Power production of converter stations for representative AT-system, all fixed variables case

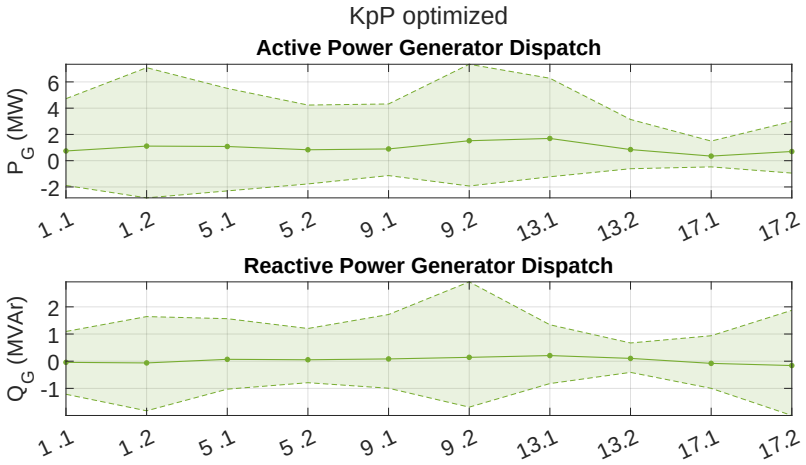

Figure 4.11: Active- and reactive power production of converter stations for representative AT-system, $K_{p,P}$ optimized case

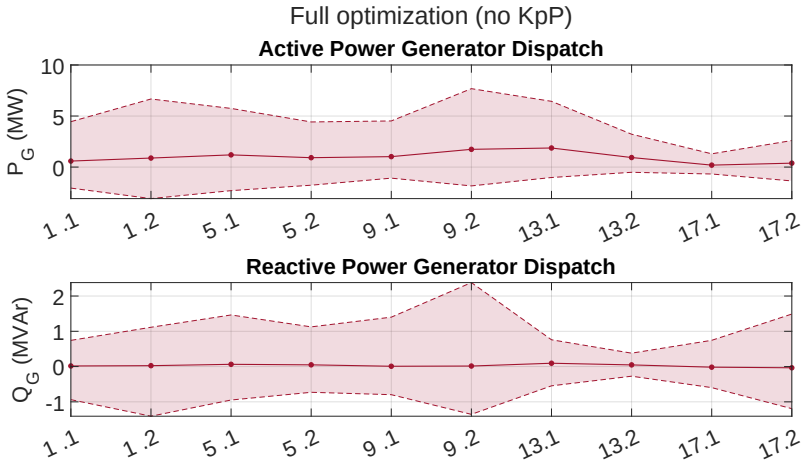

Figure 4.12: Active- and reactive power production of converter stations for the representative AT-system, full optimization without $K_{\mathrm{p,P}}$ case

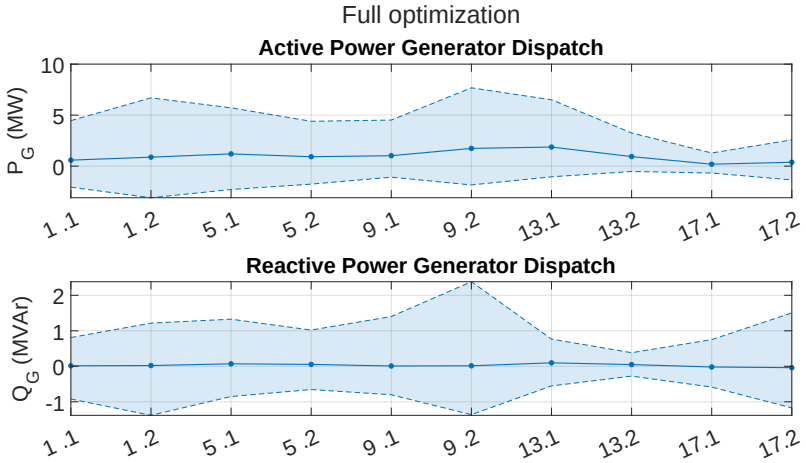

Figure 4.13: Active- and reactive power production of converter stations for the representative AT-system, full optimization case

4.3.3 BT-system

This sub-chapter shows the results of the representative BT-system.
The optimized values for different cases can be seen in Table 4.13 and 4.14:

Table 4.13: Values on variables for different cases for the BT-system

Cases:	$X_{\mathbf{q,m}}[\mathbf{p.u}]$	$X_{\mathbf{q,g}}[\mathbf{p.u}]$	$\theta_{0,16.7}[\mathbf{deg}]$	$K_{\mathbf{p,Q}}[\%]$	$K_{\mathbf{p,P}}[\%]$	$U_{0,16.7}[\mathbf{kV}]$
All variables fixed (1)	SS1 : 0.49	SS1 : 0.53	SS1 : 0	SS1 : 4	SS1 : 0	SS1 : 16.5
	SS2 : 0.49	SS2 : 0.53	SS2 : 0	SS2 : 4	SS2 : 0	SS2 : 16.5
	SS3 : 0.49	SS3 : 0.53	SS3 : 0	SS3 : 4	SS3 : 0	SS3 : 16.5
	SS4 : 0.49	SS4 : 0.53	SS4 : 0	SS4 : 4	SS4 : 0	SS4 : 16.5
	SS5 : 0.49	SS5 : 0.53	SS5 : 0	SS5 : 4	SS5 : 0	SS5 : 16.5
All variables fixed except $X_{\mathbf{q,m}}$ (2)	SS1 : 0.89	SS1 : 0.53	SS1 : 0	SS1 : 4	SS1 : 0	SS1 : 16.5
	SS2 : 0.40	SS2 : 0.53	SS2 : 0	SS2 : 4	SS2 : 0	SS2 : 16.5
	SS3 : 1.02	SS3 : 0.53	SS3 : 0	SS3 : 4	SS3 : 0	SS3 : 16.5
	SS4 : 0.40	SS4 : 0.53	SS4 : 0	SS4 : 4	SS4 : 0	SS4 : 16.5
	SS5 : 1.50	SS5 : 0.53	SS5 : 0	SS5 : 4	SS5 : 0	SS5 : 16.5
All variables fixed except $X_{\mathbf{q,g}}$ (3)	SS1 : 0.49	SS1 : 0.67	SS1 : 0	SS1 : 4	SS1 : 0	SS1 : 16.5
	SS2 : 0.49	SS2 : 0.40	SS2 : 0	SS2 : 4	SS2 : 0	SS2 : 16.5
	SS3 : 0.49	SS3 : 0.75	SS3 : 0	SS3 : 4	SS3 : 0	SS3 : 16.5
	SS4 : 0.49	SS4 : 0.40	SS4 : 0	SS4 : 4	SS4 : 0	SS4 : 16.5
	SS5 : 0.49	SS5 : 1.50	SS5 : 0	SS5 : 4	SS5 : 0	SS5 : 16.5
All variables fixed except $K_{\mathbf{p,Q}}$ (4)	SS1 : 0.49	SS1 : 0.53	SS1 : 0	SS1 : 30.0	SS1 : 0	SS1 : 16.5
	SS2 : 0.49	SS2 : 0.53	SS2 : 0	SS2 : 2.10	SS2 : 0	SS2 : 16.5
	SS3 : 0.49	SS3 : 0.53	SS3 : 0	SS3 : 30.0	SS3 : 0	SS3 : 16.5
	SS4 : 0.49	SS4 : 0.53	SS4 : 0	SS4 : −8.66	SS4 : 0	SS4 : 16.5
	SS5 : 0.49	SS5 : 0.53	SS5 : 0	SS5 : 30.0	SS5 : 0	SS5 : 16.5
All variables fixed except $K_{\mathbf{p,P}}$ (5)	SS1 : 0.49	SS1 : 0.53	SS1 : 0	SS1 : 4	SS1 : −9.22	SS1 : 16.5
	SS2 : 0.49	SS2 : 0.53	SS2 : 0	SS2 : 4	SS2 : −4.52	SS2 : 16.5
	SS3 : 0.49	SS3 : 0.53	SS3 : 0	SS3 : 4	SS3 : −9.82	SS3 : 16.5
	SS4 : 0.49	SS4 : 0.53	SS4 : 0	SS4 : 4	SS4 : −8.27	SS4 : 16.5
	SS5 : 0.49	SS5 : 0.53	SS5 : 0	SS5 : 4	SS5 : −16.20	SS5 : 16.5
All variables fixed except $\theta_{0,16.7}$ (6)	SS1 : 0.49	SS1 : 0.53	SS1 : 2.16	SS1 : 4	SS1 : 0	SS1 : 16.5
	SS2 : 0.49	SS2 : 0.53	SS2 : 7.22	SS2 : 4	SS2 : 0	SS2 : 16.5
	SS3 : 0.49	SS3 : 0.53	SS3 : 1.70	SS3 : 4	SS3 : 0	SS3 : 16.5
	SS4 : 0.49	SS4 : 0.53	SS4 : 4.46	SS4 : 4	SS4 : 0	SS4 : 16.5
	SS5 : 0.49	SS5 : 0.53	SS5 : −0.32	SS5 : 4	SS5 : 0	SS5 : 16.5
All variables fixed except $U_{0,16.7}$ (7)	SS1 : 0.49	SS1 : 0.53	SS1 : 0	SS1 : 4	SS1 : 0	SS1 : 17.18
	SS2 : 0.49	SS2 : 0.53	SS2 : 0	SS2 : 4	SS2 : 0	SS2 : 17.10
	SS3 : 0.49	SS3 : 0.53	SS3 : 0	SS3 : 4	SS3 : 0	SS3 : 17.21
	SS4 : 0.49	SS4 : 0.53	SS4 : 0	SS4 : 4	SS4 : 0	SS4 : 17.09
	SS5 : 0.49	SS5 : 0.53	SS5 : 0	SS5 : 4	SS5 : 0	SS5 : 17.19

Table 4.14: Values on combinations of variables for different cases for the BT-system

Cases:	$X_{\mathbf{q,m}}[\mathbf{p.u}]$	$X_{\mathbf{q,g}}[\mathbf{p.u}]$	$\theta_{\mathbf{0,16.7}}[\mathbf{deg}]$	$K_{\mathbf{p,Q}}[\%]$	$K_{\mathbf{p,P}}[\%]$	$U_{\mathbf{0,16.7}}[\mathbf{kV}]$
All variables fixed except $X_{\mathbf{q,m}}$ and $X_{\mathbf{q,m}}$ (8)	SS1 : 0.40	SS1 : 0.66	SS1 : 0	SS1 : 4	SS1 : 0	SS1 : 16.5
	SS2 : 0.40	SS2 : 0.40	SS2 : 0	SS2 : 4	SS2 : 0	SS2 : 16.5
	SS3 : 0.40	SS3 : 0.74	SS3 : 0	SS3 : 4	SS3 : 0	SS3 : 16.5
	SS4 : 0.40	SS4 : 0.40	SS4 : 0	SS4 : 4	SS4 : 0	SS4 : 16.5
	SS5 : 0.40	SS5 : 1.49	SS5 : 0	SS5 : 4	SS5 : 0	SS5 : 16.5
All variables fixed except $K_{\mathbf{p,Q}}$ and $K_{\mathbf{p,P}}$ (9)	SS1 : 0.49	SS1 : 0.53	SS1 : 0	SS1 : 12.07	SS1 : -10.30	SS1 : 16.5
	SS2 : 0.49	SS2 : 0.53	SS2 : 0	SS2 : 30.00	SS2 : -12.73	SS2 : 16.5
	SS3 : 0.49	SS3 : 0.53	SS3 : 0	SS3 : 30.00	SS3 : -10.71	SS3 : 16.5
	SS4 : 0.49	SS4 : 0.53	SS4 : 0	SS4 : 16.03	SS4 : -12.20	SS4 : 16.5
	SS5 : 0.49	SS5 : 0.53	SS5 : 0	SS5 : 17.04	SS5 : -13.76	SS5 : 16.5
All variables fixed except $\theta_{\mathbf{0,16.7}}$ and $K_{\mathbf{p,Q}}$ (10)	SS1 : 0.49	SS1 : 0.53	SS1 : -0.99	SS1 : 2.90	SS1 : 0	SS1 : 16.5
	SS2 : 0.49	SS2 : 0.53	SS2 : 4.24	SS2 : 14.56	SS2 : 0	SS2 : 16.5
	SS3 : 0.49	SS3 : 0.53	SS3 : -1.47	SS3 : -15.01	SS3 : 0	SS3 : 16.5
	SS4 : 0.49	SS4 : 0.53	SS4 : 1.21	SS4 : -5.94	SS4 : 0	SS4 : 16.5
	SS5 : 0.49	SS5 : 0.53	SS5 : -3.40	SS5 : 30.00	SS5 : 0	SS5 : 16.5
All variables fixed except $\theta_{\mathbf{0,16.7}}$ and $K_{\mathbf{p,P}}$ (11)	SS1 : 0.49	SS1 : 0.53	SS1 : 1.82	SS1 : 4	SS1 : -9.94	SS1 : 16.5
	SS2 : 0.49	SS2 : 0.53	SS2 : 7.05	SS2 : 4	SS2 : -6.42	SS2 : 16.5
	SS3 : 0.49	SS3 : 0.53	SS3 : 1.35	SS3 : 4	SS3 : -10.77	SS3 : 16.5
	SS4 : 0.49	SS4 : 0.53	SS4 : 4.27	SS4 : 4	SS4 : -8.51	SS4 : 16.5
	SS5 : 0.49	SS5 : 0.53	SS5 : -0.60	SS5 : 4	SS5 : -18.49	SS5 : 16.5
All variables fixed except $\theta_{\mathbf{0,16.7}}$ and $U_{\mathbf{0,16.7}}$ (12)	SS1 : 0.49	SS1 : 0.53	SS1 : 0.52	SS1 : 4	SS1 : 0	SS1 : 17.19
	SS2 : 0.49	SS2 : 0.53	SS2 : 4.91	SS2 : 4	SS2 : 0	SS2 : 17.13
	SS3 : 0.49	SS3 : 0.53	SS3 : 0.13	SS3 : 4	SS3 : 0	SS3 : 17.21
	SS4 : 0.49	SS4 : 0.53	SS4 : 2.68	SS4 : 4	SS4 : 0	SS4 : 17.19
	SS5 : 0.49	SS5 : 0.53	SS5 : -1.99	SS5 : 4	SS5 : 0	SS5 : 17.07
All variables fixed except $\theta_{\mathbf{0,16.7}}$, $K_{\mathbf{p,Q}}$, and $U_{\mathbf{0,16.7}}$ (13)	SS1 : 0.49	SS1 : 0.53	SS1 : -2.16	SS1 :~ 0	SS1 : 0	SS1 : 17.25
	SS2 : 0.49	SS2 : 0.53	SS2 : 2.54	SS2 :~ 0	SS2 : 0	SS2 : 17.25
	SS3 : 0.49	SS3 : 0.53	SS3 : -2.52	SS3 :~ 0	SS3 : 0	SS3 : 17.25
	SS4 : 0.49	SS4 : 0.53	SS4 : 0.08	SS4 : -1.61	SS4 : 0	SS4 : 17.18
	SS5 : 0.49	SS5 : 0.53	SS5 : -4.62	SS5 : 18.81	SS5 : 0	SS5 : 17.04
No variables fixed except $K_{\mathbf{p,P}}$ (14)	SS1 : 0.40	SS1 : 0.40	SS1 : 14.61	SS1 :~ 0	SS1 : 0	SS1 : 17.25
	SS2 : 0.40	SS2 : 0.40	SS2 : 18.26	SS2 :~ 0	SS2 : 0	SS2 : 17.25
	SS3 : 0.40	SS3 : 0.40	SS3 : 14.31	SS3 :~ 0	SS3 : 0	SS3 : 17.25
	SS4 : 0.40	SS4 : 0.40	SS4 : 16.35	SS4 : 1.04	SS4 : 0	SS4 : 17.24
	SS5 : 0.40	SS5 : 1.01	SS5 : 14.52	SS5 : -11.97	SS5 : 0	SS5 : 17.14
No fixed variables (15)	SS1 : 0.40	SS1 : 0.40	SS1: $-$ 0.61	SS1 :~ 0	SS1 :~ 0	SS1 : 17.25
	SS2 : 0.40	SS2 : 0.40	SS2 : 3.04	SS2 :~ 0	SS2 :~ 0	SS2 : 17.25
	SS3 : 0.40	SS3 : 0.40	SS3 : -0.92	SS3 :~ 0	SS3 :~ 0	SS3 : 17.25
	SS4 : 0.40	SS4 : 0.40	SS4 : 1.13	SS4 : 0.52	SS4 : -0.27	SS4 : 17.23
	SS5 : 0.40	SS5 : 0.87	SS5 : -1.14	SS5 : -0.78	SS5 : -3.83	SS5 : 17.11

Figure 4.14 and 4.15 shows the daily losses for the representative BT-system, whilst figure 4.16, 4.17 and 4.18 shows the voltage stability of the all fixed and full optimized cases. Lastly, figure 4.19, 4.20, and 4.21 shows the active- and reactive power production of the all fixed and full optimized cases:

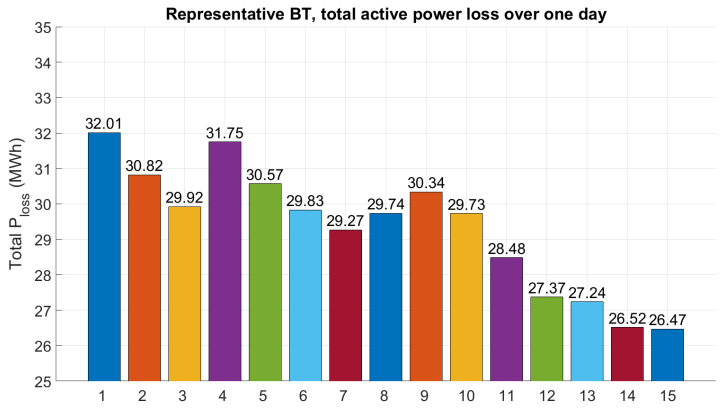

Figure 4.14: Losses for representative BT-system in [MWh]

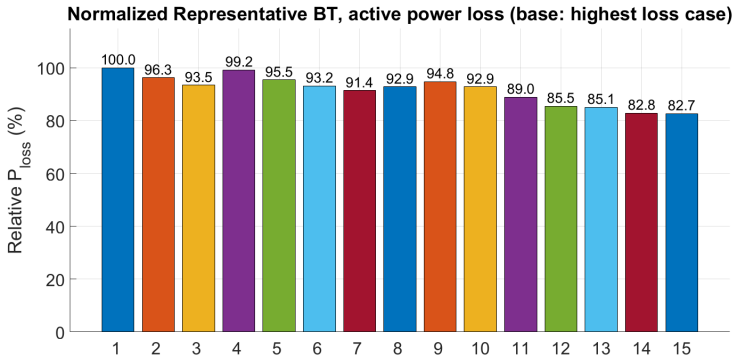

Figure 4.15: Normalized losses for representative BT-system

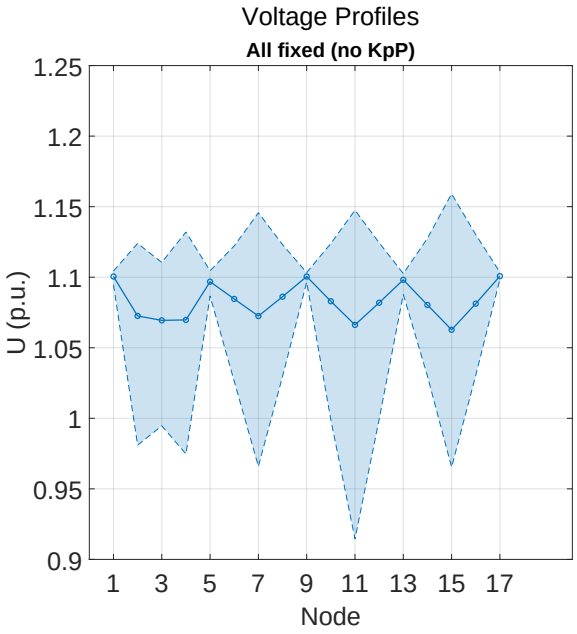

Figure 4.16: Voltage profiles for representative BT-system, all fixed case

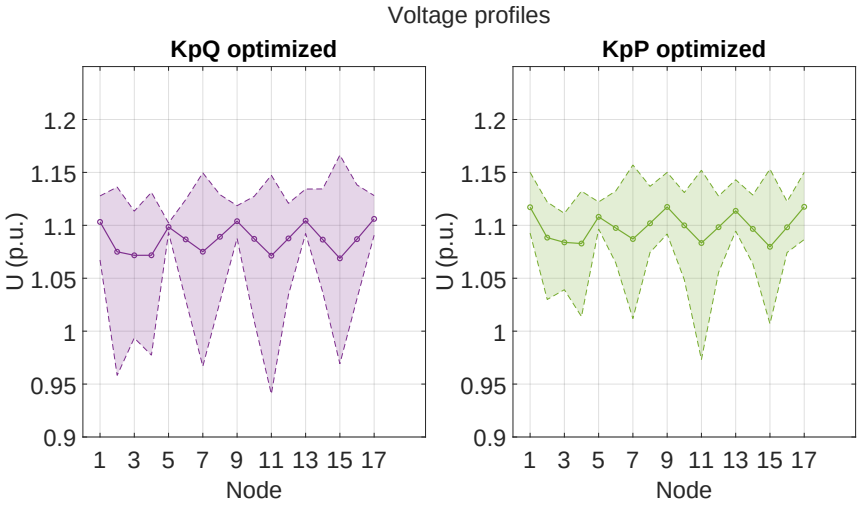

Figure 4.17: Voltage profile for the optimization of $K_{\mathrm{p,Q}}$ (left) and $K_{\mathrm{p,P}}$ (right) cases for the representative BT-system

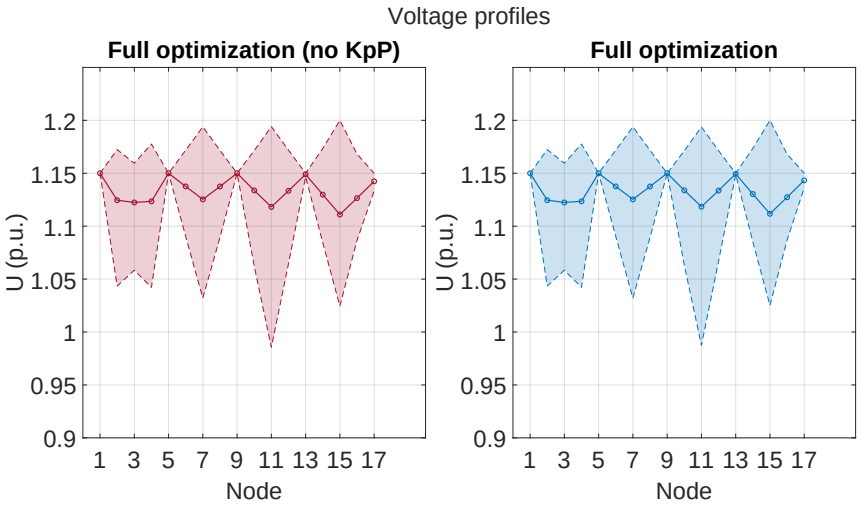

Figure 4.18: Voltage profiles for representative BT-system, full optimization without $K_{\mathrm{p,P}}$ (left), and full optimization with $K_{\mathrm{p,P}}$ (right)

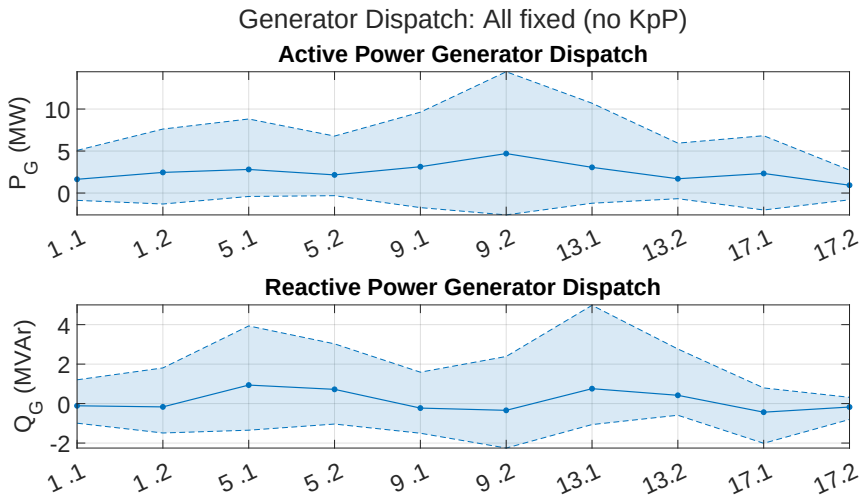

Figure 4.19: Power production for the all fixed case in the representative BT-system

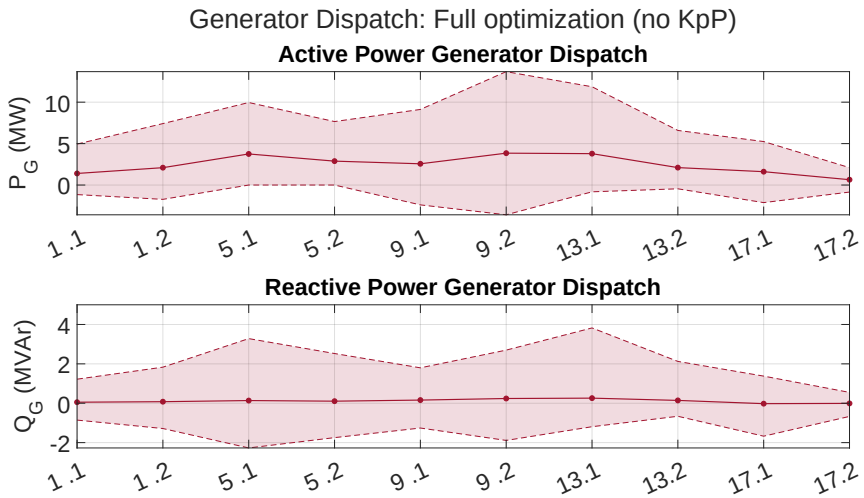

Figure 4.20: Power production for the full optimized without $K_{\mathrm{p,P}}$ case in the representative BT-system

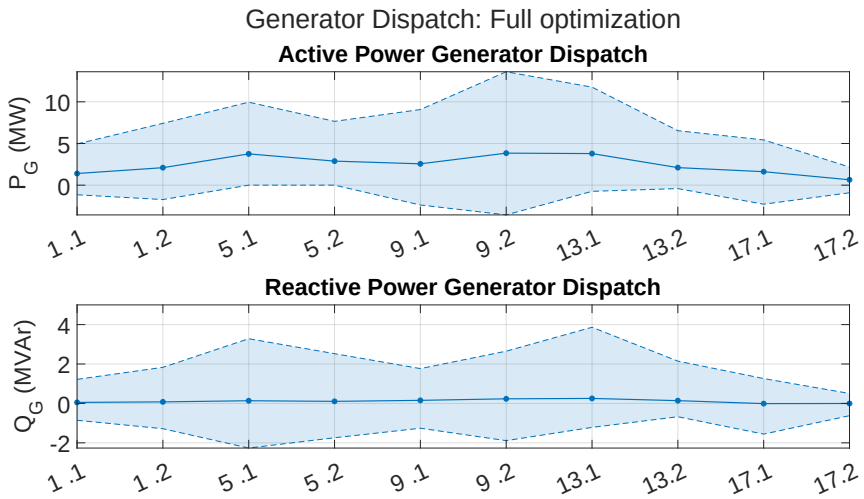

Figure 4.21: Power production for the full optimized with $K_{\mathrm{p,P}}$ case in the representative BT-system

4.4 Exaggerated converter sizes

The representative cases highlight the behavior of how losses can be reduced in realistic scenarios. In order to gain further insight into the variable optimization, simulations were performed for system with very large asymmetry on total power capacity between the substations. These simulations investigates the significance for both the AT-system and BT-system and to see how optimization changes when asymmetry increases for both systems. As before, due to a lot of plots from the simulation, all figures will not be shown in the results chapter. However, all figures of the exaggerated case for both the AT- and BT-system can be seen in A.5.

4.4.1 Converter sizes of each substation

The total system capacity was constructed with the same total system capacity as the representative case. This means that the system has the same amount of installed power, but it is distributed in a more non-uniform fashion to better understand how. The converter sizes for each system can be seen in Table 4.15:

Table 4.15: Exaggerated converter sizes for the AT- and BT-system

Substation:	**AT-system [MVA]**	**BT-system [MVA]**
1	SFC_1 : 6 SFC_2 : 5	SFC_1 : 12 SFC_2 : 12
2	SFC_1 : 27 SFC_2 : 18	SFC_1 : 25 SFC_2 : 15
3	SFC_1 : 5 SFC_2 : 5	SFC_1 : 10 SFC_2 : 13
4	SFC_1 : 23 SFC_2 : 19	SFC_1 : 25 SFC_2 : 32
5	SFC_1 : 5 SFC_2 : 7	SFC_1 : 9 SFC_2 : 8
Total system capacity:	**120**	**161**

As can be seen in Table 4.15, the total system capacity is the same as before but with a different distribution. For both exaggerated converter size cases, the majority of the installed power capacity is located in substation 2 and 4.

4.4.2 AT-system

This subsection contains results for the voltage, active- and reactive power flow as well as the total system losses for the exaggerated asymmetry in the AT-system. Table 4.16 and 4.17 show the optimized variables for the converters leading to loss reduction:

Table 4.16: Values on variables for different cases for exaggerated AT-system

Cases:	$X_{\mathbf{q,m}}[\mathbf{p.u}]$	$X_{\mathbf{q,g}}[\mathbf{p.u}]$	$\theta_{\mathbf{0,16.7}}[\mathbf{deg}]$	$K_{\mathbf{p,Q}}[\%]$	$K_{\mathbf{p,P}}[\%]$	$U_{\mathbf{0,16.7}}[\mathbf{kV}]$
All variables fixed (1)	SS1 : 0.49	SS1 : 0.53	SS1 : 0	SS1 : 4	SS1 : 0	SS1 : 16.5
	SS2 : 0.49	SS2 : 0.53	SS2 : 0	SS2 : 4	SS2 : 0	SS2 : 16.5
	SS3 : 0.49	SS3 : 0.53	SS3 : 0	SS3 : 4	SS3 : 0	SS3 : 16.5
	$SS4$: 0.49	SS4 : 0.53	SS4 : 0	SS4 : 4	SS4 : 0	SS4 : 16.5
	SS5 : 0.49	SS5 : 0.53	SS5 : 0	SS5 : 4	SS5 : 0	SS5 : 16.5
All variables fixed except $X_{\mathbf{q,m}}$ (2)	SS1 : 0.40	SS1 : 0.53	SS1 : 0	SS1 : 4	SS1 : 0	SS1 : 16.5
	SS2 : 1.50	SS2 : 0.53	SS2 : 0	SS2 : 4	SS2 : 0	SS2 : 16.5
	SS3 : 0.40	SS3 : 0.53	SS3 : 0	SS3 : 4	SS3 : 0	SS3 : 16.5
	SS4 : 1.50	SS4 : 0.53	SS4 : 0	SS4 : 4	SS4 : 0	SS4 : 16.5
	SS5 : 1.36	SS5 : 0.53	SS5 : 0	SS5 : 4	SS5 : 0	SS5 : 16.5
All variables fixed except $X_{\mathbf{q,g}}$ (3)	SS1 : 0.49	SS1 : 0.40	SS1 : 0	SS1 : 4	SS1 : 0	SS1 : 16.5
	SS2 : 0.49	SS2 : 1.03	SS2 : 0	SS2 : 4	SS2 : 0	SS2 : 16.5
	SS3 : 0.49	SS3 : 0.40	SS3 : 0	SS3 : 4	SS3 : 0	SS3 : 16.5
	SS4 : 0.49	SS4 : 1.01	SS4 : 0	SS4 : 4	SS4 : 0	SS4 : 16.5
	SS5 : 0.49	SS5 : 0.99	SS5 : 0	SS5 : 4	SS5 : 0	SS5 : 16.5
All variables fixed except $K_{\mathbf{p,Q}}$ (4)	SS1 : 0.49	SS1 : 0.53	SS1 : 0	SS1 : 19.44	SS1 : 0	SS1 : 16.5
	SS2 : 0.49	SS2 : 0.53	SS2 : 0	SS2 : 30.00	SS2 : 0	SS2 : 16.5
	SS3 : 0.49	SS3 : 0.53	SS3 : 0	SS3 : 12.93	SS3 : 0	SS3 : 16.5
	SS4 : 0.49	SS4 : 0.53	SS4 : 0	SS4 : 30.00	SS4 : 0	SS4 : 16.5
	SS5 : 0.49	SS5 : 0.53	SS5 : 0	SS5 : 30.00	SS5 : 0	SS5 : 16.5
All variables fixed except $K_{\mathbf{p,P}}$ (5)	SS1 : 0.49	SS1 : 0.53	SS1 : 0	SS1 : 4	SS1 : -4.50	SS1 : 16.5
	SS2 : 0.49	SS2 : 0.53	SS2 : 0	SS2 : 4	SS2 : -11.57	SS2 : 16.5
	SS3 : 0.49	SS3 : 0.53	SS3 : 0	SS3 : 4	SS3 : -1.20	SS3 : 16.5
	SS4 : 0.49	SS4 : 0.53	SS4 : 0	SS4 : 4	SS4 : -10.84	SS4 : 16.5
	SS5 : 0.49	SS5 : 0.53	SS5 : 0	SS5 : 4	SS5 : -10.69	SS5 : 16.5
All variables fixed except $\theta_{\mathbf{0,16.7}}$ (6)	SS1 : 0.49	SS1 : 0.53	SS1 : -4.04	SS1 : 4	SS1 : 0	SS1 : 16.5
	SS2 : 0.49	SS2 : 0.53	SS2 : -7.14	SS2 : 4	SS2 : 0	SS2 : 16.5
	SS3 : 0.49	SS3 : 0.53	SS3 : 1.19	SS3 : 4	SS3 : 0	SS3 : 16.5
	SS4 : 0.49	SS4 : 0.53	SS4 : -6.45	SS4 : 4	SS4 : 0	SS4 : 16.5
	SS5 : 0.49	SS5 : 0.53	SS5 : -6.83	SS5 : 4	SS5 : 0	SS5 : 16.5
All variables fixed except $U_{\mathbf{0,16.7}}$ (7)	SS1 : 0.49	SS1 : 0.53	SS1 : 0	SS1 : 4	SS1 : 0	SS1 : 17.07
	SS2 : 0.49	SS2 : 0.53	SS2 : 0	SS2 : 4	SS2 : 0	SS2 : 17.16
	SS3 : 0.49	SS3 : 0.53	SS3 : 0	SS3 : 4	SS3 : 0	SS3 : 17.03
	SS4 : 0.49	SS4 : 0.53	SS4 : 0	SS4 : 4	SS4 : 0	SS4 : 17.12
	SS5 : 0.49	SS5 : 0.53	SS5 : 0	SS5 : 4	SS5 : 0	SS5 : 17.10

Table 4.17: Values on combinations of variables for different cases for exaggerated AT-system

Cases:	$X_{\mathbf{q,m}}[\mathbf{p.u}]$	$X_{\mathbf{q,g}}[\mathbf{p.u}]$	$\theta_{\mathbf{0,16.7}}[\mathbf{deg}]$	$K_{\mathbf{p,Q}}[\%]$	$K_{\mathbf{p,P}}[\%]$	$U_{\mathbf{0,16.7}}[\mathbf{kV}]$
All variables fixed except $X_{\mathbf{q,m}}$ and $X_{\mathbf{q,g}}$ (8)	SS1 : 0.40	SS1 : 0.40	SS1 : 0	SS1 : 4	SS1 : 0	SS1 : 16.5
	SS2 : 0.40	SS2 : 1.00	$SS2 : 0$	SS2 : 4	SS2 : 0	SS2 : 16.5
	SS3 : 0.40	SS3 : 0.40	SS3 : 0	SS3 : 4	SS3 : 0	SS3 : 16.5
	SS4 : 0.40	SS4 : 0.98	SS4 : 0	SS4 : 4	SS4 : 0	SS4 : 16.5
	SS5 : 0.40	SS5 : 0.94	SS5 : 0	SS5 : 4	SS5 : 0	SS5 : 16.5
All variables fixed except $K_{\mathbf{p,Q}}$ and $K_{\mathbf{p,P}}$ (9)	SS1 : 0.49	SS1 : 0.53	SS1 : 0	SS1 : 24.97	SS1 : -11.25	SS1 : 16.5
	SS2 : 0.49	SS2 : 0.53	SS2 : 0	SS2 : 30.00	SS2 : -13.15	SS2 : 16.5
	SS3 : 0.49	SS3 : 0.53	SS3 : 0	SS3 : 30.00	SS3 : -12.46	SS3 : 16.5
	SS4 : 0.49	SS4 : 0.53	SS4 : 0	SS4 : 30.00	SS4 : -12.97	SS4 : 16.5
	SS5 : 0.49	SS5 : 0.53	SS5 : 0	SS5 : 25.39	SS5 : -8.29	SS5 : 16.5
All variables fixed except $\theta_{\mathbf{0,16.7}}$ and $K_{\mathbf{p,Q}}$ (10)	SS1 : 0.49	SS1 : 0.53	SS1 : 9.54	SS1 : -30.00	SS1 : 0	SS1 : 16.5
	SS2 : 0.49	SS2 : 0.53	SS2 : 6.11	SS2 : -28.16	SS2 : 0	SS2 : 16.5
	SS3 : 0.49	SS3 : 0.53	SS3 : 14.58	SS3 : 16.76	SS3 : 0	SS3 : 16.5
	SS4 : 0.49	SS4 : 0.53	SS4 : 6.92	SS4 : 30.00	SS4 : 0	SS4 : 16.5
	SS5 : 0.49	SS5 : 0.53	SS5 : 6.48	SS5 : 30.00	SS5 : 0	SS5 : 16.5
All variables fixed except $\theta_{\mathbf{0,16.7}}$ and $K_{\mathbf{p,P}}$ (11)	SS1 : 0.49	SS1 : 0.53	SS1 : 7.87	SS1 : 4	SS1 : -4.51	SS1 : 16.5
	SS2 : 0.49	SS2 : 0.53	SS2 : 4.81	SS2 : 4	SS2 : -12.26	SS2 : 16.5
	SS3 : 0.49	SS3 : 0.53	SS3 : 13.13	SS3 : 4	SS3 : -2.62	SS3 : 16.5
	SS4 : 0.49	SS4 : 0.53	SS4 : 5.49	SS4 : 4	SS4 : -10.34	SS4 : 16.5
	SS5 : 0.49	SS5 : 0.53	SS5 : 5.13	SS5 : 4	SS5 : -7.93	SS5 : 16.5
All variables fixed except $\theta_{\mathbf{0,16.7}}$ and $U_{\mathbf{0,16.7}}$ (12)	SS1 : 0.49	SS1 : 0.53	SS1 : 1.00	SS1 : 4	SS1 : 0	SS1 : 17.08
	SS2 : 0.49	SS2 : 0.53	SS2 : -1.92	SS2 : 4	SS2 : 0	SS2 : 17.07
	SS3 : 0.49	SS3 : 0.53	SS3 : 5.50	SS3 : 4	SS3 : 0	SS3 : 17.04
	SS4 : 0.49	SS4 : 0.53	SS4 : -1.26	SS4 : 4	SS4 : 0	SS4 : 17.07
	SS5 : 0.49	SS5 : 0.53	SS5 : -1.62	SS5 : 4	SS5 : 0	SS5 : 17.08
All variables fixed except $\theta_{\mathbf{0,16.7}}$, $K_{\mathbf{p,Q}}$, and $U_{\mathbf{0,16.7}}$ (13)	SS1 : 0.49	SS1 : 0.53	SS1 : 3.51	SS1 : 4.62	SS1 : 0	SS1 : 17.07
	SS2 : 0.49	SS2 : 0.53	SS2 : 0.66	SS2 : 30.00	SS2 : 0	SS2 : 17.09
	SS3 : 0.49	SS3 : 0.53	SS3 : 8.34	SS3 : 4.44	SS3 : 0	SS3 : 17.06
	SS4 : 0.49	SS4 : 0.53	SS4 : 1.31	SS4 : 30.00	SS4 : 0	SS4 : 17.07
	SS5 : 0.49	SS5 : 0.53	SS5 : 0.74	SS5 : 8.99	SS5 : 0	SS5 : 17.02
No variables fixed except $K_{\mathbf{p,P}}$ (14)	SS1 : 0.40	SS1 : 0.40	SS1 : -2.93	SS1 : 4.26	SS1 : 0	SS1 : 17.09
	SS2 : 0.40	SS2 : 0.40	SS2 : -5.09	SS2 : 30.00	SS2 : 0	SS2 : 17.11
	SS3 : 0.40	SS3 : 0.40	SS3 : 0.76	SS3 : 3.91	SS3 : 0	SS3 : 17.08
	SS4 : 0.40	SS4 : 0.54	SS4 : -4.18	SS4 : 30.00	SS4 : 0	SS4 : 17.10
	SS5 : 0.40	SS5 : 0.40	SS5 : -5.05	SS5 : 8.43	SS5 : 0	SS5 : 17.05
No fixed variables (15)	SS1 : 0.40	SS1 : 0.40	SS1 : 11.09	SS1 : 6.64	SS1 : -0.60	SS1 : 17.05
	SS2 : 0.40	SS2 : 0.40	SS2 : 8.91	SS2 : 30.00	SS2 : -4.18	SS2 : 17.04
	SS3 : 0.40	SS3 : 0.40	SS3 : 14.84	SS3 : 6.26	SS3 : -0.12	SS3 : 17.06
	SS4 : 0.40	SS4 : 0.50	SS4 : 9.73	SS4 : 30.00	SS4 : -5.21	SS4 : 17.02
	SS5 : 0.40	SS5 : 0.40	SS5 : 8.97	SS5 : 9.98	SS5 : 0.33	SS5 : 17.03

The total system losses for the same cases as shown in Table 4.16 and 4.17, can be seen in figure 4.22 and 4.23:

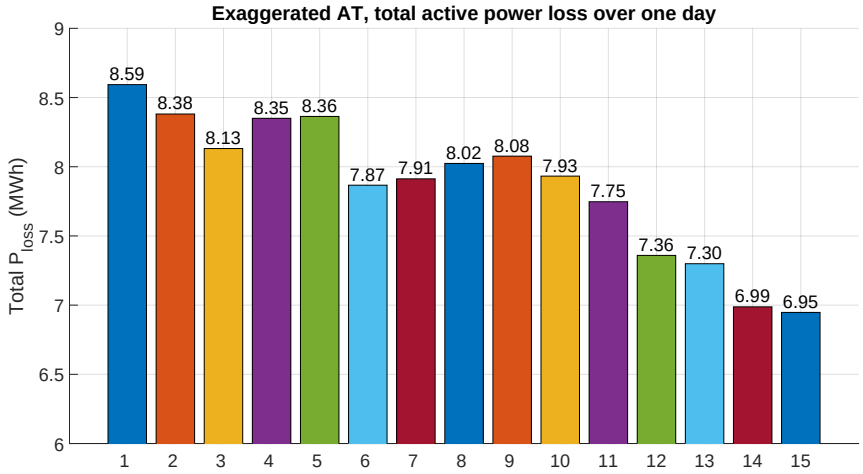

Figure 4.22: Total system losses for each case of the AT system with exaggerated converter sizes, in [MWh]

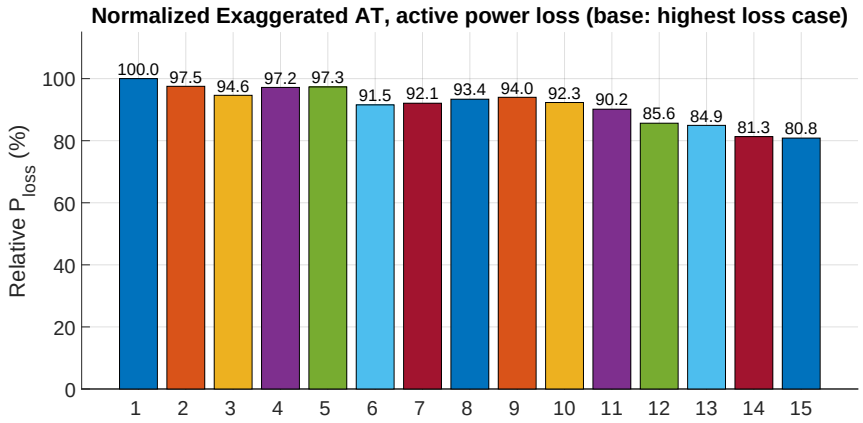

Figure 4.23: Normalized values of the total system losses for each case of the AT system with exaggerated converter sizes

Figure 4.24, 4.25, and 4.26 shows the voltage profiles of the exaggerated converter cases. The figures highlights the stability of the system and how it is affected by the loss minimization of the system:

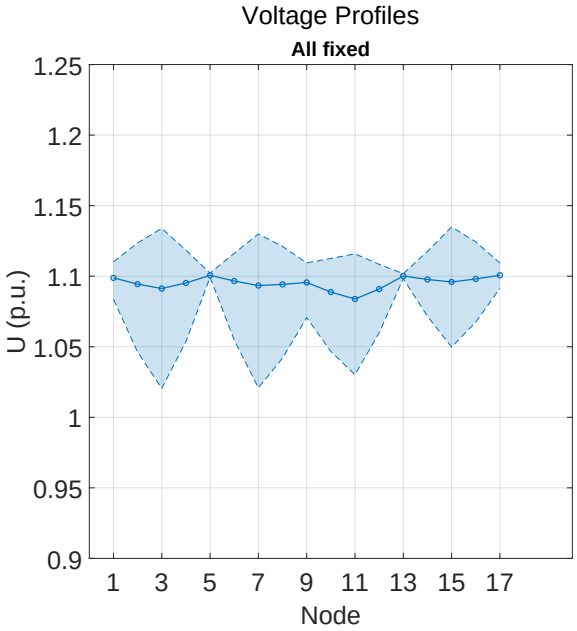

Figure 4.24: Voltage profile for the all-fixed case in the exaggerated AT-system

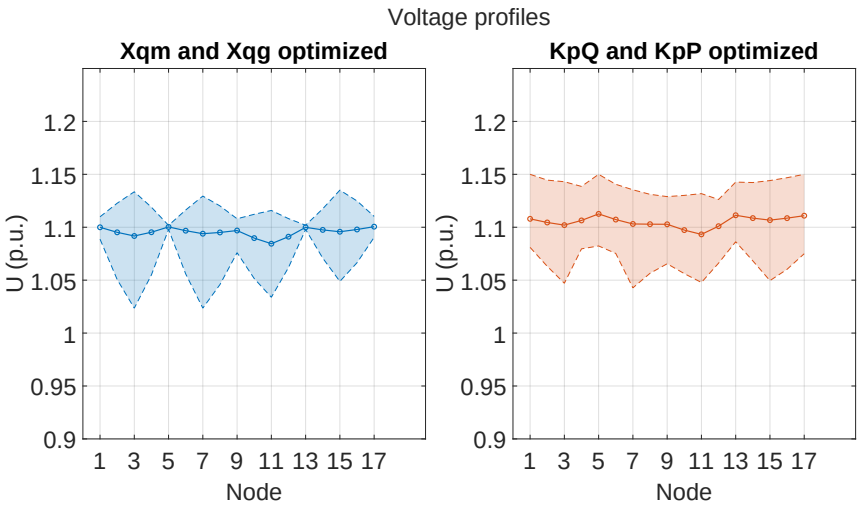

Figure 4.25: Voltage profiles for the exaggerated AT-system, $X_{\mathrm{q,m}}$ & $X_{\mathrm{q,g}}$ and $K_{\mathrm{p,Q}}$ & $K_{\mathrm{p,P}}$ cases

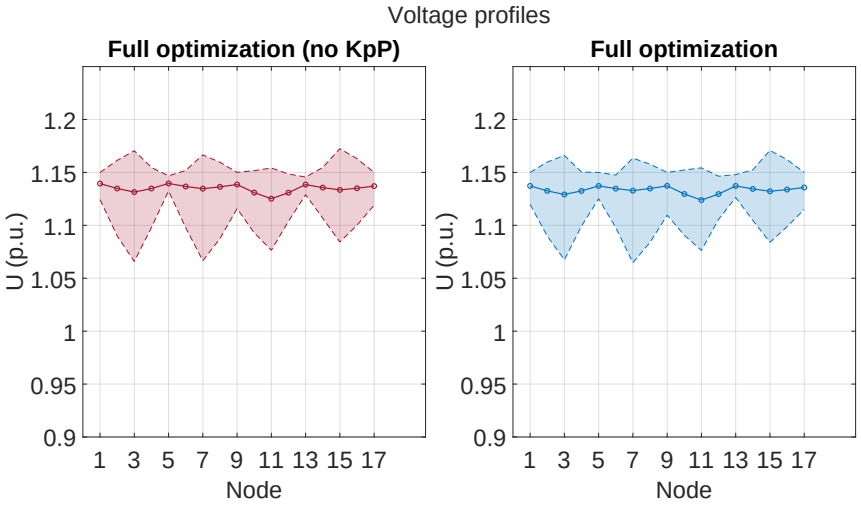

Figure 4.26: Voltage profiles for the exaggerated AT-system, full optimization with- and without $K_{\mathrm{p,P}}$

Figure 4.27, 4.28, and 4.29 shows the production of active- and reactive power for the converters in the exaggerated AT-system:

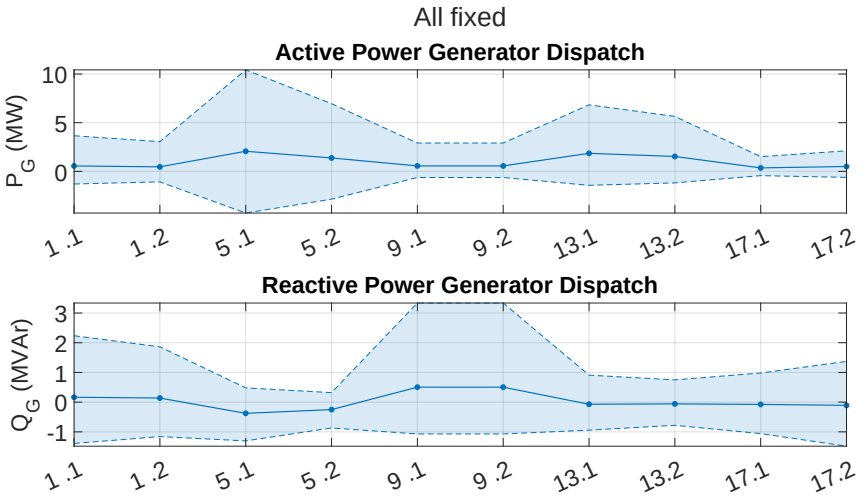

Figure 4.27: Active- and reactive power production for the exaggerated AT-system, all-fixed case

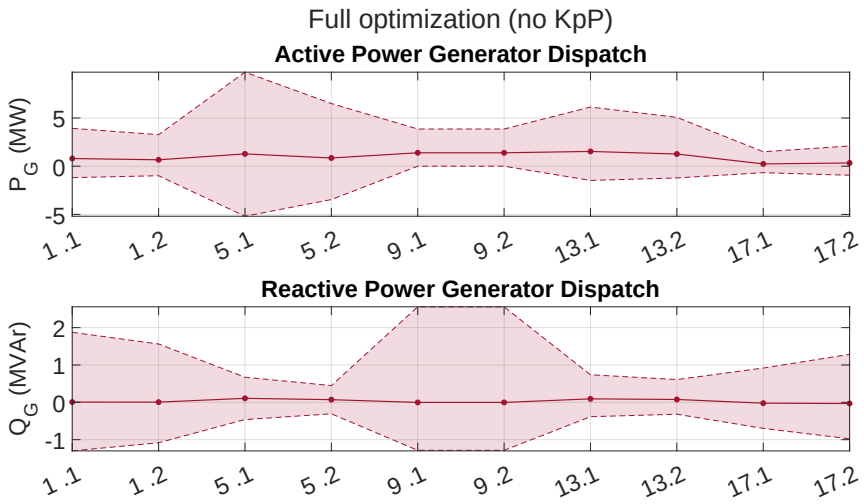

Figure 4.28: Active- and reactive power production for the exaggerated AT-system, full optimized without $K_{\mathrm{p,P}}$ case

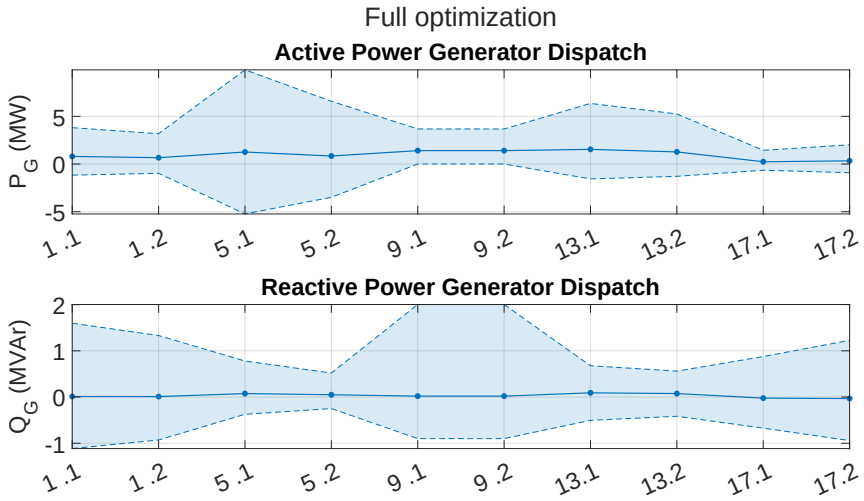

Figure 4.29: Active- and reactive power production for the full optimization case in the exaggerated AT-system

4.4.3 BT-system

This section shows the results associated with the simulations of the exaggerated BT-system. The results of the variables for different cases can be seen in Table 4.18 and 4.19:

Table 4.18: Values on variables for different cases for the exaggerated BT-system

Cases:	$X_{\mathbf{q,m}}[\mathbf{p.u}]$	$X_{\mathbf{q,g}}[\mathbf{p.u}]$	$\theta_{\mathbf{0,16.7}}[\mathbf{deg}]$	$K_{\mathbf{p,Q}}[\%]$	$K_{\mathbf{p,P}}[\%]$	$U_{\mathbf{0,16.7}}[\mathbf{kV}]$
All variables fixed (1)	SS1 : 0.49	SS1 : 0.53	SS1 : 0	SS1 : 4	SS1 : 0	SS1 : 16.5
	SS2 : 0.49	SS2 : 0.53	SS2 : 0	SS2 : 4	SS2 : 0	SS2 : 16.5
	SS3 : 0.49	SS3 : 0.53	SS3 : 0	SS3 : 4	SS3 : 0	SS3 : 16.5
	SS4 : 0.49	SS4 : 0.53	SS4 : 0	SS4 : 4	SS4 : 0	SS4 : 16.5
	SS5 : 0.49	SS5 : 0.53	SS5 : 0	SS5 : 4	SS5 : 0	SS5 : 16.5
All variables fixed except $X_{\mathbf{q,m}}$ (2)	SS1 : 0.74	SS1 : 0.53	SS1 : 0	SS1 : 4	SS1 : 0	SS1 : 16.5
	SS2 : 0.58	SS2 : 0.53	SS2 : 0	SS2 : 4	SS2 : 0	SS2 : 16.5
	SS3 : 0.40	SS3 : 0.53	SS3 : 0	SS3 : 4	SS3 : 0	SS3 : 16.5
	SS4 : 1.50	SS4 : 0.53	SS4 : 0	SS4 : 4	SS4 : 0	SS4 : 16.5
	SS5 : 0.85	SS5 : 0.53	SS5 : 0	SS5 : 4	SS5 : 0	SS5 : 16.5
All variables fixed except $X_{\mathbf{q,g}}$ (3)	SS1 : 0.49	SS1 : 0.60	SS1 : 0	SS1 : 4	SS1 : 0	SS1 : 16.5
	SS2 : 0.49	SS2 : 0.55	SS2 : 0	SS2 : 4	SS2 : 0	SS2 : 16.5
	SS3 : 0.49	SS3 : 0.40	SS3 : 0	SS3 : 4	SS3 : 0	SS3 : 16.5
	SS4 : 0.49	SS4 : 0.97	SS4 : 0	SS4 : 4	SS4 : 0	SS4 : 16.5
	SS5 : 0.49	SS5 : 0.67	SS5 : 0	SS5 : 4	SS5 : 0	SS5 : 16.5
All variables fixed except $K_{\mathbf{p,Q}}$ (4)	SS1 : 0.49	SS1 : 0.53	SS1 : 0	SS1 : 16.43	SS1 : 0	SS1 : 16.5
	SS2 : 0.49	SS2 : 0.53	SS2 : 0	SS2 : 3.84	SS2 : 0	SS2 : 16.5
	SS3 : 0.49	SS3 : 0.53	SS3 : 0	SS3 : 4.38	SS3 : 0	SS3 : 16.5
	SS4 : 0.49	SS4 : 0.53	SS4 : 0	SS4 : 30.00	SS4 : 0	SS4 : 16.5
	SS5 : 0.49	SS5 : 0.53	SS5 : 0	SS5 : 1.67	SS5 : 0	SS5 : 16.5
All variables fixed except $K_{\mathbf{p,P}}$ (5)	SS1 : 0.49	SS1 : 0.53	SS1 : 0	SS1 : 4	SS1 : −9.93	SS1 : 16.5
	SS2 : 0.49	SS2 : 0.53	SS2 : 0	SS2 : 4	SS2 : −9.19	SS2 : 16.5
	SS3 : 0.49	SS3 : 0.53	SS3 : 0	SS3 : 4	SS3 : −5.99	SS3 : 16.5
	SS4 : 0.49	SS4 : 0.53	SS4 : 0	SS4 : 4	SS4 : −11.15	SS4 : 16.5
	SS5 : 0.49	SS5 : 0.53	SS5 : 0	SS5 : 4	SS5 : −11.64	SS5 : 16.5
All variables fixed except $\theta_{\mathbf{0,16.7}}$ (6)	SS1 : 0.49	SS1 : 0.53	SS1 : 4.22	SS1 : 4	SS1 : 0	SS1 : 16.5
	SS2 : 0.49	SS2 : 0.53	SS2 : 4.85	SS2 : 4	SS2 : 0	SS2 : 16.5
	SS3 : 0.49	SS3 : 0.53	SS3 : 8.77	SS3 : 4	SS3 : 0	SS3 : 16.5
	SS4 : 0.49	SS4 : 0.53	SS4 : 2.65	SS4 : 4	SS4 : 0	SS4 : 16.5
	SS5 : 0.49	SS5 : 0.53	SS5 : 4.01	SS5 : 4	SS5 : 0	SS5 : 16.5
All variables fixed except $U_{\mathbf{0,16.7}}$ (7)	SS1 : 0.49	SS1 : 0.53	SS1 : 0	SS1 : 4	SS1 : 0	SS1 : 17.18
	SS2 : 0.49	SS2 : 0.53	SS2 : 0	SS2 : 4	SS2 : 0	SS2 : 17.19
	SS3 : 0.49	SS3 : 0.53	SS3 : 0	SS3 : 4	SS3 : 0	SS3 : 17.15
	SS4 : 0.49	SS4 : 0.53	SS4 : 0	SS4 : 4	SS4 : 0	SS4 : 17.22
	SS5 : 0.49	SS5 : 0.53	SS5 : 0	SS5 : 4	SS5 : 0	SS5 : 17.02

Table 4.19: Values of different combinations of variables for different cases for the exaggerated BT-system

Cases:	$X_{\mathbf{q,m}}[\mathbf{p.u}]$	$X_{\mathbf{q,g}}[\mathbf{p.u}]$	$\theta_{\mathbf{0,16.7}}[\mathbf{deg}]$	$K_{\mathbf{p,Q}}[\%]$	$K_{\mathbf{p,P}}[\%]$	$U_{\mathbf{0,16.7}}[\mathbf{kV}]$
All variables fixed except $X_{\mathbf{q,m}}$ and $X_{\mathbf{q,g}}$ (8)	SS1 : 0.40	SS1 : 0.59	SS1 : 0	SS1 : 4	SS1 : 0	SS1 : 16.5
	SS2 : 0.40	SS2 : 0.54	SS2 : 0	SS2 : 4	SS2 : 0	SS2 : 16.5
	SS3 : 0.40	SS3 : 0.40	SS3 : 0	SS3 : 4	SS3 : 0	SS3 : 16.5
	SS4 : 0.40	SS4 : 0.94	SS4 : 0	SS4 : 4	SS4 : 0	SS4 : 16.5
	SS5 : 0.40	SS5 : 0.65	SS5 : 0	SS5 : 4	SS5 : 0	SS5 : 16.5
All variables fixed except $K_{\mathbf{p,Q}}$ and $K_{\mathbf{p,P}}$ (9)	SS1 : 0.49	SS1 : 0.53	SS1 : 0	SS1 : 13.81	SS1 : -11.18	SS1 : 16.5
	SS2 : 0.49	SS2 : 0.53	SS2 : 0	SS2 : 26.52	SS2 : -10.84	SS2 : 16.5
	SS3 : 0.49	SS3 : 0.53	SS3 : 0	SS3 : 30.00	SS3 : -15.64	SS3 : 16.5
	SS4 : 0.49	SS4 : 0.53	SS4 : 0	SS4 : 30.00	SS4 : -13.04	SS4 : 16.5
	SS5 : 0.49	SS5 : 0.53	SS5 : 0	SS5 : 24.47	SS5 : -11.81	SS5 : 16.5
All variables fixed except $\theta_{\mathbf{0,16.7}}$ and $K_{\mathbf{p,Q}}$ (10)	SS1 : 0.49	SS1 : 0.53	SS1 : 13.39	SS1 : 13.89	SS1 : 0	SS1 : 16.5
	SS2 : 0.49	SS2 : 0.53	SS2 : 13.93	SS2 : -2.94	SS2 : 0	SS2 : 16.5
	SS3 : 0.49	SS3 : 0.53	SS3 : 17.97	SS3 : 9.96	SS3 : 0	SS3 : 16.5
	SS4 : 0.49	SS4 : 0.53	SS4 : 11.70	SS4 : -30.00	SS4 : 0	SS4 : 16.5
	SS5 : 0.49	SS5 : 0.53	SS5 : 13.25	SS5 : 27.77	SS5 : 0	SS5 : 16.5
All variables fixed except $\theta_{\mathbf{0,16.7}}$ and $K_{\mathbf{p,P}}$ (11)	SS1 : 0.49	SS1 : 0.53	SS1 : 0.04	SS1 : 4	SS1 : -10.18	SS1 : 16.5
	SS2 : 0.49	SS2 : 0.53	SS2 : 0.59	SS2 : 4	SS2 : -9.45	SS2 : 16.5
	SS3 : 0.49	SS3 : 0.53	SS3 : 4.73	SS3 : 4	SS3 : -7.02	SS3 : 16.5
	SS4 : 0.49	SS4 : 0.53	SS4 : -1.57	SS4 : 4	SS4 : -12.17	SS4 : 16.5
	SS5 : 0.49	SS5 : 0.53	SS5 : -0.03	SS5 : 4	SS5 : -11.65	SS5 : 16.5
All variables fixed except $\theta_{\mathbf{0,16.7}}$ and $U_{\mathbf{0,16.7}}$ (12)	SS1 : 0.49	SS1 : 0.53	SS1 : -2.85	SS1 : 4	SS1 : 0	SS1 : 17.19
	SS2 : 0.49	SS2 : 0.53	SS2 : -2.16	SS2 : 4	SS2 : 0	SS2 : 17.19
	SS3 : 0.49	SS3 : 0.53	SS3 : 1.22	SS3 : 4	SS3 : 0	SS3 : 17.13
	SS4 : 0.49	SS4 : 0.53	SS4 : -4.25	SS4 : 4	SS4 : 0	SS4 : 17.16
	SS5 : 0.49	SS5 : 0.53	SS5 : -3.12	SS5 : 4	SS5 : 0	SS5 : 17.09
All variables fixed except $\theta_{\mathbf{0,16.7}}$, $K_{\mathbf{p,Q}}$, and $U_{\mathbf{0,16.7}}$ (13)	SS1 : 0.49	SS1 : 0.53	SS1 : -4.53	SS1 :~ 0	SS1 : 0	SS1 : 17.25
	SS2 : 0.49	SS2 : 0.53	SS2 : -3.94	SS2 :~ 0	SS2 : 0	SS2 : 17.25
	SS3 : 0.49	SS3 : 0.53	SS3 : -0.28	SS3 :~ 0	SS3 : 0	SS3 : 17.25
	SS4 : 0.49	SS4 : 0.53	SS4 : -5.97	SS4 : 3.22	SS4 : 0	SS4 : 17.23
	SS5 : 0.49	SS5 : 0.53	SS5 : -4.83	SS5 : -3.52	SS5 : 0	SS5 : 17.16
No variables fixed except $K_{\mathbf{p,P}}$ (14)	SS1 : 0.40	SS1 : 0.40	SS1 : -5.65	SS1 :~ 0	SS1 : 0	SS1 : 17.25
	SS2 : 0.40	SS2 : 0.40	SS2 : -5.17	SS2 :~ 0	SS2 : 0	SS2 : 17.25
	SS3 : 0.40	SS3 : 0.40	SS3 : -2.35	SS3 :~ 0	SS3 : 0	SS3 : 17.25
	SS4 : 0.40	SS4 : 0.46	SS4 : -6.48	SS4 : 3.27	SS4 : 0	SS4 : 17.23
	SS5 : 0.40	SS5 : 0.40	SS5 : -5.89	SS5 : -4.46	SS5 : 0	SS5 : 17.15
No fixed variables (15)	SS1 : 0.40	SS1 : 0.40	SS1 : -1.98	SS1 :~ 0	SS1 :~ 0	SS1 : 17.25
	SS2 : 0.40	SS2 : 0.40	SS2 : -1.51	SS2 :~ 0	SS2 :~ 0	SS2 : 17.25
	SS3 : 0.40	SS3 : 0.40	SS3 : 1.34	SS3 :~ 0	SS3 :~ 0	SS3 : 17.25
	SS4 : 0.40	SS4 : 0.48	SS4 : -2.76	SS4 : 2.72	SS4 : -0.87	SS4 : 17.21
	SS5 : 0.40	SS5 : 0.40	SS5 : -2.18	SS5 : -0.04	SS5 : -1.56	SS5 : 17.14

Figures 4.30 and 4.31 shows the total system losses for each optimization case for the exaggerated BT-system:

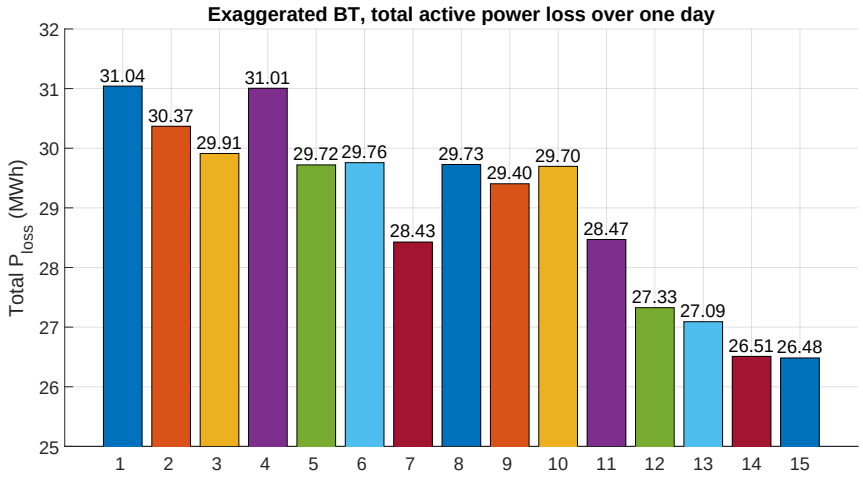

Figure 4.30: Total system losses for each case of the BT system with exaggerated converter sizes, [MWh]

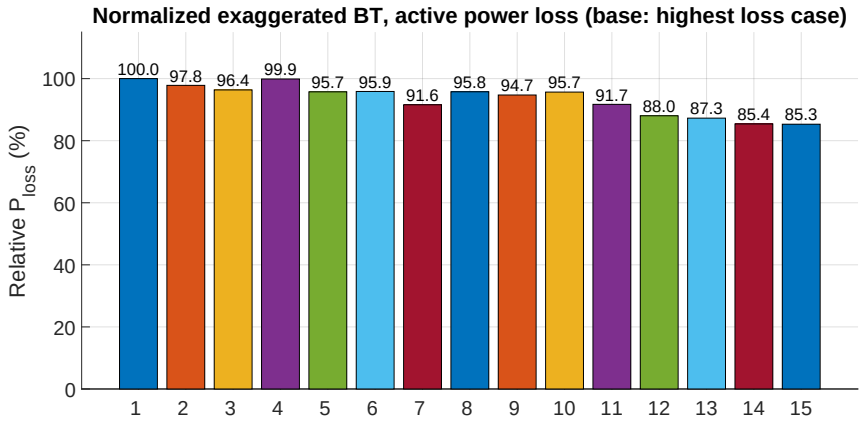

Figure 4.31: Normalized values of the total system losses for each case of the BT system with exaggerated converter sizes

Figures 4.32, 4.33 and 4.34 shows the voltage profiles for the all fixed variable case and different optimization cases:

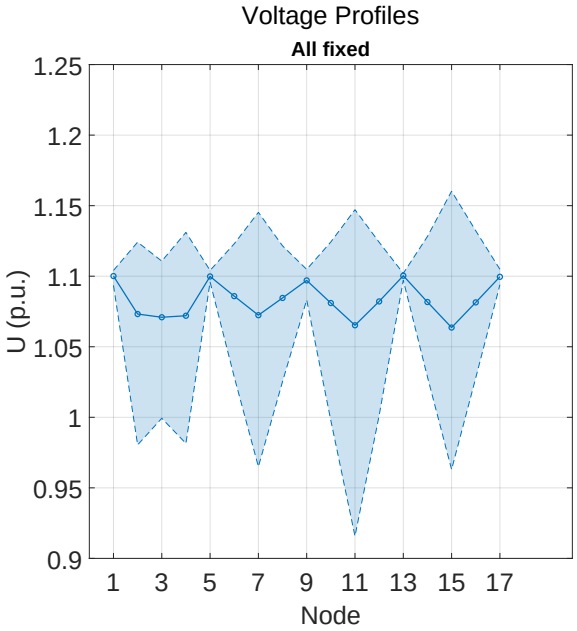

Figure 4.32: Voltage profile for the all fixed case in the exaggerated BT-system

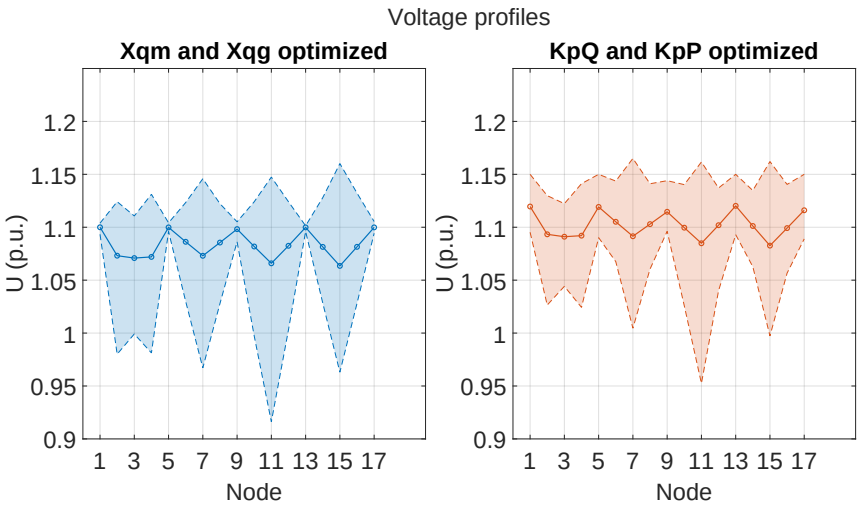

Figure 4.33: Voltage profiles for the optimization of $X_{\mathrm{q,m}}$ & $X_{\mathrm{q,g}}$ and $K_{\mathrm{p,Q}}$ & $K_{\mathrm{p,P}}$ cases in the exaggerated BT-system

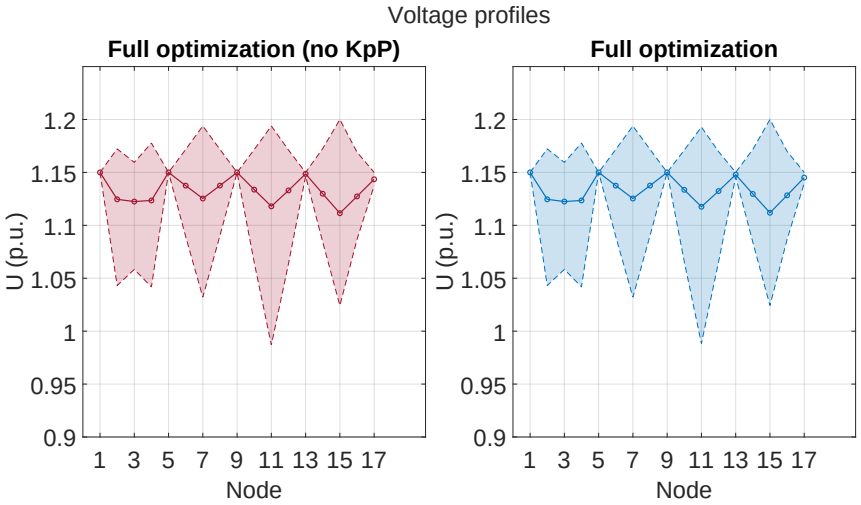

Figure 4.34: Voltage profiles for the full optimization with- and without $K_{\mathrm{p,P}}$ cases in the exaggerated BT-system

Figures 4.35, 4.36, and 4.37 shows the active and reactive power production for the all fixed and the full optimized cases:

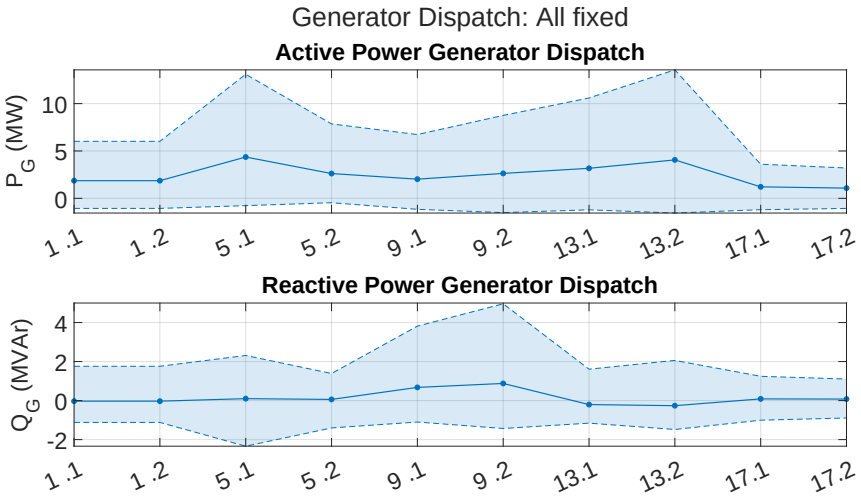

Figure 4.35: Active- and reactive power generation for the all fixed case in the exaggerated BT-system

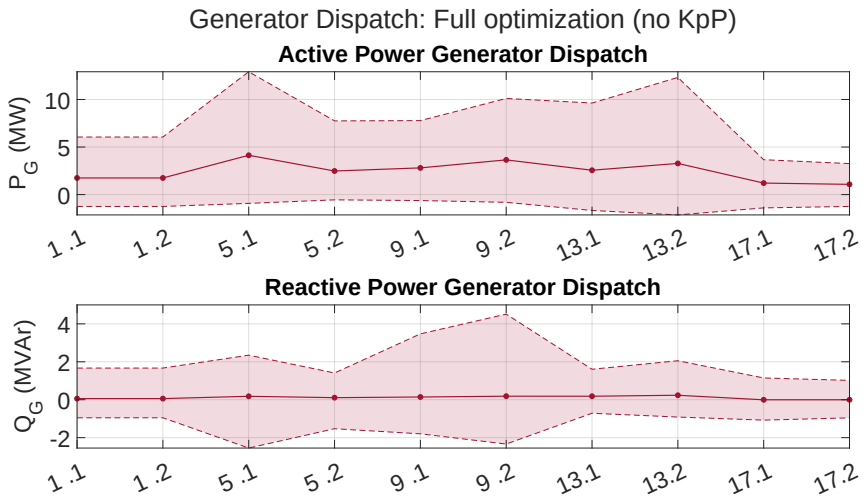

Figure 4.36: Active- and reactive power generation for the full optimization without $K_{\mathrm{p,P}}$ case in the exaggerated BT-system

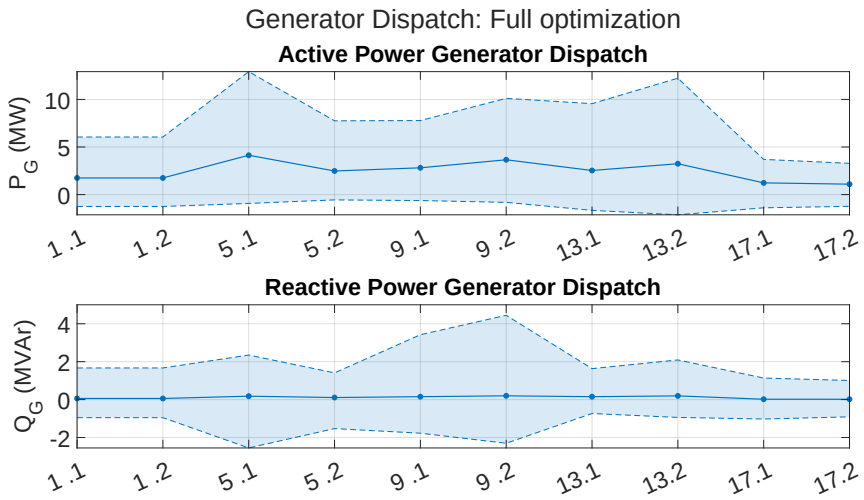

Figure 4.37: Active- and reactive power generation for the full optimization with $K_{\mathrm{p,P}}$ case in the exaggerated BT-system

4.5 Asymmetric load simulations

In order to understand the effects of the load placements and the philosophy regarding local supply, a case where the loads are connected closer to the smaller stations have been tested. This was done using the same system setup as in the exaggerated converter size cases, hence the same converter sizes as in Table 4.15. The losses and voltage profiles were not simulated for this case since the main question that is being answered with these simulations are in regards to production and thus the supply is of interest.

4.5.1 AT-system

The parameter values for different cases can be seen in figure 4.20:

Table 4.20: Values of variables for different cases in the AT-system with asymmetric load distribution

Cases:	$X_{\mathbf{q,m}}[\mathbf{p.u}]$	$X_{\mathbf{q,g}}[\mathbf{p.u}]$	$\theta_{\mathbf{0,16.7}}[\mathbf{deg}]$	$K_{\mathbf{p,Q}}[\%]$	$K_{\mathbf{p,P}}[\%]$	$U_{\mathbf{0,16.7}}[\mathbf{kV}]$
All variables fixed	SS1 : 0.49	SS1 : 0.53	SS1 : 0	SS1 : 4	SS1 : 0	SS1 : 16.5
	SS2 : 0.49	SS2 : 0.53	SS2 : 0	SS2 : 4	SS2 : 0	SS2 : 16.5
	SS3 : 0.49	SS3 : 0.53	SS3 : 0	SS3 : 4	SS3 : 0	SS3 : 16.5
	SS4 : 0.49	SS4 : 0.53	SS4 : 0	SS4 : 4	SS4 : 0	SS4 : 16.5
	SS5 : 0.49	SS5 : 0.53	SS5 : 0	SS5 : 4	SS5 : 0	SS5 : 16.5
No variables fixed except $K_{\mathbf{p,P}}$	SS1 : 0.40	SS1 : 0.40	SS1 : −2.91	SS1 : 7.63	SS1 : 0	SS1 : 16.98
	SS2 : 0.40	SS2 : 1.02	SS2 : −5.68	SS2 : 30.00	SS2 : 0	SS2 : 16.98
	SS3 : 0.40	SS3 : 0.40	SS3 : 1.45	SS3 : 7.43	SS3 : 0	SS3 : 16.98
	SS4 : 0.78	SS4 : 1.50	SS4 : −4.39	SS4 : 30.00	SS4 : 0	SS4 : 16.96
	SS5 : 0.40	SS5 : 0.40	SS5 : −5.32	SS5 : 13.35	SS5 : 0	SS5 : 16.93
No fixed variables	SS1 : 0.40	SS1 : 0.40	SS1 : 3.01	SS1 : 30.00	SS1 : −6.03	SS1 : 16.01
	SS2 : 0.40	SS2 : 0.40	SS2 : −0.75	SS2 : 30.0	SS2 : −7.89	SS2 : 16.06
	SS3 : 0.40	SS3 : 0.40	SS3 : 8.00	SS3 : 3.06	SS3 : 1.25	SS3 : 16.13
	SS4 : 0.40	SS4 : 0.40	SS4 : −0.54	SS4 : −27.04	SS4 : 0.44	SS4 : 15.98
	SS5 : 0.40	SS5 : 0.58	SS5 : 0.14	SS5 : −8.30	SS5 : 30.0	SS5 : 16.14

Figures 4.38, 4.39, and 4.40 shows the active- and reactive power generation for the AT-system:

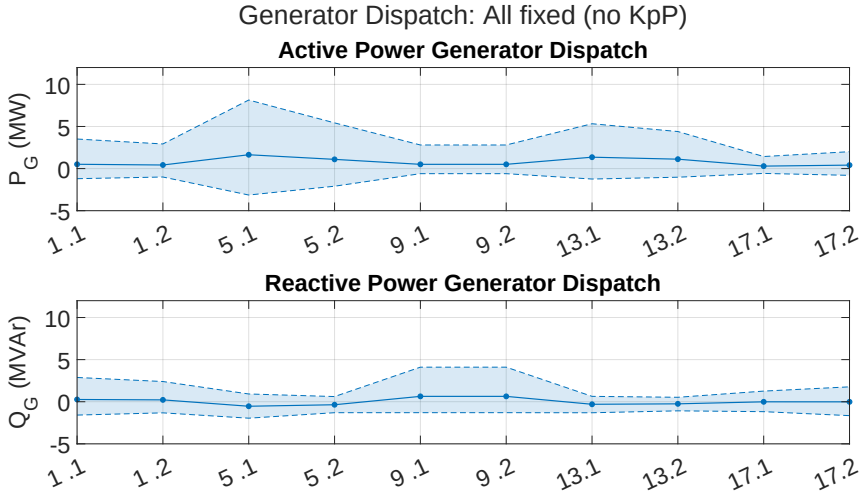

Figure 4.38: Active- and reactive power production for all fixed case with asymmetric load in the exaggerated AT-system

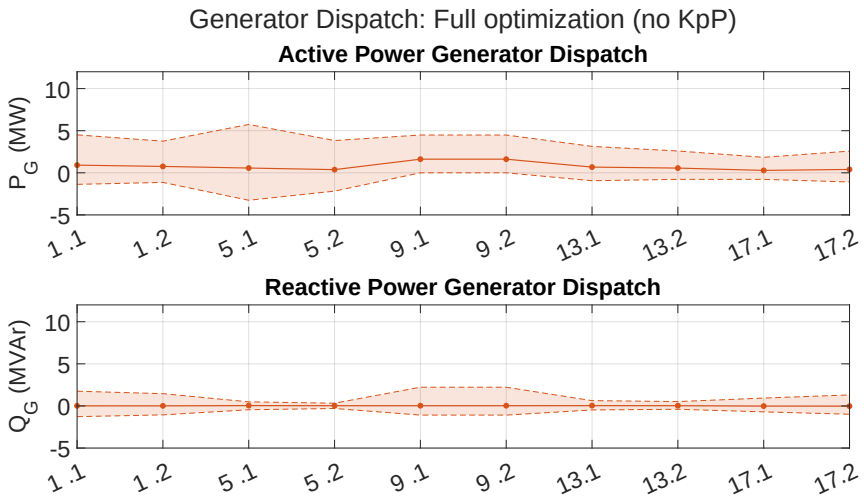

Figure 4.39: Active- and reactive power production for the full optimization without $K_{p,P}$ case with asymmetric load in the exaggerated AT-system

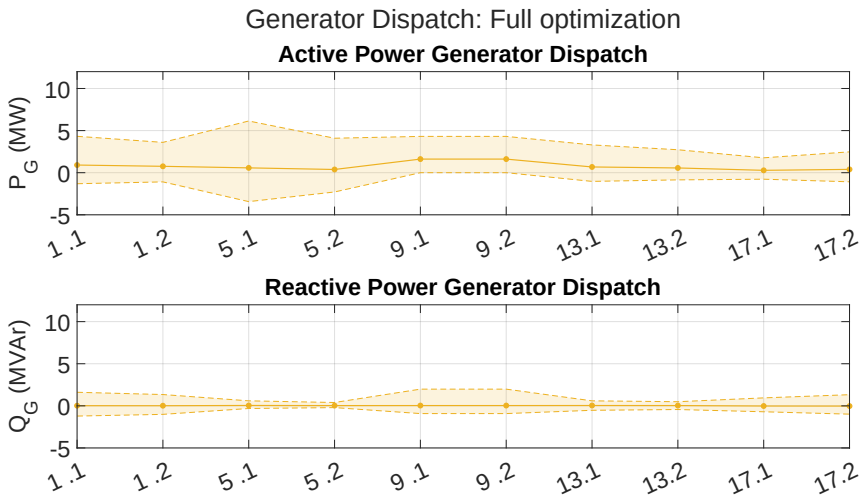

Figure 4.40: Active- and reactive power production for the full optimization case with asymmetric load in the exaggerated AT-system

4.5.2 BT-system

It is also interesting to note how this changes for a BT system. Table 4.21 shows the settings for the different cases of an asymmetrical load distribution for the BT system

Table 4.21: Values of different combinations of variables in exaggerated BT-system with asymmetric load distribution

Cases:	$X_{\mathbf{q,m}}[\mathbf{p.u}]$	$X_{\mathbf{q,g}}[\mathbf{p.u}]$	$\theta_{\mathbf{0,16.7}}[\mathbf{deg}]$	$K_{\mathbf{p,Q}}[\%]$	$K_{\mathbf{p,P}}[\%]$	$U_{\mathbf{0,16.7}}[\mathbf{kV}]$
All variables fixed	SS1 : 0.49	SS1 : 0.53	SS1 : 0	SS1 : 4	SS1 : 0	SS1 : 16.5
	SS2 : 0.49	SS2 : 0.53	SS2 : 0	SS2 : 4	SS2 : 0	SS2 : 16.5
	SS3 : 0.49	SS3 : 0.53	SS3 : 0	SS3 : 4	SS3 : 0	SS3 : 16.5
	SS4 : 0.49	SS4 : 0.53	SS4 : 0	SS4 : 4	SS4 : 0	SS4 : 16.5
	SS5 : 0.49	SS5 : 0.53	SS5 : 0	SS5 : 4	SS5 : 0	SS5 : 16.5
No variables fixed except $K_{\mathbf{p,P}}$	SS1 : 0.40	SS1 : 0.40	SS1 : 1.07	SS1 :~ 0	SS1 : 0	SS1 : 17.25
	SS2 : 0.40	SS2 : 0.71	SS2 : 2.03	SS2 : 0.68	SS2 : 0	SS2 : 17.24
	SS3 : 0.40	SS3 : 0.40	SS3 : 6.32	SS3 :~ 0	SS3 : 0	SS3 : 17.25
	SS4 : 0.50	SS4 : 1.50	SS4 : 1.10	SS4 : 1.58	SS4 : 0	SS4 : 17.24
	SS5 : 0.40	SS5 : 0.40	SS5 : 2.28	SS5 :~ 0	SS5 : 0	SS5 : 17.25
No fixed variables	SS1 : 0.40	SS1 : 0.40	SS1 : -2.26	SS1 :~ 0	SS1 :~ 0	SS1 : 17.25
	SS2 : 0.40	SS2 : 0.71	SS2 : -1.33	SS2 : 0.84	SS2 : -0.15	SS2 : 17.23
	SS3 : 0.40	SS3 : 0.40	SS3 : 3.00	SS3 :~ 0	SS3 :~ 0	SS3 : 17.25
	SS4 : 0.48	SS4 : 1.50	SS4 : -2.28	SS4 : 1.79	SS4 : -0.66	SS4 : 17.23
	SS5 : 0.40	SS5 : 0.40	SS5 : -1.04	SS5 :~ 0	SS5 :~ 0	SS5 : 17.25

Figures 4.41, 4.42, and 4.43 shows the active- and reactive power generation for the BT-system:

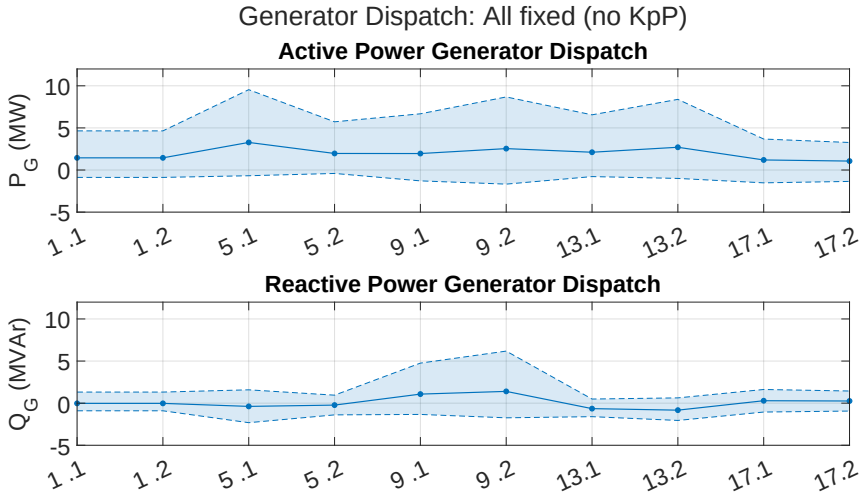

Figure 4.41: Active- and reactive power production for all fixed case with asymmetric load in the exaggerated BT system

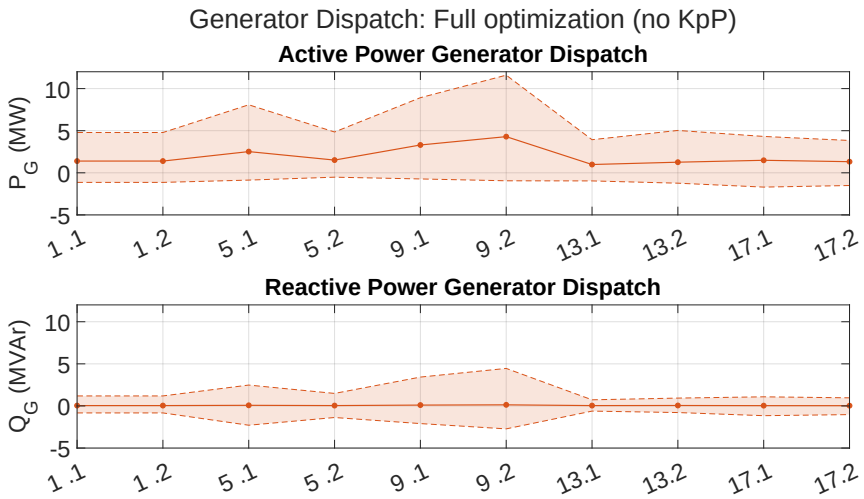

Figure 4.42: Active- and reactive power production for the full optimization without $K_{p,P}$ case with asymmetric load in the exaggerated BT system

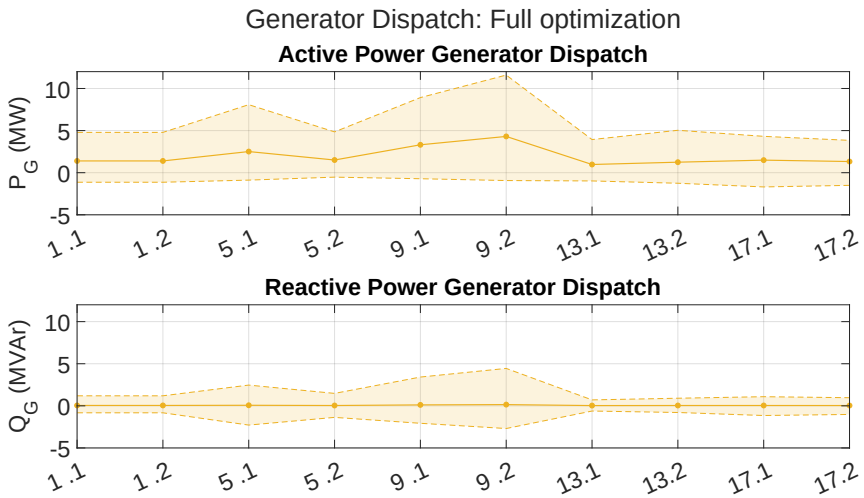

Figure 4.43: Active- and reactive power production for the full optimization case with asymmetric load in the exaggerated BT system

5
Discussion

This section seeks to discuss the results from the representative-and exaggerated AT- and BT-systems, as well as the results from the asymmetrical load scenarios. This chapter highlights what information that can be attained from the results chapter, limitations of the results and how that affects the conclusions that can be made.

5.1 Representative cases

It can be seen in figure 4.5 and 4.14 that the total amount of losses is relatively lower for the AT-system than the BT-system for the representative case. This is likely due to the configuration of the transmission line, since AT-system has electrically lower impedance than the BT-system. In order to properly see the significance of the parameter values, and to compare the two systems, the loss graphs have been normalized. The normalized figures of the AT- and BT-system can be seen in figure 4.6 and 4.15, respectively, which are normalized with respect to its highest loss scenario. The normalized figures show that the losses have decreased more in the BT-system than the AT-system, although the actual losses is less for the AT-system. This might be because the impedance in the BT-system is higher and the solver is able to find a more optimal operation point in order to minimize the losses. It could also be because of the greater capacity differences between substations in the BT-system as compared to the AT-system.
In regards to the parameters, it can be seen from the loss reduction figures, 4.6 and 4.15, that the optimization of the no-load voltage, $U_{0,16.7}$, has the most significant change in terms of active power loss reduction. The quadrature reactance on the generator side, $X_{q,g}$, also has a more significant change whilst the droop control on active- and reactive power, $K_{p,P}$ and $K_{p,Q}$, respectively, does not have any major impacts on the losses. The figures also show that $\theta_{0,16.7}$ gives a significant change in BT-system, but not as much in the AT-system. A reason for this discrepancy could be because of the difference in substation capacity between the systems. Since there is a larger asymmetry between the substations in the BT-system, which can be seen in Table 4.10 and 4.15, then the model uses the no-load angle in order to control the shared power between the stations. It can also be noticed that, for the full optimization case, the addition of droop control on the active power does not have a large influence on the total system losses. However, in terms of the voltage profile, the addition does give a significant improvement, which can be seen for the isolated optimization of droop in figure 4.8 and 4.17. An interesting setting to note is the quadrature reactances and no-load angle of the fifth station for both the AT-

and BT-system. These settings indicate that the substation on the edge gets heavily de-prioritized in power production. The reason for this is difficult to discern, but one explanation may be that this result is a modeling outlier due to the station being at the edge of the system.

5.2 Exaggerated cases

For the exaggerated cases, which have significant larger asymmetry between the substation capacities, a few differences can be noticed in comparison to the representative cases. For the total system losses in the exaggerated AT-system, which can be seen in figure 4.23, the no-load angle, $\theta_{0,16.7}$, seems to have more impact than in comparison to the representative case. This is likely due to the asymmetry in the substation capacities, which leads to the model wanting to control the load-sharing through the no-load angle. Although the optimization of $\theta_{0,16.7}$ also shows an improvement in the power losses for the BT-system, it can be seen in figure 4.31 that the no-load voltage, $U_{0,16.7}$, has the largest impact in terms of loss reduction. It can also be noticed that the optimization model is able to reduce the losses more in the AT-system than the BT-system. This could potentially be because of the different load distribution between the systems.
Further comparison between exaggerated AT- and BT- systems shows a similarity in reactive power production. On average, the reactive power production is higher in the all fixed case than the optimized cases. However, the maximum- and minimum points are quite similar, which can be seen in figures 4.10, 4.12, 4.13, 4.19, 4.20 and 4.21. This is probably since the system does not have any reactive power as load, hence the system can optimize and limit the reactive power production. The settings for $X_{\mathrm{q,M}}$, $X_{\mathrm{q,G}}$, $\theta_{0,16.7}$, seems to behave similarly across the two systems. In terms of the quadrature reactances, it can be seen in the results in Table 4.18 and 4.19 that it is the most optimal if they are as small as possible. The only exception is during the cases when they are solely optimized, since the system then uses the quadrature reactances to control the power flow of the system. For the full optimized cases, the no-load angle, $\theta_{0,16.7}$, varies across the substations and it can be noticed that the smaller substation in the middle of the system is ahead in the no-load angle than in comparison to its larger adjacent substations. A reason for this is probably that the system finds it optimal to distribute the load more evenly across the substations, hence it is ahead in angle. This explanation also goes hand-in-hand as to why the average active power production increases for the smaller and central-placed substation, which can be seen in figure 4.29 and 4.37. The optimization of $K_{\mathrm{p,Q}}$ and $K_{\mathrm{p,P}}$ across both the AT- and BT system seems to achieve similar voltage profiles, as can be seen in figure 4.25 and 4.33. With optimization solely on the voltage droops, the system tries to raise the voltage levels of the whole system and decrease the voltage dips. The voltage levels at the substations also has a larger span within the maximum and minimum values, than in comparison to the fully optimized cases. A possible reason for this may be that the model is limited in terms of optimization variables, hence the model sacrifices the voltage levels at the substations in order to decrease the system losses. This can be seen as a general improvement to the system since the most concern is usually for the voltage levels

at the load since that's where the drop is lowest and decreasing this will decrease risk of operation disruption. Since the voltage level at the load is generally of more concern the sacrifice is considered as acceptable. It can also be noticed, in figure 4.26 and 4.34, that the addition of the droop on active power barely makes any difference in terms of voltage stability for the full optimization exaggerated cases.

5.3 Asymmetric load distribution optimization

The optimization cases in figure 4.38, 4.39, 4.40, 4.41, 4.42, and 4.43 show a clear trend in how the power should be distributed to minimize system losses. For the all fixed case it seems to be optimal for the BT-system to have a relatively equal power distribution, but slightly favoring the larger stations. For the full optimized cases in the BT-system it can be seen that it is the third substation that provides for a majority of the demand. Although it is relatively smaller than the adjacent stations, it seems to be the case that it is more optimal to feed the load by local production. It is worth noting that the average production of the substations on the edges are roughly the same, indicating that the operation was already somewhat optimal. In comparison to the AT-system, it can be seen in figure 4.38, 4.39 and 4.40, that the same conclusion can be made as in the BT-system. The average reactive power generation is also decreased to zero in this system, which is most likely due to the lack of a reactive power demand present in the simulated system. The settings for the BT-system show a somewhat similar behavior to the symmetric load distribution. There are three stations in the system that have very low droop values and the highest possible no-load voltage values. From the results it can be concluded that it is more optimal to prioritize local production over larger and more geographically distant converters.

5.4 Summary and further comments

To summarize the observations of the representative- and exaggerated systems it seems to be a hierarchy in how effective the available variables are at controlling the power sharing between the substations. For the representative case, it can clearly be seen that the no-load voltage has the most significant impact for the AT-system. However, for the same case but in the BT-system, more parameters seems to give a larger impact in order to decrease the losses. The reasoning behind the difference may be that, since the BT-system has higher impedance and generally more load, the optimization of the variables becomes more important in order to decrease the system losses. For the exaggerated case it can be noticed that $U_{0,16.7}$ and $\theta_{0,16.7}$ is the most significant parameters in the AT-system. Whilst for the BT-system, the no-load angle is not as significant. As discussed, this is seemingly mainly due to the asymmetry of the power capacity between the substations. If there is a large asymmetry, then the no-load angle becomes more important in order to control the power-sharing. Across all simulations, for both the AT- and BT-

system, the model tries to set the average reactive power output to zero in order to minimize the losses. This thesis has assumed a high static value of the trains power factor ($cos(\phi)$) meaning that it only absorbs, and sends active power back during regenerative braking. But, in reality, the reactive load is dependent on the $cos(\phi)$ of the moving train. Due to the made assumption, the load lacks a reactive power demand, which explains the low reactive power output in the optimized systems. Since it is higher on average in the all fixed case than the optimized cases, the simulation model seems to optimize the converter parameters in order to decrease the reactive power flow. In terms of the parameter values, it seems to be optimal to keep the no-load voltage as high as possible and for the quadrature reactances to be as low as possible, in order to minimize active power losses. In terms of the voltage droops it can be seen that for the AT-system, it is optimal to generally keep the droop high for the larger substations, when the load is distributed in the middle. Since this applies for both the representative- and exaggerated AT-system, it is not really dependent on the substation capacity. However, for both the representative and exaggerated cases, the voltage droop is held relatively small in the BT-system. The exact reason regarding this behavior is not entirely clear. It is believed to be associated with the load profile, since the BT-system generally has more load, hence more regenerative braking than the AT-system. It may be the case that the load profile feeds back enough power to keep the voltage levels high, especially with a combination of high no-load voltage. However, since the load profile is highly limited in terms of reactive power demand, a further and more complex load model is required to draw definitive conclusions.

Through the simulation it can be seen that the structure of the system affects the results heavily, i.e the results depends greatly on the placement of the substation and loads. Due to this, the modeling becomes somewhat limited. For instance, the exaggerated cases is in a sense symmetric, since the placement of the substations has the structure of every other big and small in terms of power capacity. Another limitation is that both systems are constructed as five substations in series, which is not entirely true all the time. In order to fully understand how to control the power sharing between the substations, more complex system is needed to be investigated.

Another limitation to the modeling is the lack of complexity in the objective function. Since the objective function used in this thesis is solely to minimize losses, the modeling optimizes its given variables in order to achieve that objective. In order to make the model more realistic, it would be necessary to implement further costs to the objective function, which potentially could change the results quite a lot.

6
Conclusions and Future Work

This chapter present the main conclusions that can be drawn from the last section. It also presents potential future work within the subject, that could be done in order to reach further detailed results.

6.1 Conclusions

It appears, based on the simulations, that the current settings can be improved in terms of loss reduction. There seems to be a definite trend among all simulations, regardless of load distribution, that a reliable way to significantly reduce losses is by increasing the no-load voltage as much as possible. If there is a large asymmetry between converters, it is suggested that the no-load angle is also considered to minimize losses by sharing the load equally across the converters. In terms of voltage drop mitigation, it seems to be the case that when active power droop is solely optimized, the system is able to effectively mitigate the voltage drops. However, during the full optimization cases, when all variables are optimized, there is barely any difference in terms of improved voltage variation. This is probably because improving the voltage variation gets de-prioritized, since it is not part of the models objective function.
It can also be stated that the quadrature reactances should be set as low as possible, since that would reduce the losses further. In terms of the voltage droops, it can be noticed that during the fully optimized cases for the different BT-systems, the droop constants become very small. The reason behind this is probably due to the combination of a high no-load voltage and regenerated power from the trains. Due to limitations with the load modeling, it is not possible to draw definitive conclusions regarding the voltage droops. Hence a further improved load model, with proper regenerative braking characteristics, would be needed in order to improve the results. It seems to be the case regarding the philosophy of local supply that larger and more geographically distant converters should be de-prioritized when loads are located closer to smaller converters. Since the simulation main focus is to punish power transfer losses, it makes sense that the system finds local supply its most optimal option. However, with a further detailed objective function this results may vary.

6.2 Future Work

Although this thesis have been constructed properly and goes into details to the problem, there is a few interesting research areas within the subject that, unfortu-

nately, have not been covered due to time frame constraints. A list of interesting future works in this area can be seen below:

- **Increase the complexity of the load profile** - Since the load profile in this project have been constructed as static values, it would be interesting to see the results for a dynamic load profile. It would also be closer to reality since trains are dynamic loads. This could for instance be to include that $\cos(\phi)$ changes during regenerative braking, since it then want to absorb reactive power in order to decrease the catenary voltage.

- **Improve and expand converter models** - Due to time limit, this thesis only focused on the static converter. However, it would be interesting to see the impact of the rotary converter and how it differs to the static. A further improvement in converter modeling could be to implement loss profiles and characterization for each individual model currently in use in the railway power system.

- **Increase the system and add more asymmetry** - This thesis have used snippets of the railway power system in order to fit the time frame. For future work it would be interesting to investigate a larger system, and also add more asymmetry in terms of large and small substations.

- **Improve objective function** - All simulations in this thesis have used an objective function to minimize the active power losses in the system. The objective function could be further improved by penalizing deviation from a set point for different variables of the system, such as the voltage levels at the substations.

Bibliography

[1] M. Olofsson, "Optimal operation of the swedish railway electrical system," Doctoral thesis, KTH Royal Institute of Technology, 1996, accessed: 2026-04-13. [Online]. Available: https://www.diva-portal.org/smash/get/diva2:930128/FULLTEXT01.pdf

[2] S. R, "Railway power supply system models for static calculations in a modular design implementation," KTH Royal Institute of Technology, Stockholm, Sweden, Master's Degree Project, 2013. [Online]. Available: https://www.diva-portal.org/smash/get/diva2:839614/FULLTEXT01.pdf

[3] A. Nilsson and P. Deutschmann, "Bvs 1543.11601 - kraftförsörjningsanläggningar, autotransformersystem - systembeskrivning, utgåva 3," Trafikverket, Tech. Rep. TDOK 2014:0507, 2021. [Online]. Available: https://trvdokument.trafikverket.se/fileHandler.ashx?typ=showdokument&id=d34c22d0-8ad2-4817-98b9-b9541a4014bd

[4] E. Friman, "Impedanser för ktl och 132 kv, 30 kv och 15 kv ml," Banverket, Tech. Rep. BKE 02/28 Rev F, 2006.

[5] L. Abrahamsson and S. Östlund, "Optimizing the power flows in a railway power supply system fed by rotary converters," in *Proceedings of the ASME/IEE 2015 Joint Rail Conference (JRC2015)*, 2015. [Online]. Available: https://www.researchgate.net/profile/Lars-Abrahamsson/publication/273772588_OPTIMIZING_THE_POWER_FLOWS_IN_A_RAILWAY_POWER_SUPPLY_SYSTEM_FED_BY_ROTARY_CONVERTERS/links/550c5c0f0cf212874160def4/OPTIMIZING-THE-POWER-FLOWS-IN-A-RAILWAY-POWER-SUPPLY-SYSTEM-FED-BY-ROTARY-CONVERTERS.pdf

[6] L. J.Laury and M.Bollen, "Modified voltage control law for low frequency railway power systems," in *Proceedings of the 2017 IEEE/ASME Joint Rail Conference (JRC2017)*, Philadelphia, United States, apr 2017. [Online]. Available: https://www.diva-portal.org/smash/record.jsf?pid=diva2%3A1097264&dswid=-9982

[7] J. Laury, L. Abrahamsson, and M. H. Bollen, "A simplified static frequency converter model for electromechanical transient stability studies for 16 2/3 hz railways," 2019. [Online]. Available: https://arxiv.org/pdf/1811.04962

[8] M. Olofsson, G. Andersson, and L. Söder, "Optimal operation of the swedish railway electrical system," https://ieeexplore.ieee.org/stamp/stamp.jsp?tp=&arnumber=396056&tag=1, 1995, accessed: 2026-05-05.

[9] L. Abrahamsson, "Railway power supply models and methods for long-term investment analysis," Licentiate Thesis, Royal Institute of Technology (KTH),

2008, accessed: 2026-04-01. [Online]. Available: https://www.diva-portal.org/smash/record.jsf?pid=diva2%3A117&dswid=-5586

[10] W. Hidevik, F. Alrup, and K. Udatsjen, "Private communication," april,2026.

[11] L.Abrahamsson, "Optimal railroad power supply system operation and design - detailed system studies, and aggregated investment models," Doctoral Thesis, Royal Institute of Technology (KTH), 2012, accessed: 2026-04-01. [Online]. Available: https://www.diva-portal.org/smash/record.jsf?pid=diva2%3A574526&dswid=3097

[12] S. Nakamura, T. Fukuda, Y. Kodama, Y. Hayashi, and H. Hayashiya, "Multipurpose optimization method for energy storage system specification using measurement data of dc traction substations," *IEEJ: Transactions on Electrical and Electronic Engineering*, 2024.

[13] DIgSILENT, "Powerfactory applications," https://www.digsilent.de/en/powerfactory.html, n.d, accessed: 2026-04-02.

[14] M.Olofsson, "Power flow analysis of the swedish railway electrical system," Licentiate Thesis, Royal Institute of Technology (KTH), 1993, accessed: 2026-04-01. [Online]. Available: https://www.diva-portal.org/smash/record.jsf?dswid=-5586&pid=diva2%3A1187823

A

Appendix

A.1 Per-unit system

In order to make the different parameters of a power system network easily comparable to each other, the per-unit system can be applied. The per-unit value of a certain quantity can be calculated accordingly [2]:

$$\text{Certain Quantity in per-unit} = \frac{\text{Actual value of the quantity}}{\text{Base value of the quantity}} \tag{A.1}$$

For electrical calculations, the base power of the network is chosen as an apparent power, and then either the base voltage, impedance or current needs to be determined in order to calculate the other quantities. The base impedance and base current, for a single phase system, can be calculated accordingly [2]:

$$Z_B = \frac{V_{B,LL}^2}{S_B} \tag{A.2}$$

$$I_B = \frac{S_B}{V_{B,LL}} \tag{A.3}$$

A.2 Load profiles

This section shows the load profiles of the AT- and BT-system. The nodes 1, 5, 9, 13 and 17 is considered to be substation-nodes, hence no loads can be attached to these nodes. The rest of the nodes is considered to be load nodes. The load is supposed to imitate a moving train, hence a positive load value means that the train absorbs power to accelerate whilst a negative value is generated power from regenerative braking.

Worth mentioning, the X-axis is the number of nodes and the Y-axis is the number of minutes for the load profiles in table A.1 and A.2.

A.2.1 AT-system

The first 20 minutes of the load profile for the AT-system can be seen in Table A.1:

Table A.1: First 20 minutes of the load profile for the AT-system

	1	2	3	4	5	6	7	8	9	10	11	12	13	14	15	16	17
1	0	0	3.7411	0	0	0	0.0689	0	0	0	0.4637	0	0	0	0.2518	0	0
2	0	0	4.9310	0	0	0	0.0689	0	0	0	0.4638	0	0	0	0.7870	0	0
3	0	0	0.2664	0	0	0	0.0689	0	0	0	0.4638	0	0	0	7.4821	0	0
4	0	0	-0.9453	0	0	0	0.0689	0	0	0	0.4638	0	0	0	4.7603	0	0
5	0	0	0.9614	0	0	0	0.0689	0	0	0	0.4638	0	0	0	0.3291	0	0
6	0	0	0.6491	0	0	0	0.0689	0	0	0	0.4638	0	0	0	1.0523	0	0
7	0	0	-0.0029	0	0	0	0.0689	0	0	0	0.4767	0	0	0	6.4810	0	0
8	0	0	0.4401	0	0	0	0.0689	0	0	0	0.4767	0	0	0	-0.0352	0	0
9	0	0	-0.7929	0	0	0	0.0689	0	0	0	0.4764	0	0	0	-0.0352	0	0
10	0	0	-2.3963	0	0	0	0.0689	0	0	0	0.5643	0	0	0	-0.0352	0	0
11	0	0	-0.3249	0	0	0	0.0689	0	0	0	0.5643	0	0	0	-0.0352	0	0
12	0	0	3.2408	0	0	0	0.0689	0	0	0	0.5643	0	0	0	-0.0352	0	0
13	0	0	2.0241	0	0	0	0.0689	0	0	0	0.5648	0	0	0	-0.0352	0	0
14	0	0	-1.1741	0	0	0	0.0689	0	0	0	0.4911	0	0	0	-0.0352	0	0
15	0	0	-7.4972	0	0	0	0.0689	0	0	0	0.5927	0	0	0	-0.0352	0	0
16	0	0	-3.8825	0	0	0	0.0689	0	0	0	0.5927	0	0	0	-0.0352	0	0
17	0	0	0.6850	0	0	0	0.0689	0	0	0	0.5927	0	0	0	-0.0352	0	0
18	0	0	6.7072	0	0	0	0.0689	0	0	0	0.5927	0	0	0	-0.0352	0	0
19	0	0	7.7361	0	0	0	0.0689	0	0	0	0.5493	0	0	0	-0.0352	0	0
20	0	0	3.4982	0	0	0	0.0689	0	0	0	0.5499	0	0	0	-0.0352	0	0

A.2.2 BT-system

The first 20 minutes of the load profile for the BT-system can be seen in figure A.2:

Table A.2: First 20 minutes of the load profile for the BT-system

	1	2	3	4	5	6	7	8	9	10	11	12	13	14	15	16	17
1	0	1.6839	-0.0357	1.5093	0	0	-1.526	0	0	0	11.8115	0	0	0	6.2764	0	0
2	0	3.7377	-0.6252	0.943	0	0	0.1261	0	0	0	12.1114	0	0	0	5.1470	0	0
3	0	1.4488	0.3586	1.5307	0	0	1.3875	0	0	0	-3.2709	0	0	0	4.4469	0	0
4	0	0.9308	-1.0008	2.9443	0	0	-0.9463	0	0	0	14.0766	0	0	0	0.1798	0	0
5	0	0.9719	-0.4219	3.2075	0	0	-0.3952	0	0	0	16.2591	0	0	0	5.2252	0	0
6	0	0.1139	-0.1594	2.6639	0	0	4.0132	0	0	0	8.8982	0	0	0	4.8231	0	0
7	0	0.2648	0.511	3.670	0	0	4.5866	0	0	0	12.4539	0	0	0	4.1976	0	0
8	0	3.5388	-0.4945	5.2471	0	0	7.6502	0	0	0	6.2040	0	0	0	3.5331	0	0
9	0	1.2596	-0.4840	3.9780	0	0	10.1822	0	0	0	10.2156	0	0	0	5.1431	0	0
10	0	-0.1433	-0.7324	3.6578	0	0	3.7830	0	0	0	4.1485	0	0	0	1.6472	0	0
11	0	0.7382	-0.7324	2.2056	0	0	2.7103	0	0	0	5.9149	0	0	0	6.0344	0	0
12	0	2.4958	-0.4360	0.6020	0	0	1.0811	0	0	0	1.9553	0	0	0	5.6749	0	0
13	0	4.0462	-0.5145	1.5490	0	0	10.6114	0	0	0	3.7188	0	0	0	2.5915	0	0
14	0	3.4229	-1.0559	1.8891	0	0	7.9050	0	0	0	-1.4247	0	0	0	3.5973	0	0
15	0	2.7043	-0.3445	1.1813	0	0	4.1488	0	0	0	4.7332	0	0	0	3.9653	0	0
16	0	4.3468	-0.3445	1.5984	0	0	6.5277	0	0	0	5.1060	0	0	0	1.5339	0	0
17	0	-0.1363	0.8203	2.0262	0	0	4.2398	0	0	0	4.0359	0	0	0	1.5737	0	0
18	0	4.2066	0.4184	2.0010	0	0	5.6461	0	0	0	5.995	0	0	0	3.2133	0	0
19	0	1.8024	0.4184	0.5942	0	0	5.7885	0	0	0	6.8748	0	0	0	2.5859	0	0
20	0	0.0146	-0.0152	0.3335	0	0	4.6190	0	0	0	6.6371	0	0	0	4.3377	0	0

A.3 Y-buses

A.3.1 AT-system

The admittance matrix, Y-bus, of the AT-system network can be seen in figure A.1:

$$\begin{bmatrix}
Y_{12,0} & -Y_{12,0} & 0 & 0 & 0 & 0 & 0 & 0 & 0 & 0 & 0 & 0 & 0 & 0 & 0 & 0 & 0 \\
-Y_{12,0} & (Y_{12,0}+Y_{12}) & -Y_{12} & 0 & 0 & 0 & 0 & 0 & 0 & 0 & 0 & 0 & 0 & 0 & 0 & 0 & 0 \\
0 & -Y_{12} & 2*Y_{12} & -Y_{12} & 0 & 0 & 0 & 0 & 0 & 0 & 0 & 0 & 0 & 0 & 0 & 0 & 0 \\
0 & 0 & -Y_{12} & (Y_{12}+Y_{12,0}) & -Y_{12,0} & 0 & 0 & 0 & 0 & 0 & 0 & 0 & 0 & 0 & 0 & 0 & 0 \\
0 & 0 & 0 & -Y_{12,0} & (Y_{12,0}+Y_{23,0}) & -Y_{23,0} & 0 & 0 & 0 & 0 & 0 & 0 & 0 & 0 & 0 & 0 & 0 \\
0 & 0 & 0 & 0 & -Y_{23,0} & (Y_{23,0}+Y_{23}) & -Y_{23} & 0 & 0 & 0 & 0 & 0 & 0 & 0 & 0 & 0 & 0 \\
0 & 0 & 0 & 0 & 0 & -Y_{23} & 2*Y_{23} & -Y_{23} & 0 & 0 & 0 & 0 & 0 & 0 & 0 & 0 & 0 \\
0 & 0 & 0 & 0 & 0 & 0 & -Y_{23} & (Y_{23}+Y_{23,0}) & -Y_{23,0} & 0 & 0 & 0 & 0 & 0 & 0 & 0 & 0 \\
0 & 0 & 0 & 0 & 0 & 0 & 0 & -Y_{23,0} & (Y_{23,0}+Y_{34,0}) & -Y_{34,0} & 0 & 0 & 0 & 0 & 0 & 0 & 0 \\
0 & 0 & 0 & 0 & 0 & 0 & 0 & 0 & -Y_{34},0 & (Y_{34,0}+Y_{34}) & -Y_{34} & 0 & 0 & 0 & 0 & 0 & 0 \\
0 & 0 & 0 & 0 & 0 & 0 & 0 & 0 & 0 & -Y_{34} & 2*Y_{34} & -Y_{34} & 0 & 0 & 0 & 0 & 0 \\
0 & 0 & 0 & 0 & 0 & 0 & 0 & 0 & 0 & -Y_{34} & (Y_{34}+Y_{34,0}) & -Y_{34,0} & 0 & 0 & 0 & 0 & 0 \\
0 & 0 & 0 & 0 & 0 & 0 & 0 & 0 & 0 & 0 & -Y_{34,0} & (Y_{34,0}+Y_{45,0}) & -Y_{45,0} & 0 & 0 & 0 & 0 \\
0 & 0 & 0 & 0 & 0 & 0 & 0 & 0 & 0 & 0 & 0 & -Y_{45,0} & (Y_{45,0}+Y_{45}) & -Y_{45} & 0 & 0 & 0 \\
0 & 0 & 0 & 0 & 0 & 0 & 0 & 0 & 0 & 0 & 0 & 0 & -Y_{45} & 2*Y_{45} & -Y_{45} & 0 & 0 \\
0 & 0 & 0 & 0 & 0 & 0 & 0 & 0 & 0 & 0 & 0 & 0 & 0 & -Y_{45} & (Y_{45}+Y_{45,0}) & -Y_{45,0} & 0 \\
0 & 0 & 0 & 0 & 0 & 0 & 0 & 0 & 0 & 0 & 0 & 0 & 0 & 0 & -Y_{45,0} & Y_{45,0} & 0
\end{bmatrix}$$

Figure A.1: Y-bus matrix of the AT-system

A.3.2 BT-system

The admittance matrix, Y-bus, of the BT-system network can be seen in figure A.2:

$$\begin{bmatrix}
Y_{12} & -Y_{12} & 0 & 0 & 0 & 0 & 0 & 0 & 0 & 0 & 0 & 0 & 0 & 0 & 0 & 0 & 0 \\
-Y_{12} & 2*Y_{12} & -Y_{12} & 0 & 0 & 0 & 0 & 0 & 0 & 0 & 0 & 0 & 0 & 0 & 0 & 0 & 0 \\
0 & -Y_{12} & 2*Y_{12} & -Y_{12} & 0 & 0 & 0 & 0 & 0 & 0 & 0 & 0 & 0 & 0 & 0 & 0 & 0 \\
0 & 0 & -Y_{12} & 2*Y_{12} & -Y_{12} & 0 & 0 & 0 & 0 & 0 & 0 & 0 & 0 & 0 & 0 & 0 & 0 \\
0 & 0 & 0 & -Y_{12} & (Y_{12}+Y_{23}) & -Y_{23} & 0 & 0 & 0 & 0 & 0 & 0 & 0 & 0 & 0 & 0 & 0 \\
0 & 0 & 0 & 0 & -Y_{23} & 2*Y_{23} & -Y_{23} & 0 & 0 & 0 & 0 & 0 & 0 & 0 & 0 & 0 & 0 \\
0 & 0 & 0 & 0 & 0 & -Y_{23} & 2*Y_{23} & -Y_{23} & 0 & 0 & 0 & 0 & 0 & 0 & 0 & 0 & 0 \\
0 & 0 & 0 & 0 & 0 & 0 & -Y_{23} & 2*Y_{23} & -Y_{23} & 0 & 0 & 0 & 0 & 0 & 0 & 0 & 0 \\
0 & 0 & 0 & 0 & 0 & 0 & 0 & -Y_{23} & (Y_{23}+Y_{34}) & -Y_{34} & 0 & 0 & 0 & 0 & 0 & 0 & 0 \\
0 & 0 & 0 & 0 & 0 & 0 & 0 & 0 & -Y_{34} & 2*Y_{34} & -Y_{34} & 0 & 0 & 0 & 0 & 0 & 0 \\
0 & 0 & 0 & 0 & 0 & 0 & 0 & 0 & 0 & -Y_{34} & 2*Y_{34} & -Y_{34} & 0 & 0 & 0 & 0 & 0 \\
0 & 0 & 0 & 0 & 0 & 0 & 0 & 0 & 0 & 0 & -Y_{34} & 2*Y_{34} & -Y_{34} & 0 & 0 & 0 & 0 \\
0 & 0 & 0 & 0 & 0 & 0 & 0 & 0 & 0 & 0 & 0 & -Y_{34} & (Y_{34}+Y_{45}) & -Y_{45} & 0 & 0 & 0 \\
0 & 0 & 0 & 0 & 0 & 0 & 0 & 0 & 0 & 0 & 0 & 0 & -Y_{45} & 2*Y_{45} & -Y_{45} & 0 & 0 \\
0 & 0 & 0 & 0 & 0 & 0 & 0 & 0 & 0 & 0 & 0 & 0 & 0 & -Y_{45} & 2*Y_{45} & -Y_{45} & 0 \\
0 & 0 & 0 & 0 & 0 & 0 & 0 & 0 & 0 & 0 & 0 & 0 & 0 & 0 & -Y_{45} & 2*Y_{45} & -Y_{45} \\
0 & 0 & 0 & 0 & 0 & 0 & 0 & 0 & 0 & 0 & 0 & 0 & 0 & 0 & 0 & -Y_{45} & Y_{45}
\end{bmatrix}$$

Figure A.2: Y-bus matrix of the BT-system

A.4 Results from simulation of the representative systems

This sections contains the results of the representative AT-system and BT-system.

A.4.1 AT-system

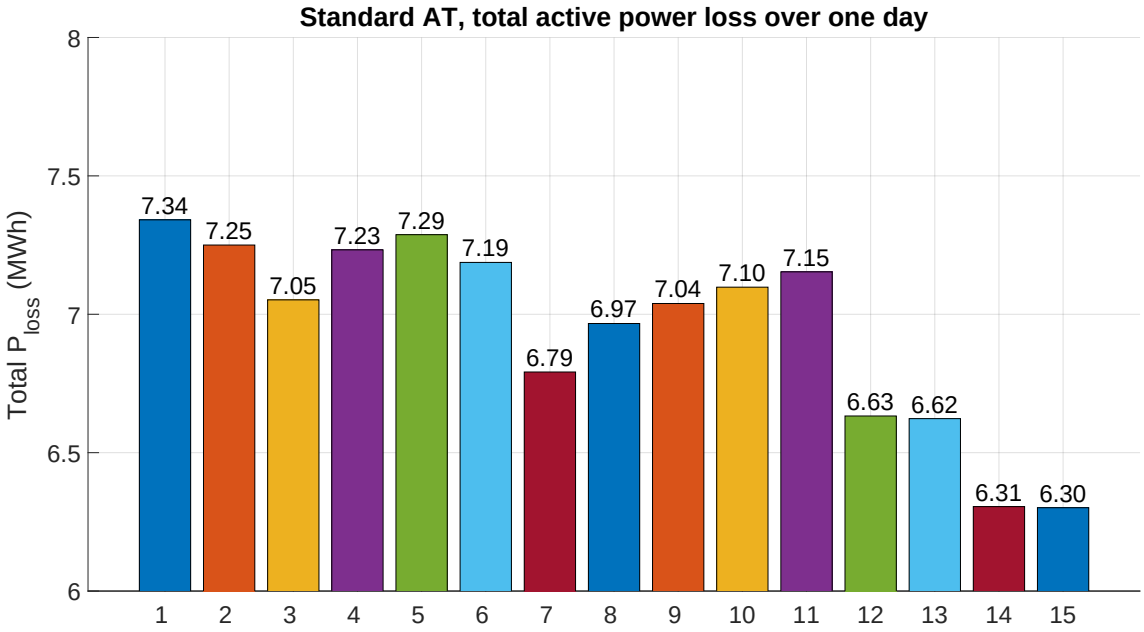

Figure A.3: System losses for each scenario in MWh

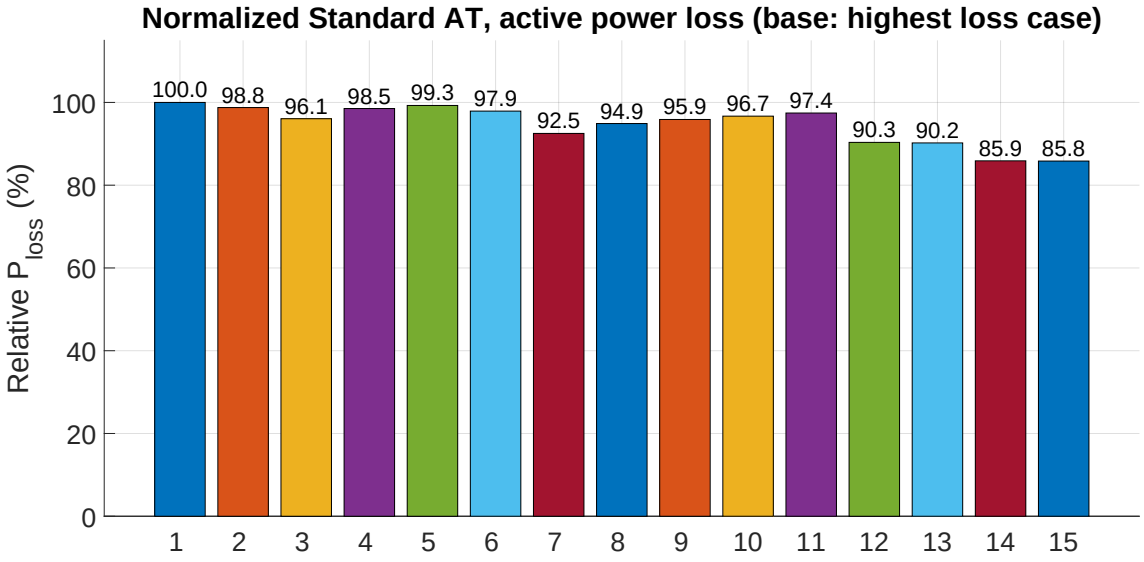

Figure A.4: System losses for each scenario in %, normalized in relation to the all fixed case

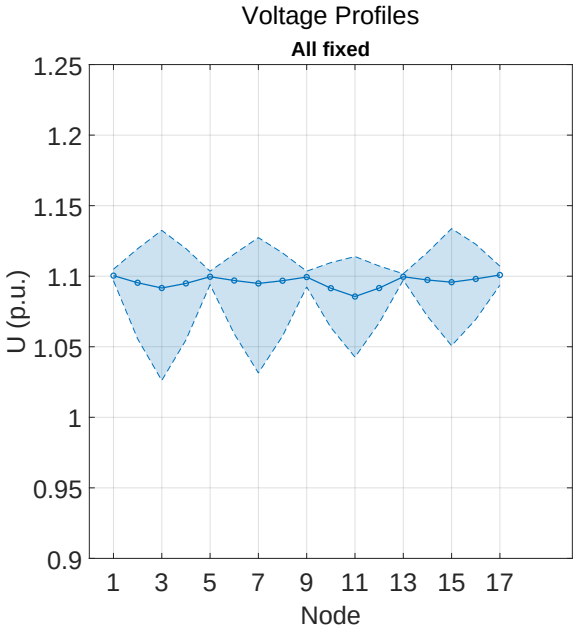

Figure A.5: Voltage profile for the all fixed case of the representative AT-system

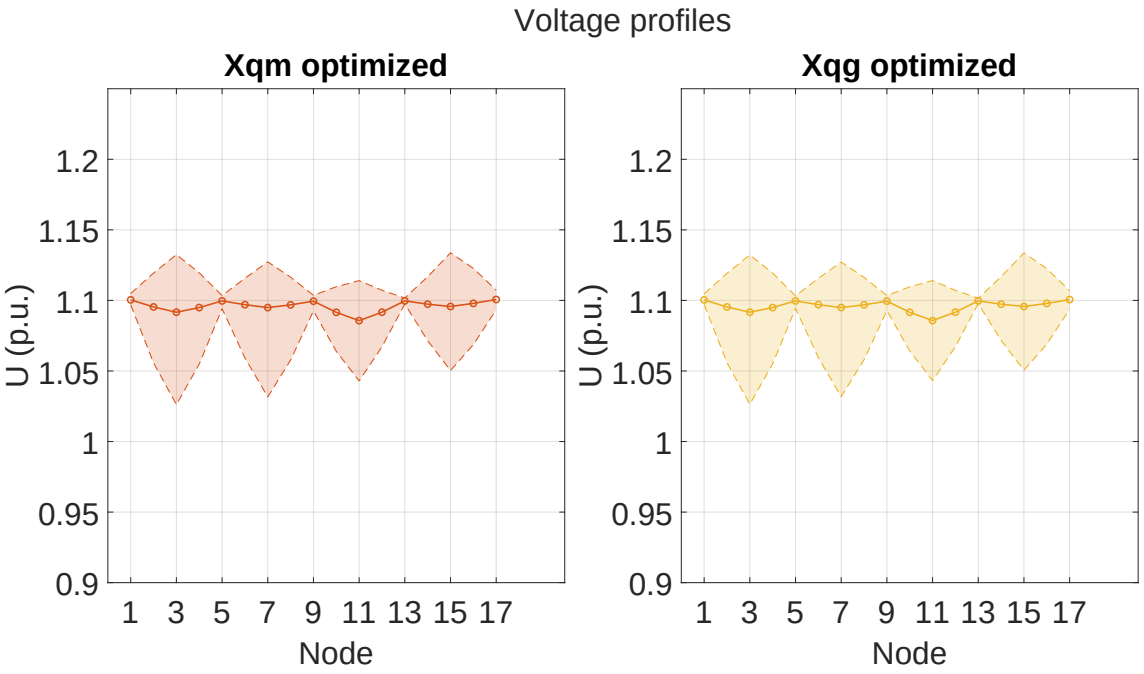

Figure A.6: Voltage profile for the optimization of $X_{\mathrm{x,m}}$ and $X_{\mathrm{q,g}}$ cases for the representative AT-system

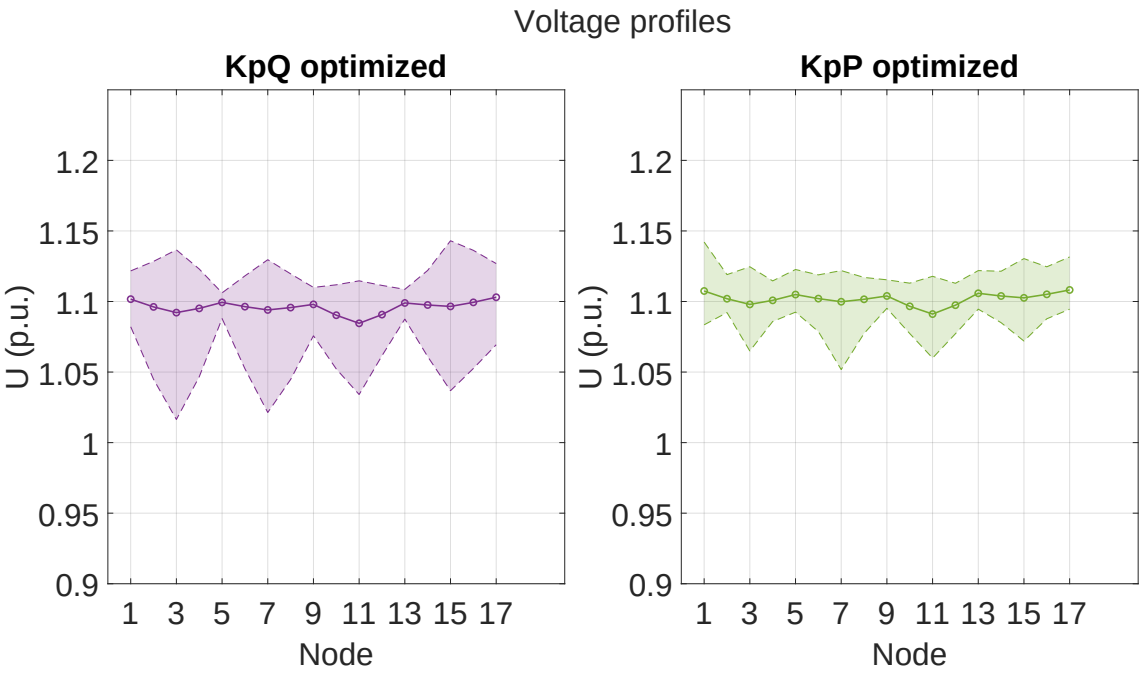

Figure A.7: Voltage profile for the optimization of $K_{\mathrm{p,Q}}$ and $K_{\mathrm{p,P}}$ cases for the representative AT-system

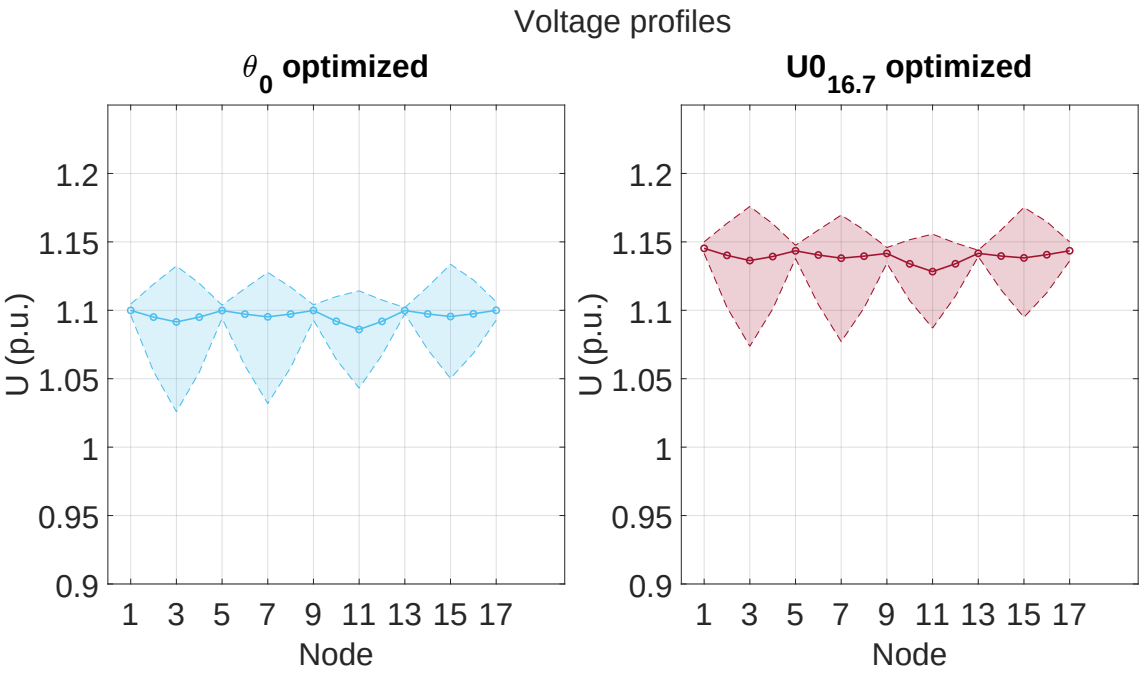

Figure A.8: Voltage profile for the optimization of θ_0 and $U_{0,16.7}$ cases for the representative AT-system

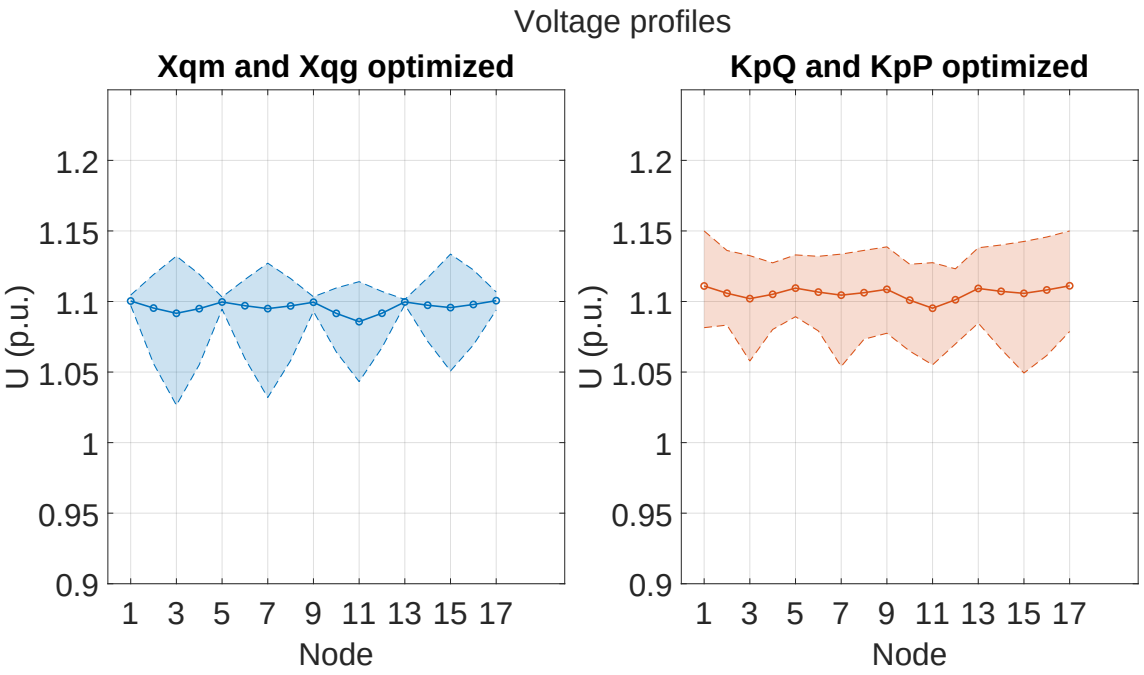

Figure A.9: Voltage profile for the optimization of $X_{\mathrm{q,m}}$ & $X_{\mathrm{q,g}}$ and $K_{\mathrm{p,Q}}$ & $K_{\mathrm{p,P}}$ cases for the representative AT-system

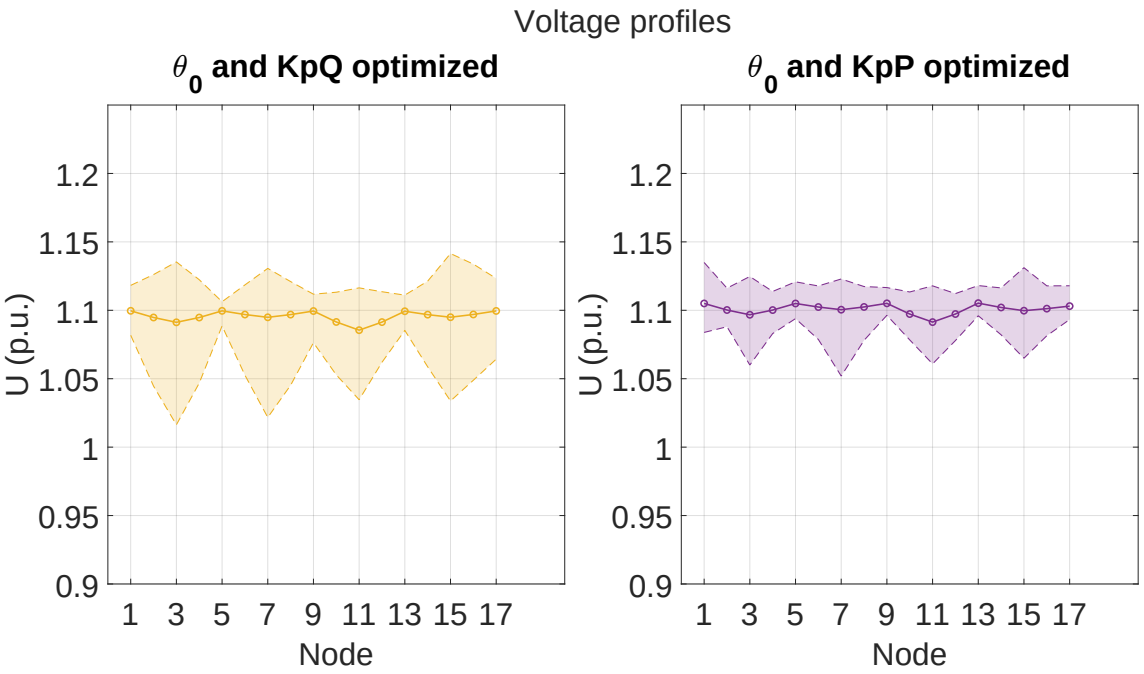

Figure A.10: Voltage profile for the optimization of θ_0 & $K_{\mathrm{p,Q}}$ and θ_0 & $K_{\mathrm{p,P}}$ cases for the representative AT-system

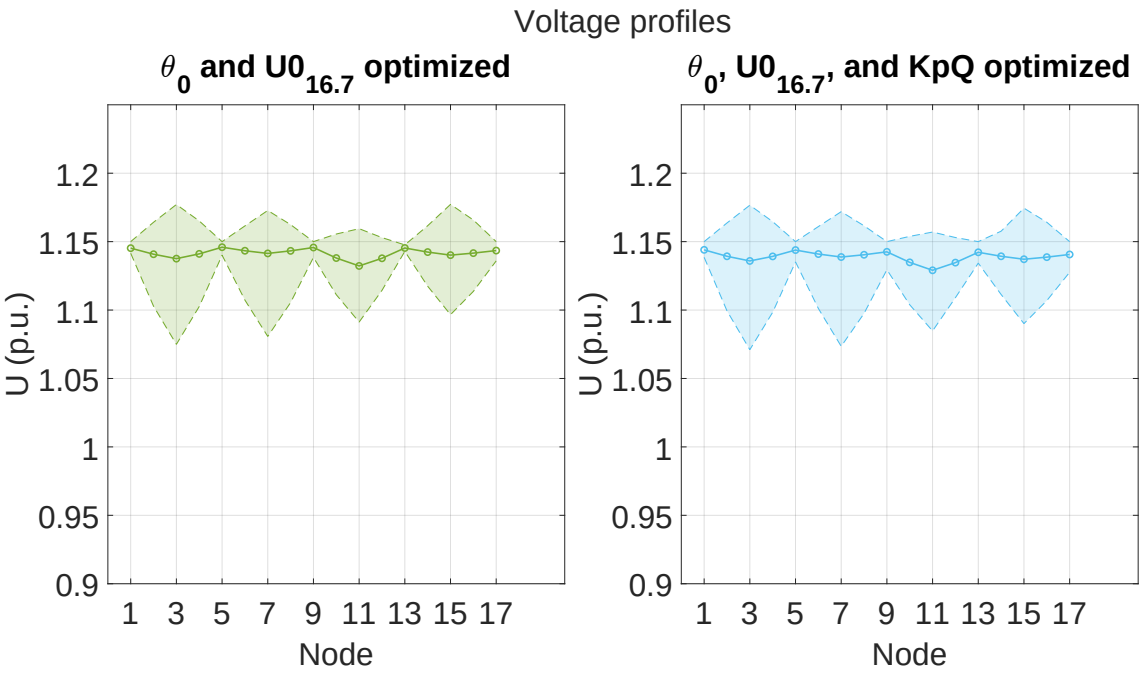

Figure A.11: Voltage profile for the optimization of θ_0 & $U_{0,16.7}$ and θ_0 & $U_{0,16.7}$ & $K_{p,Q}$ cases for the representative AT-system

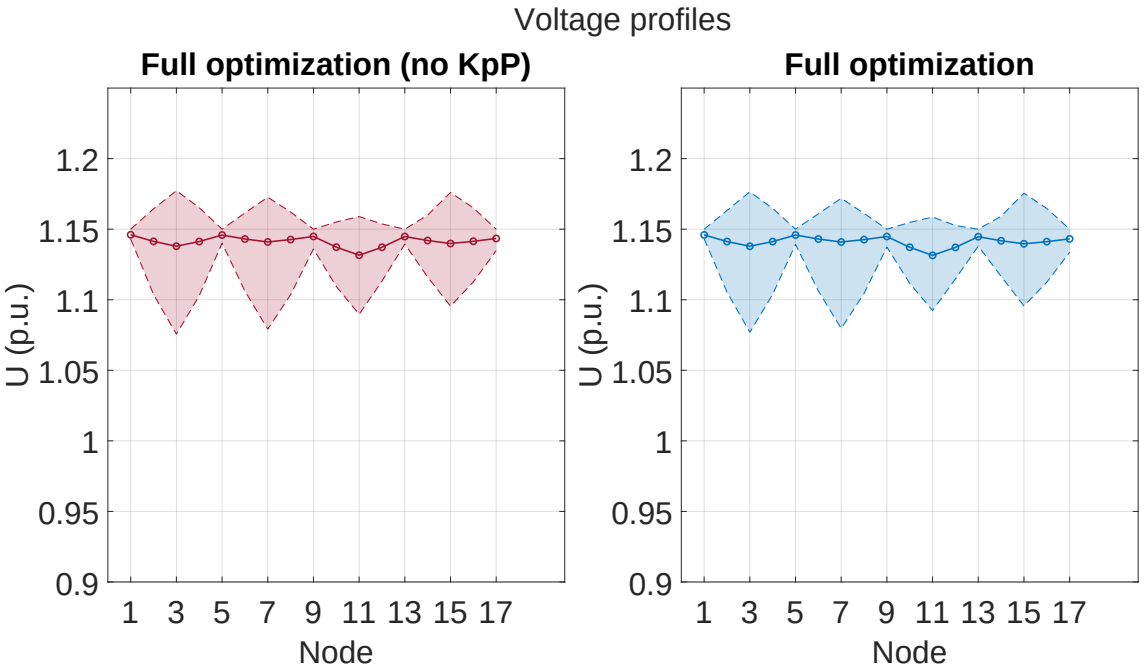

Figure A.12: Voltage profile for the full optimization with and without $K_{p,P}$ cases for the representative AT-system

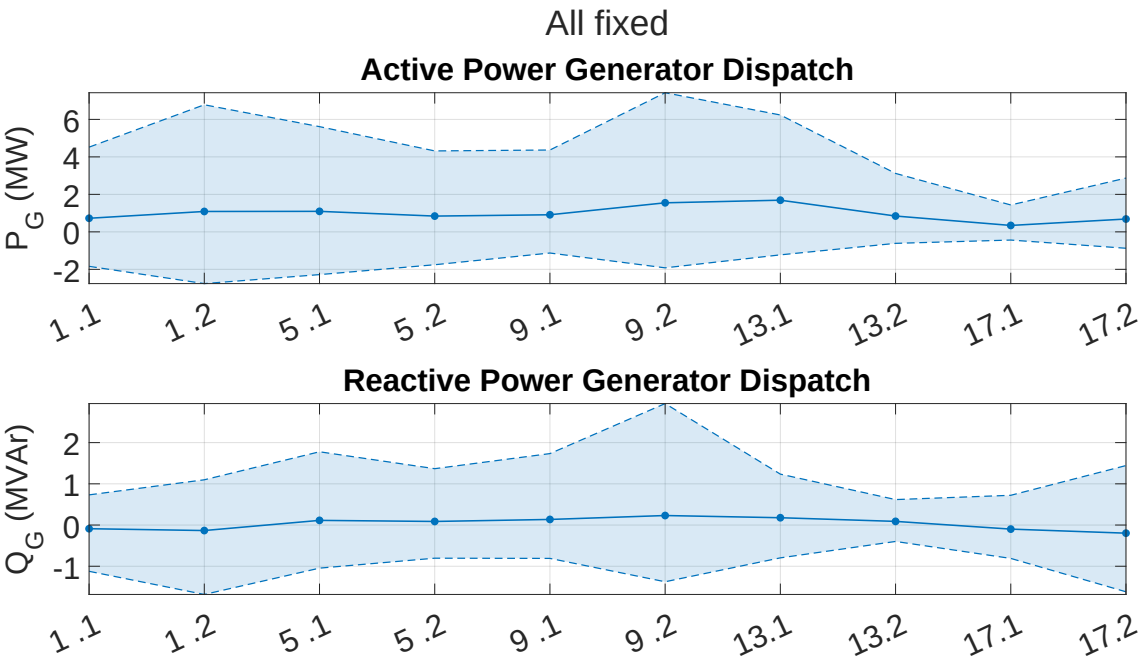

Figure A.13: Active- and reactive power generation of each substation for the All fixed case

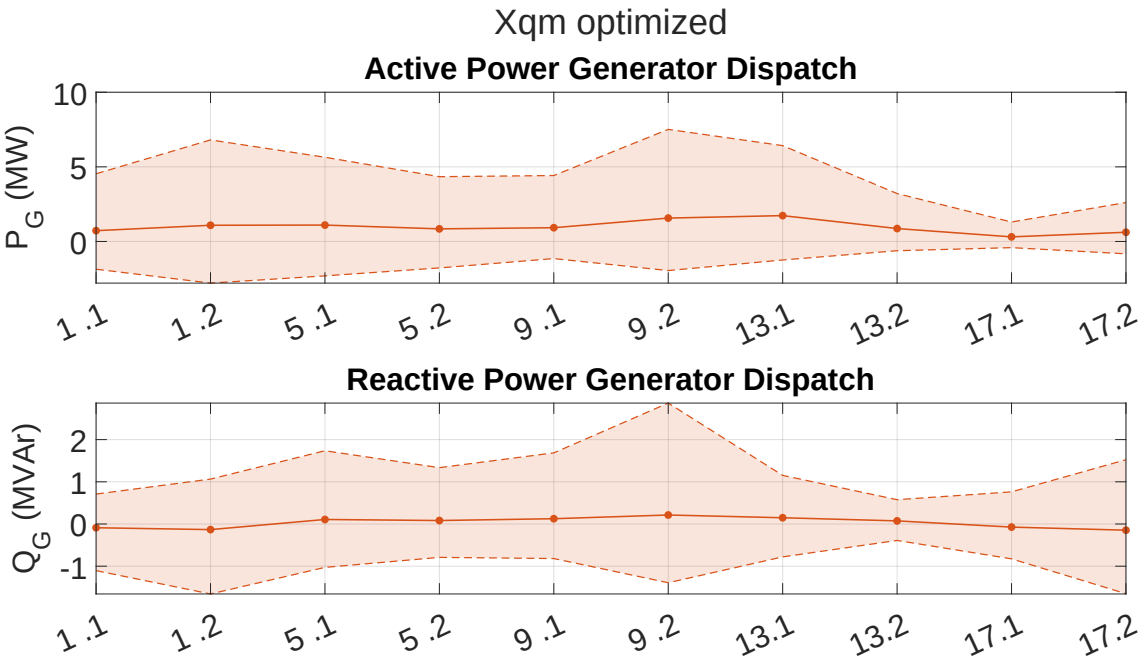

Figure A.14: Active- and reactive power generation of each substation for the optimization of $X_{q,m}$ case

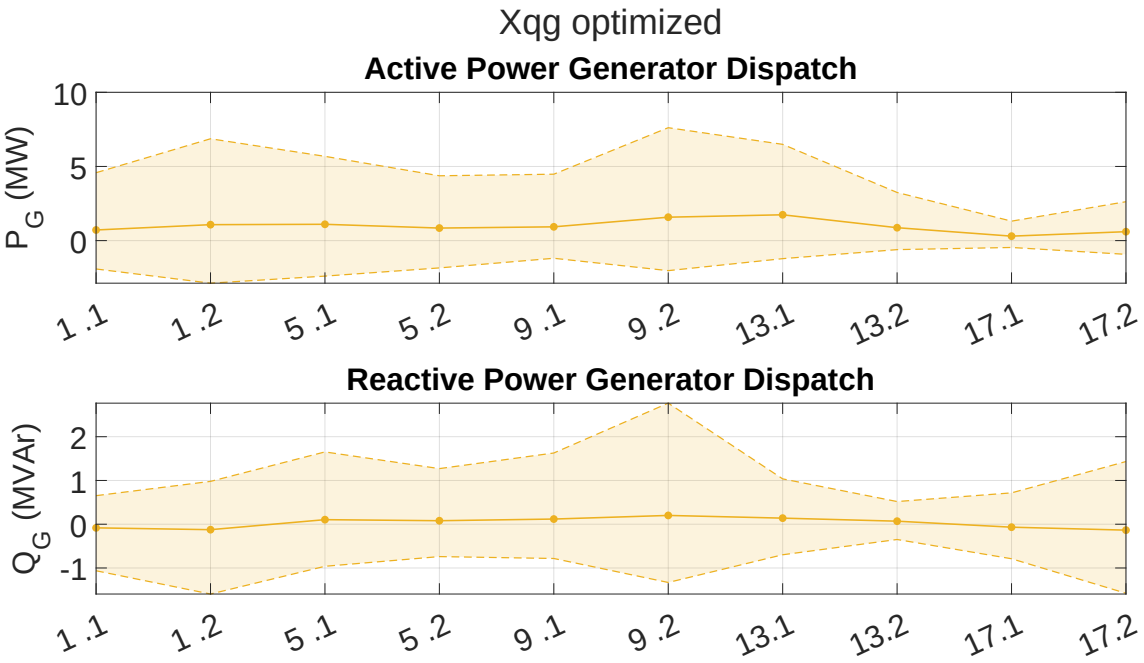

Figure A.15: Active- and reactive power generation of each substation for the optimization of $X_{q,g}$ case

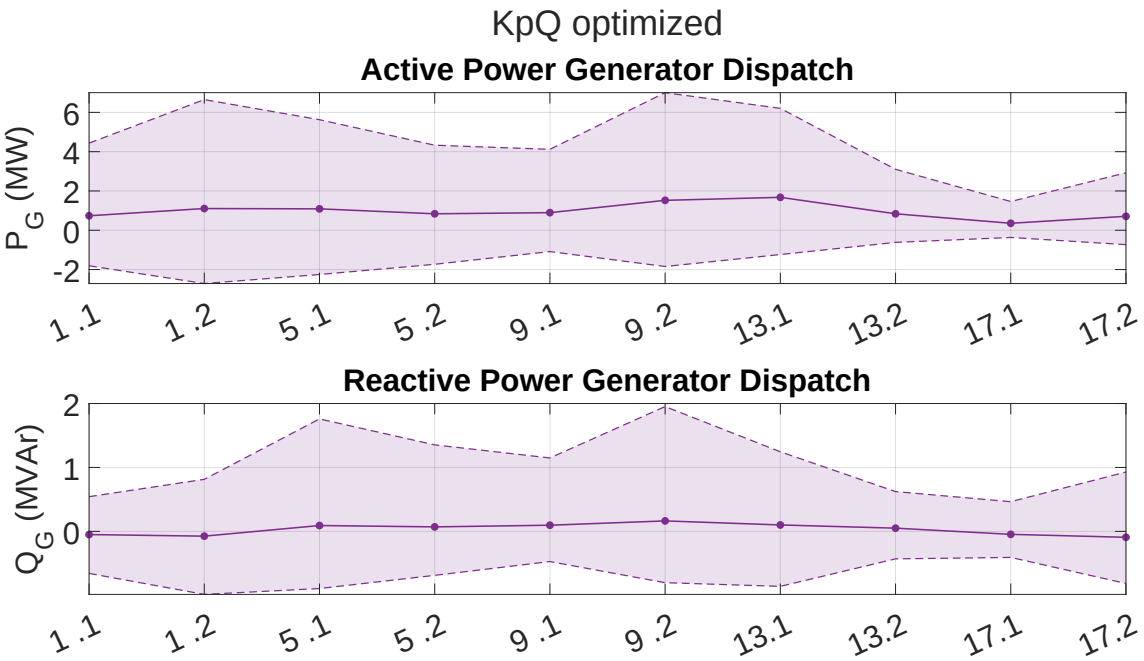

Figure A.16: Active- and reactive power generation of each substation for the optimization of $K_{P,Q}$ case

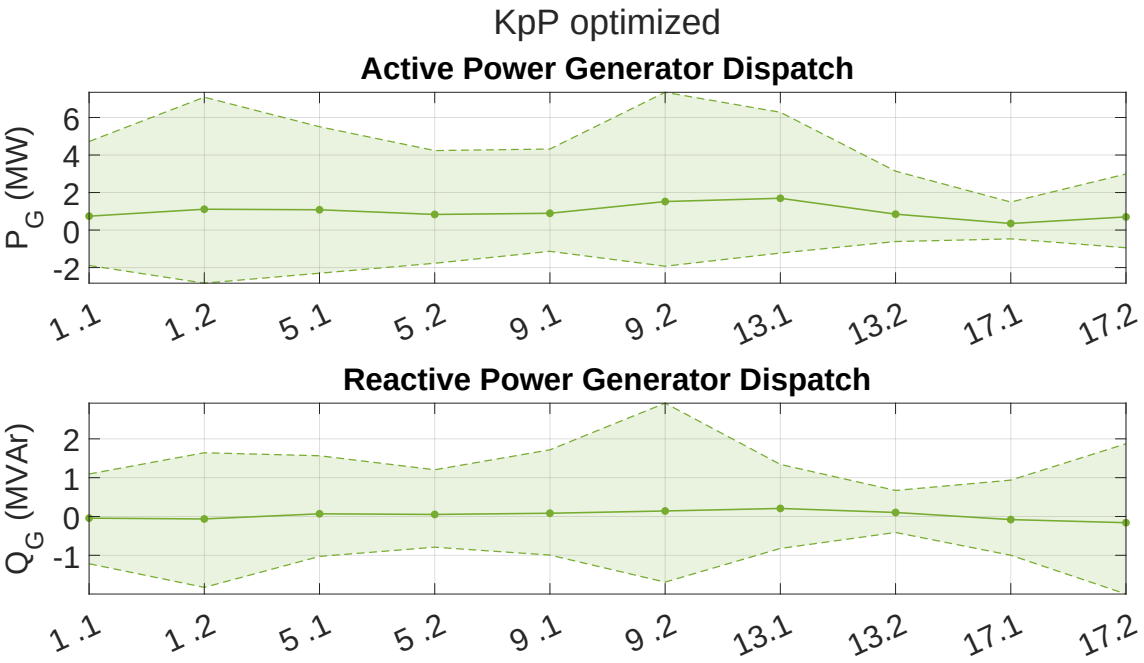

Figure A.17: Active- and reactive power generation of each substation for the optimization of $K_{\mathrm{p,P}}$ case

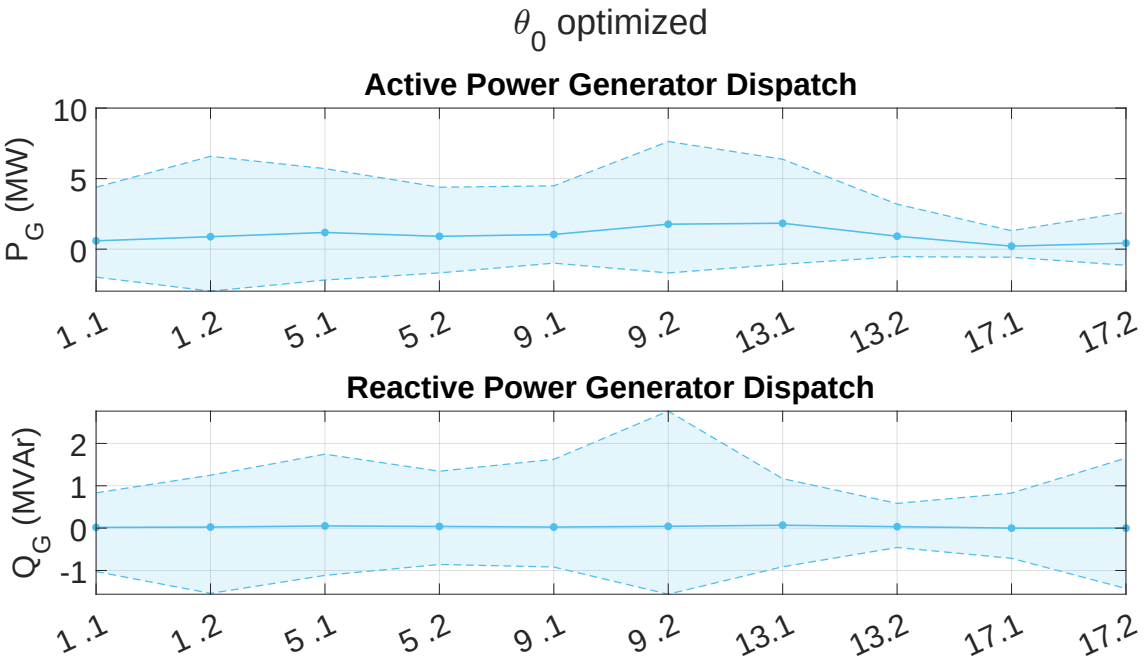

Figure A.18: Active- and reactive power generation of each substation for the optimization of θ_0 case

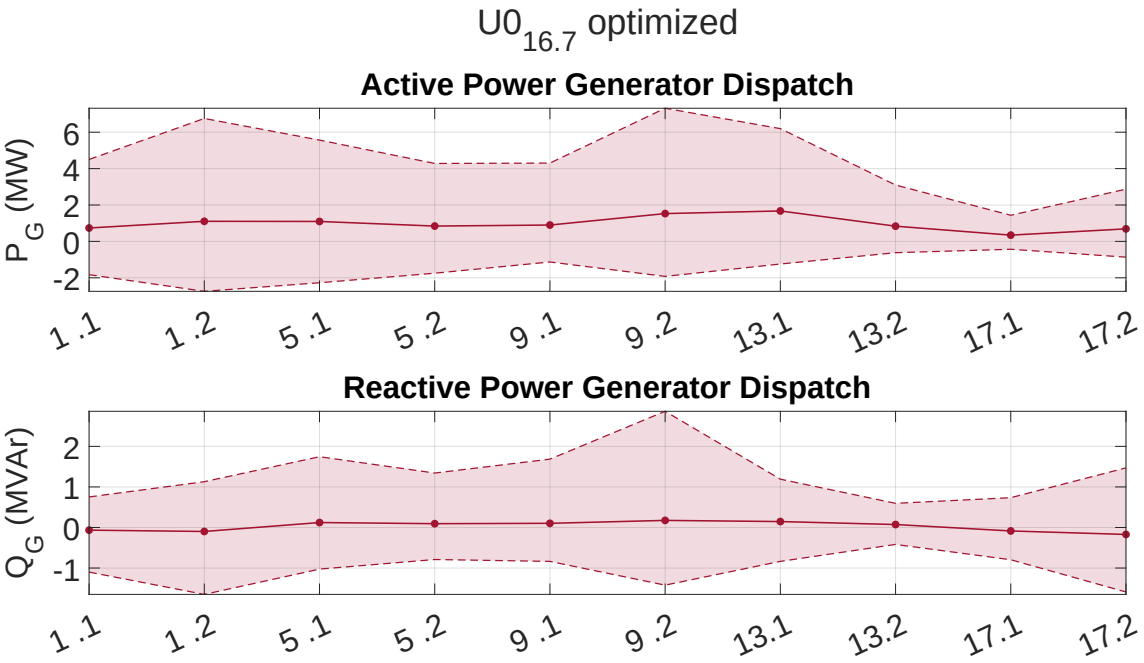

Figure A.19: Active- and reactive power generation of each substation for the optimization of $U_{0,16.7}$ case

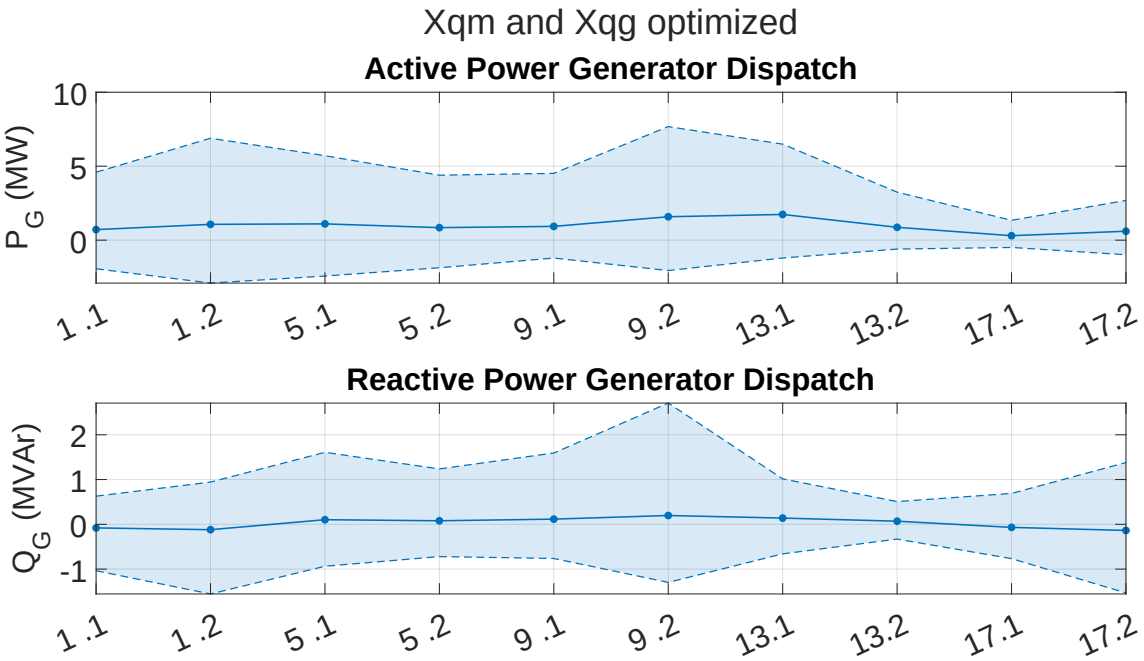

Figure A.20: Active- and reactive power generation of each substation for the optimization of $X_{\mathrm{q,m}}$ & $X_{\mathrm{q,g}}$ case

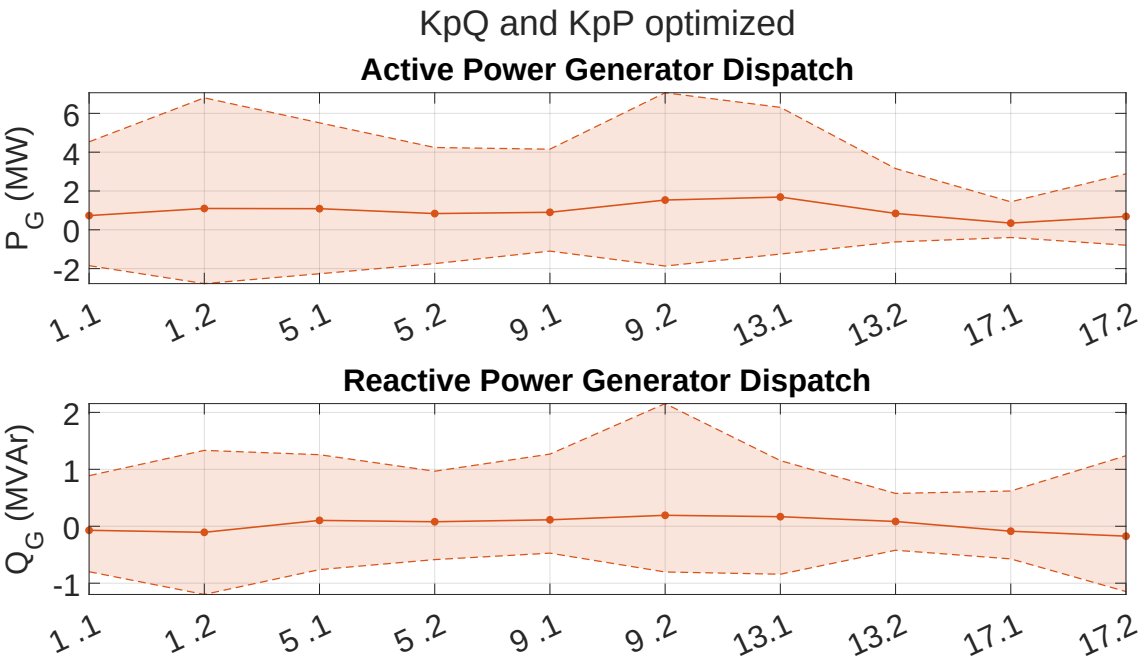

Figure A.21: Active- and reactive power generation of each substation for the optimization of $K_{\mathrm{p,Q}}$ & $K_{\mathrm{p,P}}$ case

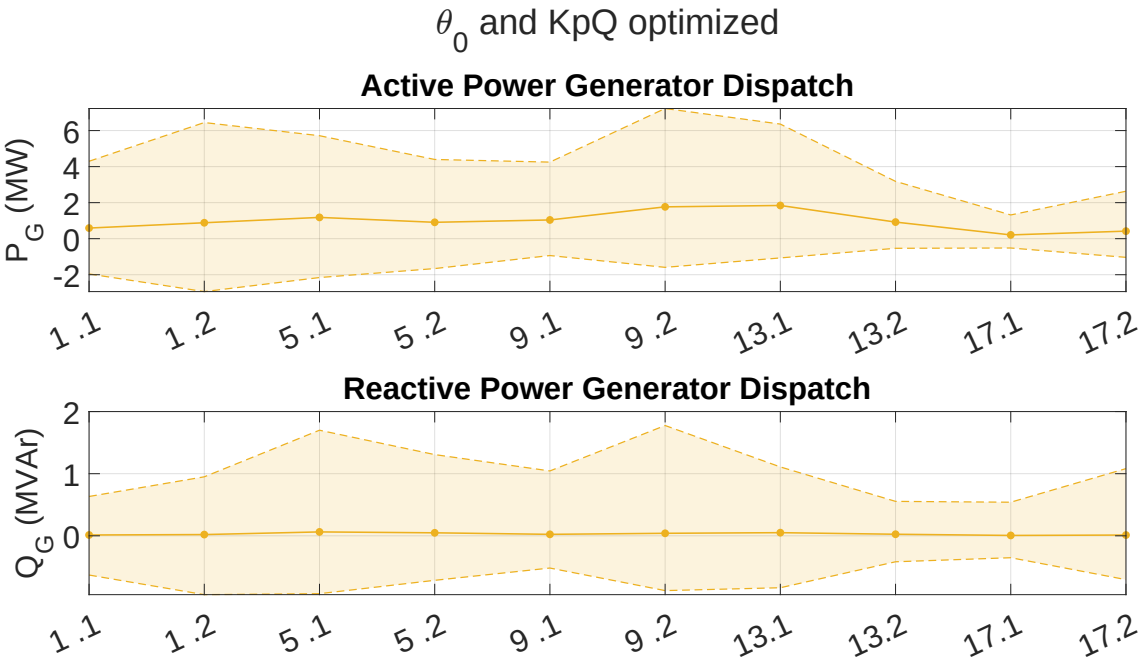

Figure A.22: Active- and reactive power generation of each substation for the optimization of θ_0 & $K_{\mathrm{p,Q}}$ case

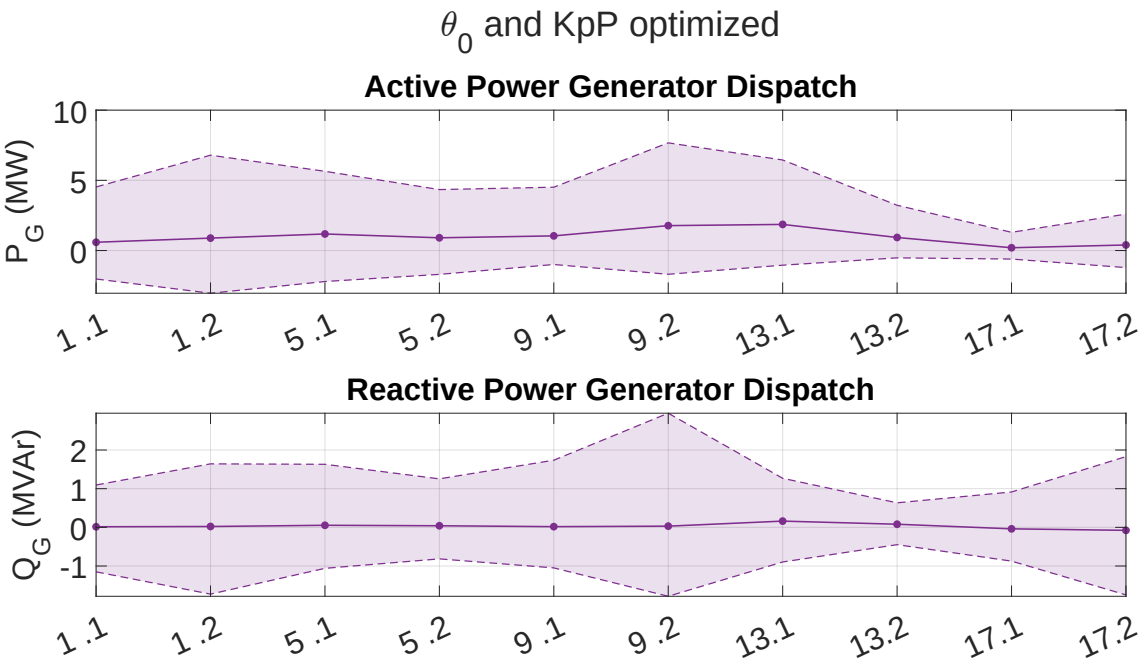

Figure A.23: Active- and reactive power generation of each substation for the optimization of θ_0 & $K_{\mathrm{p,P}}$ case

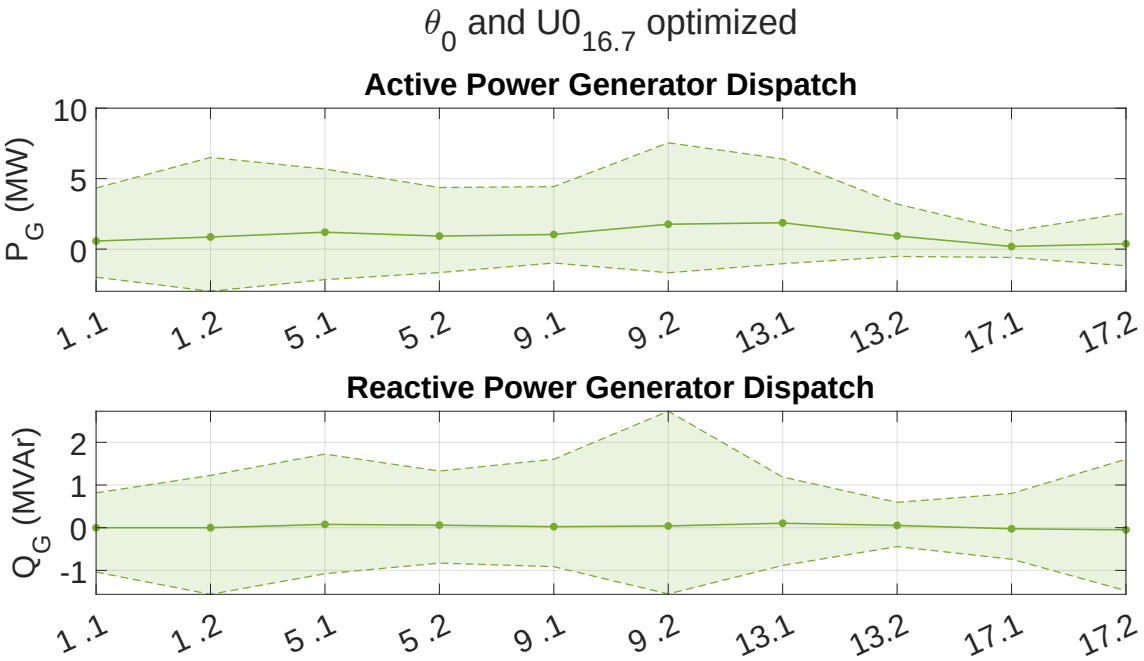

Figure A.24: Active- and reactive power generation of each substation for the optimization of θ_0 & $U_{0,16.7}$ case

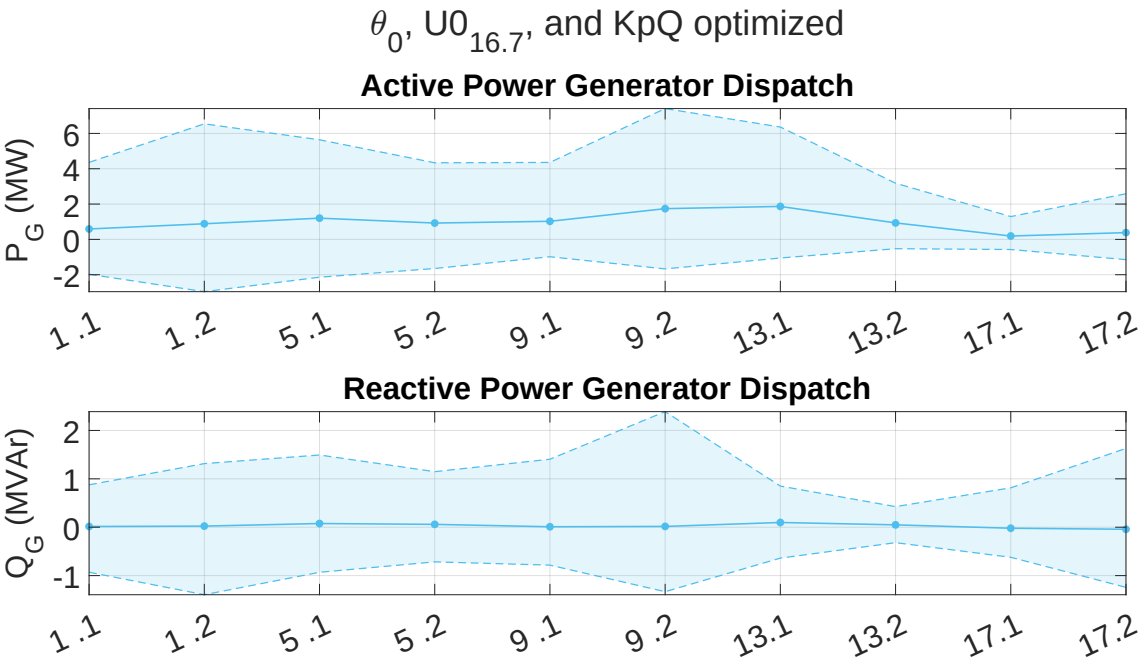

Figure A.25: Active- and reactive power generation of each substation for the optimization of θ_0 & $U_{0,16.7}$ & $K_{p,Q}$ case

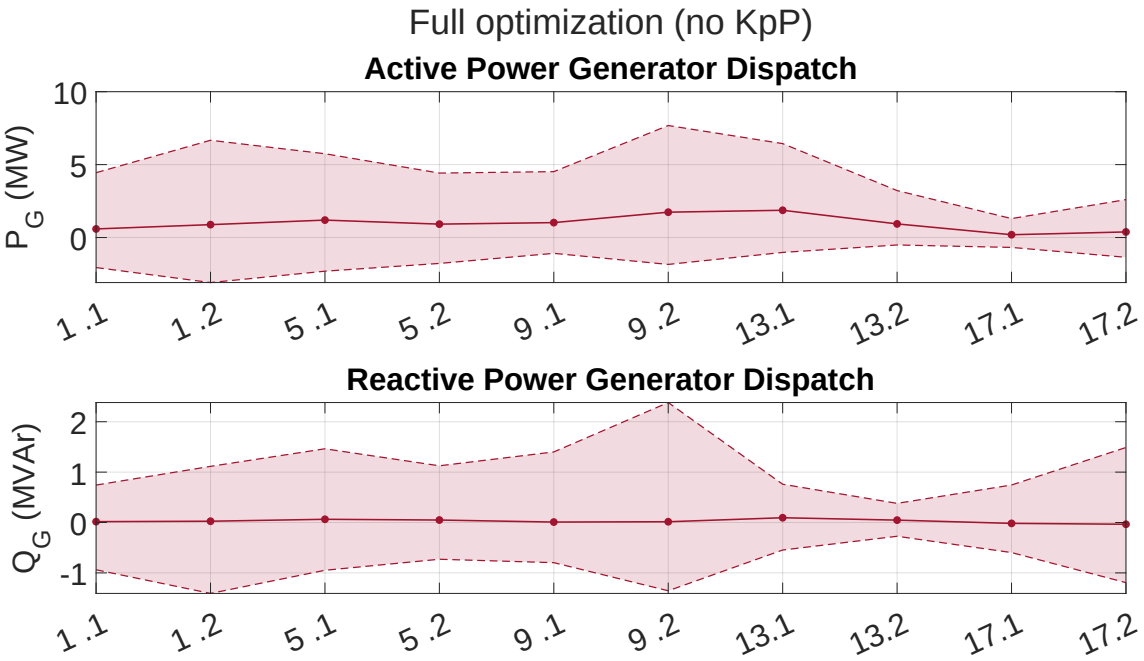

Figure A.26: Active- and reactive power generation of each substation for the full optimization without $K_{\mathrm{k,P}}$

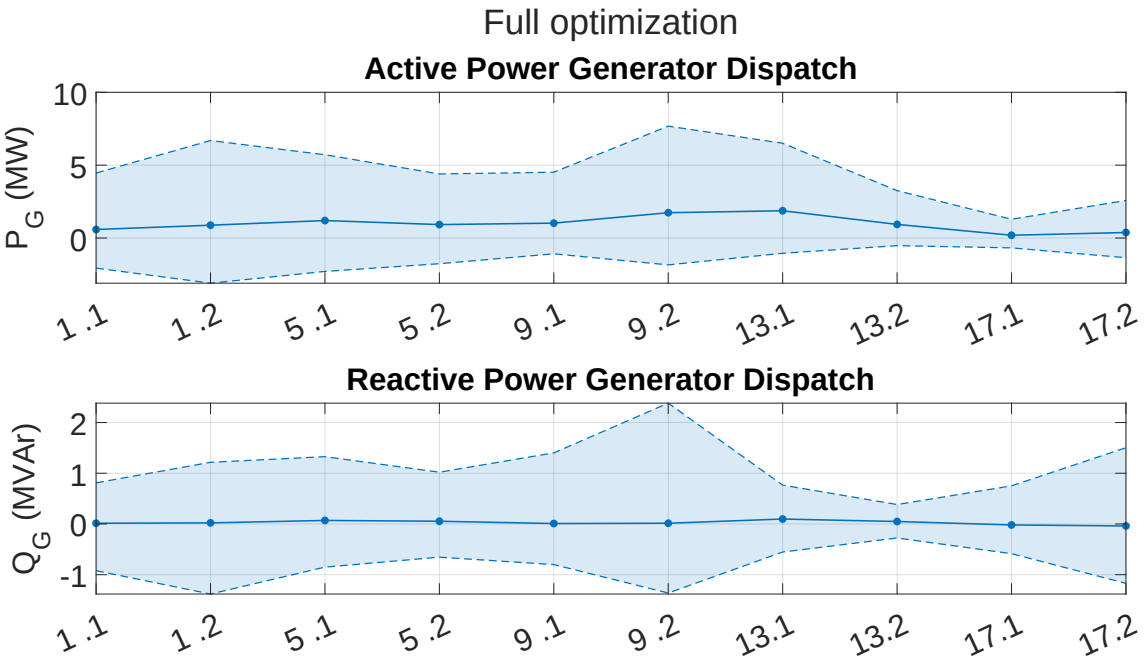

Figure A.27: Active- and reactive power generation of each substation for the full optimization with $K_{\mathrm{k,P}}$

A.4.2 BT-system

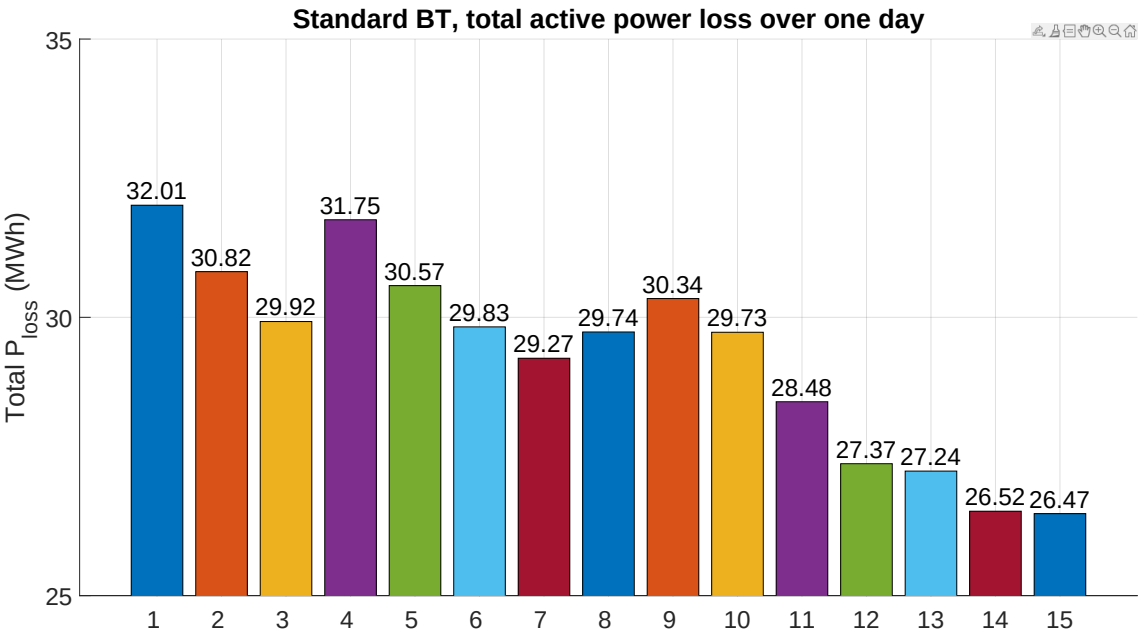

Figure A.28: Total system losses for each scenario in MWh

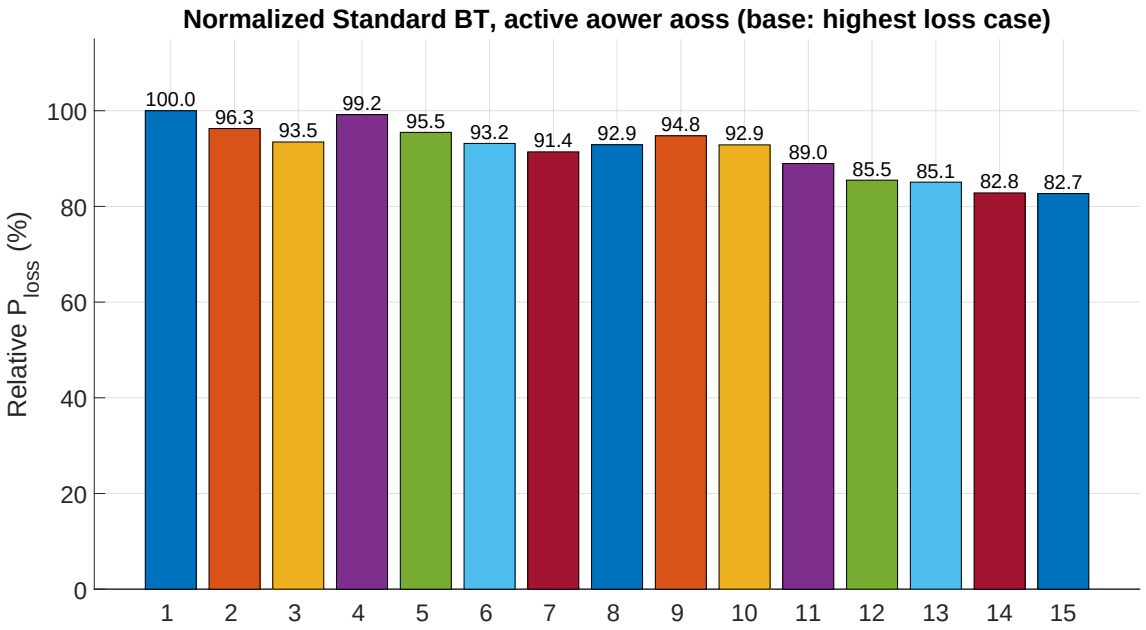

Figure A.29: Total system losses for each scenario in %, normalized in relation to the all fixed case

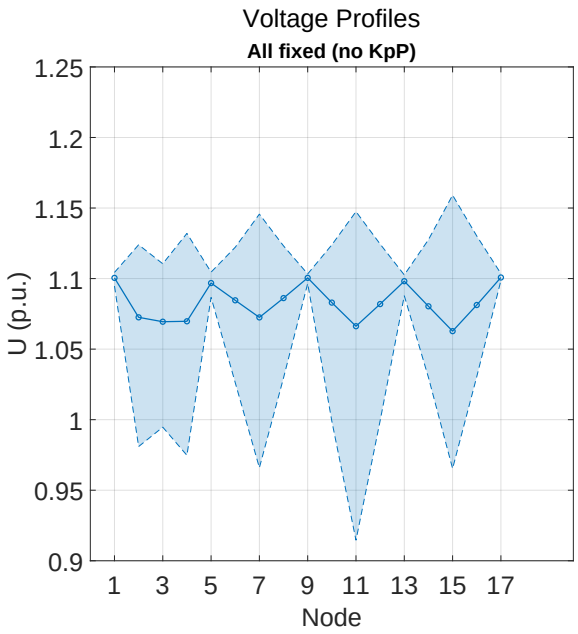

Figure A.30: Voltage profile for the all fixed case of the representative BT-system

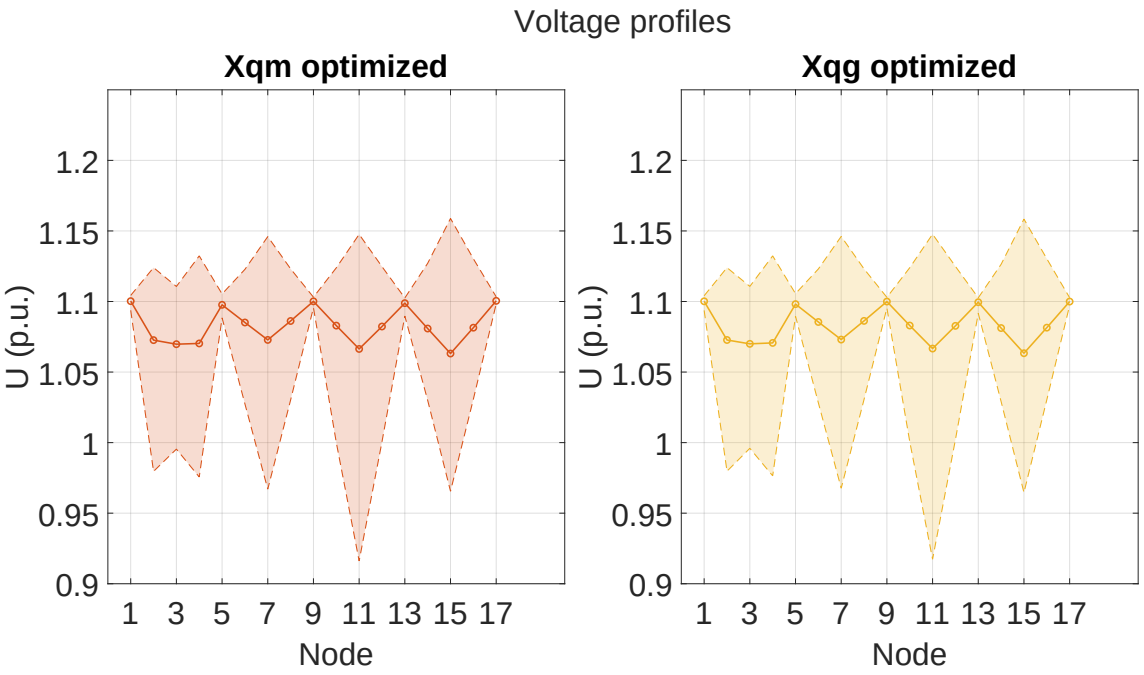

Figure A.31: Voltage profile for the optimization of $X_{\mathrm{q,m}}$ and $X_{\mathrm{q,g}}$ cases for the representative BT-system

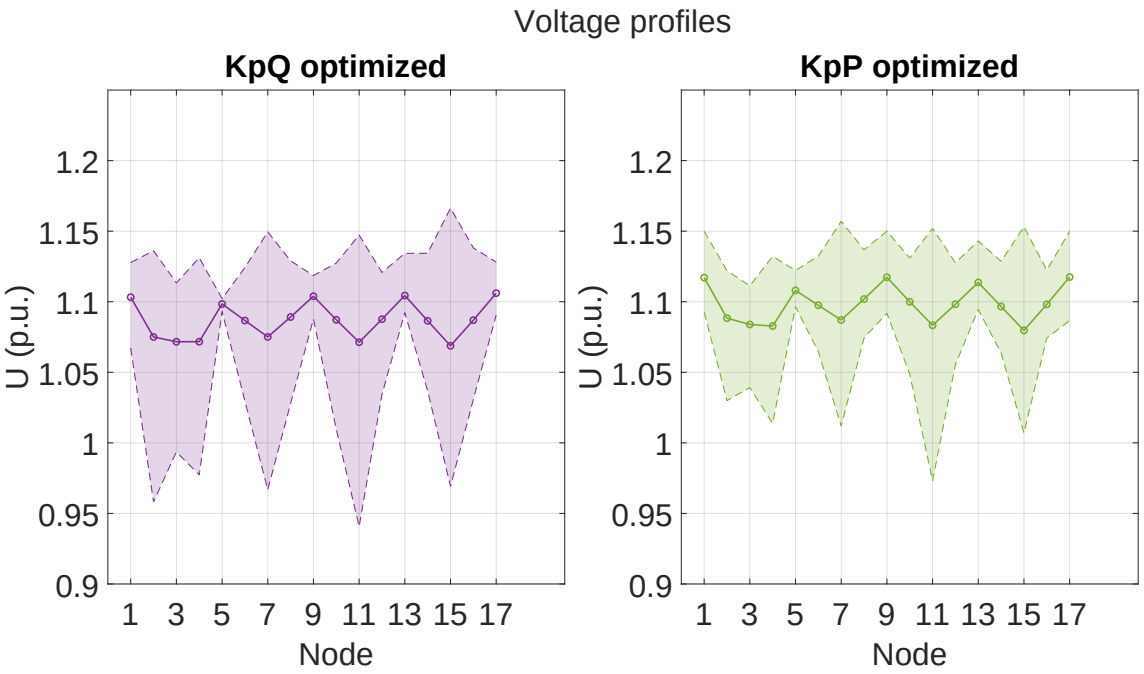

Figure A.32: Voltage profile for the optimization of $K_{\mathrm{p,Q}}$ and $K_{\mathrm{p,P}}$ cases for the representative BT-system

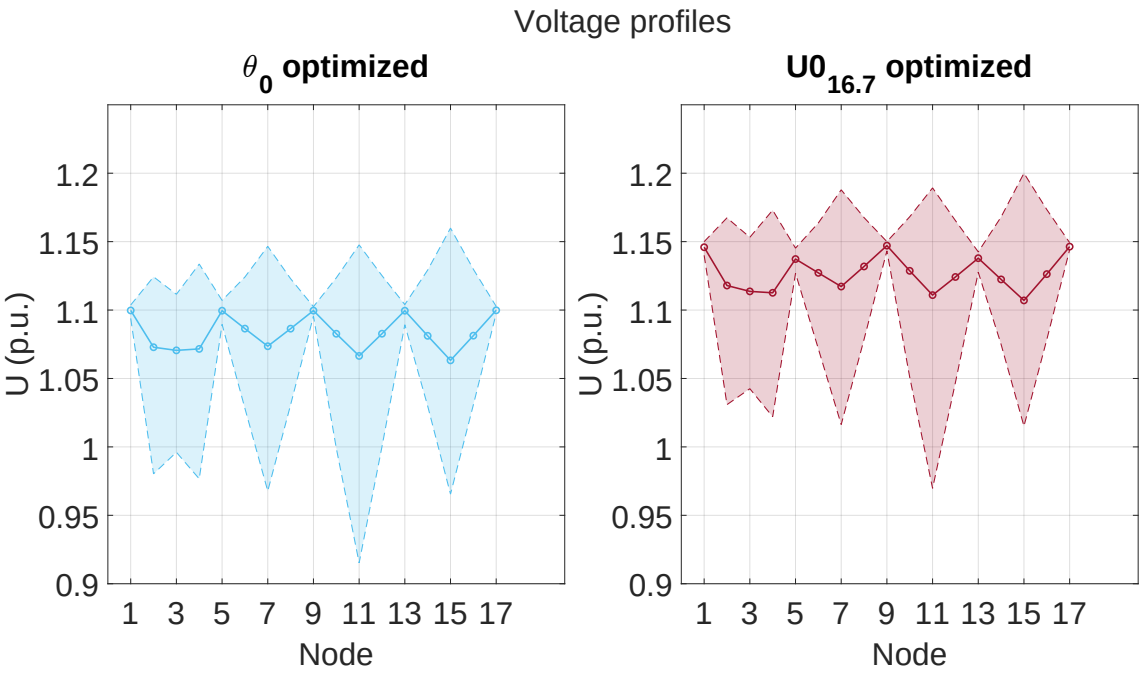

Figure A.33: Voltage profile for the optimization of θ_0 and $U_{0,16.7}$ cases for the representative BT-system

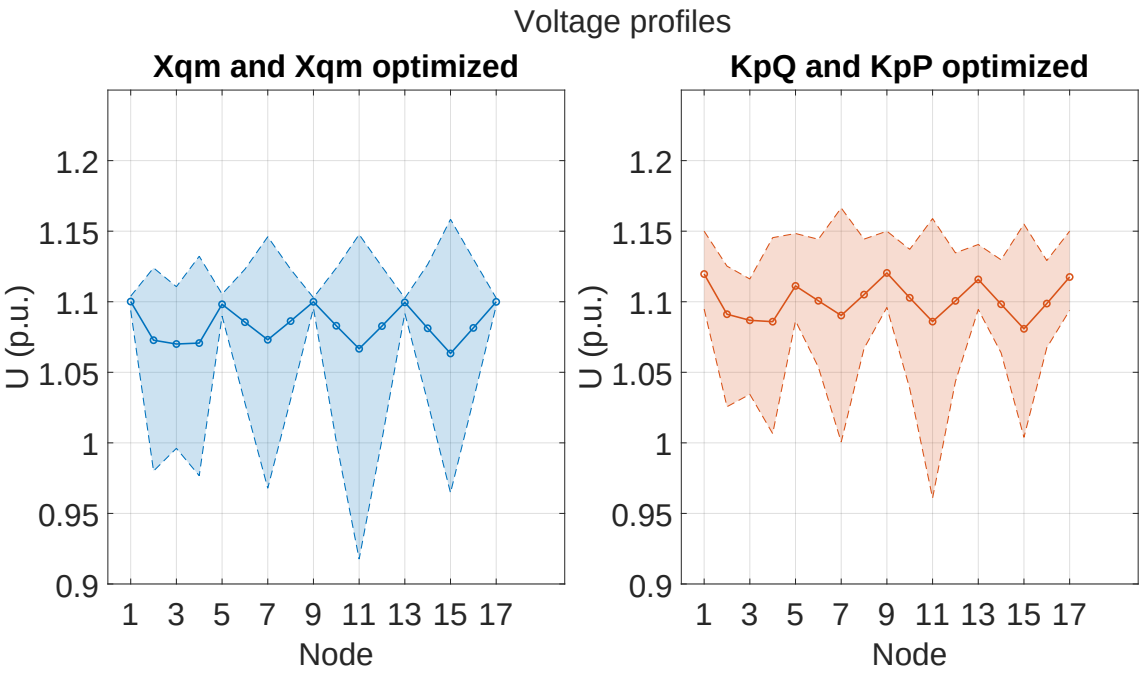

Figure A.34: Voltage profile for the optimization of $X_{\mathrm{q,m}}$ & $X_{\mathrm{q,g}}$ and $K_{\mathrm{p,Q}}$ & $K_{\mathrm{p,P}}$ cases for the representative BT-system

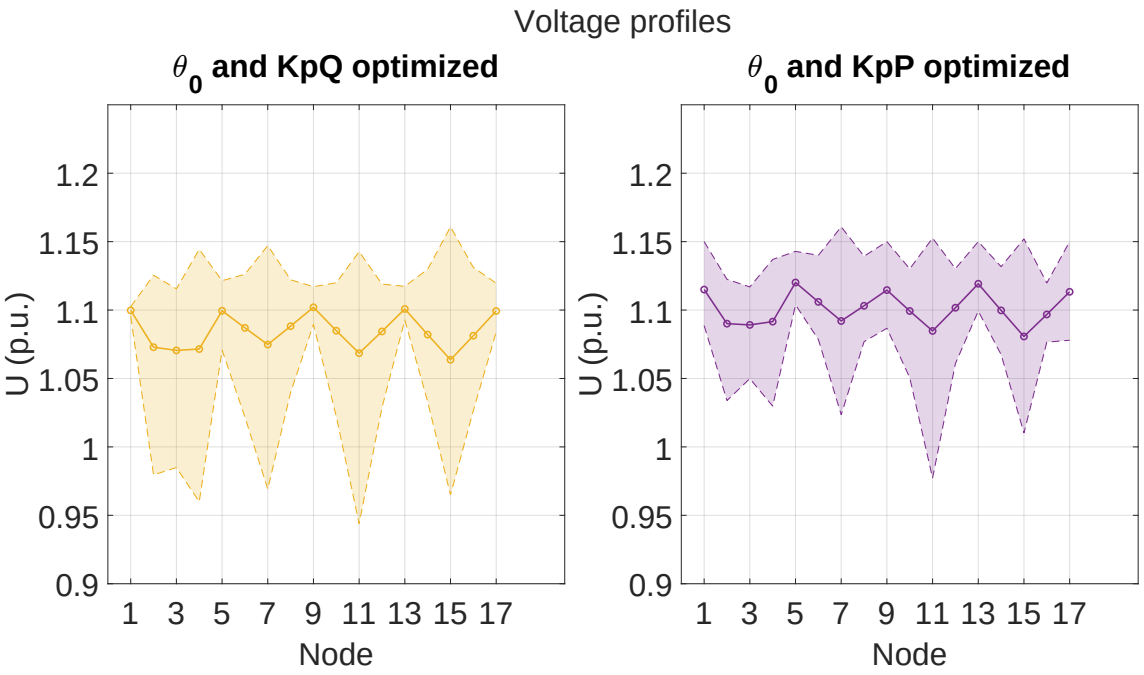

Figure A.35: Voltage profile for the optimization of θ_0 & $K_{\mathrm{p,Q}}$ and θ_0 & $K_{\mathrm{p,P}}$ cases for the representative BT-system

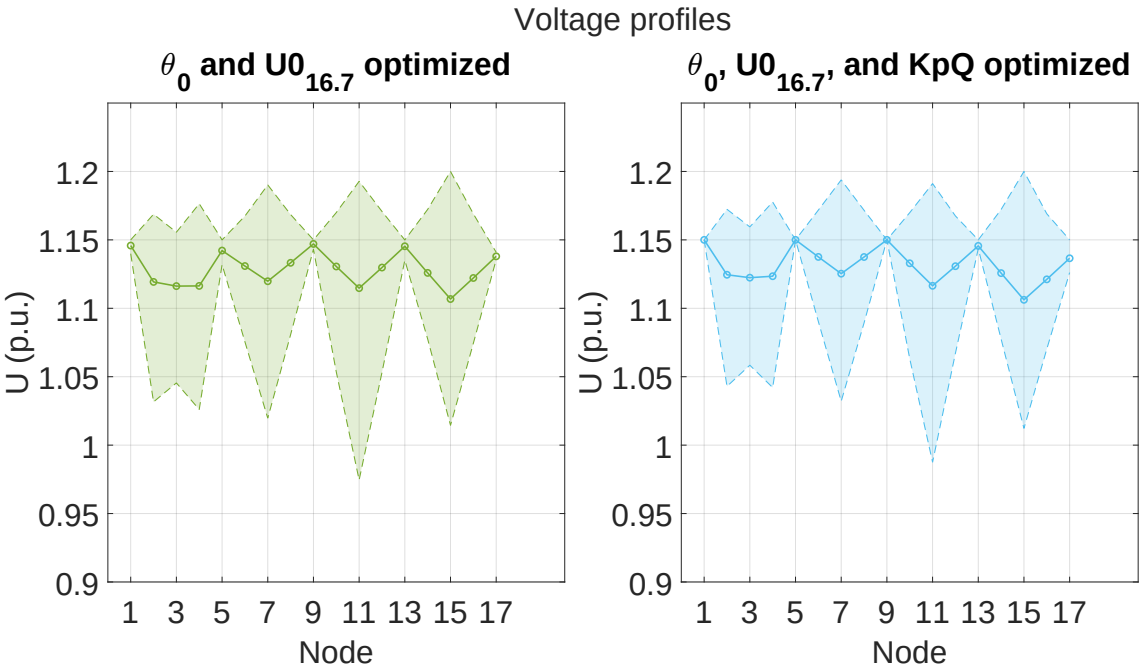

Figure A.36: Voltage profile for the optimization of θ_0 & $U_{0,16.7}$ and θ_0 & $U_{0,16.7}$ & $K_{\mathrm{p,Q}}$ cases for the representative BT-system

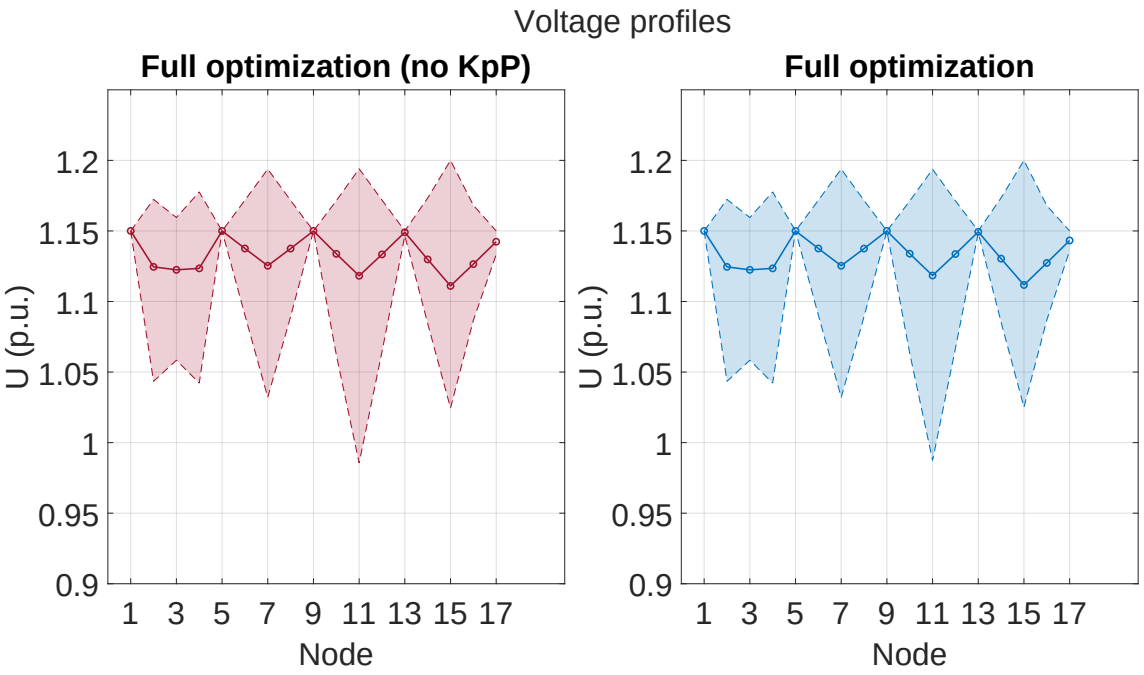

Figure A.37: Voltage profile for the full optimization with- and without $K_{\mathrm{p,P}}$

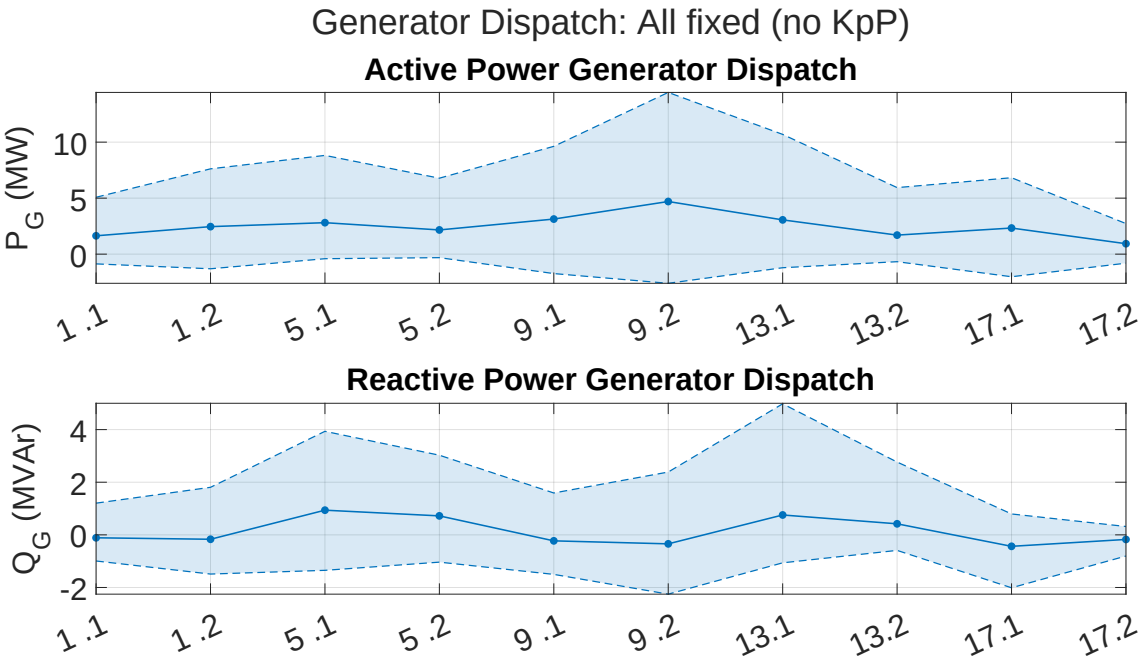

Figure A.38: Active- and reactive power generation of each substation for the all fixed case, without $K_{\mathrm{p,P}}$

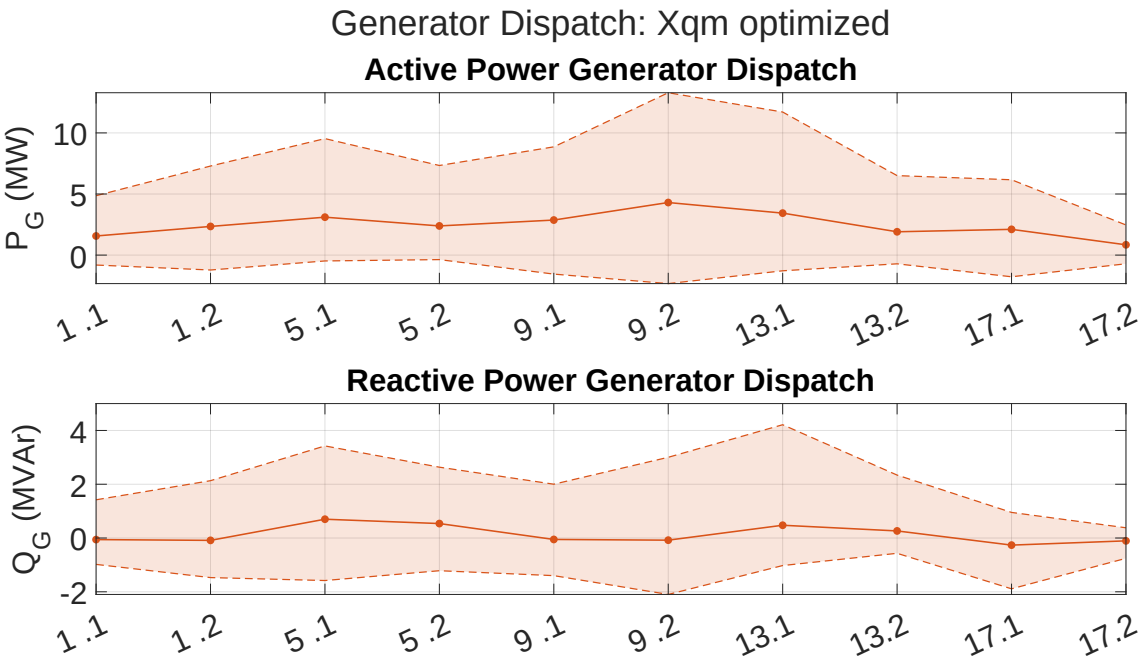

Figure A.39: Active- and reactive power generation of each substation for the optimization of $X_{\mathrm{q,m}}$ case

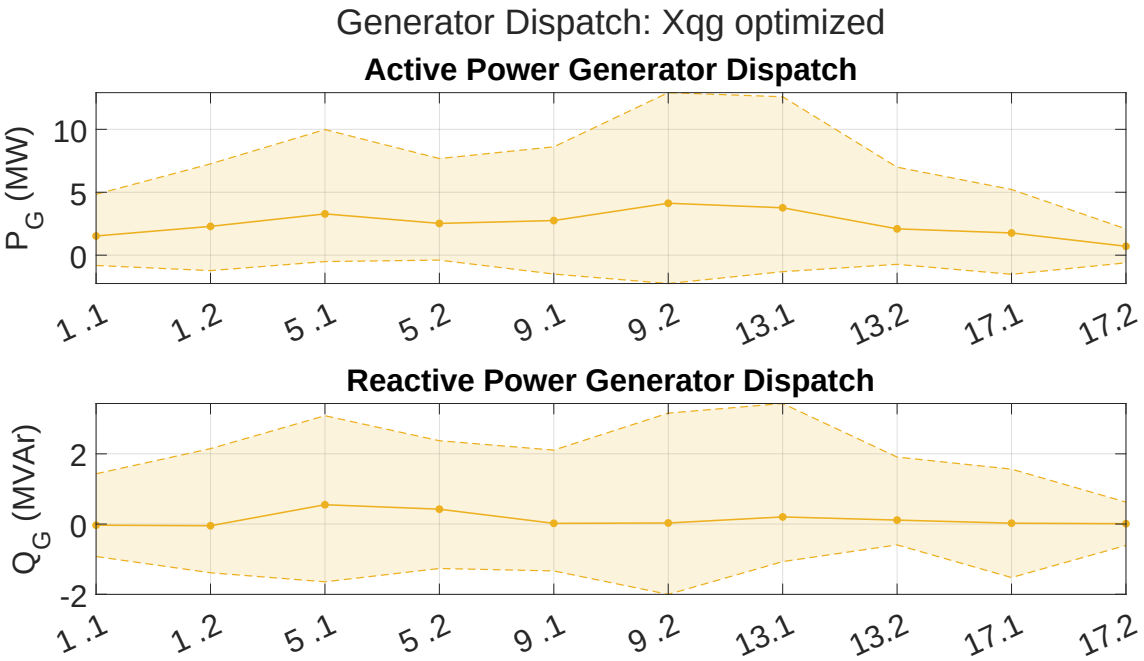

Figure A.40: Active- and reactive power generation of each substation for the optimization of $X_{\mathrm{q,g}}$ case

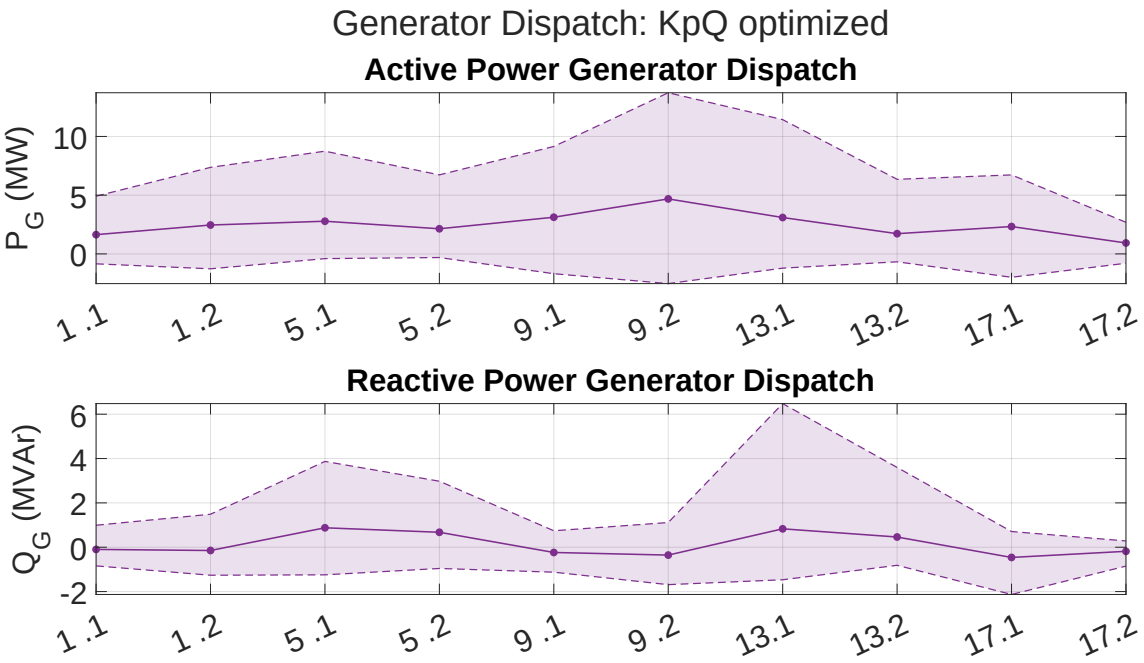

Figure A.41: Active- and reactive power generation of each substation for the optimization of $K_{\mathrm{p,Q}}$ case

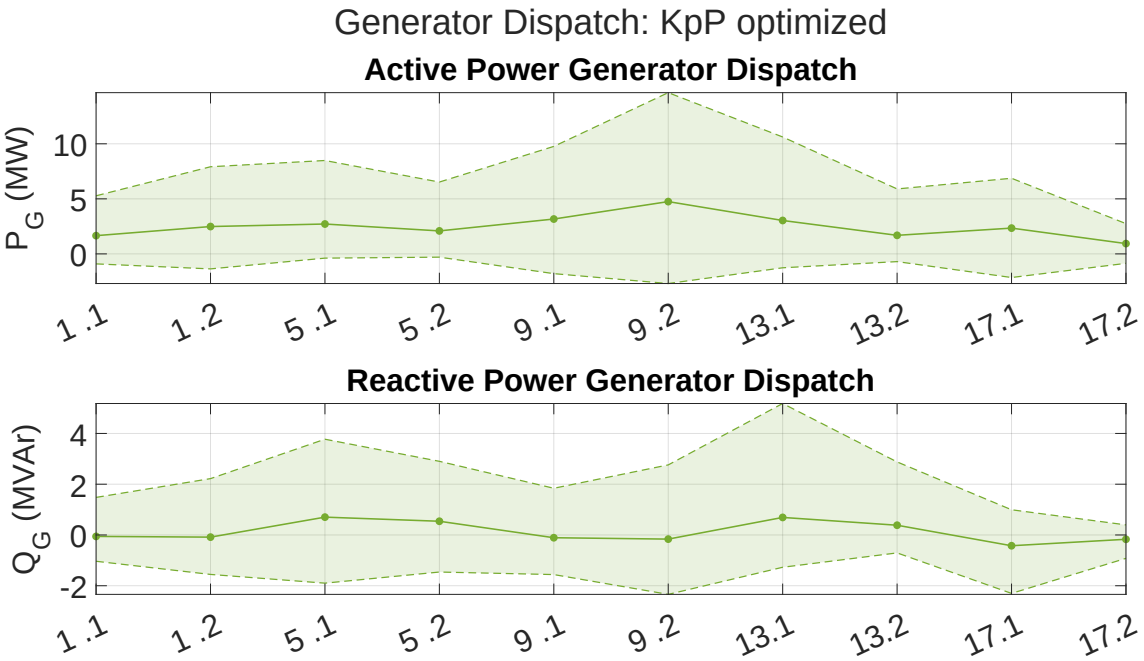

Figure A.42: Active- and reactive power generation of each substation for the optimization of $K_{\mathrm{p,P}}$ case

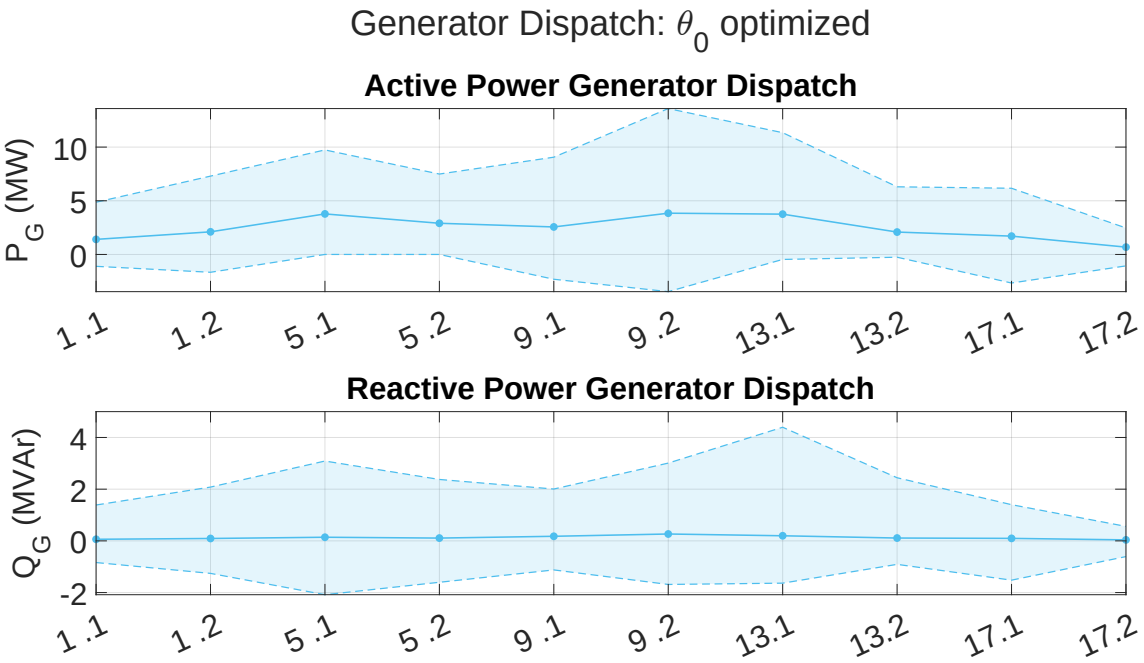

Figure A.43: Active- and reactive power generation of each substation for the optimization of θ_0 case

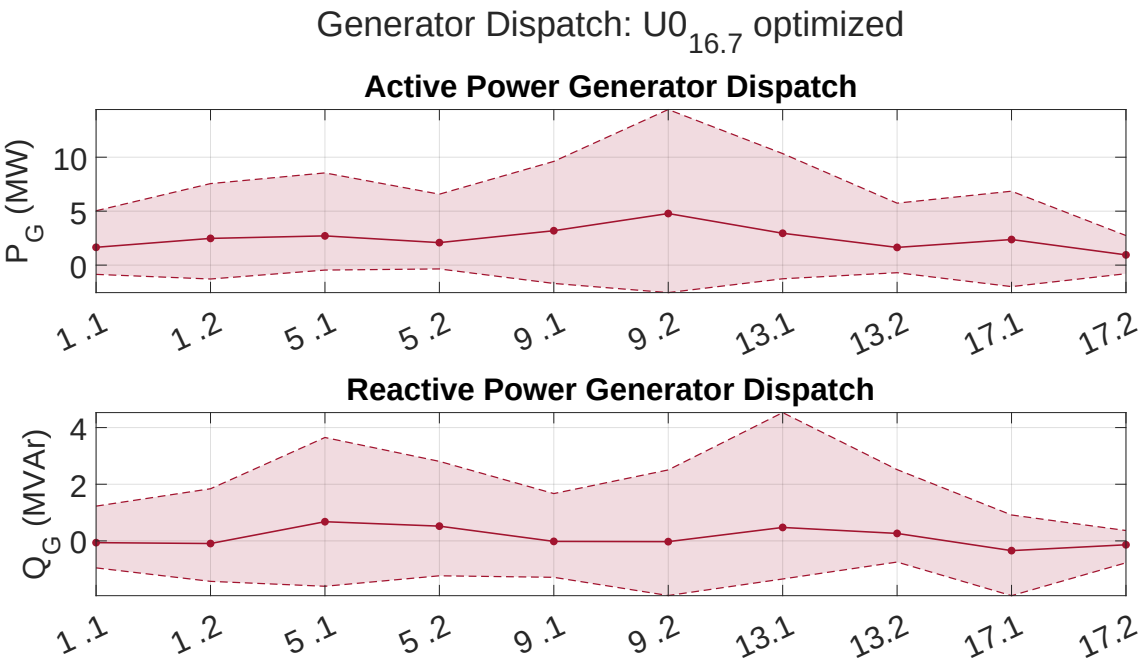

Figure A.44: Active- and reactive power generation of each substation for the optimization of $U_{0,16.7}$ case

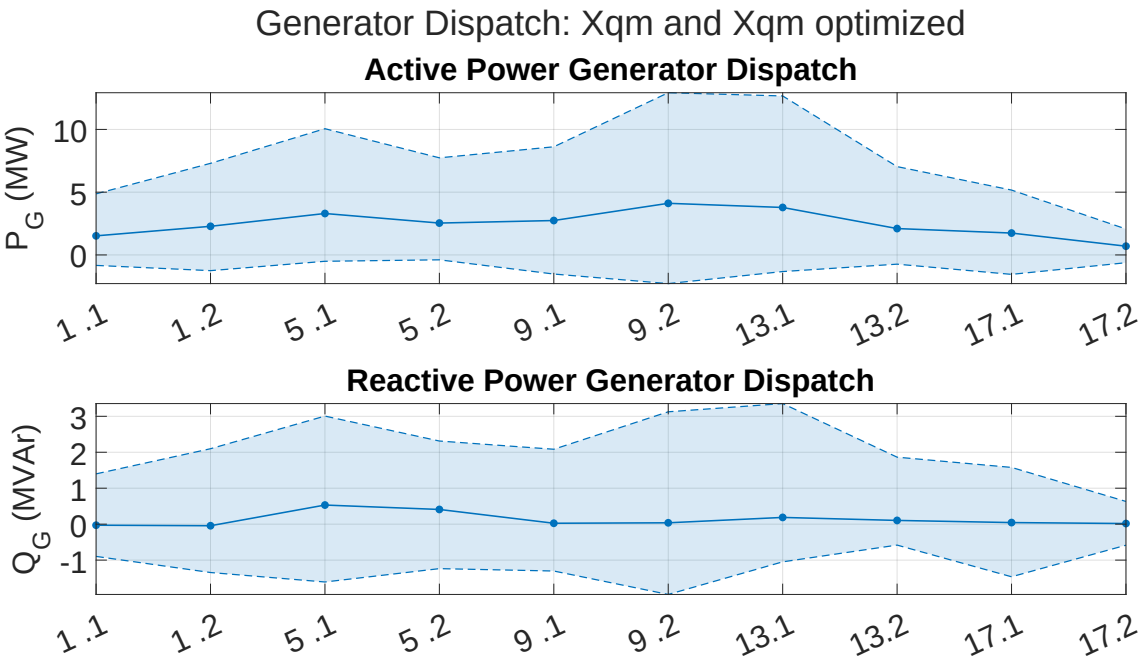

Figure A.45: Active- and reactive power generation of each substation for the optimization of $X_{\mathrm{q,m}}$ & $X_{q,g}$ case

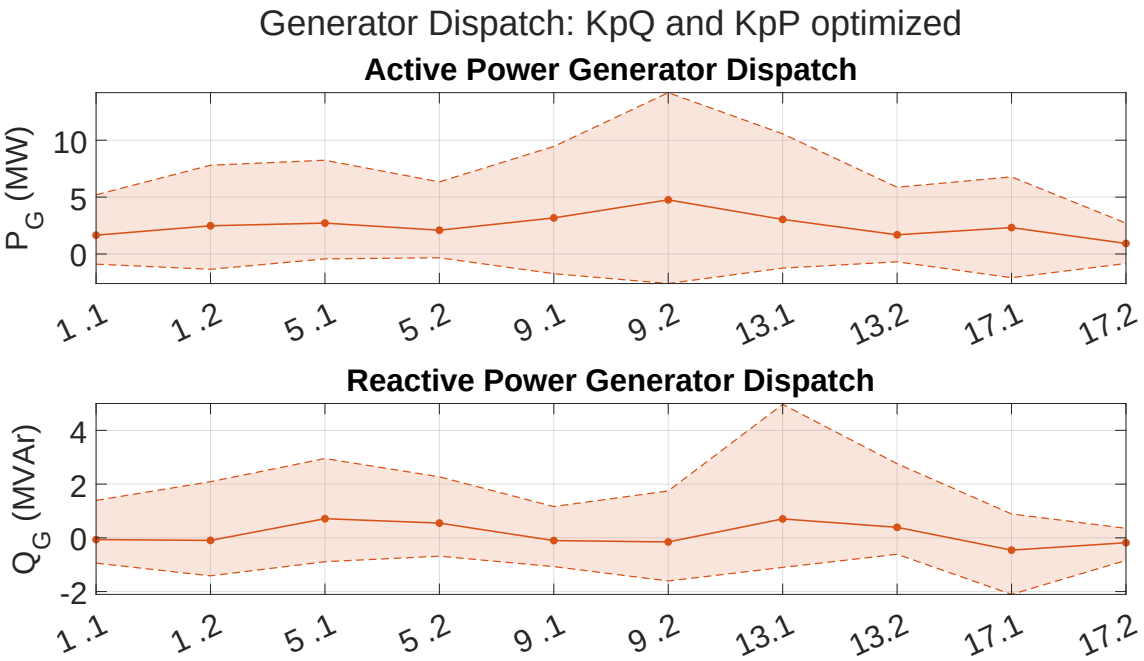

Figure A.46: Active- and reactive power generation of each substation for the optimization of $K_{\mathrm{p,Q}}$ & $K_{p,P}$ case

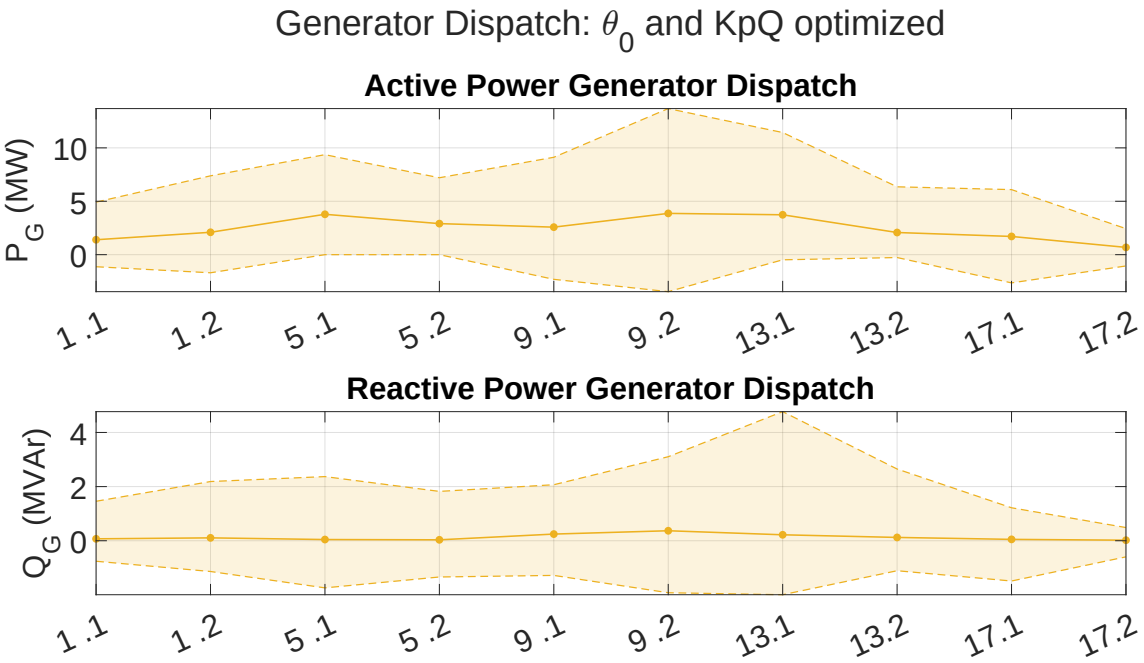

Figure A.47: Active- and reactive power generation of each substation for the optimization of θ_0 & $K_{p,Q}$ case

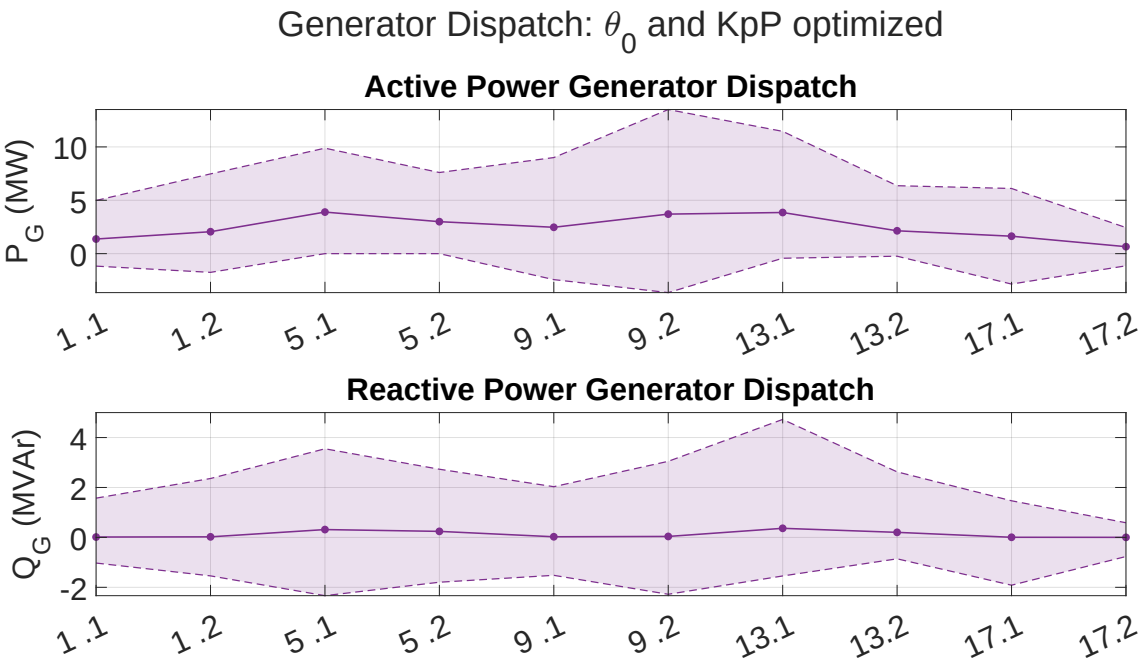

Figure A.48: Active- and reactive power generation of each substation for the optimization of θ_0 & $K_{p,P}$ case

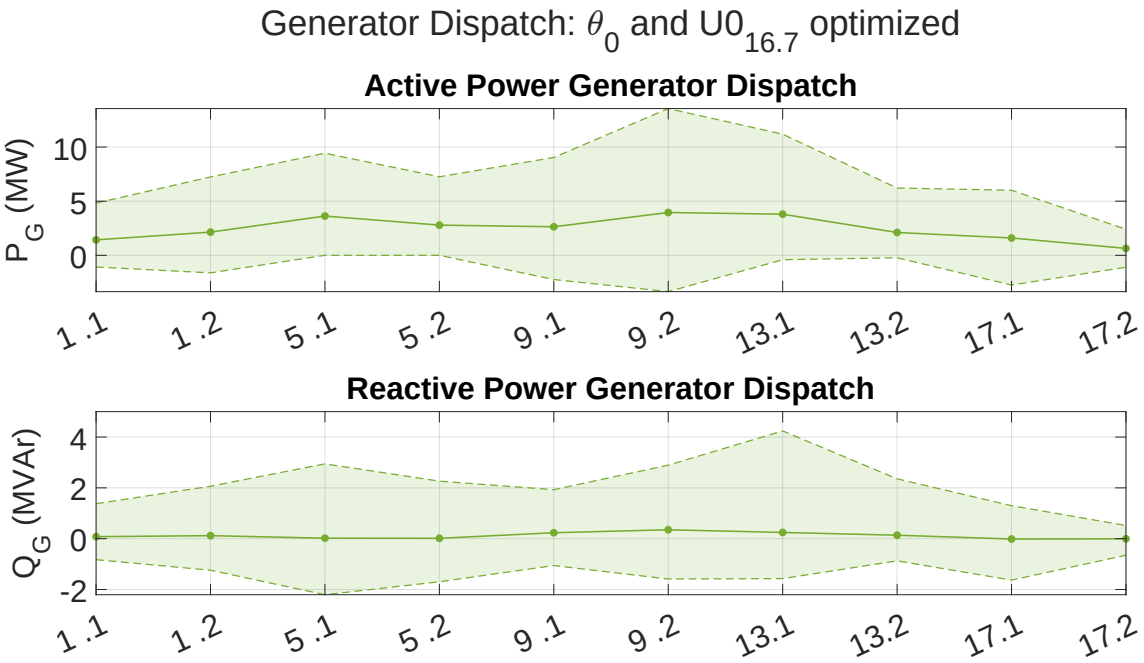

Figure A.49: Active- and reactive power generation of each substation for the optimization of θ_0 & $U_{0,16.7}$ case

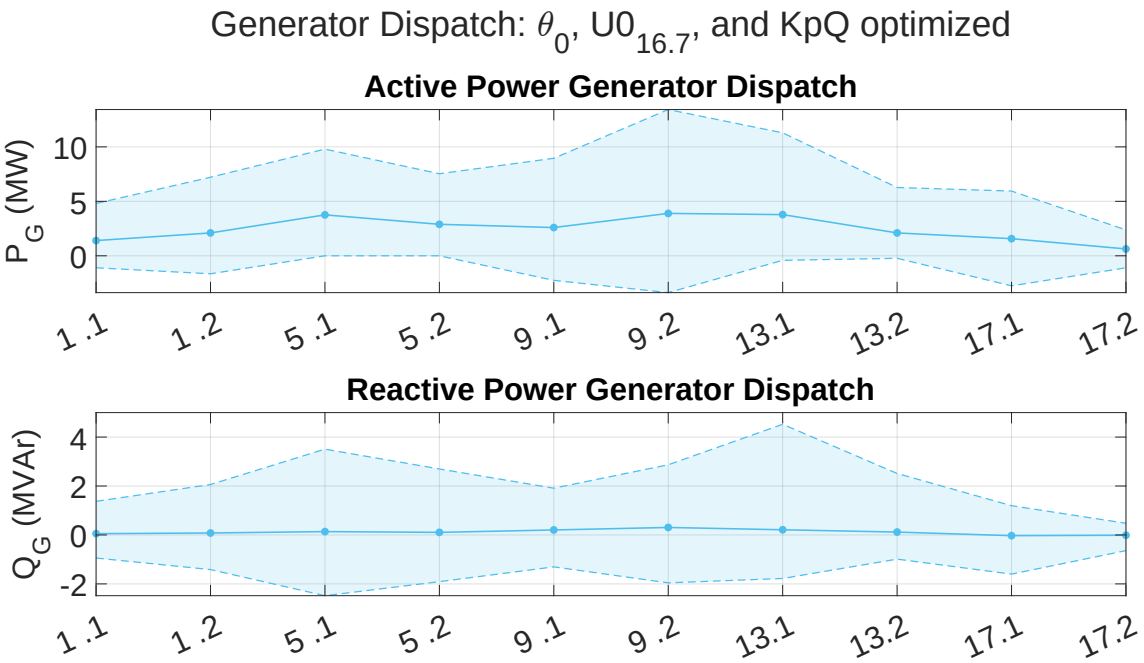

Figure A.50: Active- and reactive power generation of each substation for the optimization of θ_0 & $U_{0,16.7}$ & $K_{p,Q}$ case

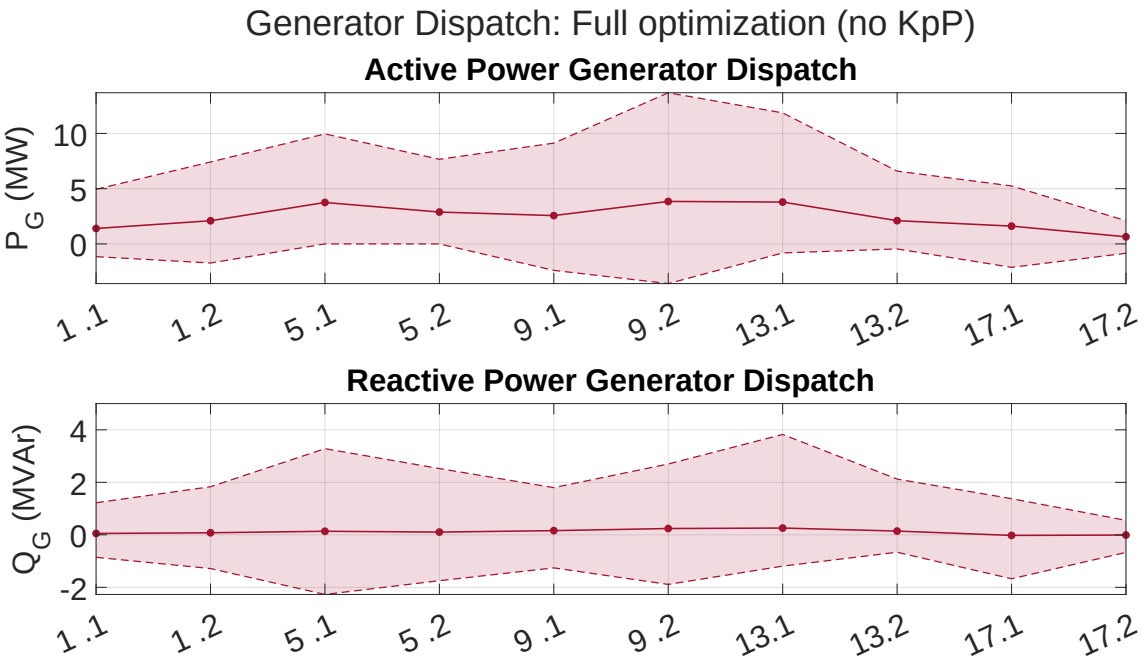

Figure A.51: Active- and reactive power generation of each substation for the full optimization case without $K_{p,P}$

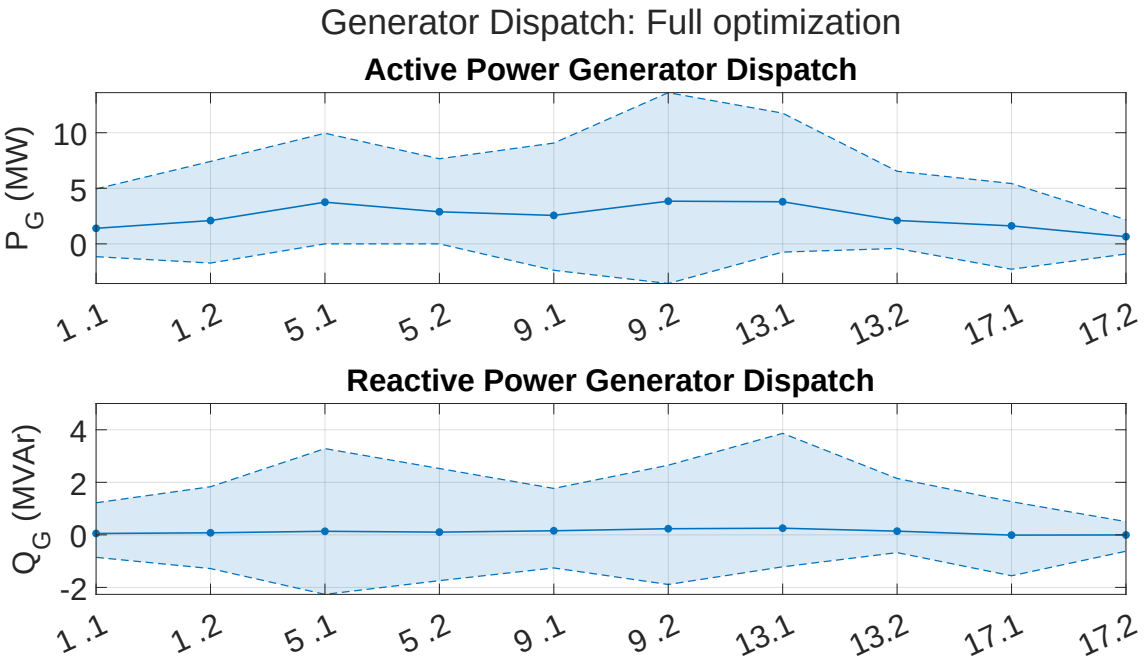

Figure A.52: Active- and reactive power generation of each substation for the full optimization case with $K_{p,P}$

A.5 Results from the simulation for the system with exaggerated converter sizes

This section contains the results from the simulation with exaggerated converter sizes for both the AT- and BT-system.

A.5.1 AT-system

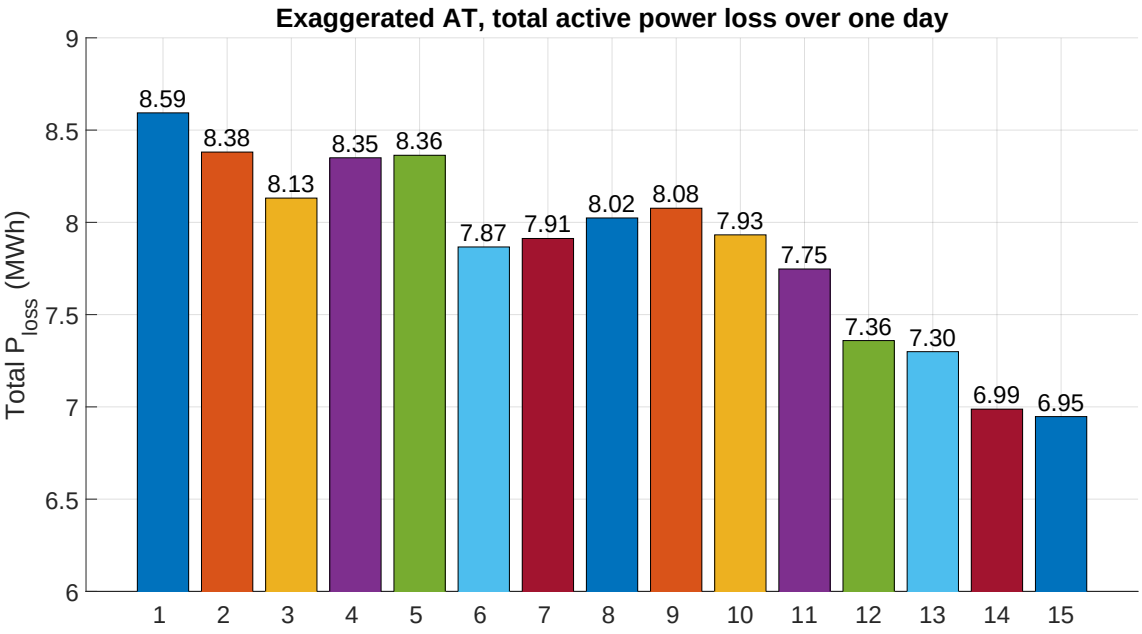

Figure A.53: Total system losses for each scenario in MWh

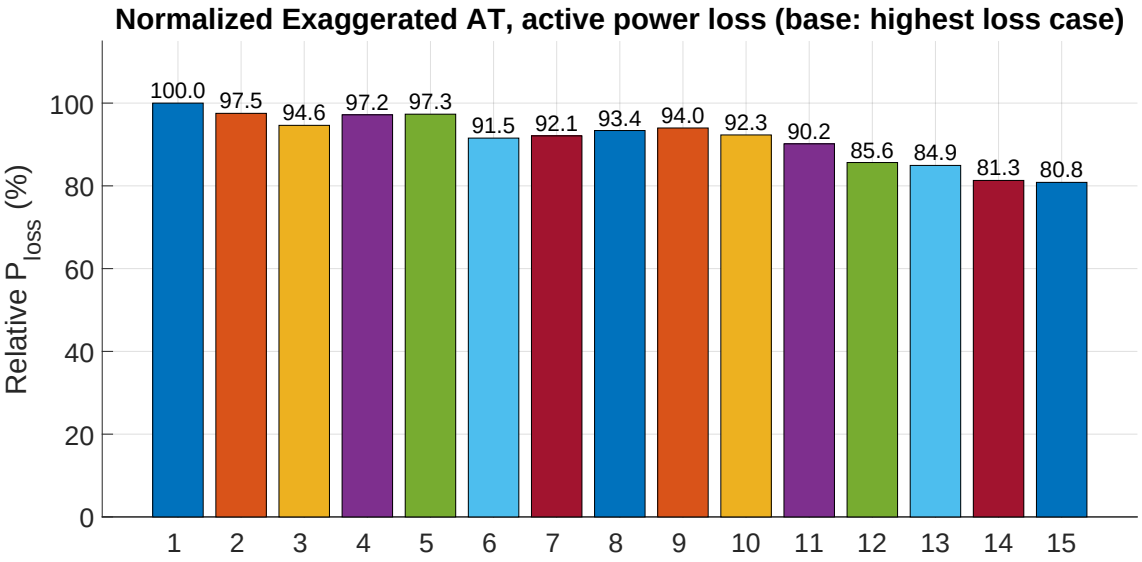

Figure A.54: Total system losses for each scenario in %, normalized in relation to the all fixed case

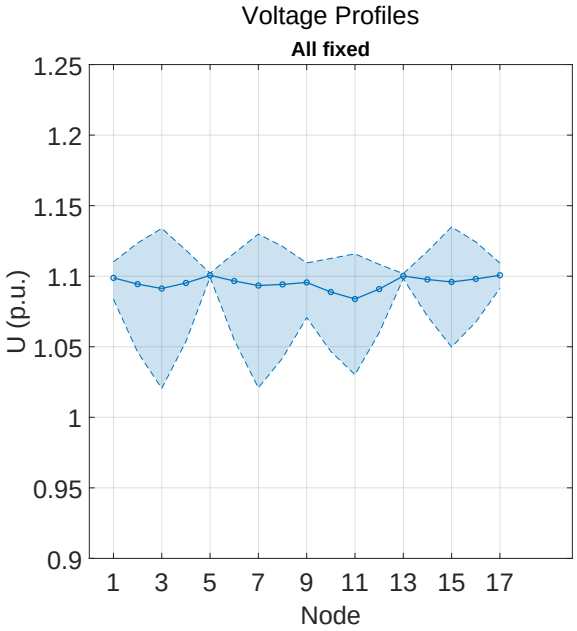

Figure A.55: Voltage profile for the all fixed case

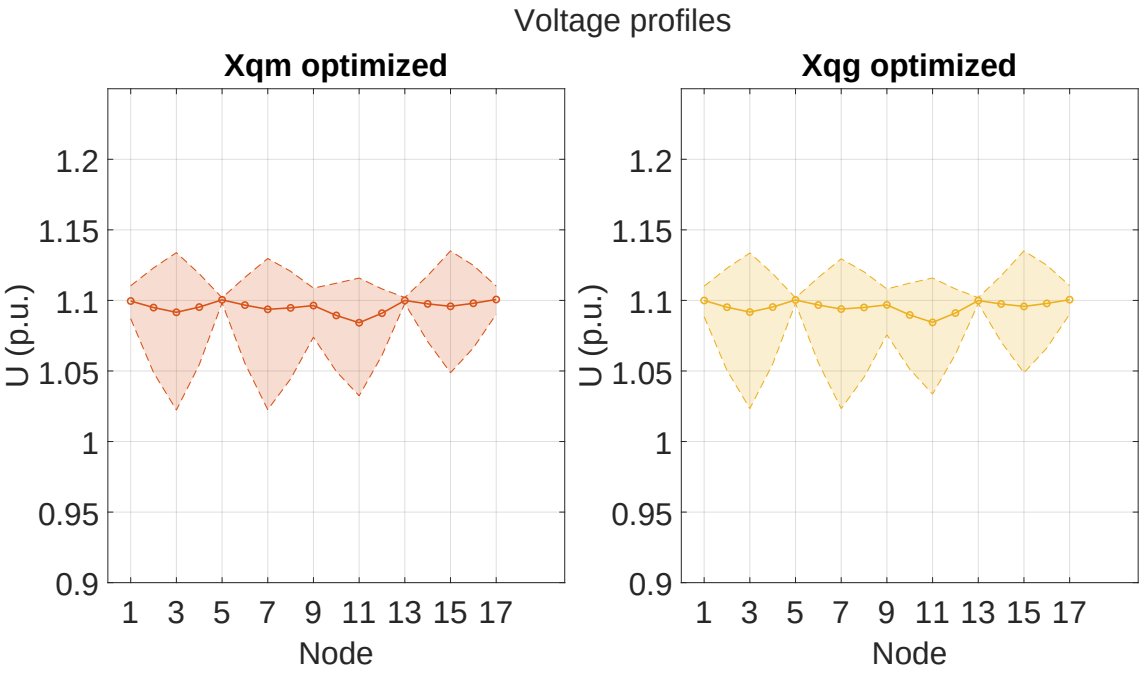

Figure A.56: Voltage profile for the optimization of the $X_{\mathrm{q,m}}$ and $X_{\mathrm{q,g}}$ cases

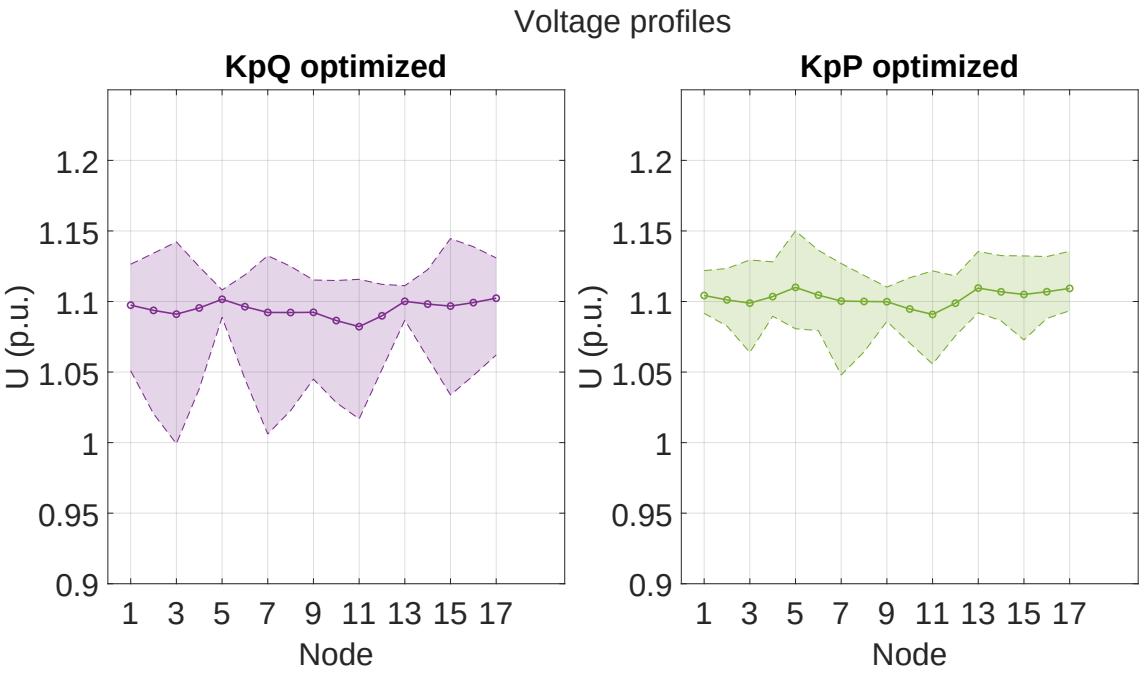

Figure A.57: Voltage profile for the optimization of the $K_{\mathrm{p,Q}}$ and $K_{\mathrm{p,P}}$ cases

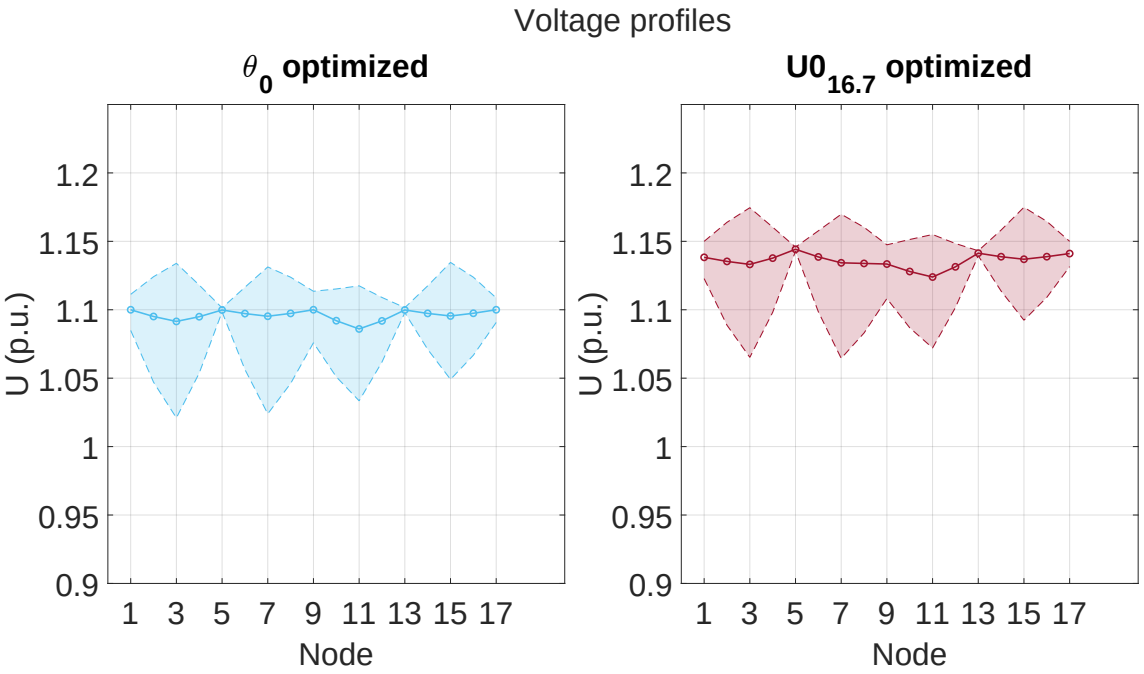

Figure A.58: Voltage profile for the optimization of the θ_0 and $U_{0,16.7}$ cases

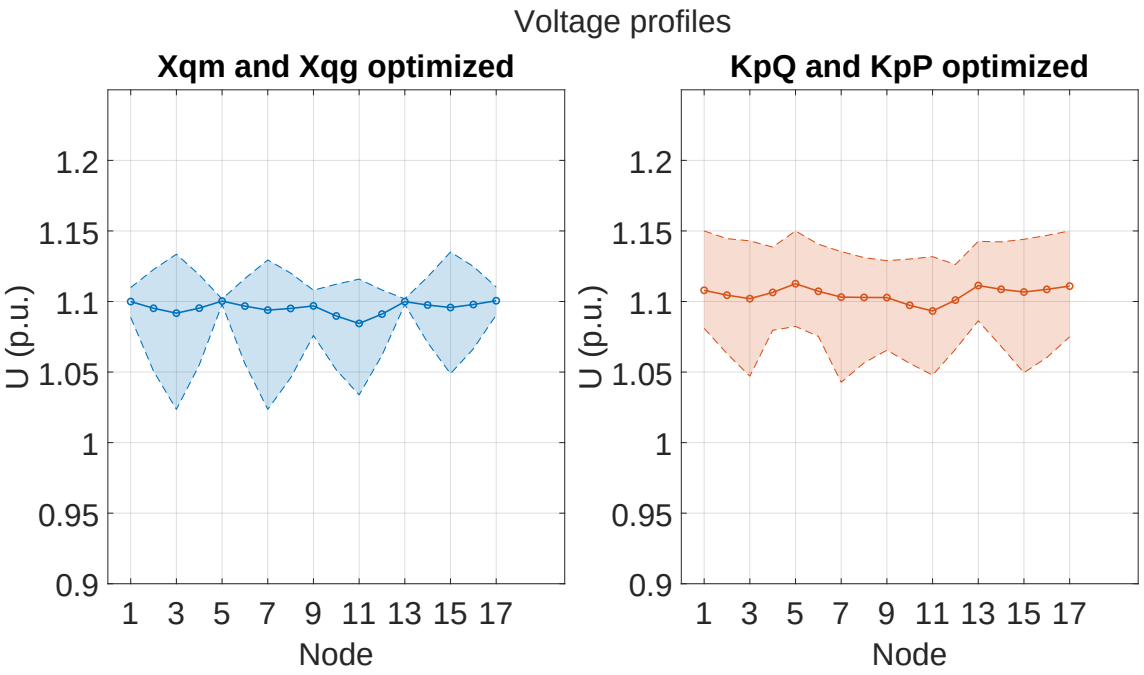

Figure A.59: Voltage profile for the optimization of the $X_{\mathrm{q,m}}$ & $X_{\mathrm{q,g}}$ and $K_{\mathrm{p,Q}}$ & $K_{\mathrm{p,P}}$ cases

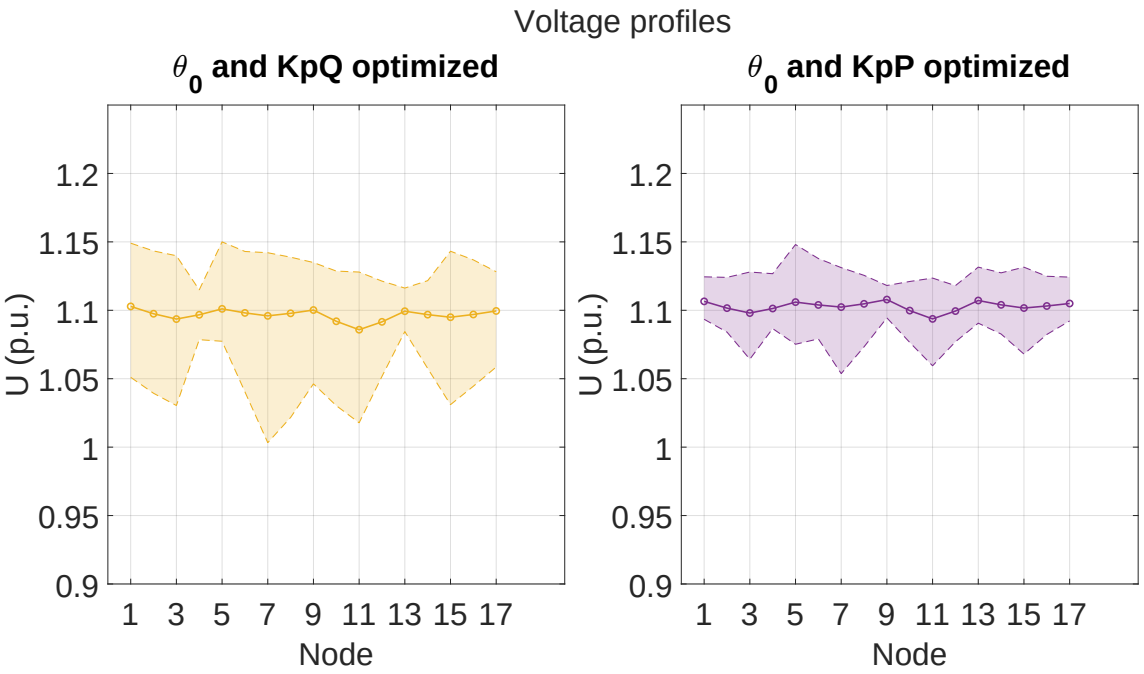

Figure A.60: Voltage profile for the optimization of the θ_0 & $K_{\mathrm{p,Q}}$ and θ_0 & $K_{\mathrm{p,P}}$ cases

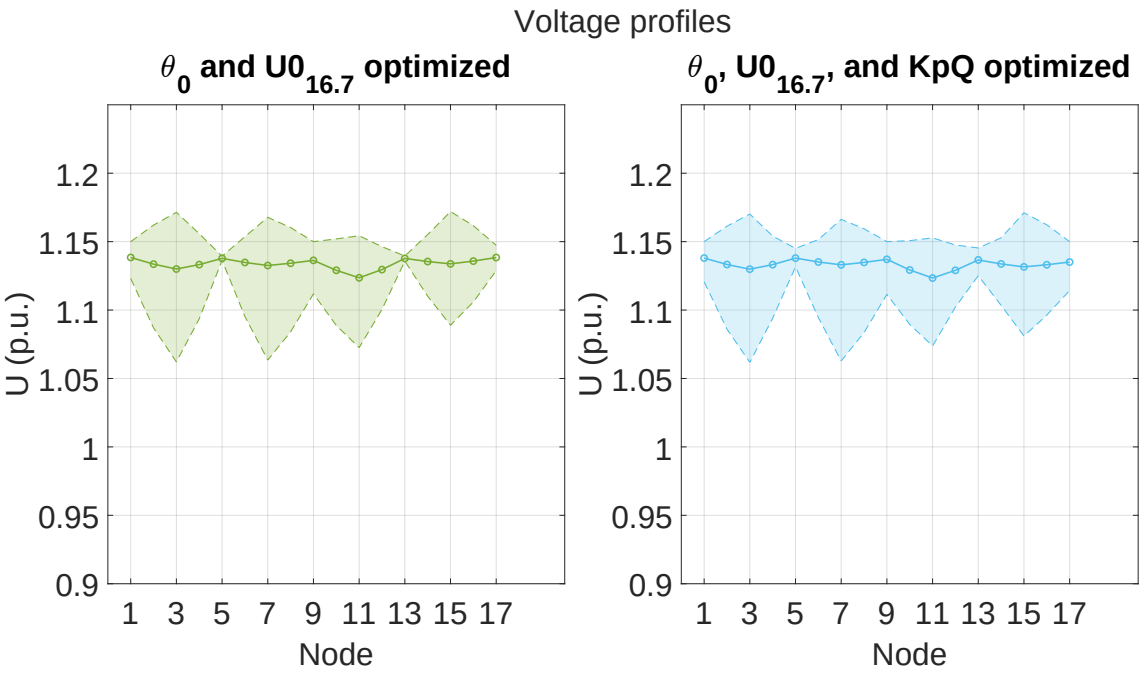

Figure A.61: Voltage profile for the optimization of the θ_0 & $U_{0,16.7}$ and θ_0& $U_{0,16.7}$ & $K_{\mathrm{p,Q}}$ cases

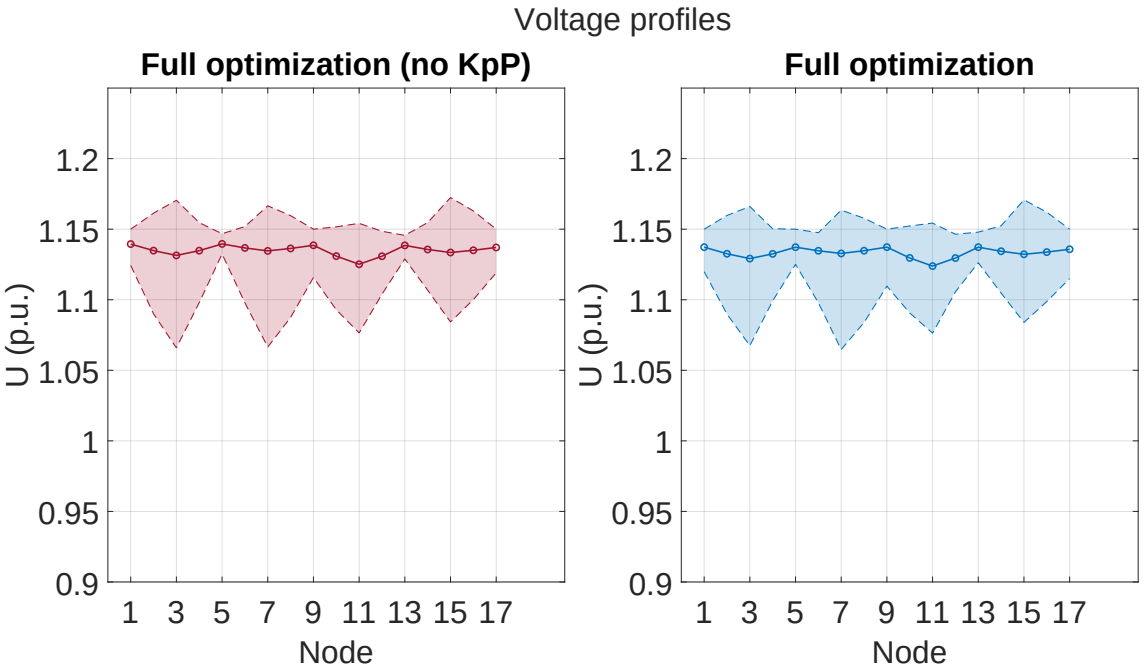

Figure A.62: Voltage profile for the full optimization cases with- and without $K_{\mathrm{p,P}}$

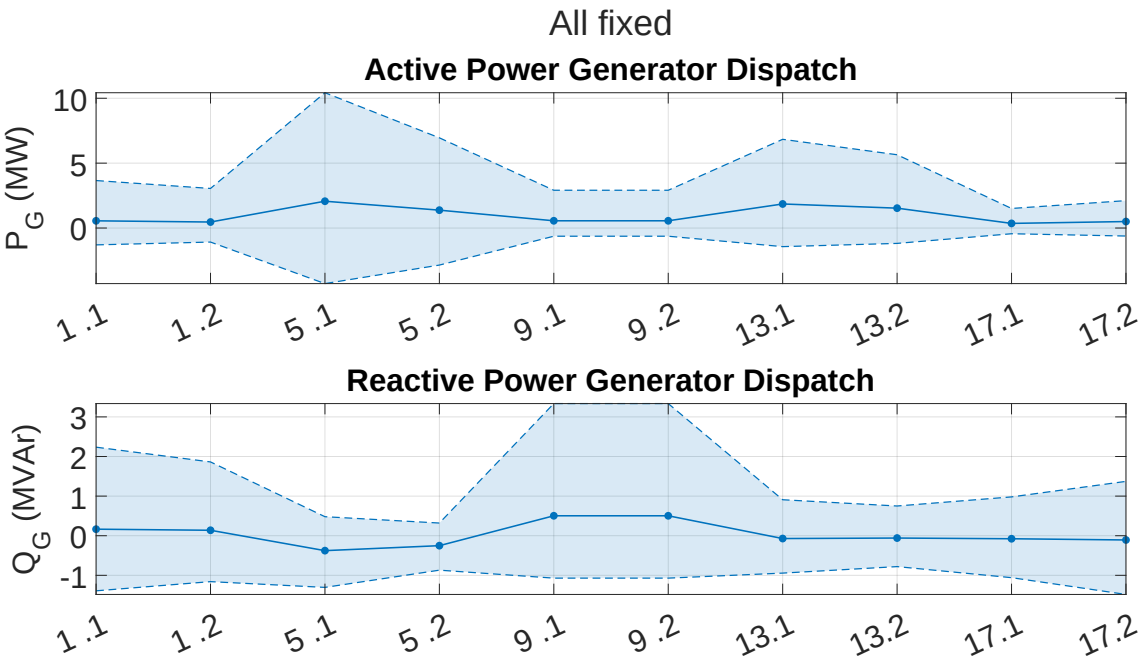

Figure A.63: Active- and reactive power generation of each substation for the all fixed case

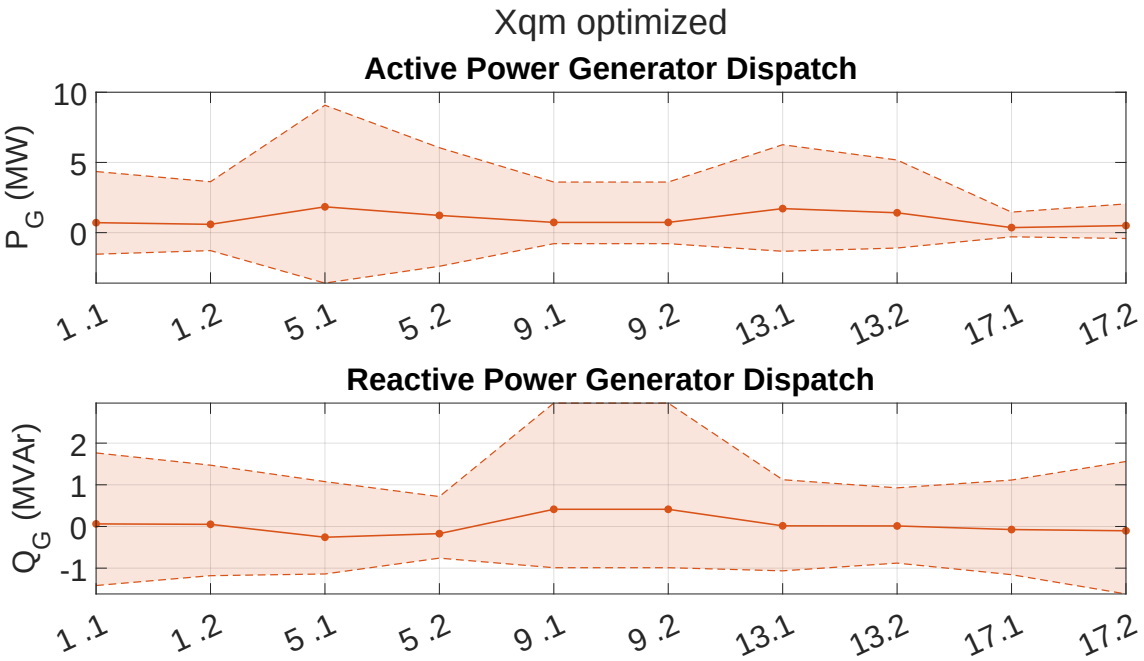

Figure A.64: Active- and reactive power generation of each substation for the optimization of $X_{\mathrm{q,m}}$ case

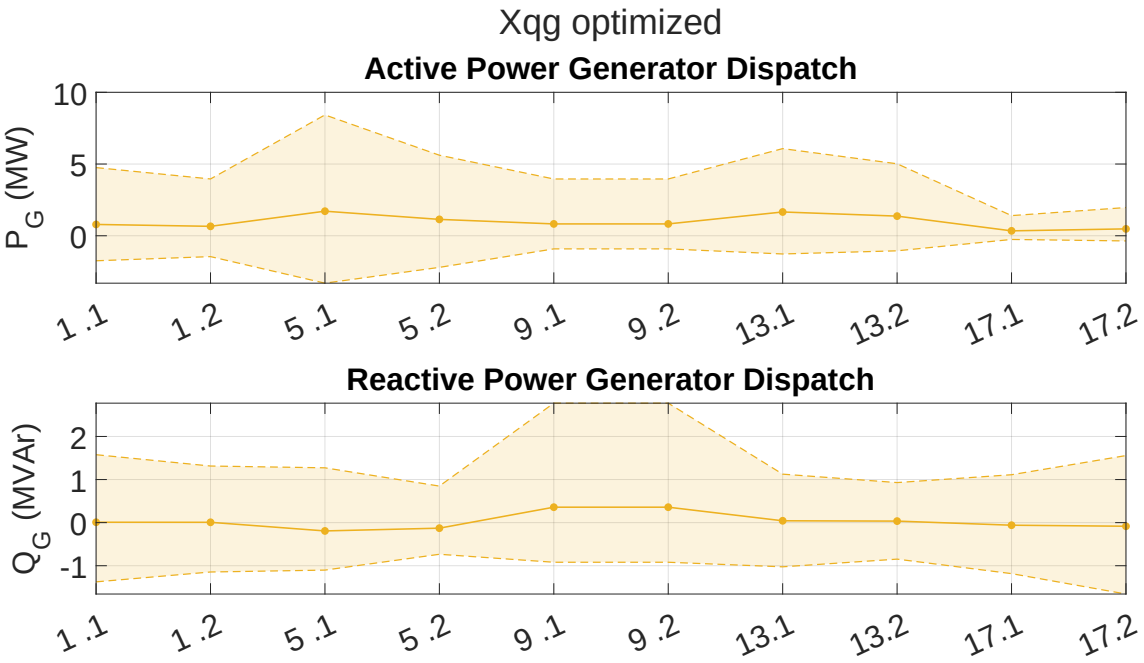

Figure A.65: Active- and reactive power generation of each substation for the optimization of $X_{\mathrm{q,g}}$ case

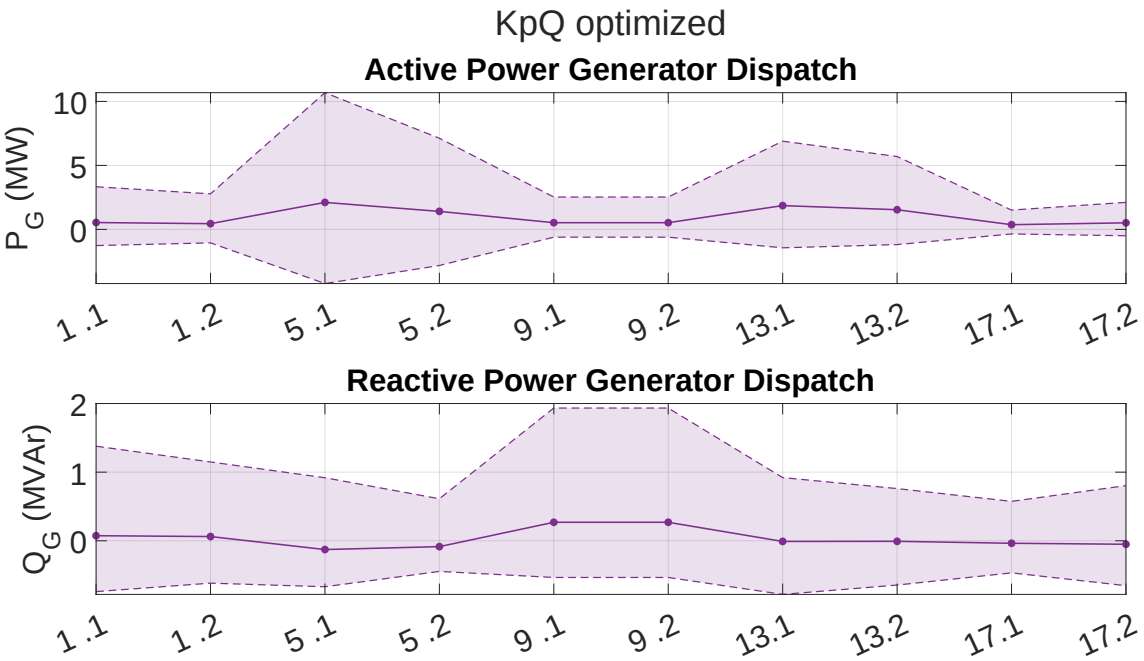

Figure A.66: Active- and reactive power generation of each substation for the optimization of $K_{\mathrm{p,Q}}$ case

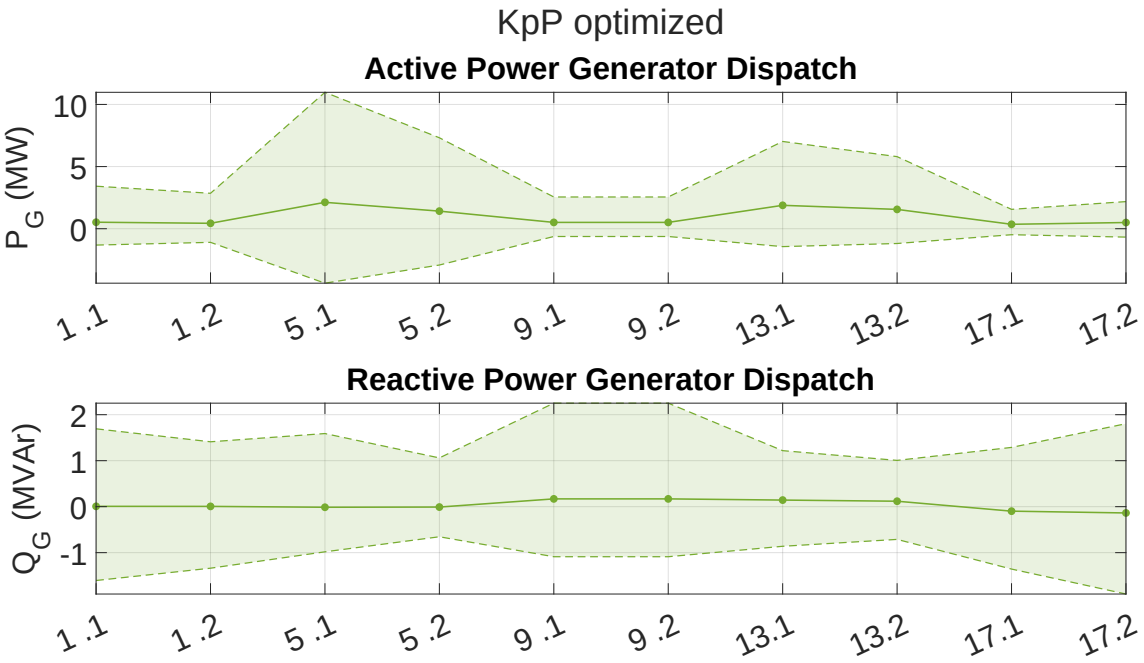

Figure A.67: Active- and reactive power generation of each substation for the optimization of $K_{p,P}$ case

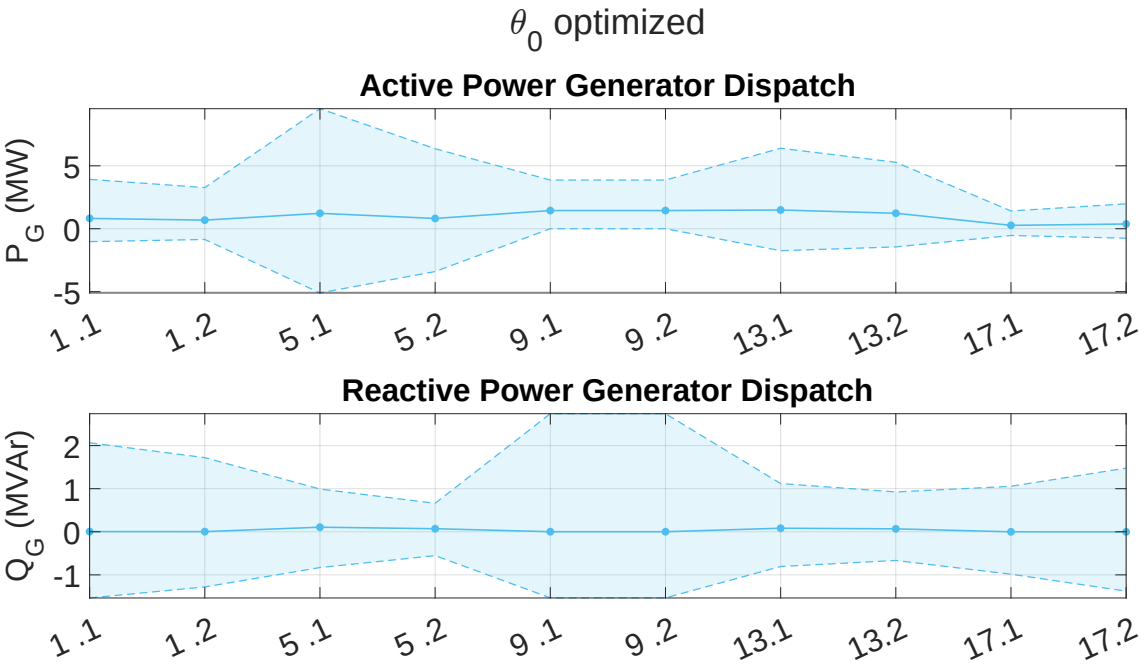

Figure A.68: Active- and reactive power generation of each substation for the optimization of θ_0 case

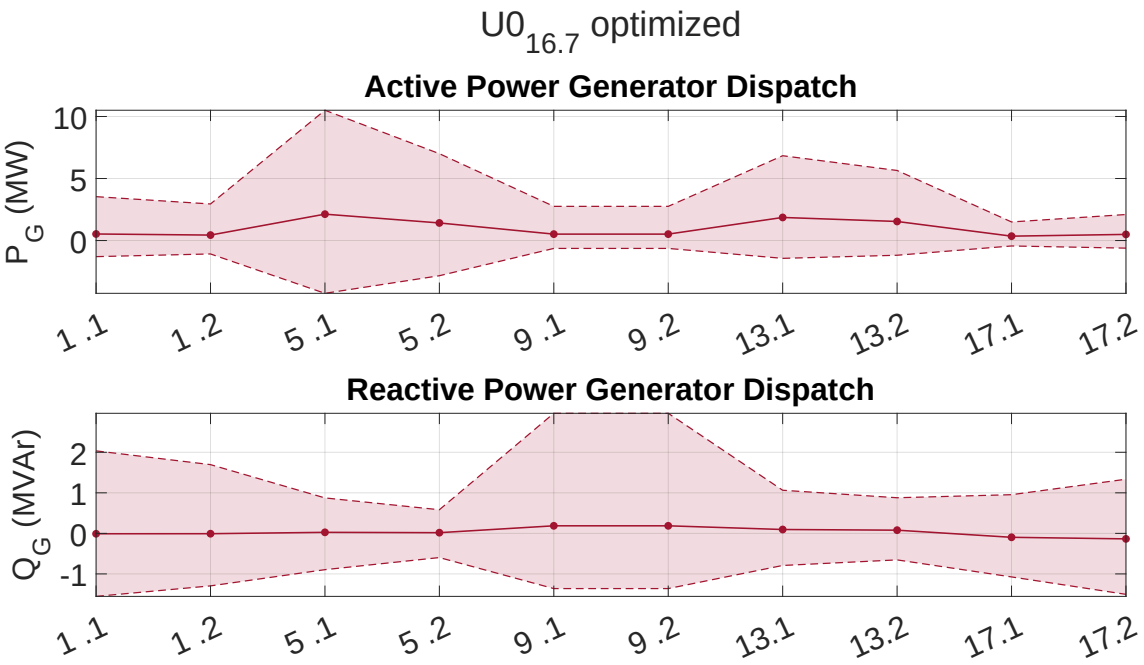

Figure A.69: Active- and reactive power generation of each substation for the optimization of $U_{0,16.7}$ case

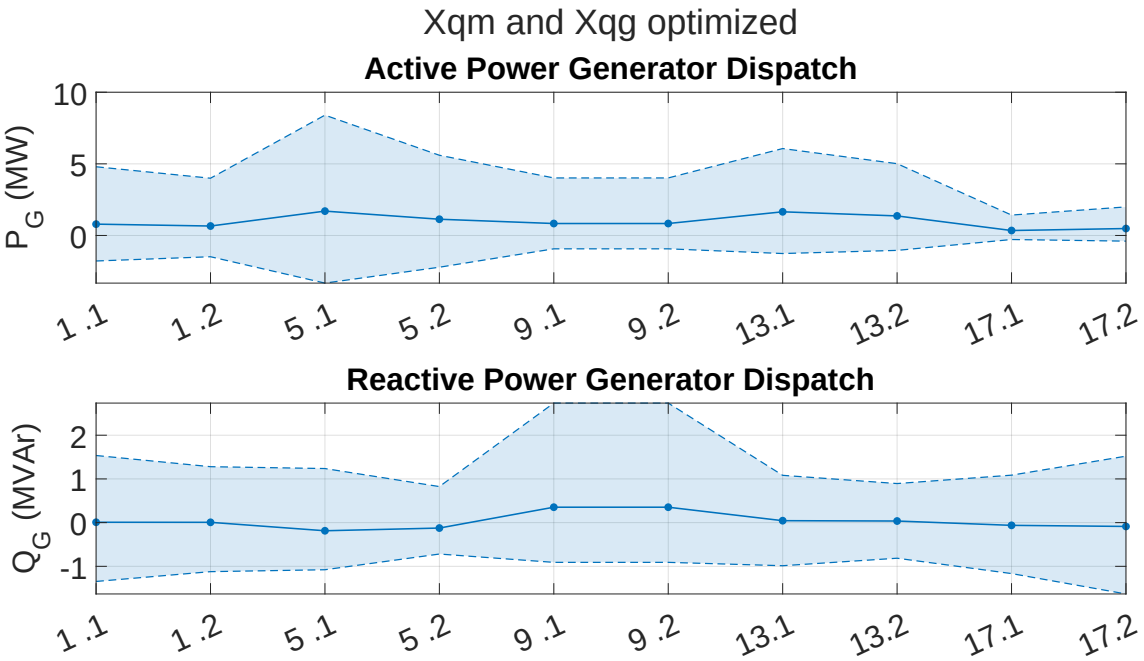

Figure A.70: Active- and reactive power generation of each substation for the optimization of $X_{\mathrm{q,m}}$ & $X_{q,g}$ case

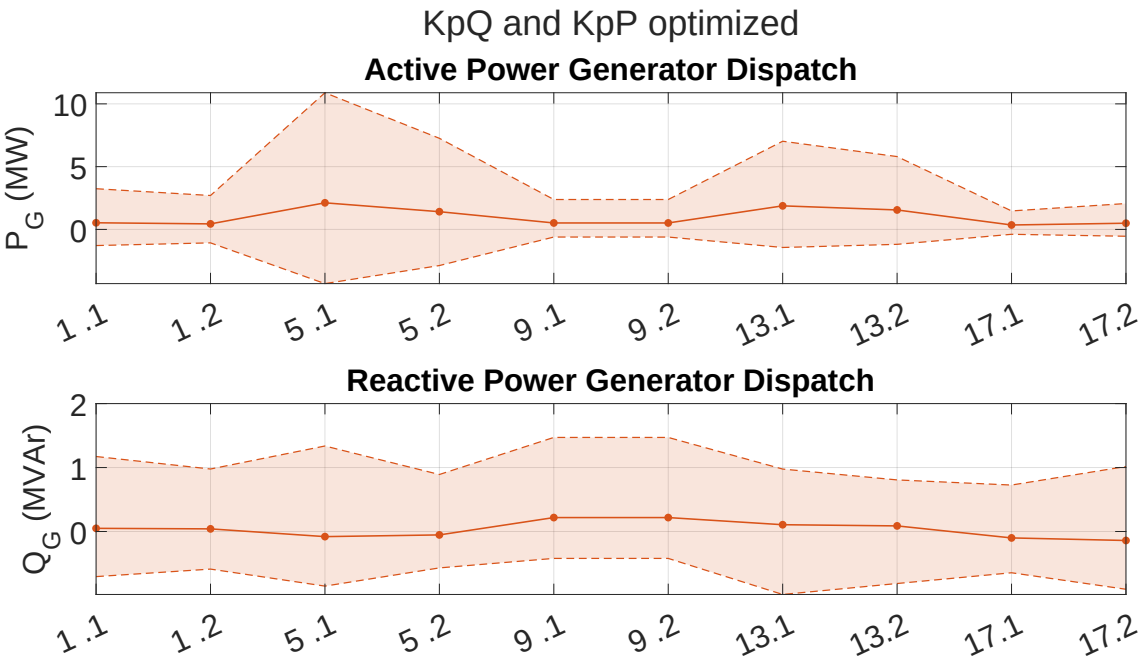

Figure A.71: Active- and reactive power generation of each substation for the optimization of $K_{\mathrm{p,Q}}$ & $K_{p,P}$ case

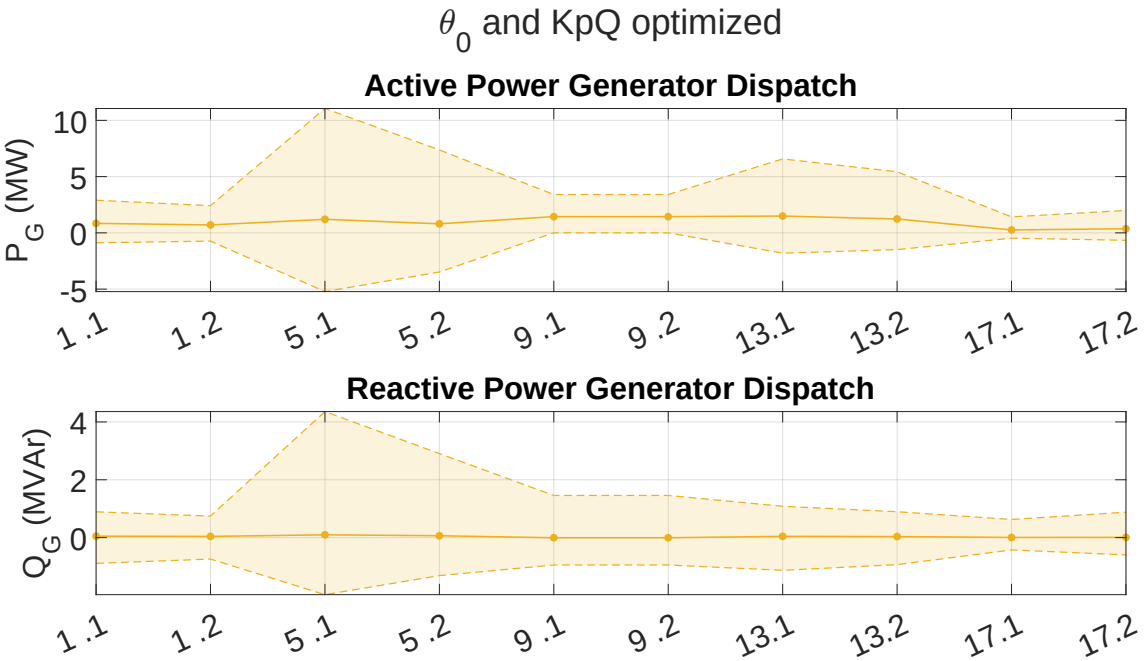

Figure A.72: Active- and reactive power generation of each substation for the optimization of θ_0 & $K_{p,Q}$ case

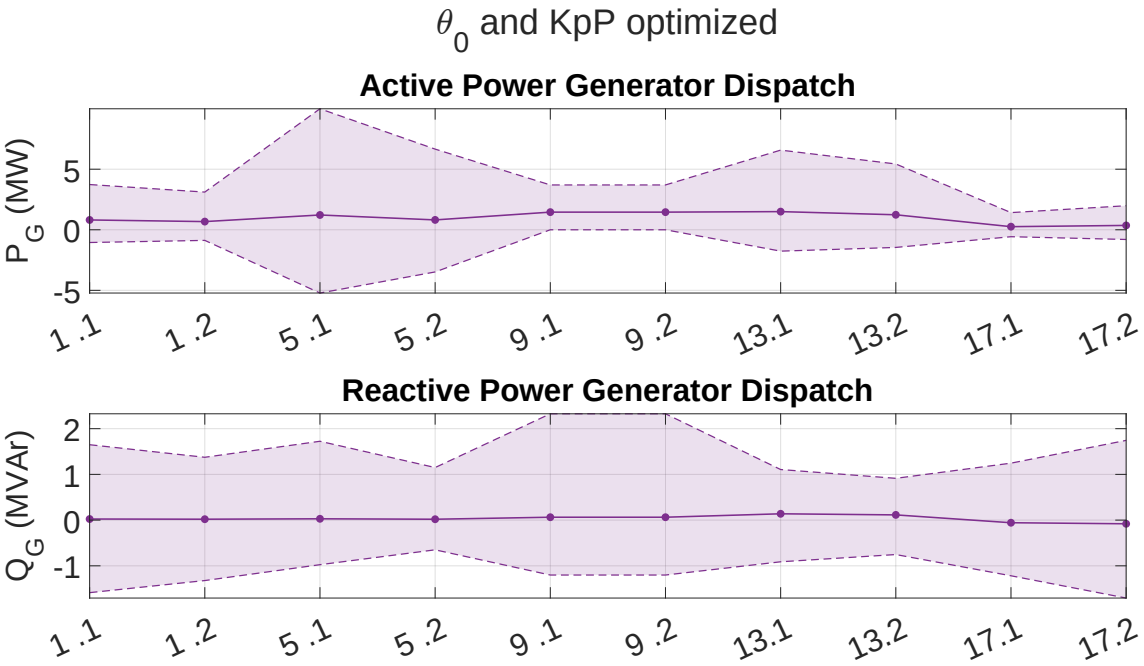

Figure A.73: Active- and reactive power generation of each substation for the optimization of θ_0 & $K_{p,P}$ case

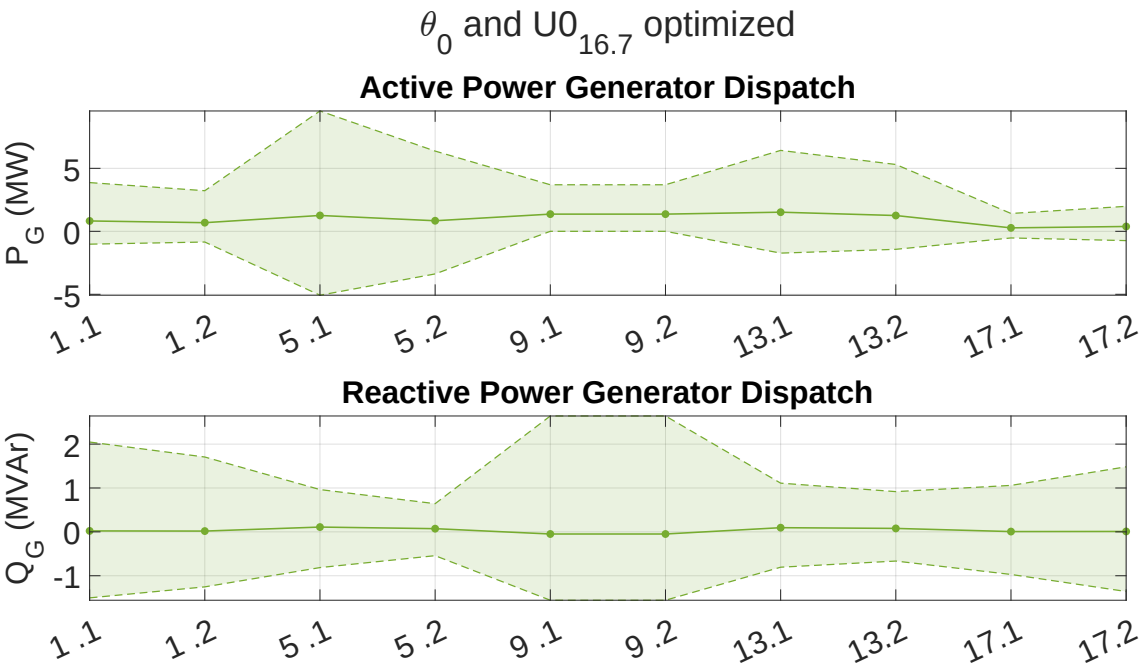

Figure A.74: Active- and reactive power generation of each substation for the optimization of θ_0 & $U_{0,16.7}$ case

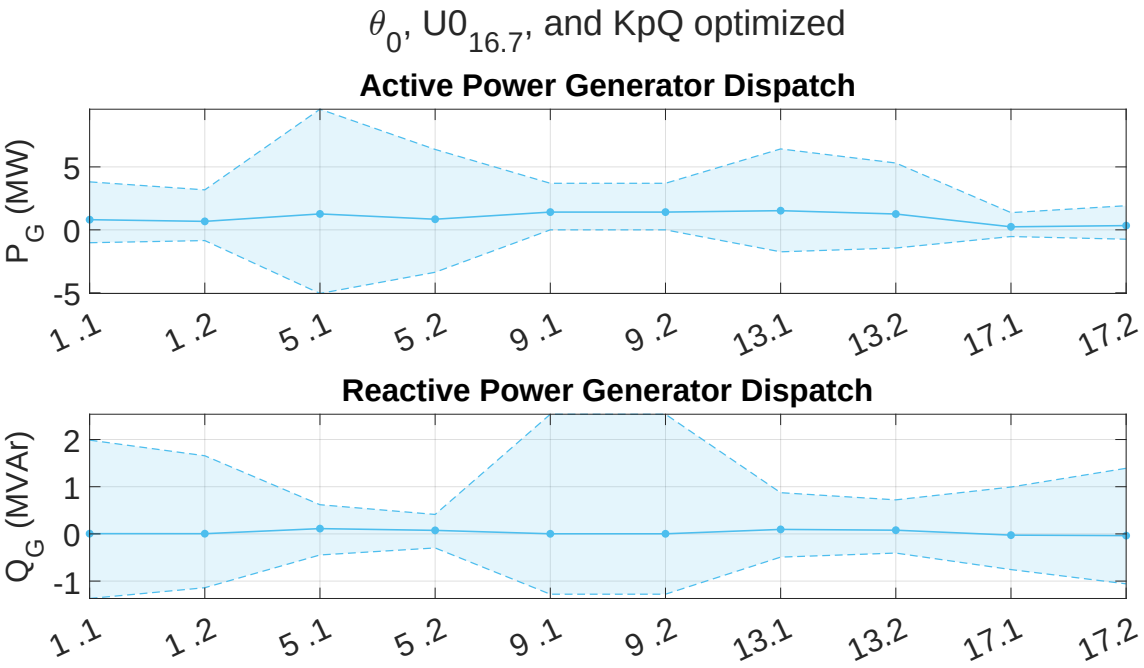

Figure A.75: Active- and reactive power generation of each substation for the optimization of θ_0& $U_{0,16.7}$ & $K_{p,Q}$ case

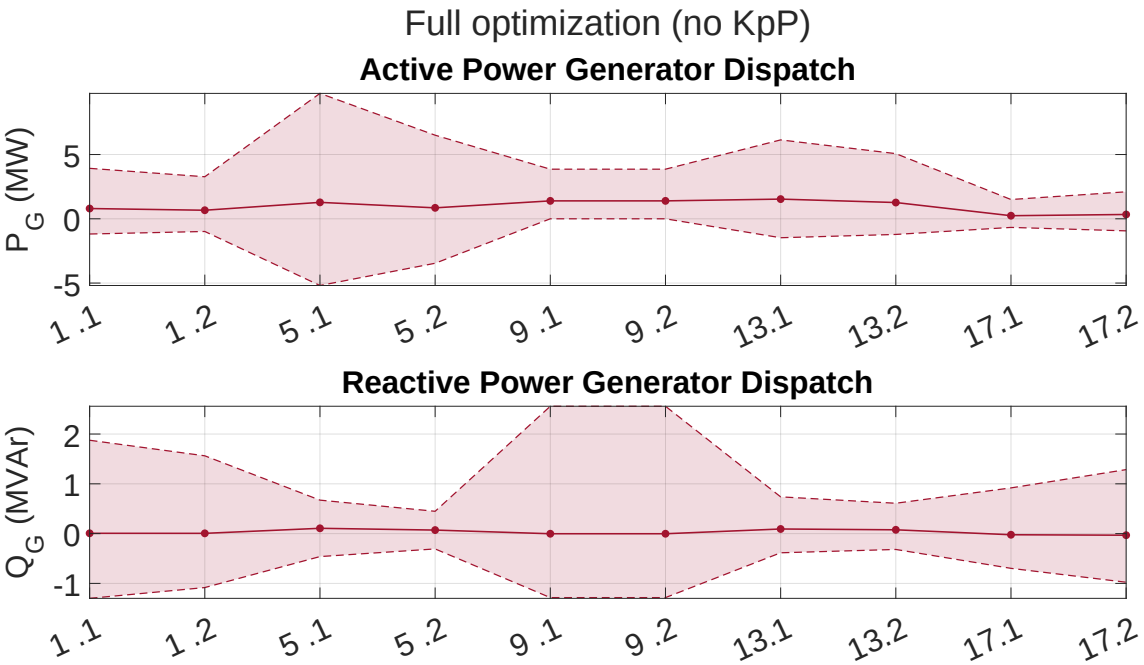

Figure A.76: Active- and reactive power generation of each substation for the full optimized case without $K_{\mathrm{p,P}}$

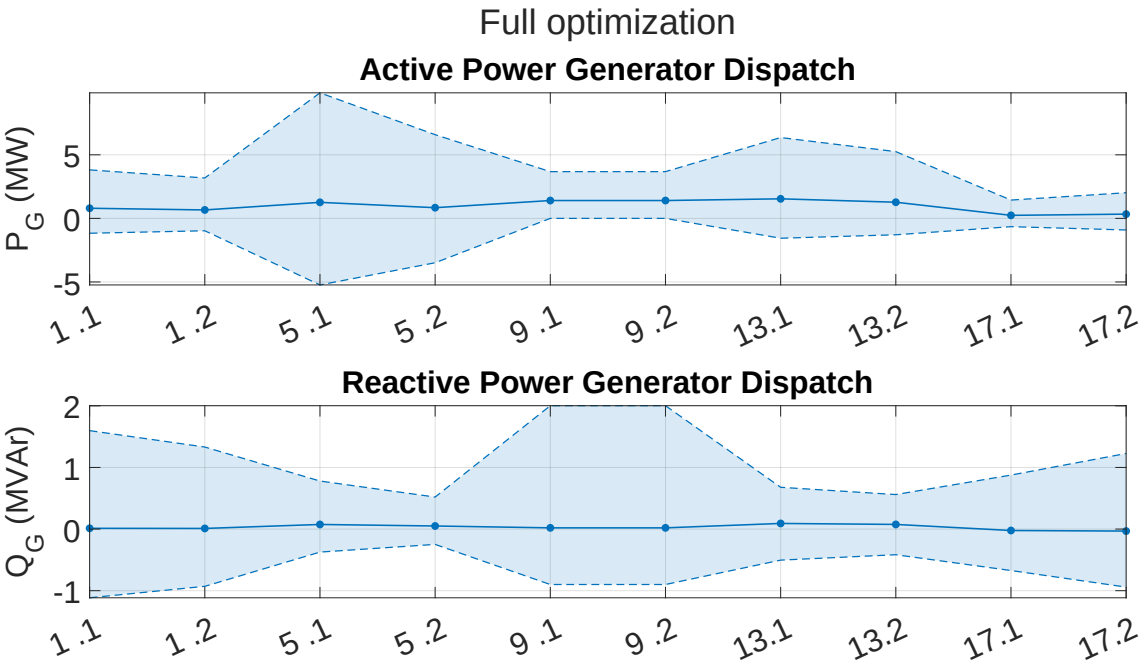

Figure A.77: Active- and reactive power generation of each substation for the full optimized case with $K_{\mathrm{p,P}}$

A.5.2 BT-system

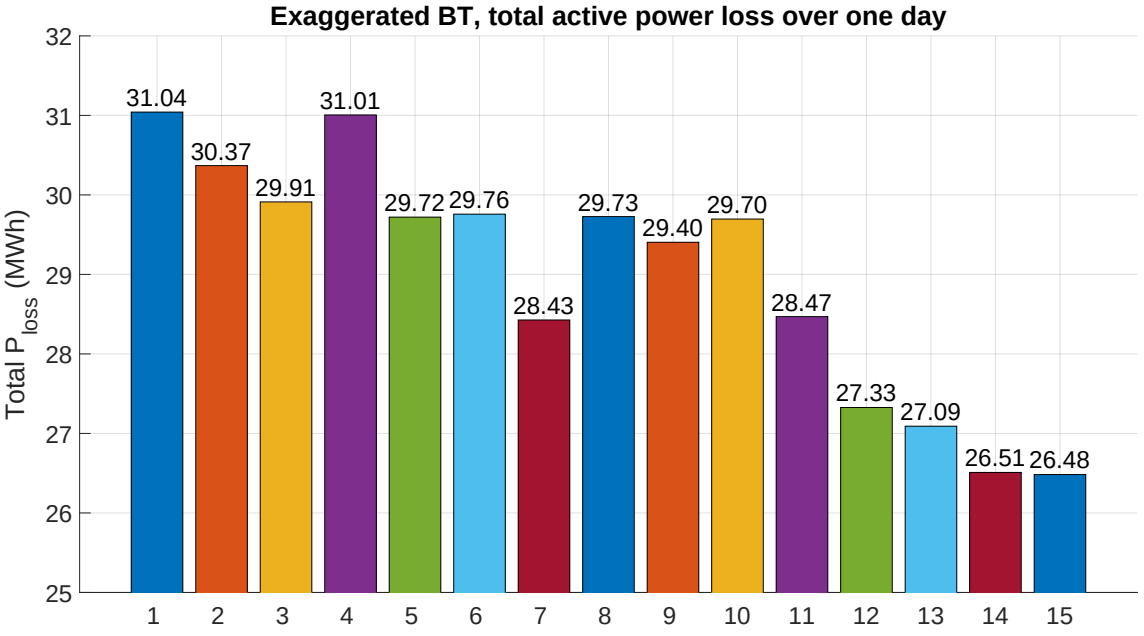

Figure A.78: Total system losses for each scenario in MWh

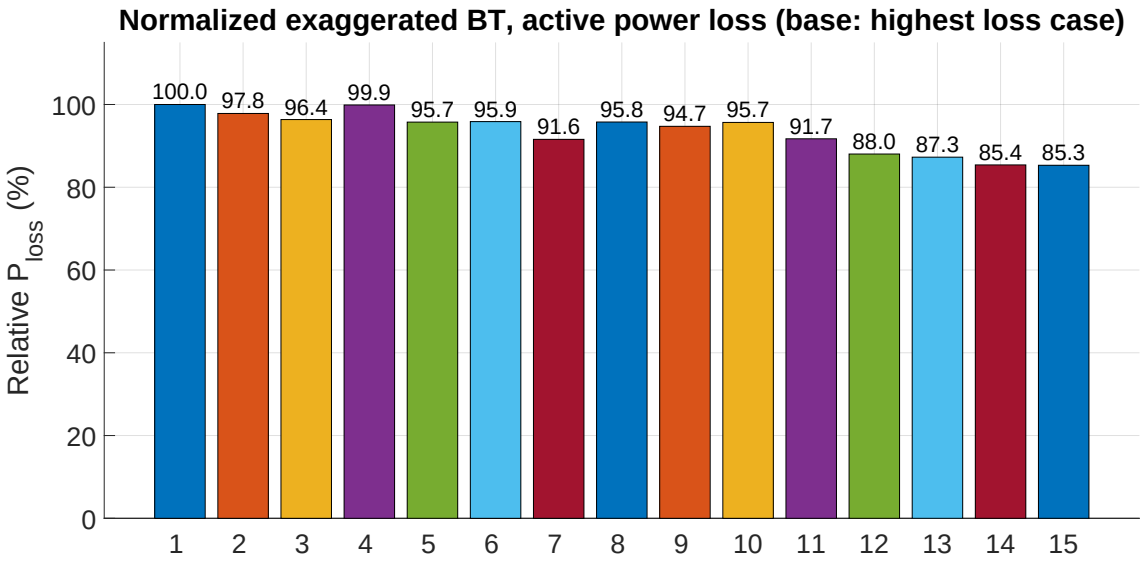

Figure A.79: Total system losses for each scenario in %, normalized in relation to the all fixed case

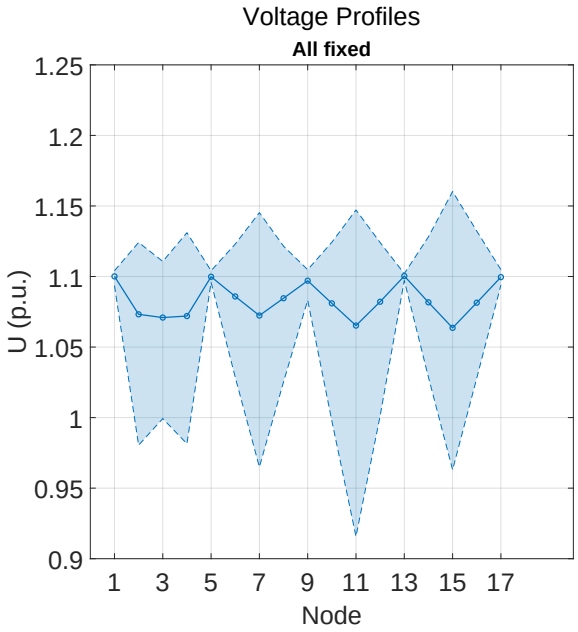

Figure A.80: Voltage profile for the all fixed case

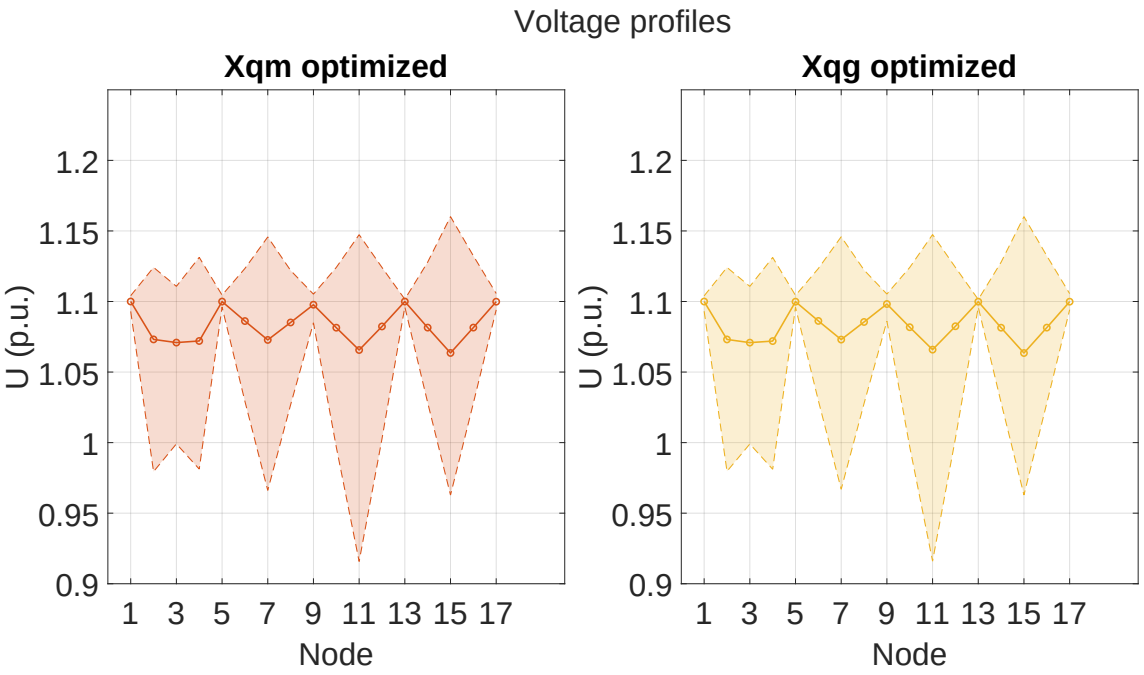

Figure A.81: Voltage profile for the optimization of $X_{\mathrm{q,m}}$ and $X_{\mathrm{q,g}}$ cases

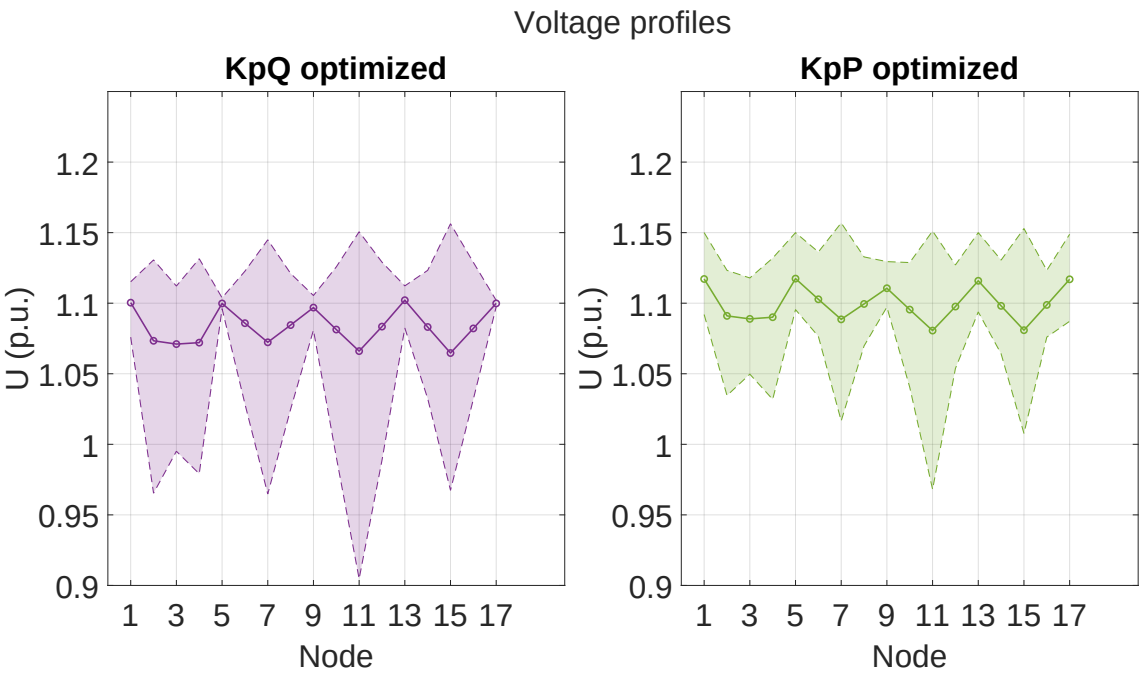

Figure A.82: Voltage profile for the optimization of $K_{\mathrm{p,Q}}$ and $K_{\mathrm{p,P}}$ cases

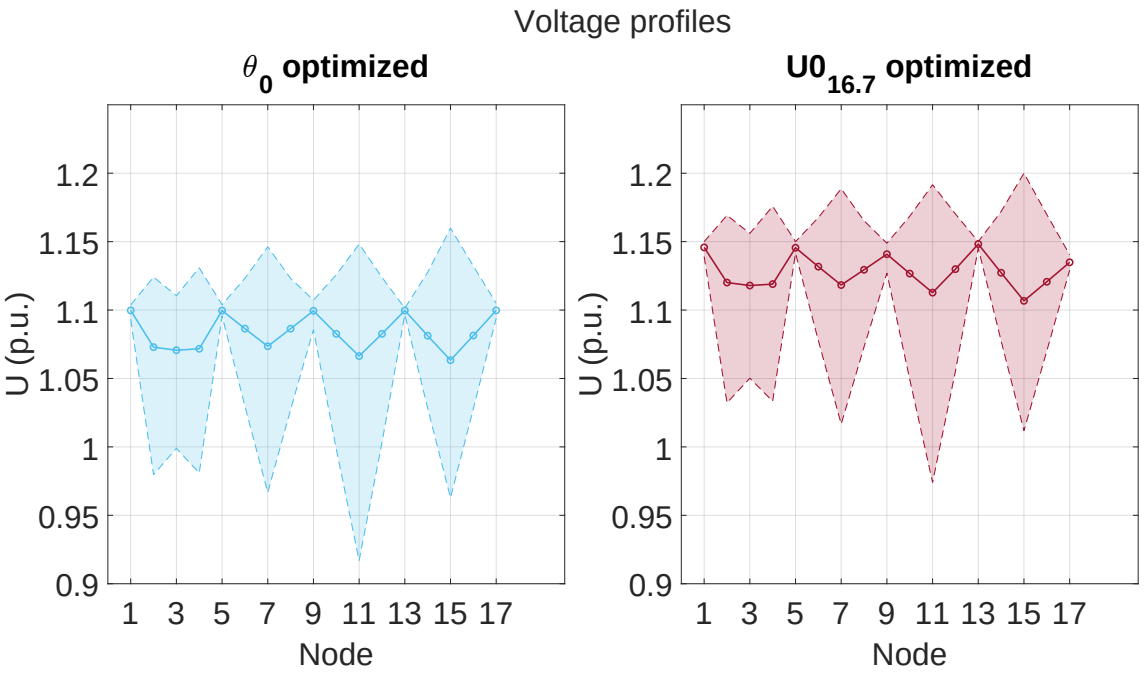

Figure A.83: Voltage profile for the optimization of θ_0 and $U_{0,16.7}$ cases

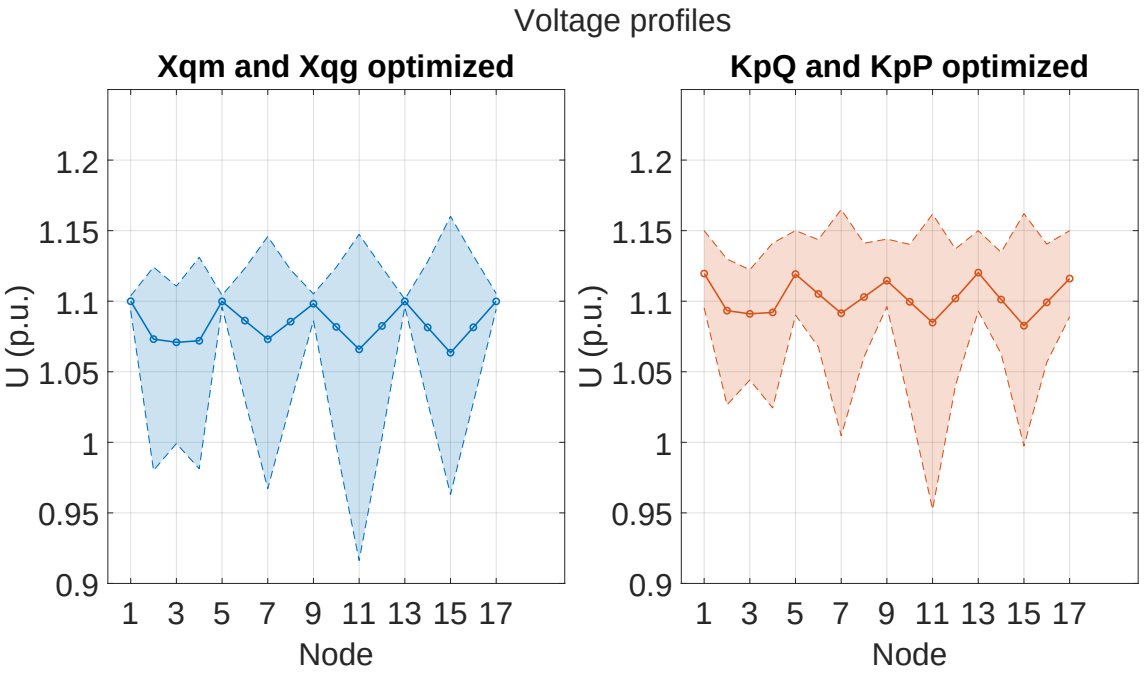

Figure A.84: Voltage profile for the optimization of $X_{\mathrm{q,m}}$ & $X_{\mathrm{q,g}}$ and $K_{\mathrm{p,Q}}$ & $K_{\mathrm{p,P}}$ cases

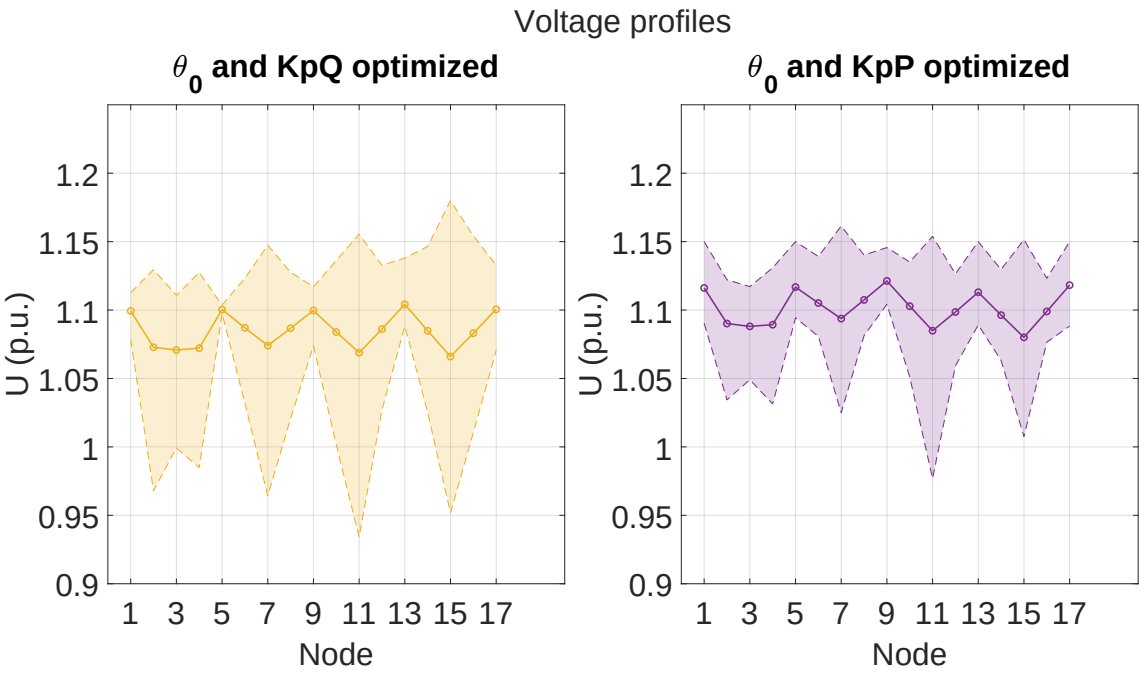

Figure A.85: Voltage profile for the optimization of θ_0 & $K_{\mathrm{p,Q}}$ and θ_0 & $K_{\mathrm{p,P}}$ cases

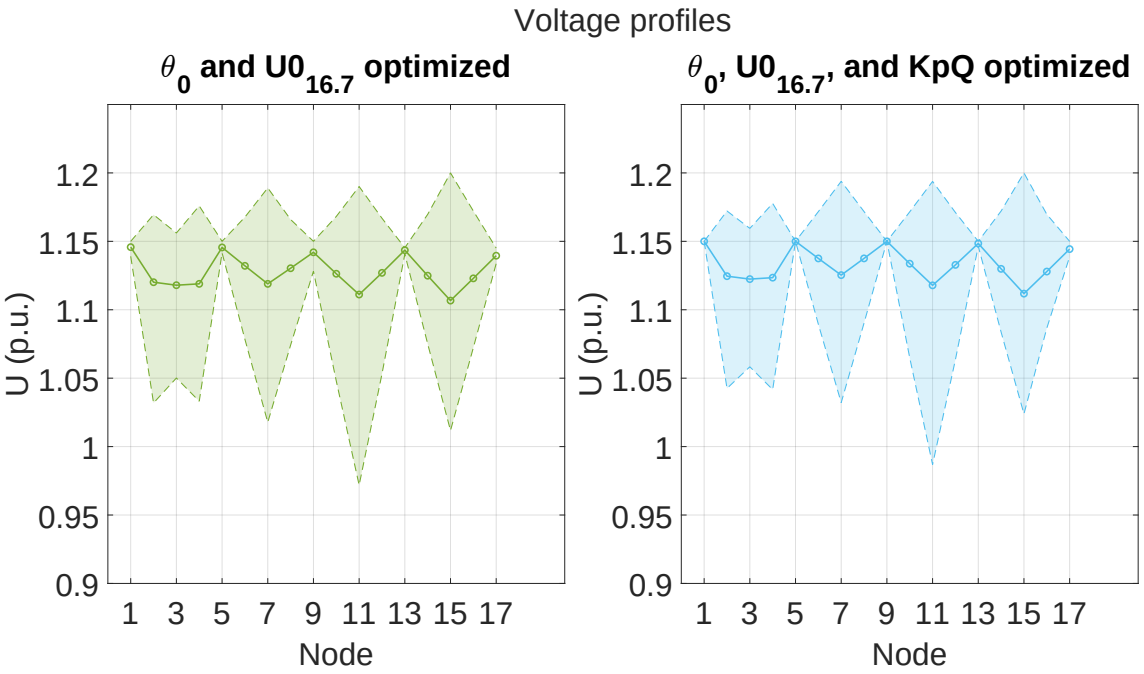

Figure A.86: Voltage profile for the optimization of θ_0 & $U_{0,16.7}$ and θ_0 & $U_{0,16.7}$ & $K_{\mathrm{p,Q}}$ cases

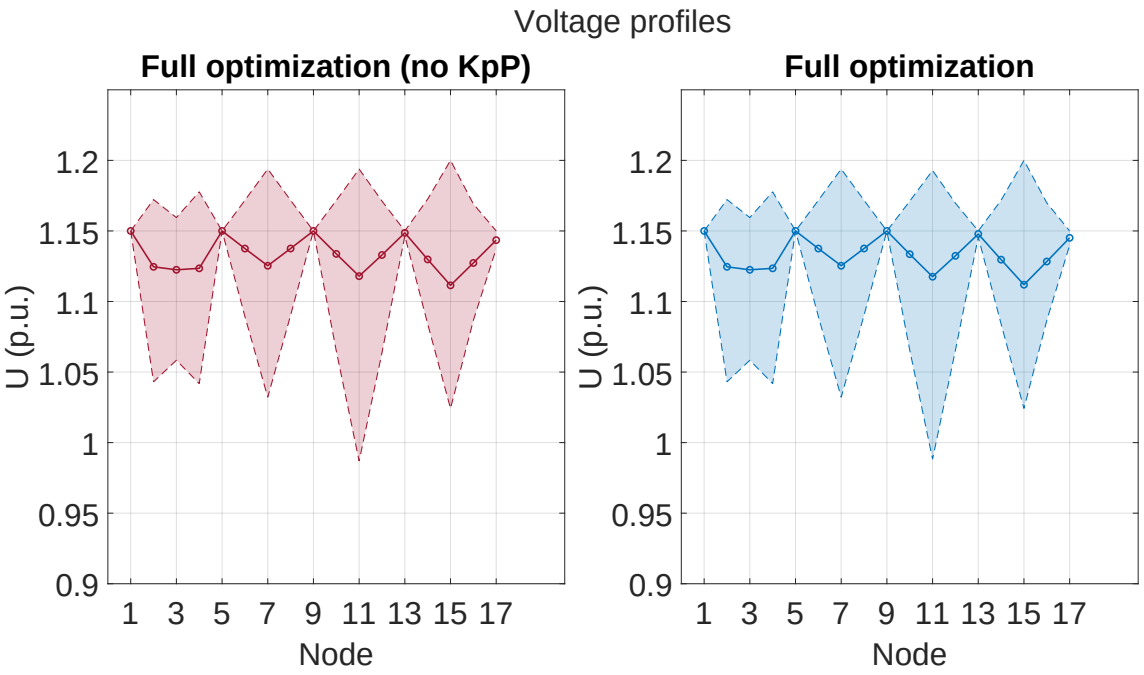

Figure A.87: Voltage profile for the full optimization cases with- and without $K_{\mathrm{p,P}}$

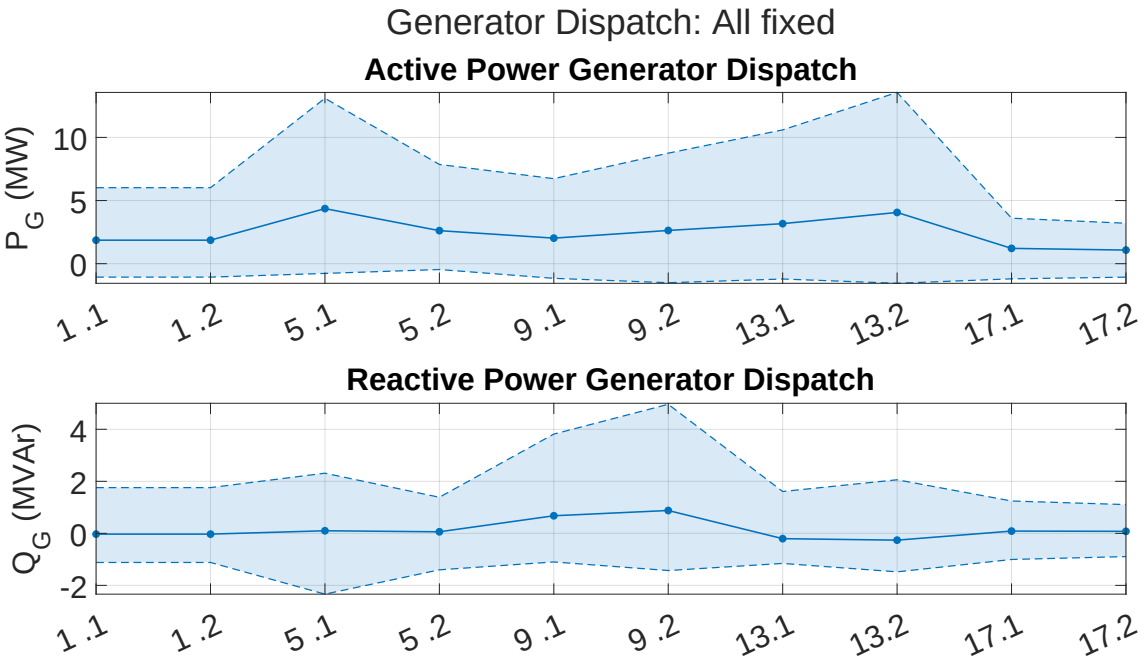

Figure A.88: Active- and reactive power generation of each substation for the all fixed case

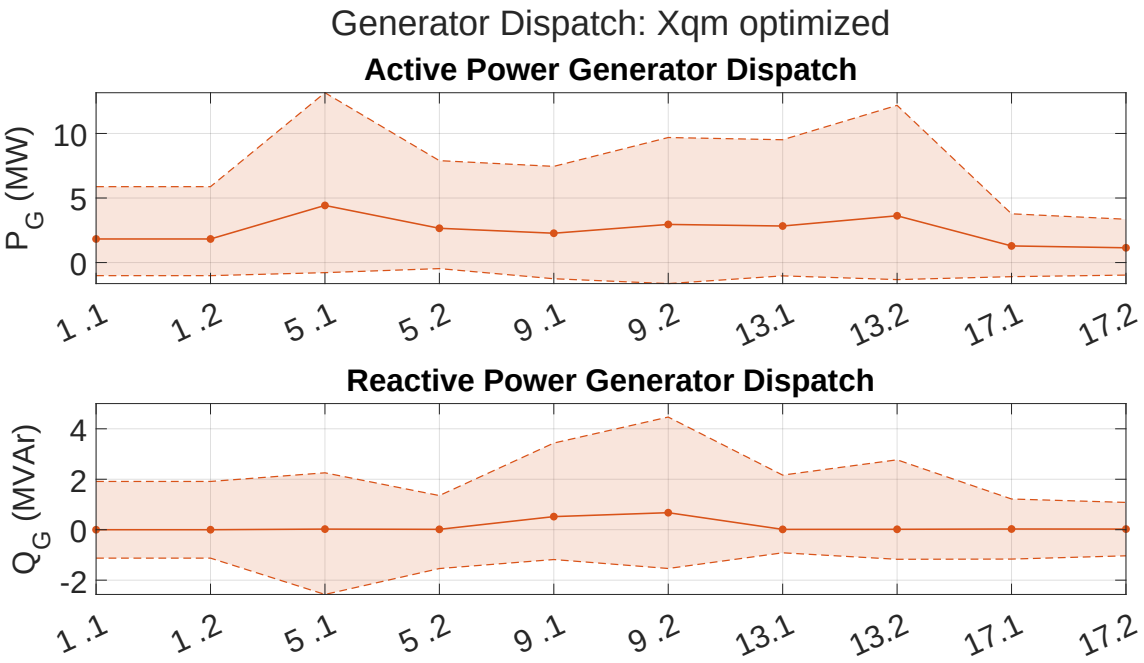

Figure A.89: Active- and reactive power generation of each substation for the optimization of $X_{\mathrm{q,m}}$ case

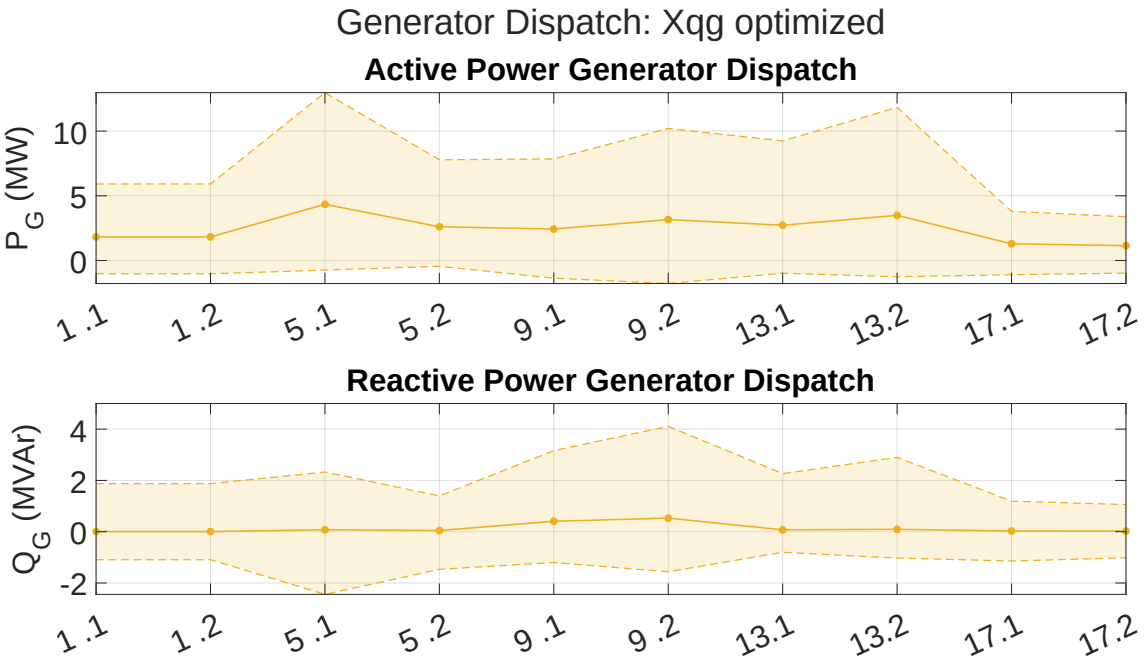

Figure A.90: Active- and reactive power generation of each substation for the optimization of $X_{\mathrm{q,g}}$ case

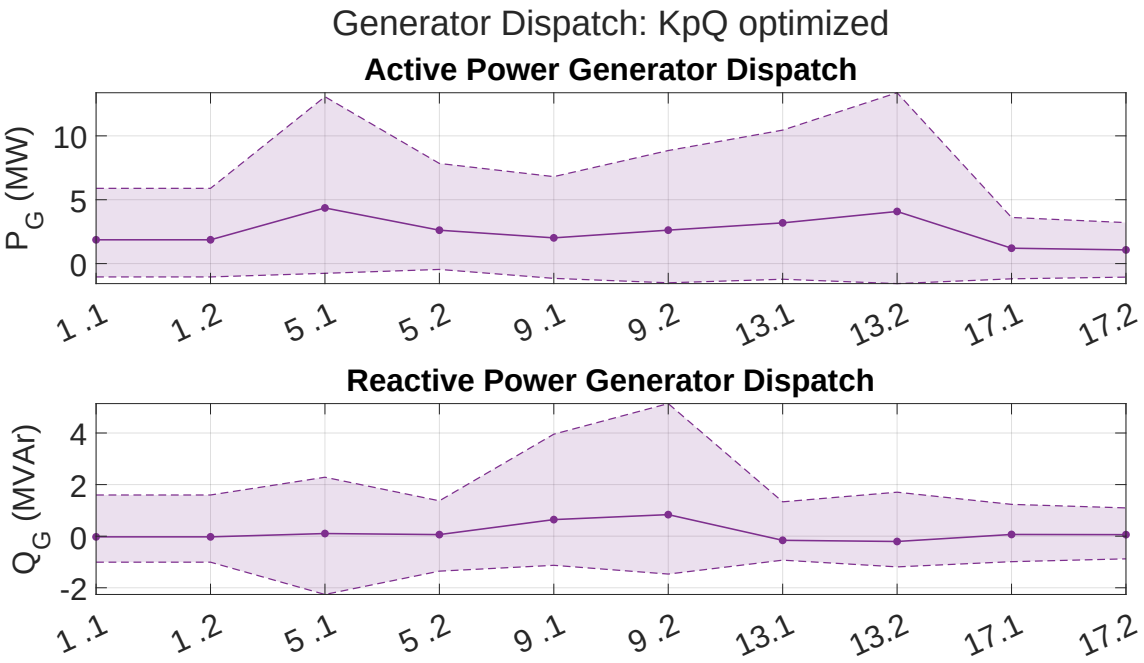

Figure A.91: Active- and reactive power generation of each substation for the optimization of $K_{\mathrm{p,Q}}$ case

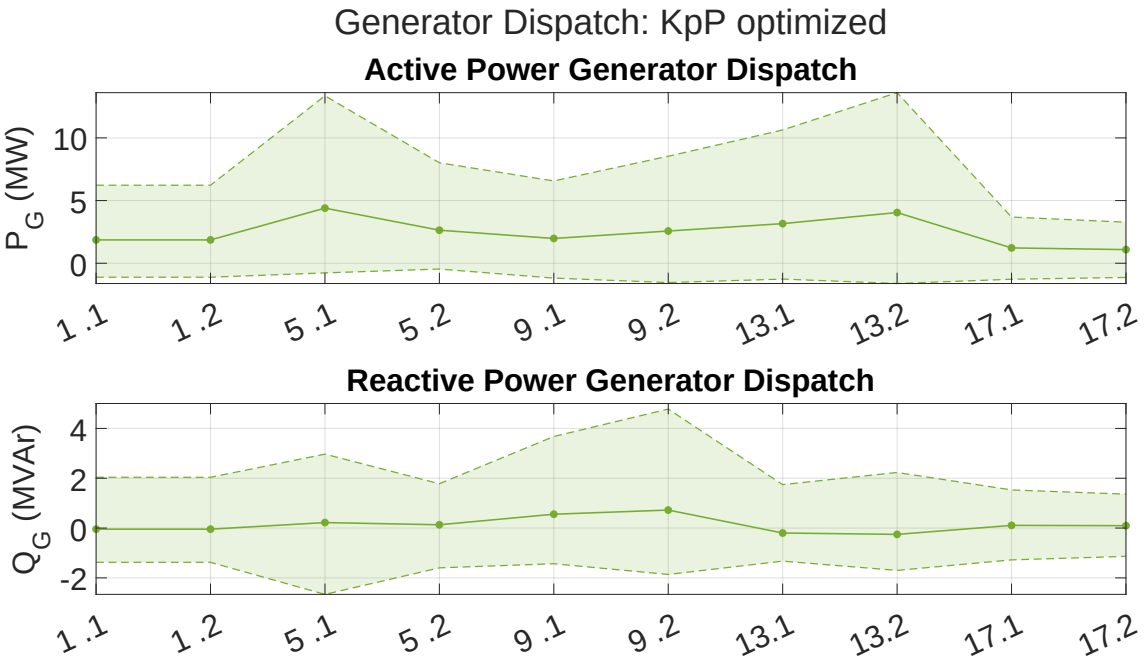

Figure A.92: Active- and reactive power generation of each substation for the optimization of $K_{\mathrm{p,P}}$ case

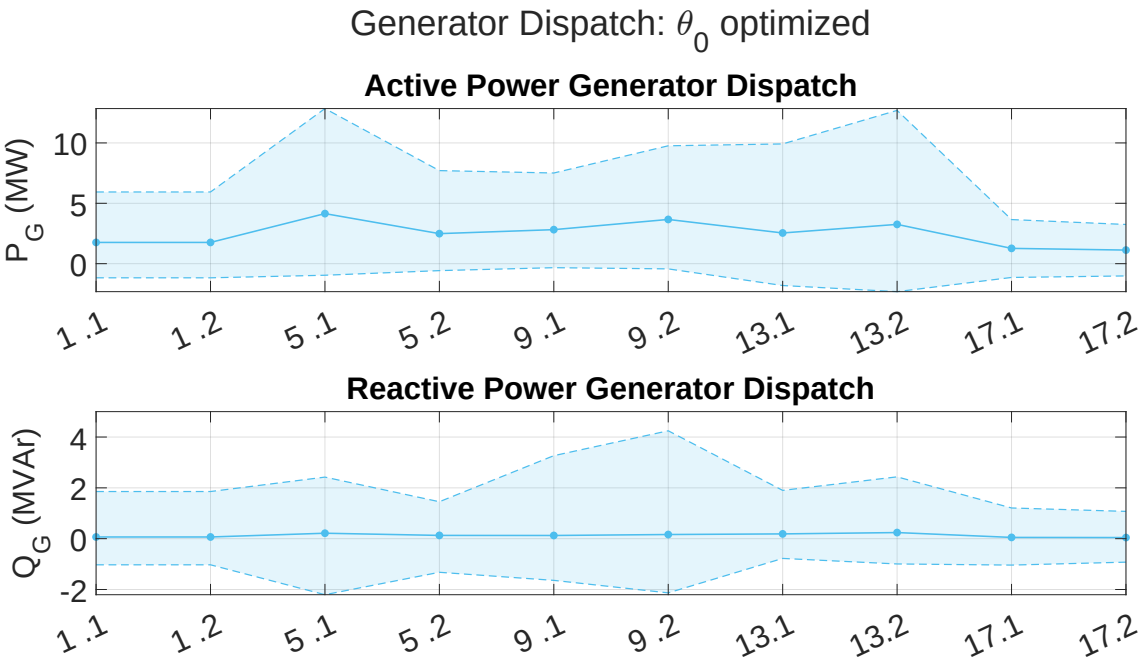

Figure A.93: Active- and reactive power generation of each substation for the optimization of θ_0 case

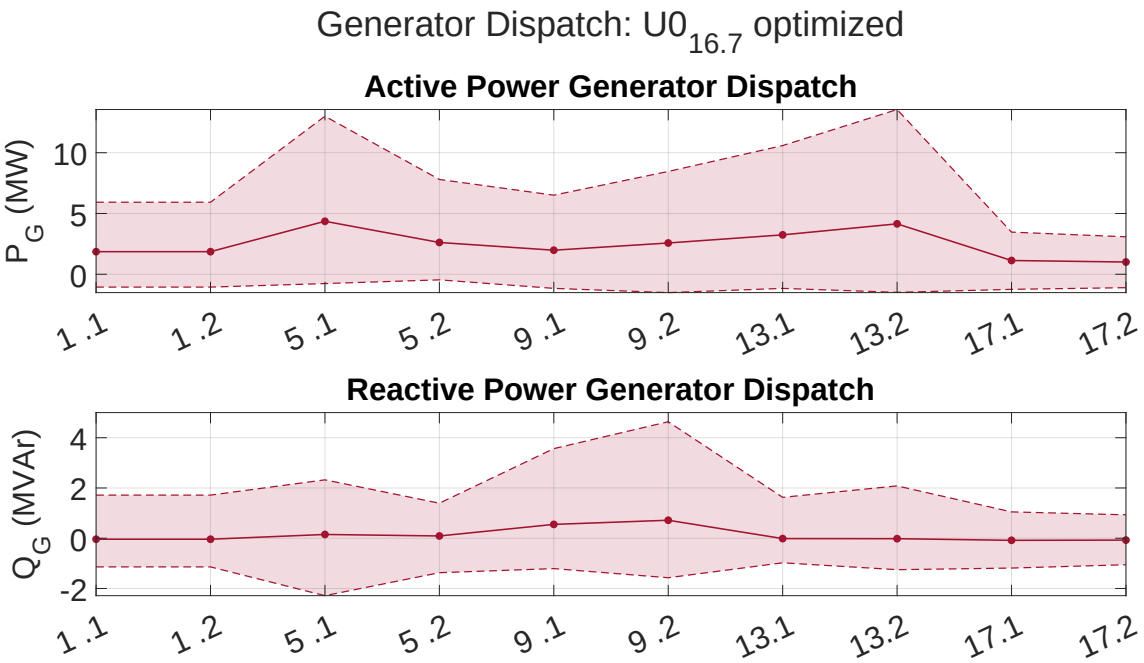

Figure A.94: Active- and reactive power generation of each substation for the optimization of $U_{0,16.7}$ case

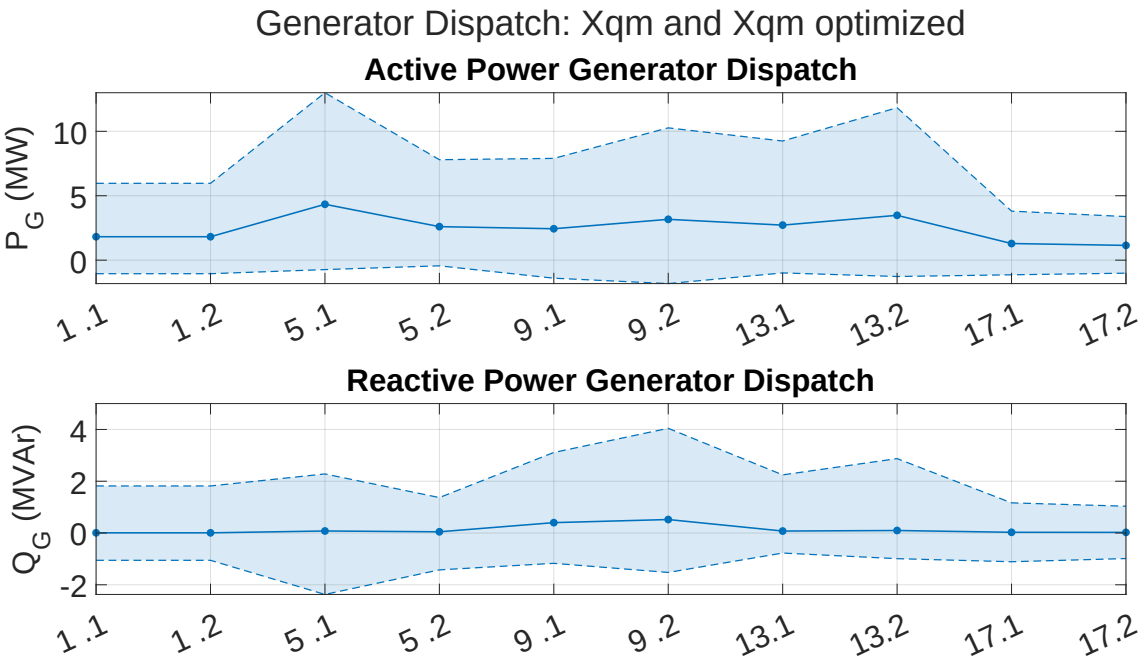

Figure A.95: Active- and reactive power generation of each substation for the optimization of $X_{\mathrm{q,m}}$ & $X_{\mathbf{q,g}}$ case

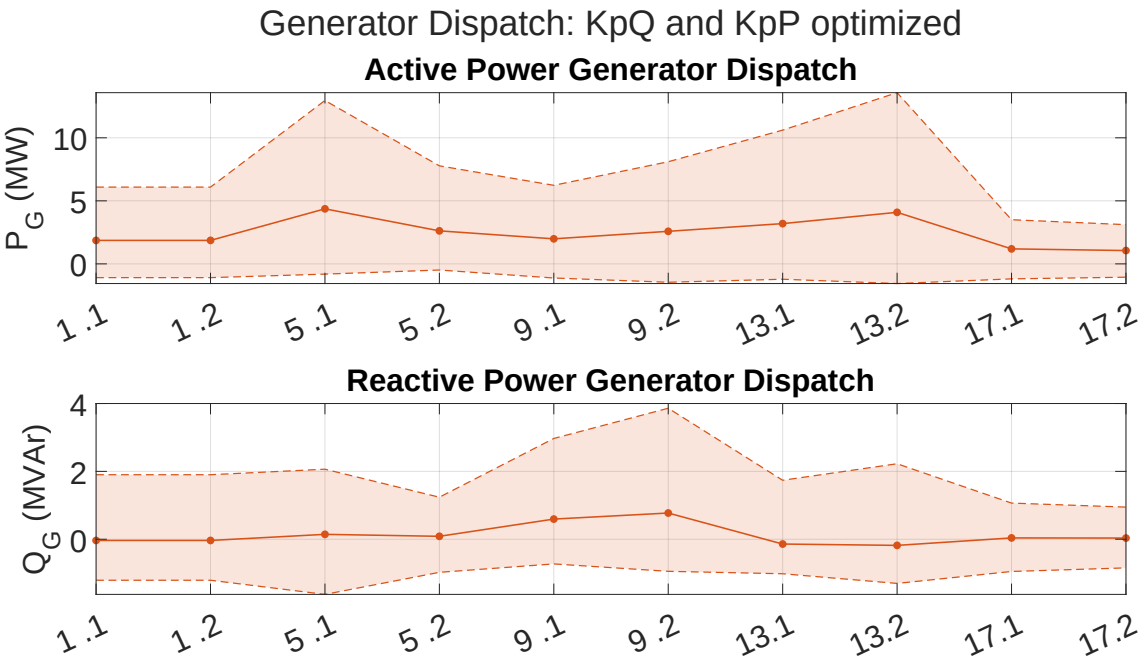

Figure A.96: Active- and reactive power generation of each substation for the optimization of $K_{\mathrm{p,Q}}$ & $K_{\mathrm{p,P}}$ case

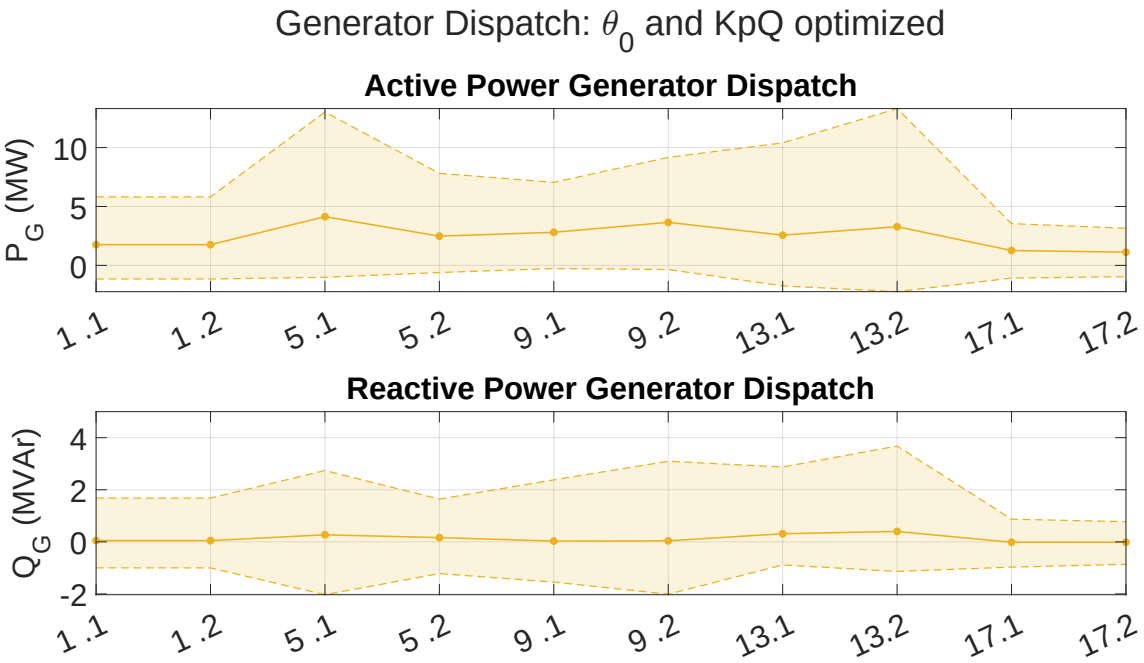

Figure A.97: Active- and reactive power generation of each substation for the optimization of θ_0 & $K_{\mathrm{p,Q}}$ case

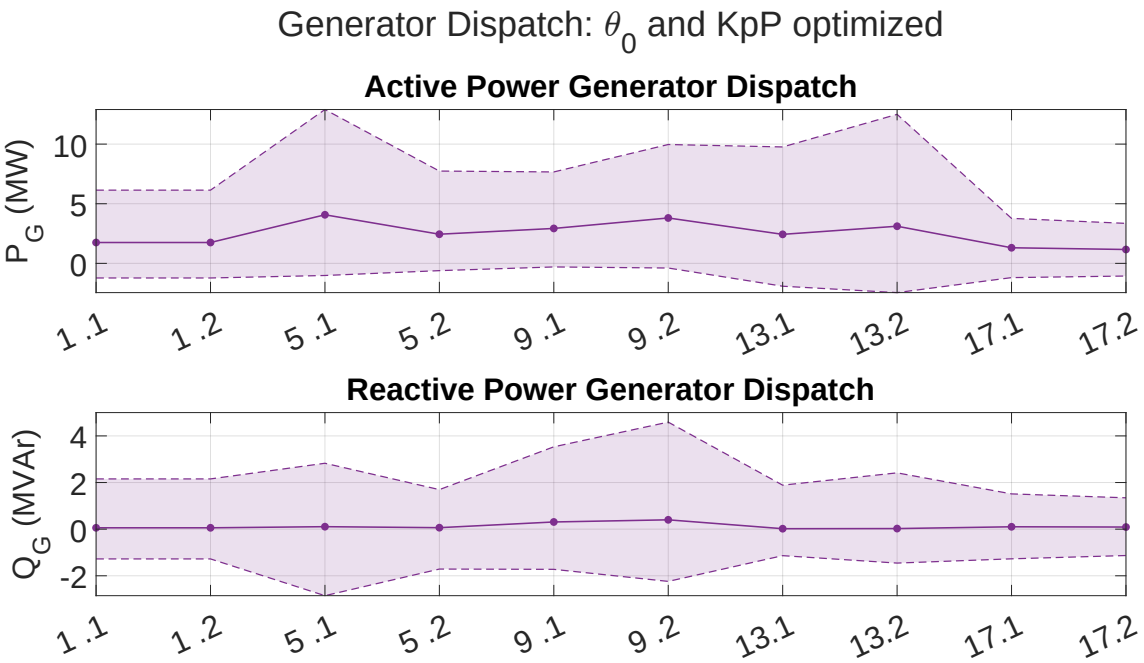

Figure A.98: Active- and reactive power generation of each substation for the optimization of θ_0 & $K_{\mathrm{p,P}}$ case

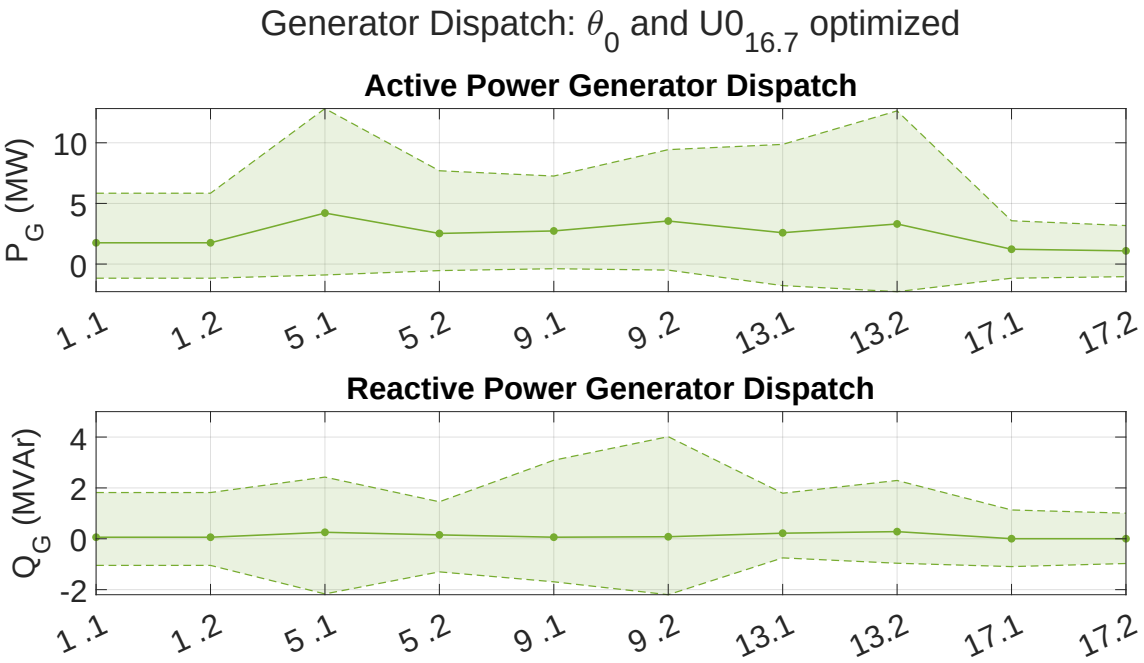

Figure A.99: Active- and reactive power generation of each substation for the optimization of θ_0 & $U_{0,16.7}$ case

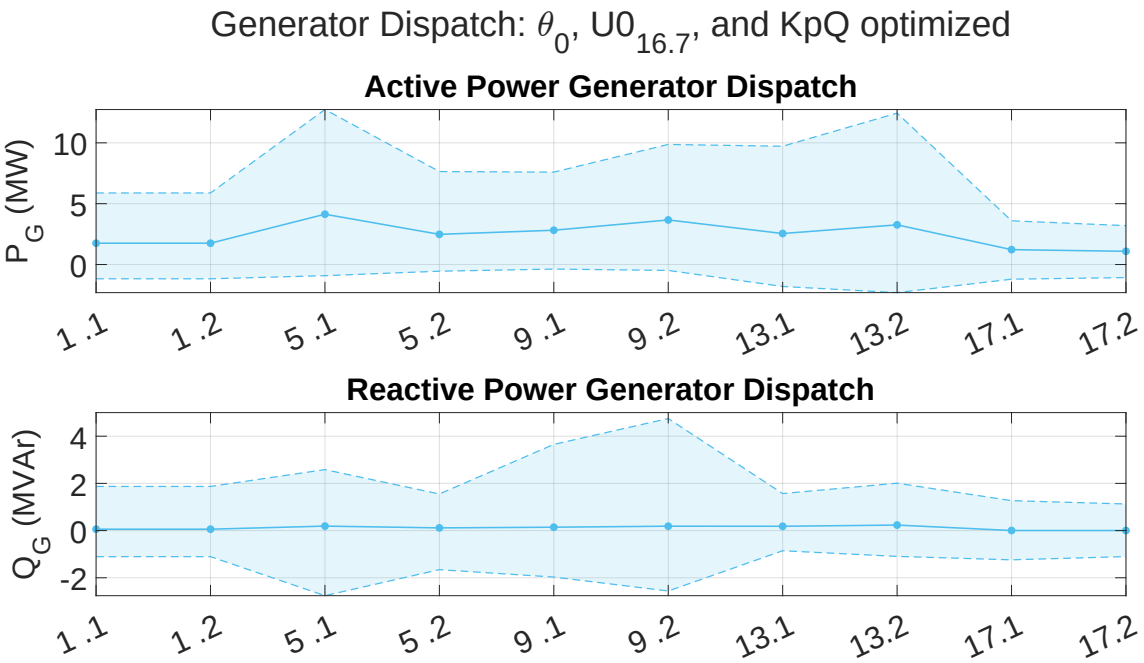

Figure A.100: Active- and reactive power generation of each substation for the optimization of θ_0& $U_{0,16.7}$ & $K_{\mathrm{p,Q}}$ case

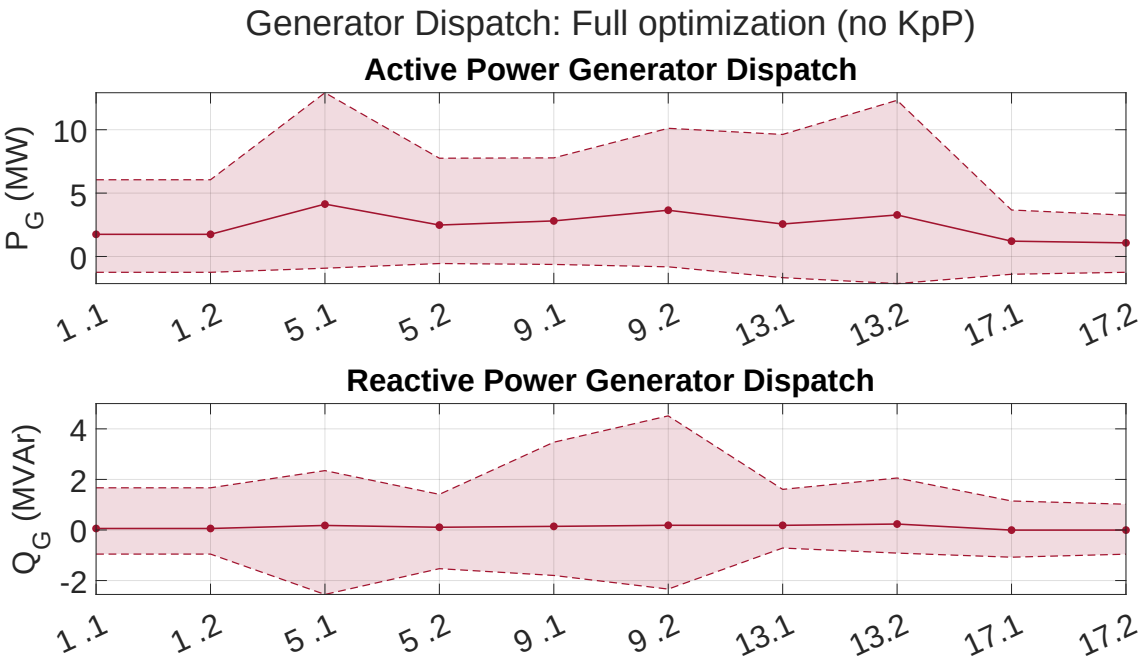

Figure A.101: Active- and reactive power generation of each substation for the full optimization without $K_{\mathrm{p,P}}$

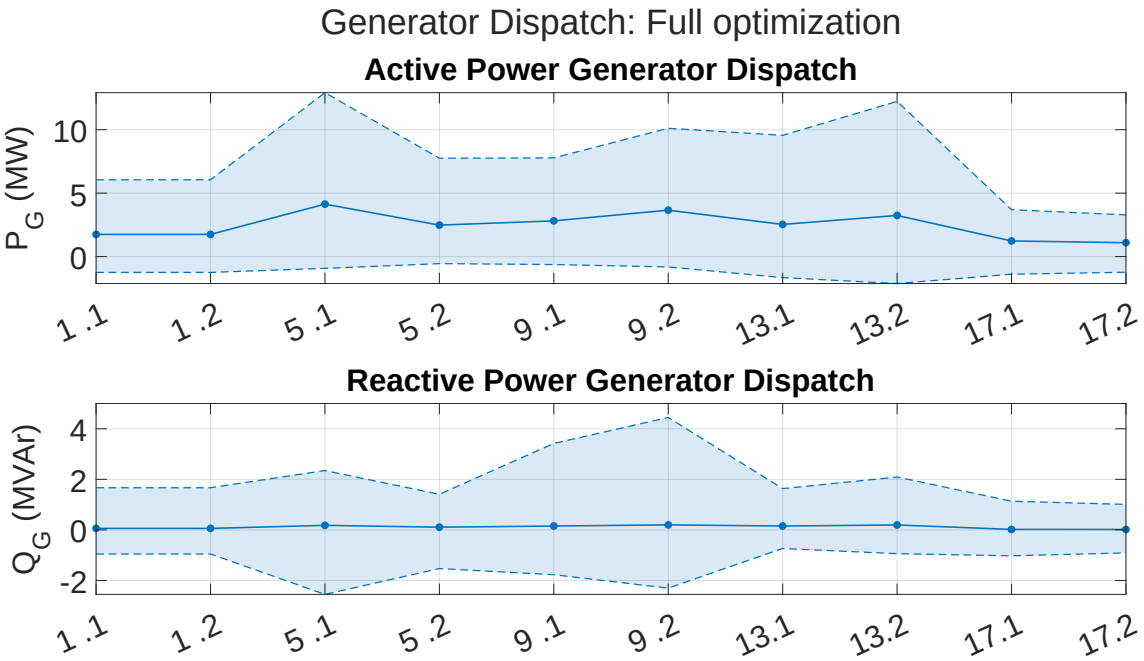

Figure A.102: Active- and reactive power generation of each substation for the full optimization with $K_{\mathrm{p,P}}$

A.6 Results from the simulation of the systems with asymmetric load positioning

This section contains the results from the simulation with asymmetric load positioning for both the AT- and BT-system.

A.6.1 AT-system

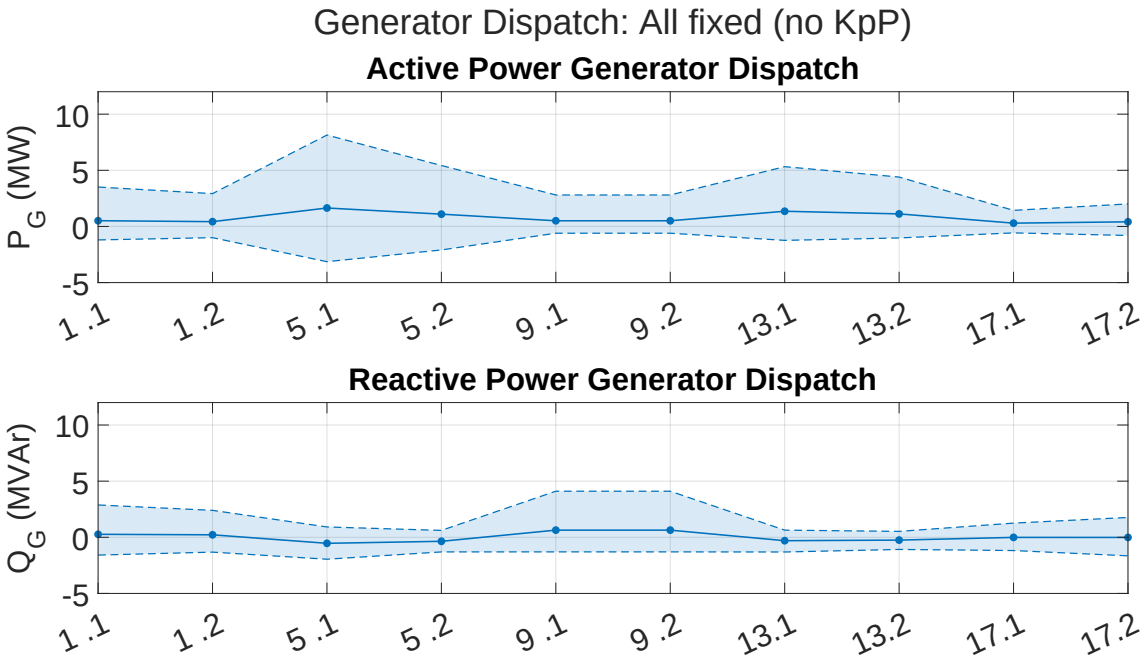

Figure A.103: Converter production for all fixed case for asymmetric load in exaggerated AT system

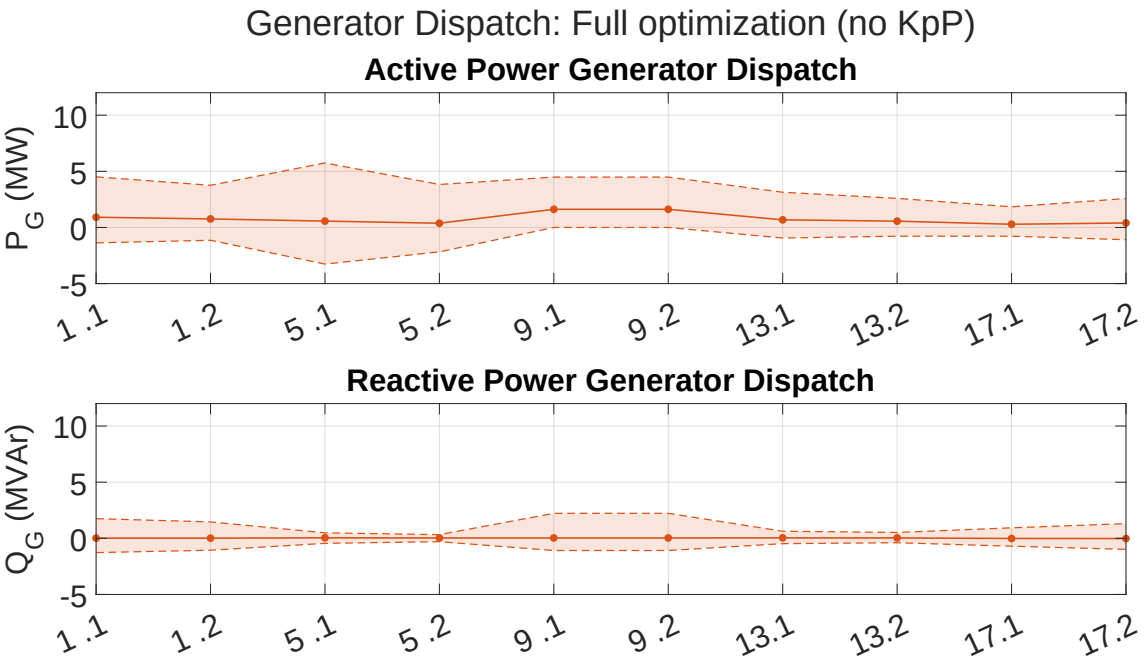

Figure A.104: Converter production for full optimization (no $K_{p,P}$) case for asymmetric load in exaggerated AT system

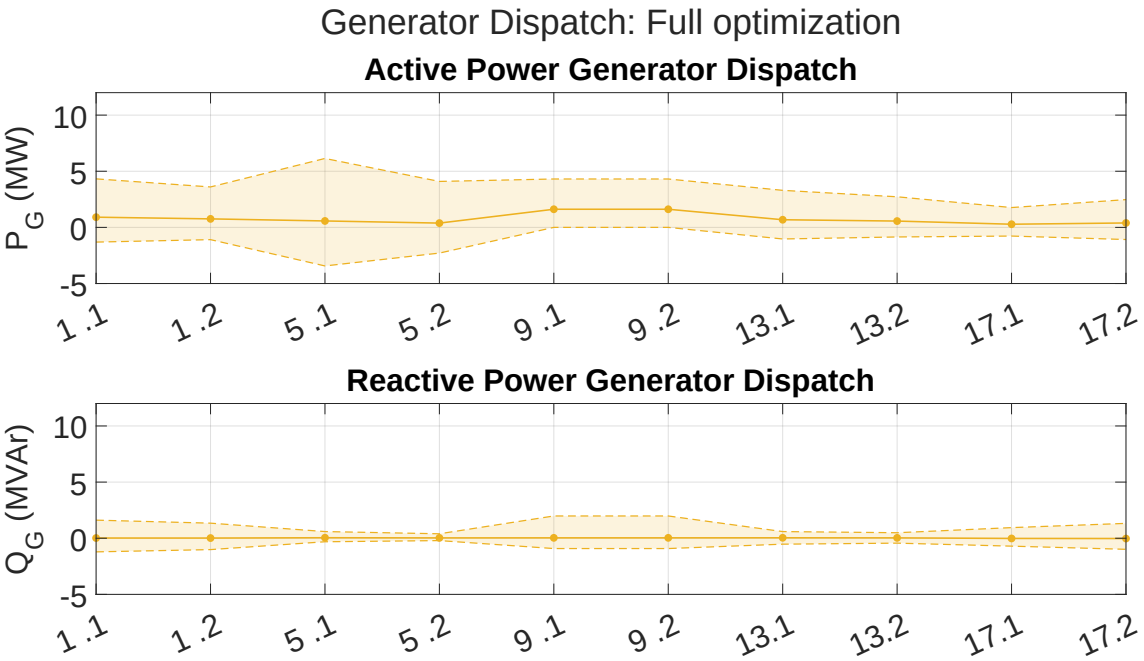

Figure A.105: Converter production for full optimization case for asymmetric load in exaggerated AT system

A.6.2 BT-system

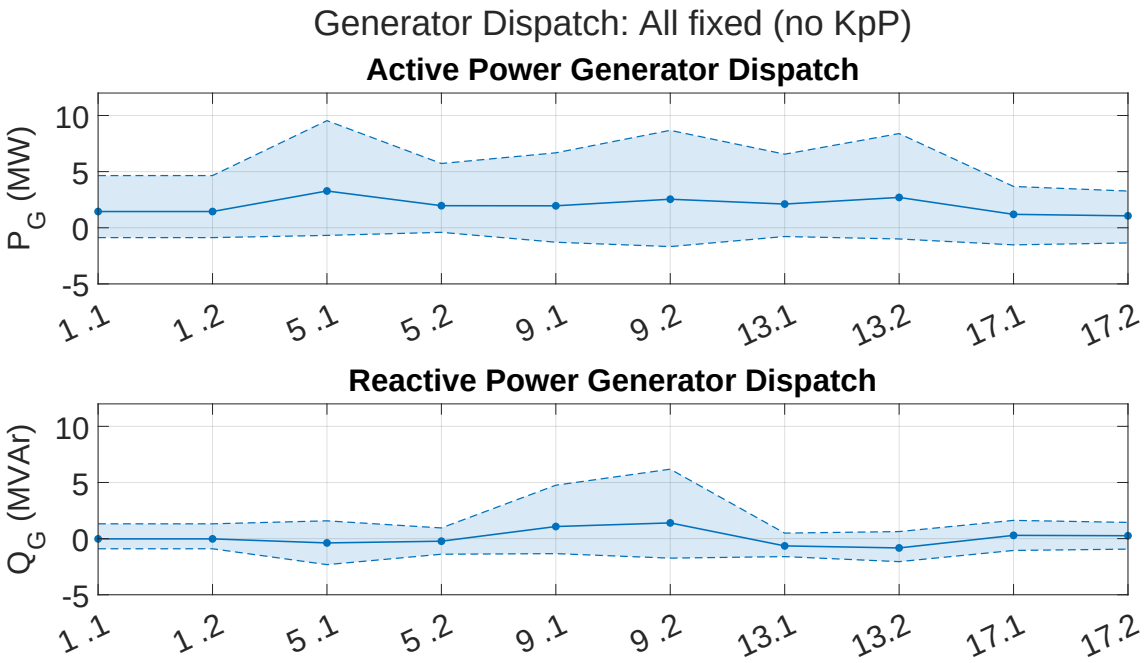

Figure A.106: Converter production for all fixed case for asymmetric load in exaggerated BT system

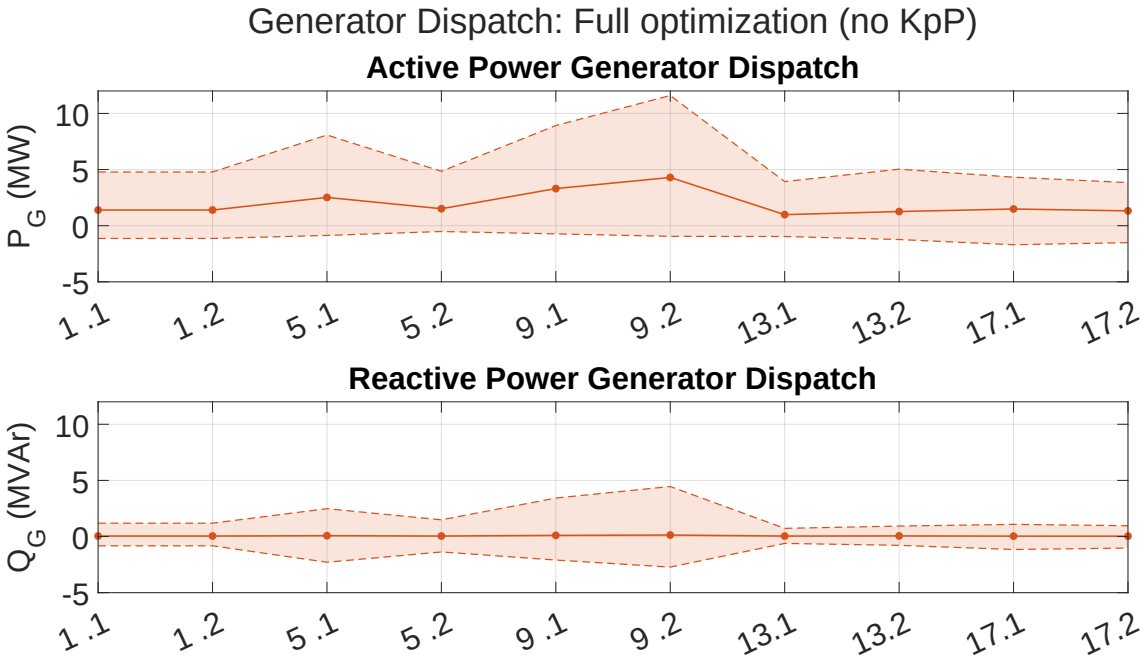

Figure A.107: Converter production for full optimization (no $K_{p,P}$) case for asymmetric load in exaggerated BT system

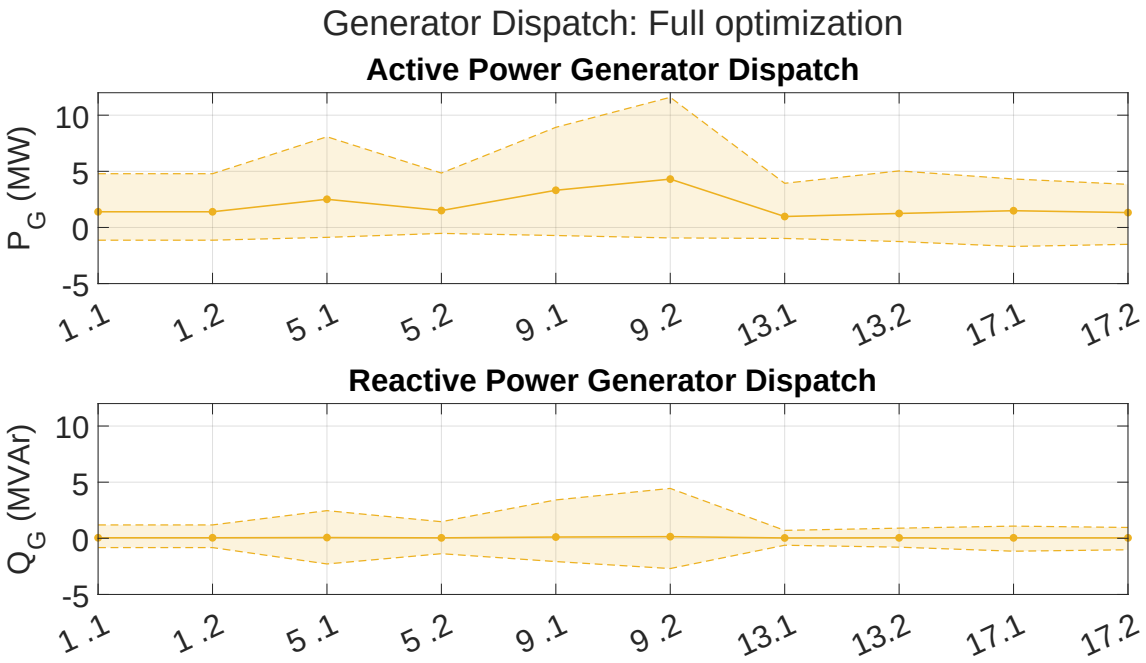

Figure A.108: Converter production for full optimization (no $K_{p,P}$) case for asymmetric load in exaggerated BT system

DEPARTMENT OF ELECTRICAL ENGINEERING
CHALMERS UNIVERSITY OF TECHNOLOGY
Gothenburg, Sweden
www.chalmers.se

CHALMERS
UNIVERSITY OF TECHNOLOGY